

DESIGN AND STRUCTURAL ANALYSIS OF ORGANIC SEMICONDUCTOR BASED ELECTRONIC DEVICES FOR BIO-MEDICAL APPLICATIONS

**A Thesis Submitted
In Partial Fulfillment of the Requirements
for the Degree of
DOCTOR OF PHILOSOPHY**

By

**SUGANDHA YADAV
(2K20/PHDEC/09)**

Under the Supervision of

Joint Supervisor

Dr. Shubham Negi

Asst. Professor, Chandigarh Univ.

Supervisor

Prof. Poornima Mittal

Professor, ECE, DTU



Department of Electronics and Communication Engineering

DELHI TECHNOLOGICAL UNIVERSITY

(Formerly Delhi College of Engineering)

Shahbad Daulatpur, Main Bawana Road, Delhi-110042. India

November, 2025

ACKNOWLEDGEMENT

I would like to express my deepest gratitude and sincere appreciation to all those who have contributed in the completion of my doctoral thesis. Their guidance, support, and encouragement have been invaluable throughout this journey.

First and foremost, I am sincerely thankful to my supervisor, Prof. Poornima Mittal, Professor, Department of Electronics and Communication Engineering, Delhi Technological University, Delhi, India for her invaluable guidance and constant support throughout my research journey. I am profoundly thankful for her unwavering commitment, encouragement, and patience. Her insightful feedback, immense knowledge, and constructive suggestions have greatly enriched my work. What I cherish most is her constant presence, always standing by my side, motivating me during difficult times, and celebrating every small success with me. I feel truly blessed and honored to have such a supportive and inspiring mentor, whose dedication has been a guiding light and whose encouragement has given me the confidence to reach new heights.

I would like to extend my profound thanks to my joint supervisor, Dr. Shubham Negi, Assistant Professor, Department of Electronics and Communication Engineering, Chandigarh University, Mohali, India. His guidance and insightful feedback were crucial to the growth and completion of my research work. It has been a privilege to learn and work under his supervision. I am deeply thankful for their supportive nature and valuable contributions, which have been a source of motivation and inspiration throughout my journey.

I express my gratitude towards the distinguished faculty members who have, time and again, guided us in various aspects of our journey. I extend my sincere regards to HoD sir, for his constant support. I wish to express my gratitude towards the DRC chairperson, the distinguished DRC members. Their expertise, constructive criticism, and valuable suggestions have significantly contributed to the refinement of my thesis. I am deeply grateful for the time and effort they devoted in reviewing and evaluating my work.

I am obliged to the esteemed faculty members of Department of Electronics and Communication Engineering, Delhi Technological University, Delhi, who provided me with a rich academic environment and facilitated my cognitive growth. Their lectures, discussions and seminars have expanded my horizons and shaped my research interests.

I express my deepest regards for Prof. Brijesh Kumar, Department of Information Technology,

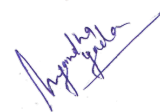
Indira Gandhi Delhi Technical University, Delhi, India, for investing his valuable time and efforts for providing deep and insightful remarks.

I am also grateful to all my colleagues and seniors of the Electronics and Communication department, especially Mr. Sachin Tyagi, Mr. Mohit Tyagi, Mr. Paritosh Chamola, Mr. Ashish Raturi, Ms. Bhawna Rawat, Ms. Yogita Chopra, Mr. Ayush, Ms. Bharti, Ms. Aparna, and Ms. Archana. I am thankful to them as they have generously contributed their time and shared their insights, without whom my study would not have been possible. Their collaborations, countless discussions and shared moments made my research journey enjoyable and intellectually rewarding. I also express my thanks all the staff members of the department for their continuous support in our academic activities.

Lastly, I would like to thank my family for their kindness, support, and patience throughout my journey. In particular, I am deeply grateful to my husband and my little daughter, Sia, whose love, encouragement, and understanding have been a constant source of strength and inspiration during my research work. Sia, though only four years old, brightened my days with her cheerful smile, making even the toughest moments lighter and more joyful.

Finally, I gratefully acknowledge the financial support provided by Delhi Technological University, Delhi. Their assistance helped me to carry out my research effectively and ensured that I had the necessary resources to complete my thesis.

To all those who have directly or indirectly contributed to my doctoral thesis, I extend my deepest gratitude. Your support, whether big or small, has played a significant role in shaping my academic and personal growth. I am profoundly grateful for your presence in my life and for the impact you have had on my journey as a researcher.



SUGANDHA YADAV
(Roll No. 2K20/PHDEC/09)



DELHI TECHNOLOGICAL UNIVERSITY

(Formerly Delhi College of Engineering)

Shahbad Daultpur, Main Bawana Road, Delhi-42

CANDIDATE'S DECLARATION

I, **Sugandha Yadav (Roll No. 2K20/PHDEC/09)**, hereby certify that the work which is being presented in the thesis entitled “**Design and Structural Analysis of Organic Semiconductor based Electronic Devices for Bio-medical Applications**”, in partial fulfilment of the requirements for the award of the Degree of **Doctor of Philosophy**, submitted in the Department of **Electronics and Communication Engineering**, Delhi Technological University is an authentic record of my own work carried out during the period from **25th August 2020 to 19th November 2025** under the supervision of **Prof. Poornima Mittal, Professor, Department of Electronics and Communication Engineering, Delhi Technological University, Delhi, India** and **Dr. Shubham Negi, Department of Electronics and Communication Engineering, Chandigarh University, Mohali, India**.

The matter presented in the thesis has not been submitted by me for the award of any other degree of this or any other Institute.

Date: 19-11-2025

Place: Delhi, India

SUGANDHA YADAV

(Roll No. 2K20/PHDEC/09)

This is to certify that the student has incorporated all the corrections suggested by the examiners in the thesis and the statement made by the candidate is correct to the best of our knowledge.

Signature of Joint-Supervisor

Signature of Supervisor

Signature of External Examiner



DELHI TECHNOLOGICAL UNIVERSITY

(Formerly Delhi College of Engineering)

Shahbad Daulatpur, Main Bawana Road, Delhi-42

CERTIFICATE BY THE SUPERVISOR(s)

Certified that **Sugandha Yadav (2K20/PHDEC/09)** has carried out their search work presented in this thesis entitled **“Design and Structural Analysis of Organic Semiconductor based Electronic Devices for Bio-medical Applications”**, for the award of **Doctor of Philosophy** from Department of Electronics and Communication Engineering, Delhi Technological University, Delhi, under our supervision. The thesis embodies results of original work, and studies are carried out by the student herself and the contents of the thesis do not form the basis for the award of any other degree to the candidate or to anybody else from this or any other University/Institution.

A handwritten signature in blue ink, appearing to read 'Shubham'.

DR. SHUBHAM NEGI

Joint Supervisor
Department of ECE
Chandigarh University
Mohali, India

A handwritten signature in blue ink, appearing to read 'Poornima'.

PROF. POORNIMA MITTAL

Supervisor
Department of ECE
Delhi Technological University
Delhi, India

Date: 19-11-2025

ABSTRACT

Organic Electronics depicts a complete paradoxical working mechanism as compared to the conventional devices and provides an alternating platform to obtain flexible, lightweight, transparent, foldable device designs with satisfactory performance. These low-cost organic devices can be further realized in various applications which is quite impressive and motivating for the research community. The present work focuses on the designing of OTFT (Organic Thin Film Transistor), OLED (Organic Light Emitting Diode), and OPD (Organic Photo Diode) for performance improvement and analyses their usage for biomedical applications.

The device structure plays a prominent role in comprehending its performance parameters. Therefore, these devices are analysed with respect to their structure to ameliorate the device performance. The conventional planar OTFT illustrates a decent current-voltage characteristics but these suffers from the limitations of grain boundary effect, large electric field requirements, and channel length constraints. A shorter length for the channel is very much needed to attain high performance TFTs. It helps in providing high drive current, fast switching, high transconductance, and good on-off current ratio (I_{on}/I_{off}). However, the reduction in channel length is quite difficult due to lithographical constraints in planar TFTs. Therefore, a short channel vertical channel OTFT is proposed which contains channel length in nano meter (nm) range. The device exhibits a significant improvement in terms of threshold voltage (V_t), maximum drain current (I_{Dmax}) and saturation mobility (μ_{sat}) in comparison to planar device.

The proposed vertical device (D₅) consists of a vertical channel between source and drain that too with a ditch-like structure. The device witnessed a significant improvement of 44 and 24 times for I_{Dmax} and μ_{sat} in comparison to the planar device (D₁). Furthermore, five other vertical-channel device structures (D₂, D₃, D₄, D₆ & D₇) are compared. Out of these structures, the proposed structure (D₅) shows remarkable performance in terms of I_{Dmax} (528 μ A) and μ_{sat} (80.8 cm²/V.s). It exhibits an increment in I_{Dmax} by 44, 2.38, 6.4, 4.4, 44 and 3.59 times as compared to the other devices; D₁, D₂, D₃, D₄, D₆ and D₇, respectively. Additionally, the proposed device exhibits a significant improvement in μ_{sat} which is higher by 24.5, 2.67, 8.32, 5.21, 73.45 and 3.6 times in comparison to D₁, D₂, D₃, D₄, D₆ and D₇, respectively. Further, to better understand the facts associated with high performance of proposed device, the vertical and horizontal cutline analysis is performed. A horizontal cutline is drawn at 5 nm below the source electrode and parameters; band energies, potential distribution, total current density,

electron/hole concentration are examined. The result of this analysis shows the strong gate control and small channel length as the primary attributes for performance enhancement.

Further, focusing on the structural aspects, an organic LED structure is proposed to design an effective light emitter for bio-medical applications. In recent years, The OLEDs have been integrated spectacularly in large panels for display and biomedical applications. Different layers used in the OLED architecture witnessed a prominent role in its performance. Herein, a CGL (Charge Generation Layer) is utilized to enhance the carrier concentration inside the EML (Emissive Layer) in OLED. This layer consists of HAT-CN (hexaazatriphenylene-hexacarbonitrile) material for electron and TAPC (1,1-bis[(di-4-tolylamino)phenyl]cyclohexane) for holes generation. In the proposed structure (L_6), the CGL layer is incorporated outside of the EML which significantly enhances the device performance. The proposed design is compared with other five CGL/non-CGL based OLED devices (L_1 , L_2 , L_3 , L_4 and L_5).

The proposed device showcased the luminescence and current values of 3636.3 cd/m^2 and 0.44 A , respectively. The obtained luminescence is about 16.8, 2.3, 1.7, 3, 1.6 times improved than that of L_1 , L_2 , L_3 , L_4 and L_5 , respectively. Thereafter, an in-depth internal analysis is performed to better analyse the behaviour of device. The proposed device is analysed and compared with other mentioned devices in terms of Langevin recombination rate, electron concentration, hole concentration, band energy, total current density, electron affinity, hole QFL (Quasi-Fermi Level), conduction current density, potential distribution, and electron/hole mobility. The results depict that the CGLs generate excess charge carriers and enhance the carrier concentration within the EML layer. Consequently, the device luminescence is enhanced and validates the Langevin's theory. Additionally, the energy levels of CGLs show a close match with the other adjacent layers, which further enhances the carrier movement from the electrodes. Thereby, the current density within the device is also improved.

The OLED device witnessed a potential use as the light source in biomedical applications. However, the detection must be carried out by the OPD. Additionally, it is desired to realize both the devices on a single substrate for smaller size and efficient sensing. Hence, an efficient CGL based organic photo diode is designed and analysed to work as a suitable light sensing element. Organic photodiodes have emerged as better alternative owing to their flexibility, reduced dark current, thin active layer, and tuneable spectral responsivity during the last decade. In the proposed device, the CGL is incorporated to enhance the exciton interaction that leads in generating more free charge carriers and thereby augment the conduction. In this work,

the proposed device (P_2) is compared with other four non-CGL (P_1) and CGL (P_3 , P_4 and P_5) based devices.

Another important aspect with CGL based devices is the position of this layer with respect to other layers. In the proposed device (P_2), the CGL is placed outside the active layer in such a manner that HAT-CN is placed near acceptor and TAPC near donor layer. Consequently, the proposed device depicts a remarkable improvement and showcased fair enough values for photocurrent (134.2 nA) and dark current (10.2 nA). The photocurrent of P_2 is increased by 34 times in comparison to the reference device (P_1). Also, on comparing with other CGL based devices; P_3 , P_4 and P_5 , the photocurrent of P_2 is enhanced by 1.6, 1.4 and 9 times, respectively. Further, the thickness optimization and internal analysis of the proposed device are also performed to better comprehend the role of layers in the OPD. The parameters; electron/hole concentration, electron current density, potential, conduction/valence band energy and electron QFL are observed and quantitatively compared. The results highlight an enhanced carrier generation due to exciton interaction with active layers and CGLs, leading to a high current generation.

The integration of OLED and OPD devices is the best suitable combination for point-of-care diagnostic in the field of sensor applications. Also, the OTFT can be used as the driver. This work proposes the methodology for bio-medical applications using organic LED and photodiode to make an efficient, flexible, and low-cost sensor. The fluorescence-based detection methodology is presented and utilized in three medical applications; corona virus detection, heart rate monitoring, and ovarian cancer detection. Primarily, the materials for both OLED and OPD devices are modified to make these devices suitable for the detection of SARS-COV-2 (Severe Acute Respiratory Syndrome Coronavirus-2) virus RNA (Ribonucleic Acid) inside human saliva sample. In OLED, the materials; DPVBi (4,4'-Bis(2,2-diphenylvinyl)-1,1'-biphenyl) & BCzVBi (4,4'-Bis(9-ethyl-3-carbazovinylen)1,1'-biphenyl) are chosen for the EML layer so that the device can emit a light of 470 nm wavelength. In case of OPD, the materials; C60 and CuPc are considered for acceptor and donor, respectively. When the emission wavelength falls on the saliva sample, fluorescence emission takes place. For a normal person, this emission is in the range of 490 nm and correspondingly OPD produces a current of 37.2 mA magnitude. However, due to the presence of SARS-CoV-2 RNA, the emission from the infected person is in the range of 525 nm, resulting in OPD current value of 63.5 mA. Thus, a healthy person can be differentiated from a Covid-19 infected patient.

Thereafter, in this work, a green color-based OLED is utilized for heart rate measurement. This OLED is based on the proposed device structure incorporating CGLs. The primary reason of choosing green color OLED is its wavelength which can be absorbed by the blood easily. Also, it has low penetration in the skin and thus provides better contrast signal. For OPD, the materials; C60 and CuPc are chosen for acceptor and donor, respectively. The methodology is based on the fluorescence emission where green light with wavelength of 497 nm falls on the blood cells. Furthermore, a different intensity of the reflected wavelength is sensed by the photodiode.

The methodology depicts that during the diastole, comparatively a higher current is produced by the OPD as the absorption by the blood cell remains less and reflection is more. On the contrary, the OPD provides low current values in the case of systole due to higher absorption of the green light as high volume of blood is available at this time. The proposed OLED exhibits current and luminescence values of 0.92 A and 8363.6 cd/m², respectively and OPD demonstrates dark current and photocurrent of 10.2 and 174.5 nA, respectively. This methodology is also applied for multiple person's and compared with some existing work in terms of excitation and detection wavelengths.

The proposed OLED and OPD are also used for the detection of Ovarian cancer. As per the requirements, the QAD (4-(5,6-dimethoxy-1-benzothiophen-2-yl)-4-oxobutanoic acid) material is opted for EML (OLED) which is responsible for producing desired wavelength of 350 nm. This OLED generates fair enough current density and luminescence values of 37.02 mA/cm² and 3636.38 cd/m², respectively. Both these devices have the same structure as the proposed devices, only the material for specific layers are changed to match the need of the application. The OLED emits the target light beam of 350 nm which falls on the urine sample. Thereafter, the altered light beam is sensed by the photodiode and produces subsequent output current. For the healthy person, the reflection occurs at 420 nm and corresponding current attains the magnitude of 31.2 nA. Whereas, for a person having ovarian cancer, the emission spectra is in the range of 440 nm and subsequent current registers a value of 47 nA. Thus, the healthy human can be easily differentiated from a cancer patient. Furthermore, it is also shown that the proposed detection technique is applicable for multiple persons. The research conducted herein shows the effective utilization of organic devices for biomedical application. The investigation of OLED and OPD highlights their effectiveness to be used for non-invasive sensing applications. This further widens up the horizons for investigating organic devices in the field of biomedical applications.

TABLE OF CONTENTS

Title	Page No.
Acknowledgement	ii
Candidate's Declaration	iv
Certificate by the Supervisor(s)	v
Abstract	vi
List of Tables	xiv
List of Figures	xvii
List of Symbols, and Abbreviations	xxi
 CHAPTER 1: INTRODUCTION	 1 – 12
1.1 ORGANIC THIN FILM TRANSISTOR	2
1.2 ORGANIC LIGHT EMITTING DIODE	3
1.3 ORGANIC PHOTO DIODE	4
1.4 DIFFERENT BIO-MEDICAL APPLICATIONS USING ORGANIC ELECTRONIC DEVICES	5
1.5 PROBLEM STATEMENT	6
1.6 OBJECTIVES	8
1.7 OBJECTIVE-WISE METHODOLOGY	8
1.8 THESIS ORGANIZATION	10
 CHAPTER 2: LITERATURE REVIEW	 13 – 56
2.1 STRUCTURAL DIVERSITY, PARAMETERS AND IMPROVEMENT TECHNIQUES FOR OLED	13
2.1.1 Basic structure and working principle of OLED	14
2.1.2 Structural diversity for OLED	15
2.1.3 Characteristics parameters of OLED	18
2.1.4 Performance improvement based on different layers	25
2.1.5 Performance comparison for blue and white OLEDs	32
2.1.6 Critical analysis for parameters and structural diversity for OLEDs	34

2.2	STRUCTURAL DIVERSITY AND PARAMETERS FOR OTFT	38
2.2.1	Performance parameters for OTFTs	38
2.2.2	Classification of OTFT based on structural diversity	39
2.2.3	Critical analysis for different OTFT structures	43
2.3	ORGANIC PHOTO DIODE	44
2.3.1	Performance parameters and importance of dark current	45
2.3.2	Layer based analysis of different OPDs in recent time	47
2.4	SOLUTION PROCESSING FABRICATION TECHNIQUES FOR FLEXIBLE ELECTRONIC DEVICES	49
2.4.1	Spin coating	49
2.4.2	Inkjet printing	50
2.4.3	Screen printing	51
2.5	DIFFERENT APPLICATIONS OF FLEXIBLE DEVICES	51
2.5.1	Bio-medical applications	51
2.5.2	Sensors	53
2.5.3	OTFT driven OLED applications	53
2.6	RESEARCH GAPS	55

CHAPTER 3: SHORT CHANNEL FLEXIBLE VERTICAL ORGANIC THIN FILM TRANSISTOR **57-76**

3.1	INTRODUCTION	57
3.2	CHARACTERISTIC ANALYSIS AND PARAMETERS EXTRACTION OF SINGLE GATE PLANAR TRANSISTOR	59
3.3	PERFORMANCE COMPARISON OF VERTICAL AND PLANAR TRANSISTORS	61
3.3.1	Cutline analysis for vertical and planar TFTs	63
3.3.2	Performance analysis of different vertical structures	65
3.4	PROPOSED VERTICAL TFT	67
3.5	INTERNAL CUTLINE ANALYSIS FOR THE PROPOSED DEVICE	72
3.5.1	Horizontal cutline analysis	72
3.5.2	Vertical cutline analysis	73
3.6	SUMMARY OF THE RESULTS	75

CHAPTER 4: CHARACTERISTICS PERFORMANCE ANALYSIS OF IMPROVED OLED AND OPD DEVICES **77-112**

4.1	INTRODUCTION	77
4.2	CHARACTERISTIC ANALYSIS AND PARAMETERS EXTRACTION OF MULTILAYERED OLED	79
4.3	PERFORMANCE ANALYSIS WITH CGL AT DIFFERENT POSITION FOR OLED	81
4.4	PROPOSED NOVEL OLED DEVICE	84
	4.4.1 Internal analysis of OLED devices	86
4.5	THICKNESS OPTIMIZATION OF THE PROPOSED OLED	96
	4.5.1 Case I: Thickness decrement in HAT-CN and TAPC layers	96
	4.5.2 Case II: Thickness decrement in only TAPC layer	96
	4.5.3 Case III: Thickness decrement in only HAT-CN layer	97
4.6	CHARACTERISTIC ANALYSIS AND PARAMETERS EXTRACTION OF OPD	99
4.7	PROPOSED OPD DEVICE	100
	4.7.1 Analysis of proposed device with positional variations of CGL	103
	4.7.2 Thickness optimization of proposed OPD	105
4.8	INTERNAL ANALYSIS OF REFERENCE AND PROPOSED OPD	107
	4.8.1 Vertical cutline analysis	107
	4.8.2 Horizontal cutline analysis	109
4.9	SUMMARY OF THE RESULTS	110

CHAPTER 5: COVID-19 DETECTION USING IMPROVED OLED AND OPD DEVICES **113-122**

5.1	INTRODUCTION	113
5.2	METHODOLOGY FOR DETECTION OF COVID-19	115
5.3	ORGANIC LED AND PHOTO DIODE UTILIZATION FOR COVID-19 DETECTION	116
	5.3.1 OLED driver circuit	117
5.4	COVID-19 FLUORESCENCE DETECTION USING OLED AND OPD DEVICES	118
5.5	SUMMARY OF THE RESULTS	121

**CHAPTER 6: PARAMETRIC ANALYSIS OF OTFT-OLED-OPD
INTEGRATION FOR HEART RATE MEASUREMENT AND OVARIAN
CANCER DETECTION 123-140**

6.1	INTRODUCTION	123
6.2	DETECTION MECHANISM FOR HEART RATE MONITORING	125
6.3	DEVICE MODIFICATION IN TERMS OF WAVELENGTH FOR HEART RATE MONITORING	126
6.3.1	Modified green OLED (H_1) for heart rate monitoring	126
6.3.2	Modified OPD (H_2) for the detection of wavelengths	128
6.4	HEART RATE MONITORING USING MODIFIED OLED AND OPD	130
6.5	DETECTION MECHANISM FOR OVARIAN CANCER	133
6.6	DEVICE MODIFICATION IN TERMS OF MATERIALS FOR OVARIAN CANCER DETECTION	134
6.7	OVARIAN CANCER DETECTION USING MODIFIED DEVICES OLED O_1 AND OPD H_2	136
6.8	SUMMARY OF THE RESULTS	139

CHAPTER 7: CONCLUSIONS AND FUTURE SCOPE 141-146

7.1	CONCLUSIONS	141
7.2	FUTURE SCOPE	144

REFERENCES	147
------------	-----

LIST OF PUBLICATIONS	172
----------------------	-----

LIST OF TABLES

S. No.	Table Caption	Page No.
Table 2.1	Comparison of three reported foldable displays.	17
Table 2.2	Comparison of different existing OLEDs in terms of luminescence and EQE during last decade.	20
Table 2.3	Some important strategies reported to improve current efficiency during last decade.	22
Table 2.4	Some important strategies reported to improve power efficiency during last decade.	23
Table 2.5	Different existing materials (with thickness) used for injection layer.	25
Table 2.6	Different materials with thickness used for transport layer in OLEDs.	27
Table 2.7	Different materials with thickness used for emissive layer in OLEDs.	29
Table 2.8	Different materials (with thickness) used for blocking layer in OLEDs.	30
Table 2.9	Different approaches used for blue OLEDs along with their performance during last decade.	32
Table 2.10	Different approaches used for white OLEDs along with their performance during last decade	33
Table 2.11	Comparison of spacer, mixed interlayer, and charge generation layers across various aspects.	37
Table 2.12	Comparison of performance parameters of different existing bottom gate top contact and bottom contact TFTs.	40
Table 2.13	Comparison of performance parameters of different existing single gate and dual gate TFTs.	41
Table 2.14	Review of different existing vertical TFTs in terms of performance parameters.	42
Table 2.15	Review of different existing organic photo diode in terms of their performance.	46
Table 2.16	Performance improvement in existing OPDs in terms of layers.	47
Table 2.17	Different bio-medical applications using OLED and OPD.	52
Table 2.18	Performance comparison of three different displays based on OTFT driven AMOLEDs.	54

Table 3.1	Materials and thickness of different layers of D ₁ .	59
Table 3.2	Material's specification for different layers of D ₁ .	59
Table 3.3	Parametric comparison of simulated (D ₁) and experimental device.	61
Table 3.4	Parametric comparison of planar (D ₁) and vertical device (D ₂).	62
Table 3.5	Materials and thickness of different regions in three vertical devices.	66
Table 3.6	Comparison of performance parameters of three vertical Devices.	66
Table 3.7	Materials and thickness of different regions of D ₂ and D ₅ .	69
Table 3.8	Parametric comparison for D ₂ and D ₅ .	69
Table 3.9	Comparison of the proposed D ₅ with existing vertical devices (simulated at common platform).	71
Table 4.1	Materials along with their thickness for each layer used in L ₁ device.	80
Table 4.2	Comparison of current and luminescence for different OLEDs (L ₁ -L ₅).	83
Table 4.3	Different values of luminescence at different CGL thickness for proposed OLED (L ₆).	98
Table 4.4	Materials used and thickness of each layer for multilayered device P ₁ .	99
Table 4.5	Parametric comparison of experimental results with multilayered device P ₁ .	100
Table 4.6	Photocurrents at different thicknesses of HAT-CN and TAPC for proposed OPD (P ₂).	106
Table 5.1	Comparison of existing research work with our work in terms of wavelength.	116
Table 5.2	Excitation and emission wavelengths with current for Covid-19 detection using OLED and OPD.	119
Table 5.3	Luminescence values of OLED (L ₆) at different voltages (0-5 V) for wavelength 470 nm.	120
Table 5.4	Current variations in OPD at different light beams from OLED for Covid-19 detection.	121
Table 6.1	Different materials used in OLED (H ₁) along with the thickness of each layer.	127
Table 6.2	Enlisting of the materials along with their thickness values for each layer of OPD (H ₂).	129
Table 6.3	Comparison of existing work with the proposed work for heart rate detection in terms of wavelength.	130
Table 6.4	Methodology for heart rate detection based on dedicated OLED wavelength values for excitation and corresponding	131

current values generated by the OPD.

Table 6.5	Luminescence values of OLED (H ₁) at different voltages (0-5 V).	132
Table 6.6	Different current values generated by OPD (H ₂) at different light beams (B ₁ -B ₁₀) for heart rate monitoring.	132
Table 6.7	Comparison of the proposed work with other researchers' work in terms of excitation and detection wavelength for ovarian cancer detection.	133
Table 6.8	Materials and thickness for OLED (O ₁).	136
Table 6.9	Technique for ovarian cancer detection using OLED and OPD.	137
Table 6.10	Luminescence values of OLED (O ₁) at various voltage from 0-5 V.	137
Table 6.11	Current variations in OPD at different light beams.	138

LIST OF FIGURES

S. No.	Figure Caption	Page No.
Fig. 1.1	Different electronic flexible devices based on organic semiconductors.	1
Fig. 1.2	Different possible bio-medical applications using OLED-OPD integration.	6
Fig. 2.1	Conventional basic structure of OLED.	14
Fig. 2.2	Multi-layered structure of OLED with holes/electrons injection and transport layers.	15
Fig. 2.3	Different structures for (a) Top (b) Inverted top and (c) Bottom emission OLED.	16
Fig. 2.4	Top view of prototype model of foldable OLED.	17
Fig. 2.5	Architecture of transparent OLED.	18
Fig. 2.6	Parametric improvement in OLEDs over the last decade in terms of (a) Luminescence, (b) EQE, (c) Luminous efficiency and (d) Current efficiency.	35
Fig. 2.7	Basic structure of OTFT.	38
Fig. 2.8	Bottom gate OTFT with (a) Top contact (TC) and (b) Bottom contact (BC) structures.	40
Fig. 2.9	Mobility variations in OTFTs based on (a) TC and BC structures and (b) Single and dual gate structures.	43
Fig. 2.10	Basic structure of organic photo diode.	45
Fig. 2.11	The flow of working mechanism for organic photo diode.	45
Fig. 2.12	(a) Processing steps of spin coating and (b) inkjet printing techniques.	50
Fig. 2.13	Pixel circuits for OTFT driven AMOLED for (a) C_1 , (b) C_2 , and (c) C_3 .	54
Fig. 3.1	Structure of BGTC planar TFT (D_1).	59
Fig. 3.2	(a) Simulated device structure of BGTC (planar) transistor and (b) Representation of layers with current flow-lines from source to drain.	60
Fig. 3.3	Transfer characteristics of experimental and simulated planar devices along with threshold voltage and (b) Drain characteristics of planar device.	61
Fig. 3.4	Device structure for vertical thin film transistor (D_2).	62

Fig. 3.5	(a) Comparison of transfer characteristics of D ₁ (planar) and D ₂ (vertical) devices along with threshold voltage and (b) Drain characteristics of D ₂ device.	62
Fig. 3.6	(a) Simulated vertical device structure (D ₂) and (b) Current flowlines inside the device.	63
Fig. 3.7	Band energy for (a) D ₁ and (b) D ₂ , Potential distribution for (c) D ₁ and (d) D ₂ , current density for I D ₁ and (f) D ₂ .	65
Fig. 3.8	Vertical structures of (a) D ₃ and (b) D ₄ devices.	66
Fig. 3.9	Comparison of transfer curves of D ₂ , D ₃ and D ₄ along with the threshold voltages.	67
Fig. 3.10	Proposed vertical TFT structure (D ₅) with a ditch in dielectric filled with organic semiconductor.	68
Fig. 3.11	(a) Simulated structure of proposed device D ₅ and (b) Current flowlines along with horizontal cutline.	68
Fig. 3.12	(a) Comparison of transfer characteristics of D ₂ and D ₅ and (b) Drain characteristics of D ₅ device.	69
Fig. 3.13	Comparison of different vertical TFTs in terms of (a) Drain current and (b) Mobility.	70
Fig. 3.14	Horizontal cutline analysis of (a) Valence band, (b) Conduction band, (c) Potential distribution, (d) Current density of D ₅ Device, I Hole concentration of D ₂ and (f) Hole concentration of D ₅ .	73
Fig. 3.15	Vertical cutline analysis of (a) Valence band, (b) Conduction band, (c) Potential distribution and (d) Current density of D ₅ Device.	74
Fig. 4.1	Structure of multilayered OLED device (L ₁).	79
Fig. 4.2	Simulated structure of OLED L ₁ showing the thickness of different materials used in the device.	80
Fig. 4.3	(a) Comparison of current for existing experiment and simulated device and (b) Combined curves of current density and luminescence for L ₁ .	80
Fig. 4.4	Different OLED structures based on positional variation of CGL (a) Below cathode (L ₂), (b) Above anode (L ₃), (c) Both sides of device (below cathode and above anode) (L ₄), and (d) Inside emissive layer (L ₅).	82
Fig. 4.5	Comparison of (a) Current and (b) Luminescence for L ₁ - L ₅ devices.	83
Fig. 4.6	CGL based Proposed OLED device (L ₆).	84
Fig. 4.7	Simulated structure of L ₆ showing the thickness of different materials.	85

Fig. 4.8	(a) Combined curves of current and luminescence for proposed device (L_6) and (b) Variation of luminescence with respect to voltage for L_1 , L_5 and L_6 .	85
Fig. 4.9	Vertical cutline at 200 μm inside proposed device (L_6).	86
Fig. 4.10	Performance comparison of all six OLED devices (L_1 - L_6) using vertical cutline in terms of (a) Hole concentration, (b) Electron concentration, (c) Total current density, and (d) Langevin recombination rate.	87
Fig. 4.11	(a) Potential distribution of the proposed device (L_6), Comparison of devices L_5 and L_6 based on (b) Conduction current density, (c) Electron affinity and (d) Acceptor trap ionized density.	89
Fig. 4.12	Horizontal cutline drawn towards cathode at 0.195 μm in proposed OLED device (L_6).	90
Fig. 4.13	Comparison of parameters for L_5 and L_6 based on horizontal cutline in terms of (a) Langevin recombination rate, (b) Conduction current density, (c) Band energy of L_5 , (d) Band energy of L_6 , and (e) Hole QFL of L_5 & L_6 .	91
Fig. 4.14	Horizontal cutline drawn towards anode at 0.215 μm in proposed OLED device (L_6).	92
Fig. 4.15	Comparison of all six devices (L_1 - L_6) using horizontal cutline in terms of (a) Hole mobility and (b) Electron mobility and (c) Langevin recombination rate.	93
Fig. 4.16	Enlarged view of devices showing (a) Net doping of L_5 , (b) Net doping of L_6 , (c) Conduction current density of L_5 and (d) Conduction current density of L_6 .	95
Fig. 4.17	(a) Luminescence comparison of Proposed OLED L_6 with thickness variation in (a) HAT-CN and TAPC both, (c) TAPC only and I HAT-CN only, with respective enlarged view in b, d and f.	97
Fig. 4.18	(a) Comparison of luminescence of device L_6 at CGL thickness (in Case I both CGLs = 12 nm, Case II bottom CGL = 12 nm and Case III, top CGL = 12 nm) and (b) Maximum luminescence for three cases.	98
Fig. 4.19	Device structure for Multilayered OPD (P_1).	99
Fig. 4.20	Simulated structure of multilayered device P_1 .	100
Fig. 4.21	Characteristics comparison for reported experiment and simulated OPDs (P_1) for (a) Dark current and (b) Photocurrent.	100
Fig. 4.22	Device structure for proposed CGL based OPD device (P_2).	101
Fig. 4.23	(a) Simulated structure of proposed device (P_2) and (b) Potential distribution inside P_2 .	102
Fig. 4.24	Comparison of multilayered device (P_1) and proposed device (P_2) based on (a) Photocurrents and (b) Dark currents.	103

Fig. 4.25	Different OPD structures (a) P ₃ with only HAT-CN, (b) P ₄ with only TAPC and (c) P ₅ with TAPC at top and HAT-CN at bottom.	104
Fig. 4.26	Photocurrent characteristics for P ₂ , P ₃ , P ₄ and P ₅ devices.	104
Fig. 4.27	Proposed OPD Performance with thickness variation (a) HAT-CN and TAPC both, (c) TAPC only and I HAT-CN only with respective enlarged view in b, d and f.	106
Fig. 4.28	Vertical cutline analysis of P ₁ and P ₂ in terms of (a) Electron concentration, (b) Hole concentration, (c) Electron current density, (d) Potential, I Conduction band energy, (f) Valence band energy and (g) QFL.	108
Fig. 4.29	Horizontal cutline analysis for (a) Band energies, (b) Potential distribution, and (c) Total current density.	110
Fig. 5.1	Covid-19 detection using OLED and OPD devices.	115
Fig. 5.2	Utilized (a) OLED and (b) OPD devices for Covid-19 detection.	116
Fig. 5.3	OLED driver circuit using V-OTFT.	118
Fig. 5.4	(a) Variation of anode voltage at node 3, and (b) Current and luminescence curves of OLED.	118
Fig. 5.5	Current with respect to wavelength variation for OPD.	120
Fig. 5.6	Comparison of the proposed work with others in terms of (a) Peak intensities, and (b) Output current produced by OPD.	120
Fig. 5.7	Currents variations in OPD at different light beams.	121
Fig. 6.1	Heart rate detection methodology using OLED and OPD devices.	125
Fig. 6.2	(a) Structure of Green OLED device H ₁ and (b) Simulated structure of device H ₁ .	127
Fig. 6.3	Simulated structure of OPD (H ₂), (b) Proposed structure of the device OPD (H ₂), and (c) Results for dark current and photo current of H ₂ .	129
Fig. 6.4	Current values of OPD (H ₂) at different wavelengths.	131
Fig. 6.5	(a) Current values of OPD at different light beams, and (b) Light intensity at different beams.	132
Fig. 6.6	Ovarian cancer detection methodology.	134
Fig. 6.7	(a) Modified structure of OLED Device (O ₁), and (b) Simulated structure of modified OLED device (O ₁) for ovarian cancer detection.	135
Fig. 6.8	Parametric analysis of OLED (O ₁) in terms of current density and luminescence.	136
Fig. 6.9	Different Current values generated by OPD at different light beams.	138

List of Abbreviations

Symbol/Abbreviation	Full Form
A-IGZO	Amorphous-Indium Gallium Zinc Oxide
AC	Alternate Current
Al	Aluminum
Alq ₃	Tris(8-hydroxyquinolinato)aluminum
AMOLED	Active-matrix OLED
AND	9,10-Di(xxiaphtha-2-yl)anthracene
BC	Bottom Contact
BczVBi	4,4'-Bis(9-ethyl-3-carbazovinylen)1,1'-biphenyl
BGBC	Bottom Gate Bottom Contact
BGTC	Bottom Gate Top Contact
Bphen	Bathophenanthroline
Bpy-p2C	Dicarbazolyl
Bpy-p3C	Tercarbazolyl
Bpy-pC	Carbazolyl
Bpy-pTC	Tert-butylcarbazolyl
C70	Fullerene-70
C8-BTBT	2,7-dioctyl[1] benzothieno[3,2-b][1]benzothiophene
CGL	Charge Generation Layer
CIE	Commission Internationale de l'Éclairage
CP-OLEDs	Circularly Polarized-Organic Light Emitting Diodes
CRISPR/Cas12a	CRISPR-associated Protein 12a (Cas12a) endonuclease
CuI	Copper(I) Iodide
CuPC	Copper Phthalocyanine
DC	Direct Current
DCJTB	4-(Dicyanomethylene)-2-tert-butyl-6-(1,1,7,7-tetramethyljulolidin-4-yl-vinyl)-4 <i>H</i> -pyran
DMPPP	1,3-Bis(N,N-dimethylphenyl)-1,3-propane-diamine derivative
DNA	Deoxyribonucleic Acid
DPVBi	4,4'-Bis(2,2-diphenylvinyl)-1,1'-biphenyl
EBL	Electron Blocking Layer
EC	Electrochromic
EIL	Electron Injection Layer
EL	Electroluminescence
EML	Emissive Layer
EQE	External Quantum Efficiency
ETL	Electron Transport Layer
HAT-CN	1,4,5,8,9,11-hexaazatriphenylene-hexacarbonitrile
HBL	Hole Blocking Layer
HIL	Hole Injection Layer

HOMO	Highest Occupied Molecular Orbital
HTL	Hole Transport Layer
Ir(ppy) ₃	Tris(2-phenylpyridine)iridium(III)
ITO	Indium–Tin Oxide
LiF	Lithium Fluoride
LUMO	Lowest Unoccupied Molecular Orbital
mCP	3,5-bis(N-carbazolyl)benzene
m-MTDATA	4,4',4''-tris[3-methyl-phenyl(phenyl)amino]-triphenylamine
MoO _x	Molybdenum Oxide
MoS ₂	Molybdenum Disulfide
mPyrPPB	mPyrPPB (1,3,5-tris(3-(3-(pyridine-3-yl)phenyl)phenyl)benzene
NiO _x	Nickel Oxide
Nm	Nano-meter
NPB	N,N'-diphenyl-N,N'-bis(1-naphthylphenyl)-1,1'-biphenyl-4,4'-diamine
OLED	Organic Light Emitting Diode
OPD	Organic Photo Diode
OSCs	Organic Semiconductor
OTFT	Organic Thin Film Transistor
PBDTT-8tTPD	Poly[(4,8-bis(2-ethylhexylthienyl)benzo[1,2-b:4,5-b']dithiophene)-alt-(thieno[3,4-c]pyrrole-4,6-dione)]
pC1B5	Phosphorus Pentachloride
PCDTBT:PC71BM	(Poly[N-9'-heptadecanyl-2,7-carbazole-alt-5,5-(4',7'-di-2-thienyl-2',1',3'-benzothiadiazole)]: [6,6]-Phenyl-C ₇₁ -butyric acid methyl ester)
PEDOT:PSS	Poly(3,4-ethylenedioxythiophene) Polystyrene Sulphonate
PEI-Zn NP	Polyethylenimine-functionalized Zinc Nanoparticles
PF-NR ₂	Poly[(9,9-bis(3'-(N,N-dimethylamino)propyl)-2,7-fluorene)-alt-2,7-(9,9-dioctylfluorene)]
Phen-DFP	Phenanthroline and Diisopropyl Fluorophosphate
Phen-m-PhDPO	3-(m-diphenylphosphinylphenyl)-1,10-phenanthroline
PHOLED	Phosphorescent Organic Light Emitting Diode
PPG	Photoplethysmography
QAD	4-(5,6-dimethoxy-1-benzothiophen-2-yl)-4-oxobutanoic acid
QFL	Quasi Fermi Level
RBD	Receptor Binding Domain
RGB	Red Green Blue
RGY	Red Green Blue Yellow
RNA	Ribonucleic Acid
SARS-CoV-2	Severe Acute Respiratory Syndrome Coronavirus-2
SPG-01T	Spiro-copolymer

SSM	Star Shaped Materials
TADF	Thermally Activated Delayed Fluorescence
TAPC	1,1-bis[(di-4-tolylamino)phenyl]cyclohexane
TC	Top Contact
TcPO ₂	Transcutaneous Oxygen Pressure
TEOLED	Top emission organic light emitting diode
TFB	[(9, 9-dioctylfluorenyl-2, 7-diyl)-co-(4, 4'-(N-(4-secbutylphenyl) diphenylamine))
TGBC	Top Gate Bottom Contact
TGTC	Top Gate Top Contact
TiO ₂	Titanium Oxide
TIPS pentacene	6,13-bis(triisopropylsilyl)ethynylpentacene
TOLED	Transparent Organic Light Emitting Diode
TPBi	1,3,5-tris(1-phenyl-1H-benzimidazol-2-yl)benzene
TPD	N,N'-Bis(3-methylphenyl)-N,N'-diphenylbenzidine
TTPA	(9,10-bis[N,N-di-(p-tolyl)-amino]anthracene)
UV	Ultra-violet
VOTFT	Vertical Organic Thin Film Transistor
<i>Ag</i>	Silver
<i>B</i>	Hole Pool–Frenkel Factor
<i>C</i>	Speed of Light
<i>E_g</i>	Energy Gap
<i>h</i>	Planck’s Constant
<i>I_D</i>	Drain Current
<i>I_{on}/I_{off}</i>	Ratio of On-State Current (<i>I_{on}</i>) to Off-State Current (<i>I_{off}</i>)
<i>K</i>	Boltzmann Constant
<i>N</i>	Electron Concentration
<i>n_i</i>	Intrinsic Concentration
<i>P</i>	Hole Concentration
<i>r_l</i>	Recombination Rate Coefficient
<i>T</i>	Effective Temperature for Charge Carriers
<i>T_g</i>	Glass Transition
<i>V_{DS}</i>	Drain to Source Voltage
<i>V_{GS}</i>	Gate to Source Voltage
<i>V_t</i>	Threshold Voltage
<i>Γ</i>	Fitting Parameter
<i>Δ</i>	Activation Energy at Zero Electric Field
<i>λ</i>	Wavelength
<i>μ</i>	Mobility
<i>μ_{sat}</i>	Saturation Mobility

CHAPTER – 1

INTRODUCTION

Recent advances in organic semiconductor-based devices owing to synthesis and development of novel high-performance OSCs (Organic Semiconductors) have spurred extensive progress in the domain of flexible electronics. The researchers have shown a lot of interest in this field and first organic thin film transistor was developed by the researcher at Mitsubishi Electric Corporation [1] in 1986. Thereafter, another successful organic device; organic light emitting diode was presented by Tang and Vanslyke [2]. The most attractive feature of organic devices is their flexibility. Also, these devices can be fabricated on unconventional substrates like cloth, plastic, glass, foil etc. which leads their realization over large area coverage.

With the instigation of soluble OSCs, printed electronics became feasible, which leads to the low-cost large area electronic circuits. These devices can be realized using simple low-cost and low-temperature fabrication processes like spin coating, direct printing, dip coating transfer printing, polymer inking, drop casting, and inkjet printing than that of high temperature fabrication processes used in silicon-based technology. It became possible as OSCs are composed of carbon-based compounds which are flexible in nature and can be made into thin layers. Organic devices can be realized into many advanced applications like printable electronic circuits, medical T-shirts, electronic magazines, sensors, OLED displays, photo detectors, etc. Researchers have also explored their usage for biomedical applications which includes cancer detection, heart rate monitoring, oxygen monitoring, and haemoglobin detection.

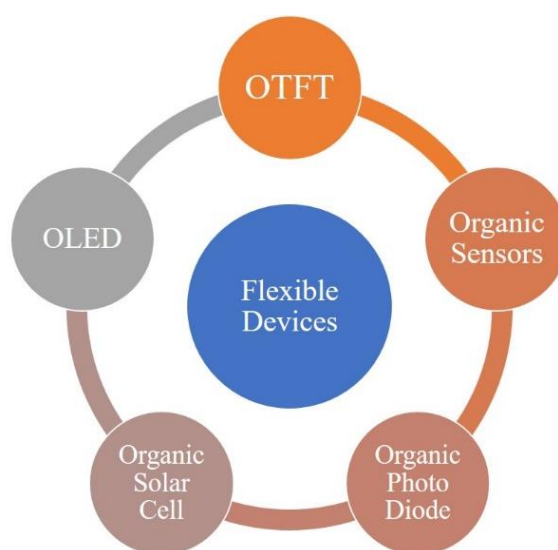


Fig. 1.1 Different electronic flexible devices based on organic semiconductors

The organic devices are suitable for applications where large area coverage is required at an effective cost. These devices have emerged as a suitable option for bendable electronics with a possibility of biodegradability. The OLED based displays have performed extremely well in terms of their efficiency, and market appeal. Flexible OLEDs can be folded without changing its functionality along with other characteristics of contrast ratio, wide viewing angle, and energy efficiency. Additionally, OPDs are also gaining a lot of attention because of their flexible and light weight nature. These devices have very good potential in providing flexible imaging arrangements and wearable health monitoring. Fig. 1.1 illustrates different organic devices that can be used in different electronics applications.

This chapter is arranged in total eight sections. The introduction about OTFT and OLED is illustrated in Section 1.1 and 1.2, respectively. Further, the OPD is discussed in terms of its need and applications in Section 1.3. Different bio-medical applications using OLED, OTFT and OPD devices are highlighted in Section 1.4 and problem statement is incorporated in Section 1.5. Subsequently, Section 1.6 and 1.7 include research objectives and their methodologies, respectively. Finally, Section 1.8 comprises the thesis organization.

1.1 ORGANIC THIN FILM TRANSISTOR

The development of organic transistors turns out to be possible due to the advent of thin film technology. During last few decades, the performance of OTFTs has shown significant improvement [3, 4]. However, there is a lot of scope of improvement in terms of its performance. These devices have been used in multiple applications; such as, digital logic circuits, memory, driving elements for flexible touch screen displays, e-paper, smart card, etc. [6, 7]. The progress in OTFT technology is attributed to the improvement in materials synthesis technology, enhanced deposition techniques, and in-depth analysis of physical structure. Perhaps, in near future, organic electronics industry would produce biodegradable and disposable organic ICs [3]. However, this can be made possible only by circumvent the shortcomings of this device. In the OTFTs, the contact resistance and higher threshold voltage restrict the performance. Also, there is a need to achieve better charge carrier injection and shorter channel length [8, 9].

Therefore, researchers have made several efforts in scaling down the dimensions of TFTs by keeping the electric field constant [10]. However, these methods are not enough to make significant improvement in cut-off frequency and transconductance of organic TFTs. On the other hand, by incorporating additional injection layer and decreasing the parasitic

capacitances, the fabrication becomes complex [11]. An appropriate way to improve the transconductance is to reduce the channel length. However, to obtain short channel device, some expensive patterning methods including stencil mask patterning and electron-beam lithography are needed [11]. But these patterning techniques increase the device cost. Additionally, these may not be suitable for OSCs as their structure can be disturbed and contaminated by processing at high temperature.

Structural modification in the device provides a good alternative in these scenarios. The researchers have already used elevated gate, dual gate, cylindrical and multiple electrode structures to enhance the device performance. However, to reduce the channel length without using complex patterning techniques, vertical channel structure can be accomplished [12-14]. Therefore, in this work a high performance VOTFT (Vertical OTFT), that too with a unique structure is proposed. In VOTFTs; gate, source, drain, and semiconductor are arranged vertically which leads to a vertical channel formation instead of horizontal in other structures. The VOTFT consists of an ultra-short channel (in nano-meter) and thus can improve the device performance significantly.

1.2 ORGANIC LIGHT EMITTING DIODE

The OLED is the most demandable commercialized device in display industry. In addition to the advantages of organic devices, OLED based displays demonstrate high color contrast, wide viewing angle, an extensive color gamut, that results in unparalleled image quality [15-17]. From the energy point of view as well, solid state devices perform extremely better, and hence the need of OLED is even more prominent [18]. The OLED also provides a high efficiency with varying lifetime depending on the material used for the color. For example, the lifetime is about 80,000 hours for red, 40,000 hours for green and 7,000 hours for yellow.

Researchers have used different methods to generate white light through OLED. However, the simplest of these is to use the three main colors; red, blue and green OLEDs. However, the field pertaining to blue OLED is still new and a lot of development is required. These blue emitters depict low stability, shorter lifetime and low efficiency as compared to green and red emitters. The development of effective blue emission materials is the primary way of developing these devices as materials affect the performance the most. Additionally, the EL (Electroluminescence) performance of these materials is required to be improved. The development of blue OLED can lead to an effective white light generation [19] that can deliver better light output with more uniformity as compared to the incandescent bulbs and compact

fluorescent lights [20]. Also, these devices are cost effective as these are realized utilizing low - cost techniques. The White OLED (WOLED) [21] uses less energy to produce a brighter light that could be more environment friendly in long run.

Organic LEDs are fabricated by depositing thin films of OSC material between the electrodes. Once the proper bias is applied, luminescence is observed. The performance of OLED depends on the charge carriers being injected in the emission layer, and their probability of finding each other as per the Langevin's theory for low mobility charge carriers. Therefore, to enhance the device performance, the researchers have utilized an array of layers to enhance the carrier injection within the device. The charge injection, charge transport and charge blocking layers have been utilized effectively to improve the device performance [22]. A lot of research is carried out with respect to these layers. The investigation shows that the addition of only basic layers cannot increase the device performance up to great extent and some other layers needs to be incorporated.

Therefore, some novel layers; charge generation [23], spacer [24] and mixed interlayer [25] have also been explored. Out of these layers, investigation pertaining to CGL (Charge Generation Layer) is still ongoing. Therefore, the present research focuses on enhancing the device performance using these CGLs. The work intends to conduct the positional analysis of the CGLs. Since these layers generate and inject the charge carriers within the device, therefore, these are influential in enhancing the device performance in terms of EL emission [23].

These layers are a combination of an n type and a p type material. These layers generate electrons and holes, respectively, when the proper external voltage is applied. The generated charge carriers get injected into the emission layer and thus increase their concentration [26]. Higher the concentration of charge carriers in the EML (Emissive Layer), higher is the probability of these carriers finding the opposite type of carriers and recombining. Thereby, as per Langevin's theory, emission within the device can be greatly improved.

1.3 ORGANIC PHOTO DIODE

Organic semiconductor based devices display a unique combination of polymeric materials and benefits of a semiconductor [27, 28]. These can also be used for the development of degradable electronic devices [29]. Researchers have started using these devices in biomedical applications as well. With the similar intent, OPD (Organic Photodiode) is explored in the present research work.

The conventional silicon-based photodiodes are very sensitive to a wide range of wavelengths (ultraviolet to in-red). On the other hands, organic semiconductor-based photodiode can particularly identify a designated range of light wavelengths and produces a corresponding current. This is possible due to their molecular design [30]. The materials used in OPDs can be altered chemically which leads to faster charge extraction and dynamic range adjustments [31]. The OPDs have been explored widely by various researchers using several techniques to improve the performance parameters including photocurrent, responsivity, dark current, and EQE (External Quantum Efficiency) [32-35].

In this research work, OPD device is explored for possible utilization in the biomedical applications. The work focuses on possibility of using OLED and OPD on a single substrate. Therefore, to reduce the fabrication complexity, similar methodologies are opted for OPD that are being investigated for OLED. Thus, impact of CGLs on the structure of OPD is analysed. The performance improvement in the device is explored with respect to the positional variation of the CGLs.

1.4 DIFFERENT BIO-MEDICAL APPLICATIONS USING ORGANIC ELECTRONIC DEVICES

The portable and low-cost bio-medical devices are gaining a lot of attention in the market. The people want to be self-aware about their health and make a knowledgeable decision in this aspect. Organic devices being thin and flexible in nature [36, 37] provide an excellent candidate to be utilized for such applications. Additionally, these can be used to make wearable sensors. The OTFTs, OLEDs and OPDs; all three of them have been explored by researchers for different biomedical applications. The OLEDs have been extensively used in the large panels and high-quality displays. Recently, researchers have shown its utilization as a source of light as well to diagnose different diseases [38, 39]. Separately, OPDs have been explored a lot for the detection of light in biosensing devices [40]. The OTFTs have also not remained untouched. The nanoelectromechanical and microelectromechanical systems based technologies have been investigated along with organic transistor for some biomedical applications.

Some of the applications wherein these organic devices have been investigated either in unison or separately are illustrated in Fig. 1.2. There are some instances, where all three devices (OTFT, OLED and OPD) have been used together in healthcare applications. These devices have become popular especially when non-invasive light-based detection is required.

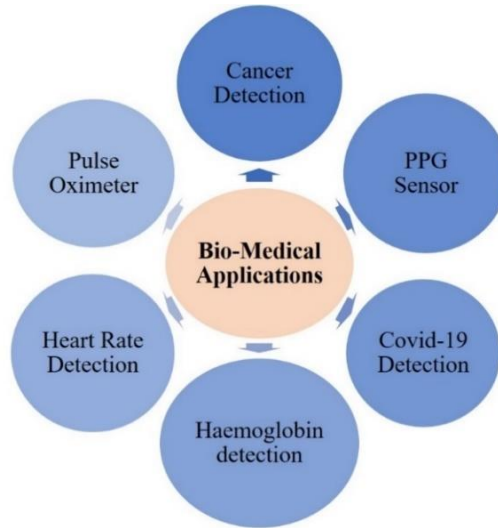


Fig. 1.2 Different possible bio-medical applications using OLED-OPD integration

The reason being high sensitivity and selectivity of these devices towards light. Additionally, being low power devices, these can be effectively used for portable applications. Therefore, the research work undertaken herein explores the possibility of using OLED and OPD devices in cohesion for biomedical application using light based non-invasive methods. These devices are investigated for the detection of SARS-COV-2 virus and Ovarian cancer. Further, prospect of measuring heart rate is also explored.

1.5 PROBLEM STATEMENT

The OLEDs have consistently depicted an increasing performance over the time owing to synthesis of novel materials. The OTFT has also illustrated satisfactory performance but still there is a scope of improvement. Their performance is mainly restricted due to high threshold voltage and contact resistance. Additionally, the injection barrier is also observed to be higher in these devices. Several methodologies have been applied to resolve these issues. The most prominent is to scale down the device dimensions while maintaining a constant electric field. Still, this has not resulted in significant outcomes. Additionally, reducing the device dimensions results in multiple short channel effects as well. The solution of these problems can be achieved by using VOTFT. In these vertical transistors, the source and drain are placed in a vertical arrangement resulting in small channel length often in nano meter range. The device mitigates a lot of short channel issues because of strong gate control. Moreover, due to the formation of short channel, the device performance in terms of threshold voltage and carrier injection can be improved significantly.

The OLED device is presently considered as the most sought-after device in display technology. However, their application should not be restricted to displays only. These are capable of generating extremely close values of wavelengths that results in a higher order color gamut. This property can be utilized effectively in numerous medical applications wherein the light-based detection is prominent. Using OLED in such applications can result in a high sensitivity and selectivity. However, inherently, OLEDs are not curated for such applications.

Hence, the device development aspect should focus on enhancing and modifying the OLED performance with respect to the color of light and luminescence to tailor OLEDs for biomedical applications. Some efforts in this aspect have been undertaken wherein; the researcher have tried to enhance the device performance by either developing materials as per the requirement or altering the device structure. Both the methodologies are effective to improve the luminescence, current density and lifetime which are some aspects wherein OLED can be improved. Material related aspect is often highly limited and focuses on specific application. On the other hand, structural aspects are more generalized and the performance has shown improving trends.

The researchers have explored utilization of different layers for device performance improvement. Some of these are charge injection, charge transport and blocking layers. However, these layers have been saturated for further enhancing the device performance. Therefore, some novel layers are investigated which include spacer layer, mixed interlayer (MI) and CGLs. These layers can also be incorporated in the OPD structure. This opens the possibility of fabricating both the devices on a single substrate. Since, these layers provide an opportunity to develop both the devices on a single substrate, therefore, a compact, low-power, and portable sensing device can be investigated for its effective use in bio-medical applications. This can impact the sensor technology drastically. At present, the silicon devices are used which often results in a higher cost. Contrary to this, the organic devices are flexible and robust in nature.

An OLED–OPD device combination can effectively function as a biosensor for disease detection. When the light emitted from the OLED passes through a biological sample (such as blood, urine, or saliva), the elements present in the sample alter the properties of the transmitted light in terms of either intensity or wavelength. If these variations are efficiently detected and distinguished by a detector, the device can identify whether the sample is infected or affected by a particular disease or virus. This mechanism, along with the OLED's flexibility, low operating voltage, and biocompatibility, makes such devices highly suitable for biomedical

sensing applications. The OLED-OPD combination can be further utilized for monitoring the heart rate, diagnosis for the cancer, and Covid-19 detection. The main aim of this work is to investigate organic devices OTFT, OLED and OPD in terms of their structure and layers utilization such that their combination can be explored for bio-medical applications.

1.6 OBJECTIVES

The primary goal of this research is to propose low power and high performance OTFT, OLED and OPD devices for biomedical applications. The novel structures are proposed and analyzed for these devices. Furthermore, the proposed devices are utilized for Covid-19 detection, heart rate measurement, and ovarian cancer detection. To carry out the whole research work, following four objectives are formulated:

Objective 1:

Design and structural analysis of high performance flexible vertical thin film transistor and comparison with existing OTFTs.

Objective 2:

Investigation of charge generation layers and positional analysis for performance improvement of OLED and OPD devices.

Objective 3:

Covid-19 disease detection using proposed OLED, OPD and OTFT devices.

Objective 4:

Characteristic analysis of proposed OLED and OPD devices with selected materials and their utilization for heart rate monitoring and detection of ovarian cancer.

To attain these objectives, the systematic methodologies are followed, encompassing both analytical and experimental perspective. The methodologies are aligned with the overall goal of this work so that the objectives can be effectively addressed and assessed.

1.7 OBJECTIVE-WISE METHODOLOGY

The following methodologies are followed to attain the formulated objectives:

Methodology for Objective 1

To accomplish objective 1, firstly, a novel structure of short channel vertical TFT is proposed. The efforts have been made in the direction to achieve high performance by incorporating some

structural variation in an existing vertical structure. The proposed structure demonstrates improved performance in terms of V_t , I_{Dmax} and μ_{sat} . This device is further compared with six other devices having planar and vertical structures. Additionally, for better understating the facts associated with the performance enhancement, horizontal and vertical cutline analysis of proposed device is also incorporated.

Methodology for Objective 2

In this objective, the OLED and OPD devices are explored for further utilization in the bio-medical applications. First, a new structure of blue OLED device with CGL is proposed. The novel structure is deeply investigated and compared with other five similar devices. Moreover, detailed internal analysis is also incorporated to understand the device physics on the basis of different parameters. These parameters are hole/electron concentration, recombination rate of charge carriers, electron affinity, conduction current rate, band energies, hole QFL, acceptor trap density, ionized density, net doping and hole/electron mobility.

Next, for the purpose of detection, a high performance CGL based organic photodiode is proposed and compared against the reference non CGL based device. The proposed structure is also compared with three other CGL based structures. This work also incorporates the thickness optimization of the proposed devices. Additionally, internal device analysis is performed using the vertical cutline methodology. Herein, important internal device parameters: electron/hole concentration, electron current density, potential, conduction/valence band energy and electron QFL are investigated and compared to establish details for better performance outcomes.

Methodology for Objective 3

This objective aims to investigate utilization of OLED and OPD devices to develop a portable sensor for Covid-19 detection. Herein, the OLED is utilized as the light emitter whereas, the OPD is utilized as light detector. First, the light from OLED falls on the saliva sample which excites the sample and fluorescence emission occurs. This emission takes place at different wavelengths for the presence of SARS-CoV-2 DNA (Deoxyribonucleic Acid) and the normal person. This difference in emission wavelength is detected by the OPD. Subsequently, the OPD produces different current values at two different wavelengths, which helps in detecting the Covid-19.

Methodology for Objective 4

Herein, the goal is to depict utilization of novel OLED and OPD devices for monitoring the heart rate and detection of ovarian cancer. For heart rate measurement, the detection methodology is based on the emission of wavelength from OLED and detection of reflected light by the OPD. A target light beam is emitted from the OLED and falls on the human blood tissues. Some of this light is absorbed by the blood and the reflected light is detected by the photo-diode. Correspondingly, a photo current is produced which reflects the variation in heart rate. A high current is achieved for lower heart rates and vice-versa.

For ovarian cancer detection, a light beam from organic LED is used to excite the urine sample. The urine sample emits a fluorescence light at a specific wavelength. However, for an ovarian cancer patient, the wavelength of fluorescence emission is altered. This is due to the presence of specific compounds found in the patient's urine sample. The variation in light emission wavelength is detected by a photodiode. Thereby, two different photo currents are produced by the photodiode. Accordingly, ovarian cancer is detected based on the produced currents.

1.8 THESIS ORGANIZATION

The complete thesis is arranged in seven chapters. Primarily, a brief introduction based on the concerned issue and motivation behind the study is included in each chapter. Conjointly, the key observations are outlined at the end. A concise overview of each chapter is outlined as follows –

Chapter 1: Introduction

This chapter focuses on introducing the field of organic electronics and important characteristics of OSC based devices are discussed. The current progress in the organic electronic devices; OTFT, OLED and OPD is demonstrated and the areas wherein the gaps are required to be addressed are highlighted. The chapter also includes the objectives and their methodologies for the research work. The chapter concludes with an organization of complete thesis work as well.

Chapter 2: Literature Review

In this chapter, a detailed literature review for the OTFTs, OLEDs and OPDs is presented. A chronologic advancement for these organic devices is shown to highlight the systemic progress made so far. OTFTs are investigated in terms of V_t , I_{Dmax} , I_{on}/I_{off} and μ_{sat} to understand the methods deployed for their enhancement. Moreover, OLEDs are also explored in terms of

different performance parameters; EQE, luminescence and current density. Furthermore, the various OPDs are reviewed in terms of material used in various layers, dark current and photocurrent. The attempts are made to observe the performance of organic electronic devices based on fabrication techniques, different structures, dimensional parameters, materials for different layers and their vital usage. Based on the review, the technical gaps that need to be mitigated are highlighted.

Chapter 3: Short channel flexible vertical organic thin film transistor

In this chapter, the performance enhancement of organic TFT based on the structural modification is analysed. Herein, a vertical channel based TFT having ditch in the dielectric filled with semiconductor is proposed which is further compared with six different planar and vertical organic transistors in terms of V_t , I_{Dmax} , I_{on}/I_{off} and μ_{sat} . The chapter also includes the internal device analysis using horizontal and vertical cutline to understand the facts for performance improvement and the parameters; band energies, potential distribution, current density and electron/hole concentration are demonstrated.

Chapter 4: Characteristics performance analysis of improved multilayered OLED and OPD devices

In this Chapter, the charge generation layer based blue OLED is proposed. This device is compared with five other CGL and non-CGL based devices in terms of current and luminescence. Furthermore, a CGL based OPD is designed using the similar methodology for its performance enhancement. This OPD is compared with four other devices in terms of photo current and dark current. In addition to this, cutline analysis is performed for both OLED and OPD to understand the device behaviour. Thickness optimization is carried out for the proposed OLED and OPD devices to achieve the best results. The chapter highlights the possibility of integrating OLED and OPD devices on a single substrate for the development of low-power, low-cost portable sensors.

Chapter 5: Covid-19 detection using proposed OLED, OPD and OTFT devices

In this chapter, the light-based detection methodology for the Covid-19 is discussed. An in-depth investigation is performed on proposed OLED and OPD devices to develop a sensor suitable for the detection of SARS-COV-2 virus RNA by analysing human saliva sample. The presented methodology is based on the fluorescence detection. Further, it investigates the utilization of the OTFT for driving the OLED. Finally, OPD is explored for the detection of Covid-19 in different persons with varying attributes.

Chapter 6: Heart rate monitoring and ovarian cancer detection using OLED and OPD devices

In this chapter, the methodologies for heart rate monitoring and fluorescence -based ovarian cancer detection using combined arrangement of OLED and OPD are discussed. The OLED and OPD are modified in terms of CGL and active layer's materials to make these devices suitable for the detection. These methodologies are also investigated for multiple persons. Further, a comparison of the proposed work with other reported work is also highlighted.

Chapter 7: Conclusions and Future Scope

In this chapter, a comprehensive discussion of significant outcomes of the proposed work is summarized. Conjointly, some of the essential future directions are highlighted for further research to be carried out in the field of low-cost organic electronics.

The chapters are followed by the list of references referred to carry out this research work. Afterwards, all the research papers (published, submitted and under progress) based on the research work are listed.

CHAPTER-2

LITERATURE REVIEW

A gradual and noteworthy advancement on the organic electronics front has been endowed with an alternative design platform, especially in the application areas of large area displays and flexible analog/digital circuits. Over the last few decades, significant research and development have been witnessed for the organic material-based devices, motivated by the need of bio-medical applications. These advancements in performance are credited by introducing novel structures, layers, materials, and fabrication techniques. In this chapter, these organic devices; OTFT, OLED and OPD are reviewed in terms of their performance parameters, structural advancements, materials, and applications.

This chapter is arranged into six different sections. In Section 2.1, the OLED device is explored in terms of structural diversity, performance improving techniques, parameters and materials. Afterwards, in Section 2.2, the literature review based on OTFT is incorporated. This section covers different aspects of TFTs in terms of working mechanism, structure, performance parameters and materials. Furthermore, organic photo diode is discussed in Section 2.3. Thereafter, different solution processing fabrication techniques for these organic devices are discussed in Section 2.4, while Section 2.5 highlights different applications based on OTFT, OLED and OPD devices. Finally, in Section 2.6, the research gaps are framed.

2.1 STRUCTURAL DIVERSITY, PARAMETERS AND IMPROVEMENT TECHNIQUES FOR OLED

Electroluminescence in organic materials was first observed by Andre Bernanos in 1950 [41] and first direct current electroluminescence under Vacuum on crystal of anthracene was observed in 1963 [42]. Later in 1965, W. Helfrich and W. G. Schneider [43] have developed double injection recombination electroluminescence through hole and electron electrodes in an anthracene crystal. Subsequently, the first organic light emitting diode was reported in 1987 using a two-layered structure with ETL/HTL (Electron/Hole Transport Layers) for recombination of carriers [44].

The OLED based displays have witnessed most promising outcomes owing to better display quality, flexibility, wide viewing angle and varieties of colors. With the instigation of soluble OSCs, printing electronics became feasible in a similar approach as to print on a paper. Organic LEDs can be processed near the room temperature, thereby promising to produce low-cost

large area flexible displays. These organic LEDs exhibit low power consumption, high contrast ratio, faster response time and good luminescence characteristics.

2.1.1 Basic structure and working principle of OLED

The organic LED is an electronic device that comprises emissive and conducting layers, as shown in Fig. 2.1. These layers are sandwiched between the anode and cathode electrodes. These layers contain thin organic materials, which are often less than 500 nm [45] and a bright light gets generated on biasing. In general, carbon-based materials are used to form the layers, wherein, the brightness and color can be enhanced by altering the properties of these materials. Also, these devices are energy efficient as OLED displays do not require backlighting due to their self-luminous nature.

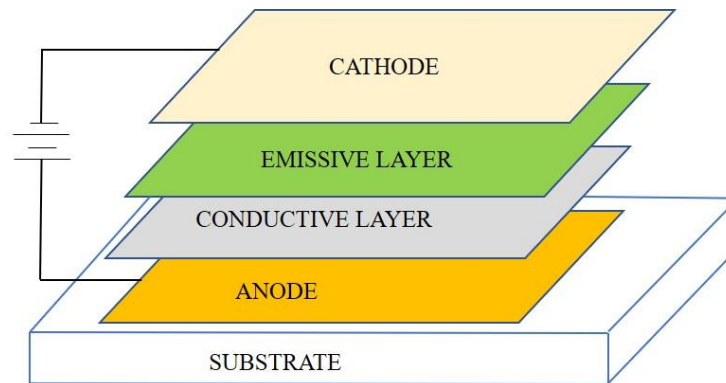


Fig. 2.1 Conventional basic structure of OLED

In OLEDs, the process of light emission is categorized in 1) injection, 2) transportation, 3) recombination, of charge carriers and 4) light emission. First, the electrons and holes get injected into the LUMO (Lowest Unoccupied Molecular Orbital) and HOMO (Highest Occupied Molecular Orbital) levels from cathode and anode, respectively [46]. These energy levels act like conduction and valence band, respectively. The work function difference between the electrode and OSC plays an important role for the injection of charge carriers. Further, these carriers move towards the OSC and within the EML [47]. This recombination of electrons and holes leads to the generation of energy in the form of photons and light is produced [48].

Sometimes, recombination does not occur within the EML due to mobility difference in the holes and electrons [49]. Thus, the major recombination takes place in the vicinity of cathode only, as the mobility of holes is usually higher than that of electrons in organic materials. This problem can be resolved by incorporating transport, injection and blocking layers in the OLED structure [50, 51]. The ETL/HTL get utilized for high carrier's recombination however,

sometimes these charge carriers do not inject properly due to energy barrier between these layers and electrodes [52, 53]. Therefore, the electron/hole injection layers (EIL/HIL) are introduced. These layers form an intermediate energy level between the HOMO/LUMO and the work function of the electrode and thus liable to reduce the energy barrier. In general, holes move faster than the electrons and reach to the EML early [54] due to their higher mobility. To restrict the movement of holes and match with the mobility of electrons, HBL (Hole Blocking Layer) is incorporated.

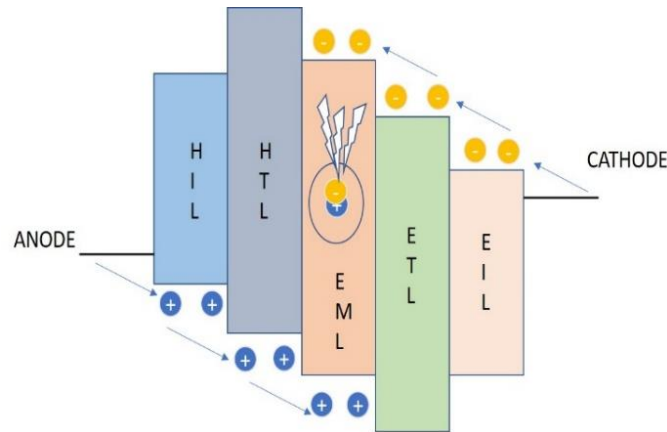


Fig. 2.2 Multi-layered structure of OLED with holes/electrons injection and transport layers

A multilayered OLED structure is shown in Fig. 2.2, where electrons and holes traverse to the EML through respective injection and transport layers. These electron and holes recombine in the EML and produces energy in the form of photons. In addition to these layers, some more layers are introduced by the researchers to augment the performance of OLED devices. These layers include mixed interlayer (MI) [23], CGL [24] and spacer layers [25].

2.1.2 Structural diversity for OLED

The device structure plays an important role to improve the performance of OLED devices. Different structures like top-emitting, foldable and transparent OLEDs are proposed by researchers to achieve good performance in terms of efficiency, current density and durability [55]. These structures are discussed in details in the following sub-sections.

a. Top-emitting OLED

Top-emitting organic LEDs (TEOLEDs) are invariably utilized in active-matrix OLEDs as thin-film transistors can be implanted under these OLEDs [56]. The researchers have preferred ITO (Indium Tin Oxide) anode-based OLEDs for the credit and debit cards [57]. Figure 2.3 illustrates different structures for a) top, b) inverted top and c) bottom emission OLEDs. The top emitting OLED shows strong microcavity effects because of the reflective contacts at both

sides (bottom and top) [58]. In bottom emitting OLED, the light is emitted via transparent bottom contact of ITO.

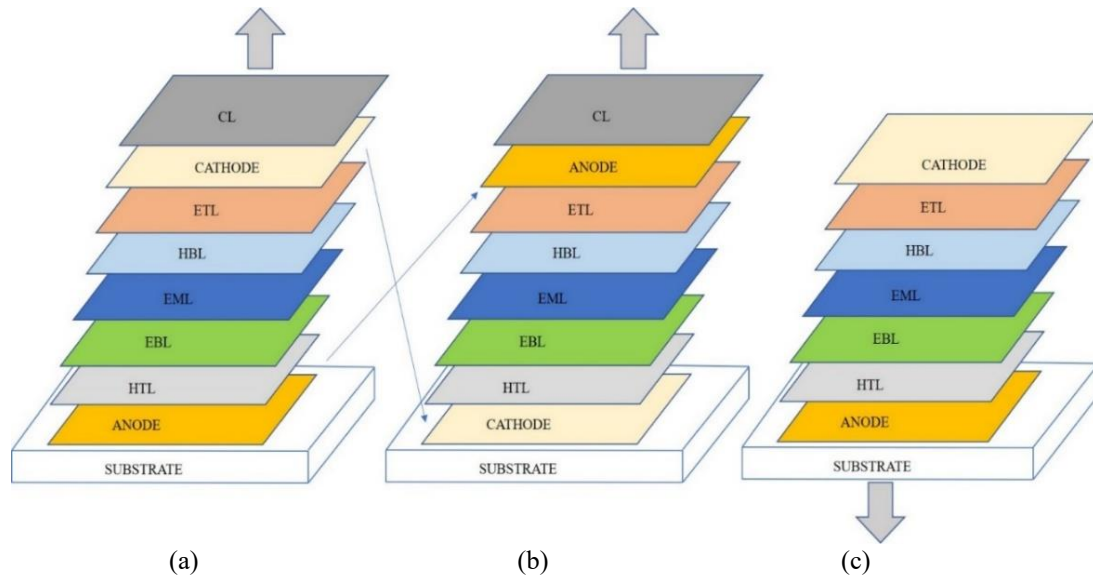


Fig. 2.3 Different structures for a) Top, b) Inverted top and c) Bottom emission OLED

In 2017, Qu *et al.* [59] demonstrated a transparent conductive oxide and scattering grid-based top-emitting green OLED that led to an improvement of 30% for external quantum efficiency. Further, Liu *et al.* [60] in 2018, used mixed interlayer of Poly (9-vinylcarbazole) and Poly [(9, 9-dioctylfluorenyl-2,7-diyl)-co-(4,4'-(N-(4-secbutylphenyl) diphenylamine))] (TFB) between emitting layer and the PEDOT:PSS (poly(3,4-ethylenedioxythiophene) polystyrene sulphonate) electrode to significantly improve the hole injection from the electrode. Research reports demonstrate a variety of materials opted for different layers and use of mixed interlayer to enhance the performance of TEOLEDs.

b. Foldable OLED

The foldable OLEDs can be realized using flexible substrate and are liable for big screen curved televisions, GPS devices, mobile phones, etc. These OLEDs are benefited in terms of high contrast image, faster response time and crisper resolution. Figure 2.4 shows the top view of prototype model. If the scan drivers of high bending resistance are placed on both sides of the display, then the display can be bent parallel to the flexible printed circuit and IC area. Some reported foldable displays with their specifications are summarized in Table 2.1. In 2015, Takahashi *et al.* [61] designed a 13.3-inch, 8K×4K, 664-ppi, high-resolution foldable organic LED display using crystalline oxide semiconductor FETs. Afterwards, Watanabe *et al.* [62] reported an 8.67-inch foldable display complying with an in-cell touch sensor.

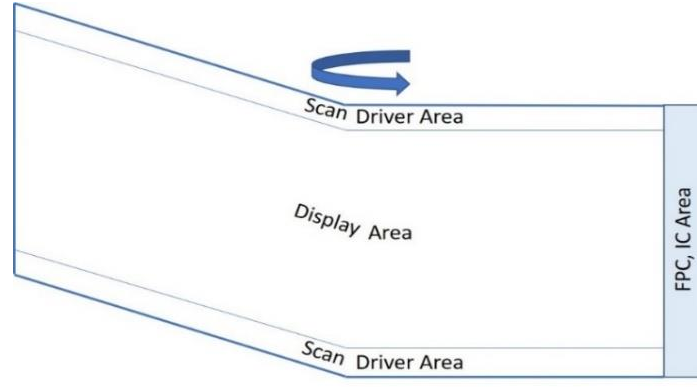


Fig. 2.4 Top view of prototype model of foldable OLED

Table 2.1. Comparison of three reported foldable displays

Aspect	Takahashi <i>et al.</i> [61]	Watanabe <i>et al.</i> [62]	Idojiri <i>et al.</i> [63]
Screen size	13.3 inches	8.67 inches	13.3 inches
Driving Method	Active matrix	Active matrix	Active matrix
Number of effective pixels	4320×RGB×7680	1080×RGBY×1920	4320×RGB×7680
Pixel pitch	12.75 μm×RGB×38.25 μm	0.100 mm×0.100 mm	12.75 μm×RGB×38.25 μm
Pixel density	664 ppi	254 ppi	664 ppi
Aperture Ratio	40.1%	46.0%	44.3%
Pixel arrangement	RGB stripe	RGBY checker	RGB stripe
Source driver	Chip on glass	Chip on film	Chip on film
Scan driver	Integrated	Integrated	Integrated

Here, the OLED and sensors were able to work appropriately even after 10^5 folding operations including 5 mm as the radius of curvature. Further, in 2019, De *et al.* [64] proposed a 3-D touch sensor technology. It included pressure sensitive adhesive and transparent layer to permit a high resolution static/dynamic pressure sensing. Further in 2020, Zhang *et al.* [65] developed a 17.3-inch wide quad high definition foldable AMOLED (Active-Matrix OLED) display with 10-bit depth.

c. Transparent OLED

These OLEDs are transparent in nature and one can see through these devices as photons can travel in both directions. The technology used in these OLEDs is Passive-Matrix OLED/Active-Matrix OLED. These devices exhibit good contrast even in bright sunlight and are used in laptops and mobile phones [66]. Figure 2.5 shows a see-through image of a transparent OLED. To determine the display region, Qin *et al.* [66] formulated the calculation; $DL \times B_1 / (B_1 + B_2)$ on the basis of diffraction lens aperture DL, background distance B_1 and viewer distance B_2 . In 2017, Shu *et al.* [67] introduced an ITO-free, inkjet-printed transparent organic LED, wherein, high emission brightness with PEDOT:PSS and ITO were obtained as $16,000 \text{ cd/m}^2$ and $50,000 \text{ cd/m}^2$, respectively.

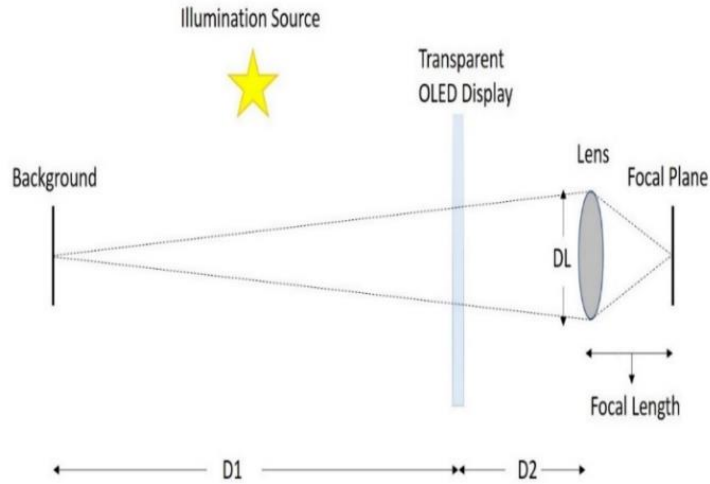


Fig. 2.5 Architecture of transparent OLED

Further, Tsai *et al.* [68] reported a flexible T-OLED (transparent-OLED) with FlexUP™ technology, wherein, a flexible EC (Electrochromic) shutter was placed (as a light blocking layer) behind the T-OLED to improve the ambient contrast ratio. Total transmittance of T-OLED/EC was reported as 54.2%. In 2020, Song *et al.* [69] demonstrated a highly reliable and transparent cathode for T-OLED applications. The silver (Ag) and aluminum (Al) metals were utilized for the fabrication of cathode by thermal evaporation. The current efficiencies of T-OLED were obtained as 18 and 36 cd/A from top and bottom sides emission, respectively.

In conclusion, top-emission flexible OLEDs are ideal for biomedical applications as they provide high brightness and efficient light extraction of top-emission designs with the mechanical adaptability of foldable devices. Compared to transparent OLEDs, these offer superior light output without compromising spectral control that too with their realization on the wearable substrates. This combination of efficiency, spectral precision, and mechanical versatility makes top-emission flexible OLEDs particularly suitable for sensitive and miniaturized biomedical sensors. A variety of materials is reported for different layers and mixed interlayers can be used to enhance the performance of TEOLEDs.

2.1.3 Characteristics parameters of OLED

The applicability of a device is determined by quantitative means for performance parameters and electrical characteristics. Essential prerequisites for a good OLED include a high magnitude for luminance, current density, current efficiency and power efficiency. These parameters are greatly affected by position of different layers, work function difference of adjacent layers and nature of material. Different performance parameters and techniques for their improvements are discussed in the successive sub-sections.

a. Luminescence

The intensity of light emitted per unit area is defined as luminescence [70]. The luminescence depends on excitation of the system and subsequent emission of the photons. In case of OLED, the luminescence depends mostly on the type of organic material, color of light, and supply voltage. In 2015, Gomez *et al.* [71] reported adenine material for hole injection layer. The maximum luminescence was improved from 12,500 to 45,000 cd/m² on glass due to better hole injection.

In 2018, Zhuo *et al.* [72] reported a white OLED that showed a luminescence of 9296 cd/m² with RGB (Red-Green-Blue) in double light emitting layer. Furthermore in 2020, Klein *et al.* [73] utilized Copper (I) and Silver (I) complexes with a new type of Tridentate N,P,P-Ligand and achieved a luminance of 10,000 cd/m² for green OLED based on compound 8 having 2 wt% concentration. This luminescence was higher as compared to other devices with 4 and 8 wt% concentrations. Further in 2020, Zheng *et al.* [74] utilized a host material; 3,5-bis(N-carbazolyl)benzene into organic layers to enhance the efficiency of inkjet-printed blue OLED. With this material, luminescence was improved by 5 times and achieved as 3743 cd/m². These reports illustrate a strong luminescence dependence on the electrode and the materials of different layers (emissive, electron/hole transport, and electron/hole injection) and improvement is observed even changing their concentrations.

b. External Quantum Efficiency

The ratio of number of emitted photons to the total electrons is known as external quantum efficiency. In 2012, Park *et al.* [75] incorporated a twisted material using anthracene with xylene, wherein, the EQE was obtained as 5.26%. Thereafter, in 2016, Rajamalli *et al.* [76] utilized blue TADF (Thermally Activated Delayed Fluorescence) emitters of BPy-pC (carbazolyl), BPy-pTC (tert-butylcarbazolyl), BPy-p2C (dicarbazolyl) and BPy-p3C (tercarbazolyl). The device using BPy-p3C dopant showed the maximum EQE of 23.9%. This value was almost 6 times higher than the EQE of device having BPy-pC dopant. In 2020, Han *et al.* [77] reported extremely high efficiency of 103% by using light extraction layer with high refractive index. Additionally in 2021, Lu *et al.* [83] developed a pair of chiral green Ir(III) containing dual stereo chiral centres and achieved the maximum EQE of 30.5%. Here, the researchers tried to resolve the challenges of CP-OLEDs using chiral emitters which provided high phosphorescence quantum yields and circularly polarized luminescence property.

Table 2.2. Comparison of different existing OLEDs in terms of luminescence and EQE during last decade

Year	Ref.	Luminescence (cd/m ²)	EQE (%)	Observations
2024	[78]	-	10	The EQE was improved as the hybrid local and charge transfer mechanism utilized both singlet and triplet excitons. This minimizes non-radiative losses in Near-Infrared fluorescence and exceeded the exciton usage limit of traditional fluorescent emitters.
2023	[79]	69311	10.3	Aggregation-induced emission mechanism prevented quenching and ensured strong luminescence in the solid state, which is essential for blue OLEDs. The emitter exhibited intrinsically strong radiative efficiency due to high photoluminescence quantum yield and thus contributed to higher EQE.
2022	[80]	-	32	High-efficiency reverse intersystem crossing has converted non-radiative triplets into radiative singlets which provided exceptionally high EQE through superior exciton management.
2022	[81]	-	14.3	Triplet harvesting via sensitizer dramatically boosted the exciton utilization efficiency. Novel acceptor design enhanced the charge transfer and radiative recombination.
2021	[82]	9156	-	The luminescence increased from 265 to 9156 cd/m ² , while the corresponding color variation remained visually indistinguishable.
2021	[83]	92,455	30.5	High phosphorescence quantum yield (~93%) provides efficient radiative recombination. Semi-transparent cathode design improves light extraction and enhances EQE and current efficiency values. Low efficiency roll-off maintains stable high luminescence at elevated brightness.
2021	[84]	32,710	18.9	The doped EMLs exhibited a high photoluminescence quantum yield, which contributed to an efficient radiative recombination and consequently enhanced device luminance. The in-situ annealing during deposition improved the hole transport characteristics, thereby facilitating better charge balance within the device.
2021	[85]	-	25.5	The emitters exhibited efficient TADF behaviour with short delayed fluorescence lifetime (1.1 μ s) and it provided effective harvesting of triplet excitons. The non-doped solution-processed device architecture maintained an efficient exciton utilization and reduced quenching, which contributed in a high external quantum efficiency of 25.5%.
2020	[86]	15,000	126.2	The hybrid tandem configuration with TADF and phosphorescent units facilitated efficient exciton utilization, thereby enhancing EQE. The integration of light extraction structures with four-color emission design effectively reduces optical losses and thus resulting in high luminescence.
2020	[87]	1031	9.3	The dimethyl methylene bridge makes the molecule more rigid, which reduces non-radiative losses and allows stronger ultra-violet (UV) emission. The shallower LUMO energy level improves charge balance and exciton utilization, leading to a record-high EQE for ultraviolet OLEDs.

2020	[73]	10,000	16.4	The rigid tridentate ligand design provides strong molecular stability and suppresses non-radiative losses, which results in very high photoluminescence quantum yields (up to 90%).
2020	[74]	3743	5.03	The introduction of mCP (3,5-bis(N-carbazolyl)benzene) as a host material enhanced the charge transport balance, thereby improving exciton recombination efficiency and overall device performance.
2020	[88]	5200	21.0	The integration of through-space charge transfer/ through-bond charge transfer effects with a multi-donor–acceptor design enables efficient utilization of triplet excitons via multichannel reverse intersystem crossing, leading to high EQE.
2019	[89]	1273	20.2	The material Triphenylamin- Phenanthro[4,5-abc]phenazine-11,12-dicarbonitrile showed a high photoluminescence quantum yield (73–87%) in doped films. This efficient light emission in the deep red /near-infrared region plays a key role in achieving the high EQE of the devices.
2018	[72]	9296	4.09	Fine-tuning the DCJTB (4-(Dicyanomethylene)-2-tert-butyl-6-(1,1,7,7-tetramethyljulolidin-4-yl-vinyl)-4H-pyran) doping level in Alq ₃ (tris(8-hydroxyquinolato)aluminum) allows the device to maintain balanced emission while minimizing the energy loss.
2018	[85]	5000	30.3	The small singlet–triplet energy gap ($\Delta E_{ST} = 0.03$ eV) makes it easier for triplet excitons to be converted into light through the TADF process, which greatly enhances the EQE of the CP-OLEDs (Circularly Polarized-Organic LED).
2017	[90]	100	9.4	The solution-processable carbazole–triazine dendrimers enable efficient exciton utilization and uniform emissive films, which improved the luminescence and EQE of the OLED device.
2016	[16]	5219	2.39	The simple triaryl benzene–benzothiadiazole–benzene molecule utilizes multiple emissive states to achieve efficient exciton recombination, resulting in improved luminescence and EQE in the WOLED device.
2015	[91]	-	2.56	The SSM (Star-Shaped Material) produces bright near-UV emission at 408 nm and achieves an EQE of 2.56%, while also serving as an effective host for high-efficiency blue OLEDs.
2014	[70]	49,993	5.12	The weak donor–acceptor interaction in tetraphenylethene-p-nitrophenyl butyrate leads to efficient solid-state emission, allowing to achieve very high luminance (49,993 cd/m ²) along with an EQE of 5.35%.

Some more approaches reported to augment the luminescence and EQE for the OLEDs are summarized in Table 2.2. Majority of the approaches pointed towards addition of multiple emissive states to have better exciton recombination. Fine tuning of the doping level in Alq₃ material (generally used as ETL (Electron Transport Layer) and EML) also allows the device to maintain a balanced emission that too with minimizing the energy loss and to achieve a high brightness. Additionally, aggregation-induced emission mechanism is liable to prevent

quenching and thus enabled a strong luminescence. At the outset, working on EML is highly impactful to tune the OLED characteristics and thus establishes a scope to work further.

c. Current efficiency

The ratio of luminescence over current density is defined as current efficiency [92-94]. Numerous efforts have been reported over the time to improve the current efficiency. A heterojunction organic bipolar charge injection layer with zinc phthalocyanine: fullerene is reported by Chen *et al.* [8]. Here, the maximum current efficiency was reported as 36.5 cd/A, which is 2.4 times higher on comparing with single unit device. Additionally, Zhuo *et al.* [72] developed a double EML for red-green emission. The device showed an improvement by 10 times in current efficiency.

Table 2.3. Some important strategies reported to improve current efficiency during last decade

Year	Ref.	Current Efficiency (cd/A)	Observations
2023	[92]	47.85	By incorporating bulky and rigid ligands, the Iridium (III) complexes effectively reduced the quenching losses and resulted in a remarkable current efficiency of 47.85 cd/A.
2023	[93]	85.6	The heteroatom-based chiral design, combined with close-lying excited states and strong intra-/intermolecular interactions, produced highly efficient TADF emission, and achieved a high current efficiency.
2022	[94]	15.0	The printed silver electrodes provided a good conductivity and transparency and thus led to a good current efficiency and brighter emission in the OLEDs.
2021	[83]	105.6	The dual-chiral Iridium (III) complexes, with high phosphorescence quantum yield and optimized device design have improved the current efficiency and recorded high EQE in CP-OLEDs.
2020	[95]	70.0	Doping CuI into the CuPc HTL improved the hole injection and transport and that led to a higher current efficiency and overall OLED performance compared to PEDOT:PSS.
2018	[96]	24.9	Incorporating 4,4',4''-tri(Ncarbazolyl)triphenylamine as a co-host enhanced the charge balance and exciton recombination, which resulted in an improved current efficiency of 24.9 cd/A and high EQE.
2018	[97]	2.75	The flexible printed substrates support efficient device operation and authors have reported current efficiency comparable to the OLEDs on glass.
2017	[98]	52.1	The embossed Aluminum Oxide nanosphere structure improves light extraction and charge recombination and it resulted in a high current efficiency of 52.1 cd/A.
2015	[99]	24.8	An optimized double-dopant mixture improved the charge balance and energy transfer in the EML and thus provided a higher current efficiency of 24.8 cd/A.

Mohan *et al.* [95] utilized CuI (Copper(I) Iodide) as dopants into CuPc (Copper Phthalocyanine) to refine HTL and attained current efficiency as 70 cd/A. Thereafter, Lu *et al.*

[83] designed some conventional devices utilizing chiral complexes as dopants. Here, the current efficiency is obtained as 105.6 cd/A. Some important strategies opted to improve the current efficiency during last decade are illustrated in Table 2.3, wherein a strong trend towards inclusion of layers is observed. In some reports, it is shown that the addition of hole injection and transport layers led to a higher current efficiency. Surprisingly, the use of double EML yielded ten times improved current efficiency. Selection of material is another important concern specifically for emission layer. A high fluorescent material can significantly augment the current efficiency. Also, the layer thickness optimization is crucial for efficient exciton recombination and energy transfer.

d. Power efficiency

The power efficiency refers to the ratio of luminous flux with respect to the power consumption of the device. In 2018, a WOLED was reported with high power efficiency of 31.0 lm/W [100]. Then in 2019, Han *et al.* [101] proposed a blue TADF using a fused B-N emitter. The device exhibited a very good power efficiency of 33.3 lm/W. In 2020 Han *et al.* [77], presented a WOLED device with an internal light extraction layer of high refractive index. The power efficiency of the device was achieved as 93.2 lm/W. Some important strategies reported to improve power efficiency during last decade are mentioned in Table 2.4.

Table 2.4. Some important strategies reported to improve power efficiency during last decade

Year	Ref.	Power Efficiency (lm/W)	Observations
2023	[60]	47.2	The combination of a mixed HTL and cohost minimized the exciton quenching and thus enhanced the charge transport. This led to a high-power efficiency of 47.2 lm/W.
2023	[92]	84.0	The sterically hindered, rigid ligand design reduces the energy loss and quenching. Thus, it results in a very high-power efficiency in the Iridium (III) OLED.
2023	[102]	7.7	The dielectric-nanomesh design boosts the light extraction and reduces operating voltage. It leads to a significantly high-power efficiency in the OLEDs.
2022	[95]	74.1	Incorporating CuI into the CuPc HTL enhances the charge transport and reduces injection barriers, resulting in a power efficiency of 74.1 lm/W.
2021	[103]	87.2	A low-triplet-energy, high-mobility interlayer with exciton confinement improves the charge flow and light emission and thus led to a high-power efficiency in the blue OLED.
2021	[104]	68.9	Depositing the EML at 60°C refines molecular alignment and light emission and subsequently improves the charge flow. Thereby a higher power efficiency is obtained in the OLED.
2020	[105]	57.2	The charge flow and light emission is improved by adding lithium to the nickel oxide HIL. This resulted in a high power efficiency in the OLED.
2020	[77]	93.2	A hollow light extraction layer combined with a hemispherical lens can be introduced for significant

			improvement in power efficiency for WOLEDs. Herein, it is improved from 26.5 to 93.2 lm/W.
2019	[101]	33.3	The use of a TADF assistant dopant with a narrow blue emitter improves energy transfer and reduces losses and subsequently results in a high power efficiency.
2018	[100]	31	The combination of an exciplex host and efficient energy transfer to the orange emitter increases the power efficiency.
2018	[72]	5.80	WOLEDs exhibits bright, efficient, and color-stable emission using double-layer structure and DCJTb doping in Alq ₃ .
2016	[16]	2.60	The multi-state emission of the triaryl molecule enhances the brightness and power efficiency of the WOLED.
2014	[91]	8.69	Charge transport and emission quality can be improved using SSM as the host and emitter. This leads to a better power efficiency and improves the color purity in the OLEDs.

In 2021, Cui *et al.* [104] utilized emission layers with different substrate temperatures ranges from 30°C to 100°C in the OLED devices. The maximum power efficiency is reported as 68.9 lm/W at 60°C. Furthermore, in 2022, a highly efficient device with the power efficiency of 74.1 lm/W was proposed by Mohan *et al.* [95]. In this device, CuI as dopants was added into CuPc to enhance HTL. Recently in 2023, Qi *et al.* [102] presented a dielectric-nano mesh OLED device with the peak power efficiency of 7.7 lm/W which is 1.8 times improved as compared with ITO-OLED.

e. Operational lifetime

Despite numerous advantages linked with OLEDs, the problem of their short lifetime is a matter of concern. Some researchers have tried to address this issue by inclusion of double EML with an ETL of LiF-doped TPBi ((1,3,5-tris(1-phenyl-1H-benzimidazol-2-yl)benzene)), wherein the operational lifetime was improved by 35 times [106]. Thereafter in 2017, Chang *et al.* [107] developed a solution-processed phosphorescent OLED with mixed-hosts system and TFB material. Here, the green OLED showed a lifetime of 310 hours and yellow of 1200 hours.

Further, in 2021, Le *et al.* [108] opted the approach of shifting the recombination area away from interfacial mixing region. This significantly improved the lifetime from 14 to 42 hours. Further, in 2023, Guo *et al.* [109] tried to dope a fluorescent emitter into (2-(4-(10-(3-(9H-carbazol-9-yl)phenyl)anthracen-9-yl)phenyl)-1-phenyl-1H-phenanthro[9,10-d]imidazole) to accelerate the reverse intersystem crossing process. This resulted in a high lifetime of 110 hours. Additionally, in 2023, Wong *et al.* [110] synthesized C⁺C⁺N carbazolygold(III) complexes using oligophenyls substituents. Here, the device showed quite high operational lifetime up to 470,700 hours with luminescence of 100 cd/m². Addition of some specific layers

like hole/electron injection layer, hole/electron transport layer, blocking layer makes an OLED very efficient and improves the parameter.

2.1.4 Performance improvement based on different layers

A multilayered OLED structure contains stacked layers of cathode, EIL/HIL, ETL/HTL, EML, blocking layer and anode. In this section, some vital layers are discussed which play an important role to improve the performance parameters of OLED. For each layer, some specific materials are explored and discussed.

a. Electron/hole injection layer

Charge injection layers are vital to reduce the energy barrier between the HOMO/LUMO of semiconductor and the work function of the electrodes. Selection of material and thickness of this layer is essential to determine adequate amount of charge carrier injection. Subsequently, different materials along with thickness used by researchers for injection layer are summarized in Table 2.5.

Table 2.5. Different existing materials (with thickness) used for injection layer

Year	Ref.	Materials		Thickness (nm) (EIL, HIL)	Observations
		EIL	HIL		
2024	[111]	-	TCTA	20	Luminous efficiency: improved by 6.17%
2023	[112]	TPBi	HAT-CN	10, 40	Transient EL measurement is used to identify degradation origin. Exciplex-type co-hosts show potential for improved stability.
2021	[113]	-	PEDOT:PSS/MoS ₂	40	The electroluminescent characteristics of devices using PEDOT:PSS and hybrid HILs are investigated. Maximum current efficiency: 72.7 cd/A
2020	[105]	-	Li:NiO _x (Nickel Oxide)	-	In this work, a low-temperature, solution-processed Li-doped NiO _x was developed as a novel HIL for OLEDs. Current efficiency: 55.8 cd/A Power efficiency: 7.2 lm/W
2019	[114]	PEDOT:PSS	-	-	For green emission- EQE: 30.8% Luminous efficiency: 111.9 cd/A For bluish-green emission- EQE: 27.2% Luminous efficiency: 83.8 cd/A
2018	[115]	MoO _x (Molybdenm Oxide)	-	-	Luminous efficiency: 7.9 cd/A (improved by 43.6 %) Power efficiency of 5.9 lm/W (improved by 73.5%)
2017	[116]	Zinc oxide	-	-	Maximum efficiency: 58.5 cd/A Maximum luminance: 11,660 cd/m ²

2017	[117]	-	PEDOT:PSS and MoO _x	-	UV OLEDs with 4.4% EQE were reported by employing solution-processed PEDOT:PSS+MoO _x .
2016	[118]	Polyethyleneimine	-	10	Current density: 20 mA/cm ² The obtained lifetime is substantially greater than that of the LiF/Al reference OLED.
2016	[119]	HAT-CN	-	10	Studied impact of impurities in OLED fabrication. Devices employing high-purity materials exhibited a lifetime nearly nine times longer.
2015	[120]	PF-NR ₂	-	-, 7	It is revealed that interface dipole model alone is insufficient to account for the electron injection capability of the aliphatic amine group-EIL.
2015	[71]	-	Adenine	10	The outcomes enhanced the utility of DNA bases for green electronics and provide practical methodologies to utilize cellulose as a biodegradable platform.

In 2015, Gomez *et al.* [71] realized a high-performance OLED by replacing substrate and HIL with cellulose and DNA nucleobase adenine. The HIL material improved the luminance and emission efficiency both by 5 times owing to wide energy level. Additionally, in 2016, Stolz *et al.* [118] proposed an OLED with EIL layer of polyethyleneimine. Surprisingly, it increased the device lifetime by 1000 hours with a reasonable current density of 20 mA/cm². In 2017, Zheng *et al.* [117] applied the combination of PEDOT:PSS and MoO_x for HIL. This material is helpful in providing improved surface work function and enhanced hole injection capacity. With better durability, the EQE and radiance were obtained as 4.4% and 12.2 mW/cm².

Thereafter, in 2020, Wang *et al.* [105] reported a novel material; Li:NiO_x for the HIL that led to quite high performance in terms of current efficiency, power efficiency, low turn-on voltage, and EQE of 55.8 cd/A, 57.2 lm/W, 3.1 V and 17.1%, respectively. In 2021, Zhu *et al.* [113] realized a hybrid material; PEDOT:PSS/MoS₂ (Molybdenum Disulfide) quantum dot for HIL. The device with this HIL showed an improvement of 28% in current efficiency than that of with single PEDOT: PSS material. These reports highlight a remarkable performance improvement based on materials for HIL/EIL that are capable to increase the charge injection and thus to augment their recombination further.

b. Electron/hole transport layer

Like charge injection layers, these are used to better transporting the charge carriers by diminishing the energy level difference. Table 2.6 comprises different materials along with thickness for the transport layer. To design high performance OLEDs, Lu *et al.* [121] reported a genetic algorithm to examine the combination of molecular materials. It was reported that

pyridine-based central core with acridine-based fragments are excellent host molecules due to good energy alignment with common electrode materials.

In 2019, TSAI *et al.* [114] proposed a novel high triplet energy and cross-linkable hole transporting material (N, N- N, N-bis(4-(6-((3-ethyloxetan-3-yl) methoxy)hexyloxy)phenyl)-3,5-di(9H-carbazol-9-yl)benzenamine). The highest external quantum efficiency/luminous efficiency (η_L) among the reported devices with double HTLs were recorded as 27.2%/83.8 cd/A for green and 30.8%/111.9 cd/A for blue emission. Further, Zhang *et al.* [125] demonstrated an ultra-thick (105 nm) MoO₃ HTL based highly stable hybrid OLED. This device showcased current efficiency and power efficiency as 60.87 cd/A and 58.84 lm/W, respectively with excellent hole mobility and efficient hole injection which reduced the turn-on voltage at 2.65 V. Afterwards, in 2020, Nagar *et al.* [123] proposed a high-performance device by utilizing TiO₂ (Titanium Oxide) doped TPBi as an ETL. The device showed good properties for yellow emission and outstanding electron mobility. The current efficiency, power efficacy and EQE were achieved as 53.9 cd/A, 56.1 lw/W and 15.5%, respectively.

Table 2.6. Different materials with thickness used for transport layer in OLEDs

Year	Ref.	Materials		Thickness (nm) (ETL, HTL)	Observations
		ETL	HTL		
2025	[122]	Alq ₃	NPB	40, 30	EQE: 10.14%
2024	[111]	BPhen (4,7-diphenyl-1,10-phenanthroline)	PEDOT: PSS	30, 40	Maximum brightness: 152.3 cd/m ² Current density: 1892 mA/cm ² Luminous efficiency: improved by 6.17%
2023	[112]	TPBi	NPB	40, 60	The research highlights the critical need for novel, efficient bipolar exciplex host materials to realize more stable PhOLED (Phosphorescent OLED) devices.
2020	[123]	TiO ₂ -doped TPBi	-	35	Maximum power efficiency: 56.1 lm/W Current efficiency: 53.9 cd/A EQE: 15.4% The enhancement is primarily due to enhanced electron transport, strong hole blocking capability, and a decrease in barrier height.
2020	[124]	-	NPB	25	The device achieved the deepest blue reported in OLEDs, with CIE (Commission Internationale de l'Éclairage) color coordinates of (0.162, 0.028). Maximum EQE: 4.43%
2019	[125]	-	MoO ₃	105	Luminance: Improved by 8 times than that of conventional devices. Turn-on voltage is also lower than that of conventional devices.
2019	[114]	-	DCDPA		EQE: 30.8% Luminous efficiency: 111.9 cd/A

2018	[126]	TPBi	NPB	NA, 10	Varying TPBi thickness in electron-only devices reveals electron transport changes and confirmed recombination zone and charge balance. Current efficiency: 80 cd/A
2018	[127]	BPe	NPB	65, 50	Due to improved exciton utilization and recombination–emission zone separation, lifetime is improved by 4.1 times for 9,10-Di(naphth-2-yl)anthracene (ADN) blue and 34.8% for Alq ₃ green emission.
2018	[115]	-	NPB	55	The hole injection and performance-enhancing mechanism of MoOx in OLEDs is explained.
2018	[72]	TPBi	NPB	15, 25	Maximum brightness: 9296 cd/m ² Current efficiency: 10.17 cd/A Power efficiency: 5.80 lm/W
2014	[91]	TPBi	TCTA doped NPB	-	Current efficiency: 10.37 cd/A Power efficiency: 8.69 lm/W
2012	[128]	Alq ₃ & BPhen	NPB	-	Power efficiency: 30 lm/W
2011	[129]	Alq ₃	NPB	-	The enhanced performance in this study is significant for practical use, indicating Cu as an alternative route for TOLED applications.
2010	[130]	Alq ₃	NPB	-	Compared to the undoped device, the operating voltage of <i>p</i> type doped blue OLEDs is reduced by 1.5 V. Half luminance decay: 3800 hours

These reports indicate the benefit of adding transport layer to improve the device efficiency. Addition of multiple transport layers that too with proper balancing of energy barriers (through materials) may lead to even lower turn-on voltage that gives insight towards low power consumption devices. The xylene and naphthalene-based fragments are suggested for ETL, while acridine and triphenylamine based fragments are good for HTL because of their strong electron donating property.

c. Emissive layer

This layer plays a major role in OLEDs as recombination of holes and electrons should occur here that further leads to the light emission. The emission wavelength of light from this layer depends on band gap of material and thus color of emission too. Table 2.7 summarizes different materials and thickness for EML. In 2011, Kim *et al.* [131] reported an OLED with high efficiency consisted of ambipolar blends of electron and hole transport polymers. This device exhibited maximum EQE of 13.6% and luminous efficiency of 44.6 cd/A. Then, Zhao *et al.* [132] in 2012, utilized a double EML structure in blue/orange complementary WOLED that resulted in improved spectral density and better luminance of 20,000 cd/m². Afterwards in 2013, Erickson *et al.* [133] proposed an approach for determining the location and spatial extent of the exciton recombination area in an organic LED.

Table 2.7. Different materials with thickness used for emissive layer in OLEDs

Year	Ref.	Material for EML	Thickness (nm) (EML)	Observations
2025	[122]	TTPA ((9,10-bis[N,N-di-(p-tolyl)-amino]anthracene))	40	EQE: 10.14% This work offered a new route to stable, low-cost, high-performance fluorescent OLEDs.
2024	[78]	Rubrene Host: Red Dopant	40	Non-doped OLEDs demonstrated high exciton utilization efficiency and Near-Infrared emission: <ul style="list-style-type: none"> • 55.6% @694 nm • 82.8% @736 nm • 42.3% @756 nm
2024	[111]	Bis[2-(diphenylphosphino)phenyl]ether oxide	30	Luminous efficiency was improved by 6.17% in the device using guest–host co-deposition compared with others.
2023	[112]	DiPhenylDiPhenylBenzene- acceptor conjugated	20	Degradation mechanism of PhOLEDs was explored using different host types: single hosts, exciplex-type co-hosts, and exciplex-free co-hosts.
2021	[134]	Alq ₃	50	OLET operating at low voltage (5 V) was reported. OLET performance is significantly improved by incorporating an appropriate HBL.
2020	[135]	BEPP (bis(2-(2-hydroxyphenyl)-pyridine) beryllium) and TCTA: Ir(ppy) ₃ (Tris(2-phenylpyridine)iridium(I II))	-	The dual-active layer device witnessed 39% EQE with CIE (0.57, 0.42).
2019	[136]	Poly methyl methacrylate: Zinc Sulfide	40	This work showed reduced band gap (~3.3 eV), multi-color photoluminescence, fast decay (~4.8 ns), and ~249% higher conductivity.
2017	[137]	TCTA: (Irmpy) ₃	30	Achieved high-efficiency green OLEDs (18 lm/W) in device sizes of 0.44 cm ² and 4 cm ² .
2014	[91]	SSM doped DSA-Ph	20	Developed a SSM with carbazole/arylamine backbone. Achieved near-UV EL as an emitter at 408 nm with EQE of 2.56%.
2013	[133]	TCTA: BPhen: Ir(ppy) ₃	100	Demonstrated an experimental method to locate exciton recombination zones in OLEDs which is applied to double-EML, mixed-EML, and graded-EML device architectures.
2012	[138]	DCzPPy: bt2Iracac	20	Introduced an organic capping layer (TAPC) to tune emission and spectra and showed that optimized capping layer thickness enhances the total emission and achieves spectral matching.
2010	[130]	TBADN & DSA-ph	-	Developed a low-voltage operating, high-stability blue OLEDs with emission peak at 470 nm. Operating voltage is reduced by 1.5 V compared to undoped device.

The reports which are mentioned above highlight an insight towards the importance of emissive layer. Some reports demonstrate a significant improvement in luminous efficiency after inclusion of this layer. The performance can be further augmented by using multiple EMLs that can significantly increase the electron-hole recombination rate due to shrinking the band gap between different materials. Thickness optimization for this layer is another important aspect to be taken care of and it can lead to a reduction in operating voltage for the device.

d. Blocking layer

Charge blocking layers are incorporated to block the movement of one type of carriers towards the respective electrode before arrival of another type of carrier in the EML. Generally, the mobility of hole is higher than electrons which results in early arrival of holes to the EML as compared to electrons and leads a reduction in recombination rate. To resolve this, hole blocking layer is introduced to block the hole carriers. Similarly, EBL (Electron Blocking Layer) can be utilized. These layers are beneficial for enhancing efficiency of organic LED by raising electron/hole recombination.

Table 2.8. Different materials (with thickness) used for blocking layer in OLEDs

Year	Ref.	Materials		Thickness (nm) (EBL, HBL)	Observations
		EBL	HBL		
2025	[122]	TCTA	-	10	This work demonstrated that triplet states in TTPA play a key role through hot-exciton processes. EQE: 10.14%
2022	[139]	-	Ytterbium	1	Introduced a thin ytterbium interlayer between organic layer and cathode to block Ag migration. Lifetime is increased from 33/37/27 hours to 128/254/244 hours (R/G/B).
2021	[134]	-	TPBi and BCP	10, 10	It is concluded that device performance depends strongly on energy-level alignment, highlighting the priority of efficient charge injection over blocking.
2019	[140]	TCTA	-	-	Doped Alq ₃ ETL with TCTA as EBL yields the best performance. At 1000 cd/m ² brightness, EQE is improved by 27.8% compared to device using only NPB as both EBL and HTL.
2018	[127]	-	1,3-Bis(N,N-dimethylphenyl)-1,3-propane-diamine derivative (DMPPP)	10	Added DMPPP interlayer to enable triplet diffusion and block singlet quenching by Alq ₃ .

					Achieved 86.1% intrinsic triplet-triplet annihilation up conversion efficiency in Alq ₃ /DMPPP/ADN tri-layer OLED.
2018	[141]	-	mPyrPPB (1,3,5-tris(3-(3-(pyridine-3-yl)phenyl)phenyl)benzene)	25	Designed hole blocking materials mPyrPPB and 1,3,5-tri(mpyrid-2-yl-phenyl)benzene)), combining pyrimidine and phenylene segments. Compared to reference device, EQE, current efficient and power efficiency are improved by 38%, 35%, 54%, respectively.
2018	[126]	TCTA	-	5	Optimizing TCTA effectively balances charges, confines recombination zone, and improves PhOLED efficiency with low roll-off.
2018	[115]	-	Bphen		The proposed OLEDs achieved current efficiency as 7.9 cd/A (improved 43.6%) and power efficiency as 5.9 lm/W (improved 73.5%).
2017	[142]	-	Phenanthroline and diisopropyl fluorophosphate (Phen-DFP)	150	New phenanthroline derivative Phen-DFP is synthesized for electron transport/hole blocking in OLEDs. The research highlights trade-offs between electron transport, triplet energy, hole blocking, efficiency, and device stability.
2016	[119]	-	2,4,6-tris(biphenyl-3-yl)-1,3,5-triazine	10	Studied impact of impurities in OLED fabrication. It is concluded that strict purity control is critical not only for emitters but also for all OLED materials.
2016	[143]	3-(m-diphenylphosphinylphenyl)-1,10-phenanthroline (Phen-m-PhDPO)		10	An electron transport/hole blocking material Phen-m-PhDPO is utilized for red, green phosphorescent and blue fluorescent OLEDs. Enabled high power efficiency and operational stability.
2015	[144]	-	9,9-dimethyl-10-(9-phenyl-9H-carbazol-3-yl)-9,10-dihydroacridine	10	High triplet energy (2.99 eV). Improved quantum efficiency. 8 times longer lifetime in blue PhOLEDs.

Table 2.8 illustrates some important work related to addition of blocking layers and their subsequent benefits. As shown in this table, some reports have shown several-fold improvements in efficiency and lifetime after adding HBL. In general, there is a high need of blocking the holes than the electrons due to their high mobility in organic materials. However, some researchers have reported the performance dependance on selection of material for electron blocking layer too. Like, Soman *et al.* [140] in 2019, explored the effect of different

EBLs, wherein TCTA material was found most effective in blocking the electrons and enhancing the recombination rate. Also, EQE was observed higher by 27.8% than that of using NPB (N,N'-diphenyl-N,N'-bis(1-naphthylphenyl)-1,1'-biphenyl-4,4'-diamine) material. These results give an insight to wisely choose the materials for these layers.

2.1.5 Performance Comparison for Blue and White OLEDs

Three main colors; red, blue, and green are required for white lighting and full color display. The researchers have reported RGB emitters in recent times [145, 146]. The light of color is determined based on the wavelength spectrum, where a dedicated range of wavelength is used to identify the color of emission. The wavelength of emission depends on the energy band gap of the material and thus selection of material is of great concern while designing the OLED devices. Here, different approaches used by the researchers for blue (Table 2.9) and white (Table 2.10) color emission OLEDs are summarized.

Table 2.9. Different approaches used for blue OLEDs along with their performance during last decade

Year	Ref.	Approach	Performance Parameters
2024	[147]	Designed Boron based ultra narrow blue emitter	EQE: 36.4% Current efficiency: 49.1 cd/A Power efficiency: 51.4 lm/W
2023	[148]	Reported Multi resonance TADF material based high performance Blue OLED	EQE: 36.2% Roll off: 4.9% Luminance: 1000 cd/m ²
2022	[149]	Reported a bi-layer structure of blue emitting layer	EQE: 14% Lifetime: 450 hours
2021	[150]	Designed and synthesized a novel deep blue fluorescent material 2,6-di-tert-butyl-1,5-bis-(3,5-di-tert-butyl-phenyl)-naphthalene	EQE: 7.8% Current efficiency: 11.52 cd/A Power efficiency: 10.33 lm/W
2021	[151]	Designed a pure blue hyper fluorescence OLED	EQE: 32% Good stability of 18 hours at an initial luminance of 1000 cd/m ² . Narrow emission.
2020	[152]	Five blue thermally activated delayed fluorescence emitters by varying the alkyl substituent of acridine to adjust the energy levels.	High photoluminescence quantum yields between 75% to 85%. Maximum EQE: 24.1%
2020	[153]	Fabricated inkjet-printed blue OLED using 3,5-bis(N-carbazolyl)benzene as a host material.	EQE: 5.03% Luminescence: 3743 cd/m ²
2018	[154]	Designed and synthesized a deep blue hybrid local and charge transfer based on triphenylbenzene.	The maximum exciton utilizing efficiency of 9-(4-(Triphenylboron)phenyl)carbazole and arbazole-Triphenylboron derivative were obtained as 85% and 86%, respectively.
2017	[155]	Developed blue pyrimidine emitters for TADF OLED.	The effect of nitrogen was investigated on the photophysical properties. The EQE was obtained of 25%.
2016	[76]	Synthesized blue TADF emitters BPy-pC, BPy-pTC, BPy-p2C and BPy-p3C using carbazoly, t-butyl	Single triplet energy gap (ΔE_{ST}) is reduced from 0.29 eV to 0.05 eV.

		carbazolyl, dicarbazolyl and tercarbazolyl as electron donating unit and 4-benzoylpyridine as electron accepting unit respectively.	EQE: 23.9%.
2012	[75]	Synthesized new rigid and highly twisted materials made of anthracene with xylene as the core unit.	Using BDNA, device exhibited maximum EQE of 5.26%.

Table 2.10. Different approaches used for white OLEDs along with their performance during last decade

Year	Ref.	Approach	Performance Parameters
2024	[156]	Presented TADF based warm WOLED	High color rendering index of 87 Correlated Color Temperature of 3216 K Luminance of over 5300 cd/m ²
2022	[157]	Designed low voltage, high luminance, top emitting, three-wavelength WOLED	Luminescence: 170,000 cd/m ² Color gamut: 136% (as compared to RGB)
2021	[158]	Fabricated high-efficiency fluorescent dual-wavelength WOLED	Luminescence: 21,070 cd/m ² Current efficiency: 18.09 cd/A Power efficiency: 8.77 lm/W
2021	[17]	Fabricated WOLED using a single host of bis(1-phenylisoquinoline) (acetylacetonate) iridium(III) and 1,3-bis(9-carbazolyl)benzene with iridium (III) bis[(4,6-difluorophenyl) pyridinato-N,C2']picolinate as red and blue phosphorescent, respectively.	Luminescence: 9156 cd/m ² . Decay time of excitons was also calculated to observe the emission mechanism using electroluminescence and transient photoluminescence technique.
2020	[77]	Designed an internal light extraction layer using high refractive index material for white organic LED.	The maximum EQE without and with light extraction structure were obtained as 35.6 and 103%, respectively. Power efficiencies without and with light extraction are calculated as 26.5 and 93.2 lm/W at 100 cd/m ² , respectively.
2020	[86]	Demonstrated highly efficient WOLED fabricated with a blue-red unit based on a TADF and a phosphorescent yellow-red unit using an exciplex host based on a modified hybrid tandem structure.	Luminous efficacy: 150.7 lm/W EQE: 126.2% The color rendering index: 80 at 1000 cd/m ² . The T50 lifetime: 12,600 h at 1000 cd/m ² .
2018	[100]	Fabricated highly efficient warm WOLED by energy transfer from exciplex host to orange dopant.	EQE: 18.7% Power efficiency: 31.0 lm/W Current efficiency: 35.3 cd/A
2016	[159]	To improve the optical power of red color, quantum dot nanocrystals dispersed in photoresist film are applied to WOLED.	40.2% enhancement in optical power is noticed in WOLED using quantum dot dispersed PR film.
2016	[160]	Designed WOLED based large area lighting panels using dip coating process in air having emission area of 72×72 mm ² .	Non-uniformity of film decreased from 49 to 15% on reducing the withdrawal speed from 1 to 0.06 mm/s. Uniformity of dip coated film is improved by adding buffer zone to the panel.
2016	[16]	Applied a benzene-benzothiadiazole-benzene core based new triaryl molecule in WOLED device.	The maximum brightness: 5219 cd/m ² Current: 6.5 cd/A

			The device also exhibited good color quality with CIE coordinates of (0.38, 0.45) and 4500K color temperature.
2014	[161]	Synthesized WOLED based on temperature sensitive β -diketonate complex of molecular formula $[\text{Eu}_{0.45}\text{Tb}_{0.55}(\text{btfa})_3(4,4'\text{-bpy})(\text{EtOH})]$ (btfa ⁻ , 4,4,4-trifluoro-1-phenyl-1,3-butanedionate; 4,4'-bpy, 4,4'-dipyridyl; EtOH, ethanol).	The emission color coordinates are varying from (0.521, 0.443) to (0.658, 0.335) by changing the temperature from 11 to 298 K.

It is quite difficult to produce a high-performance blue emission due to the wide band gap of materials that makes it complicated to insert charges into blue emitters. However, over the span of years, researchers have synthesized high quality materials with low band gaps. In 2020, Han *et al.* [152] varied the alkyl substituent of acridine to adjust the energy levels and subsequently, five blue thermally activated delayed fluorescence emitters DAc-C1 to DAc-C5 were designed. The maximum EQE was obtained as 24.1% based on DAc-C2 OLED which is 1.42 times more than the DAc-C1 based device (EQE = 17.0%). Also, a high photoluminescence quantum between 75% to 85% was achieved.

White inorganic LEDs are being used commercially for indoor and outdoor lighting and automotive lighting. On the other side, white organic LEDs are used as low-cost alternatives [16] for back-lights in flat panel displays. White OLED can be designed as flexible panels with superior white color balance and wide viewing angles. In 2016, Chen *et al.* [160] designed a WOLED using dip coating technique with an emission area of $72 \times 72 \text{ mm}^2$. Dip-coating process is useful for removing the material pile-up near the metal grids which results in uniform light emission across the whole panel. Here, non-uniformity is reduced from 49% to 15% by decreasing the withdrawal speed from 1 to 0.06 mm/s.

Recently in 2021, Lee *et al.* [17] designed a white organic LED utilizing a single host of bis(1-phenylisoquinoline)(acetylacetonate) iridium(III) and 1,3-bis(9-carbazolyl)benzene with iridium(III) bis[(4,6-difluorophenyl) pyridinato-N,C2']picolinate as red and blue phosphorescent, respectively. In this work, luminescence was improved from 265 to 9156 cd/m^2 . These reports added new possibilities for developing highly efficient, low-cost materials to increase the emission and other parameters for OLEDs.

2.1.6 Critical analysis for parameters and structural diversity for OLEDs

This section summarizes the productive approaches to design and improve the OLEDs. The researchers showcased noteworthy advancements for luminescence, EQE, luminous efficiency and current efficiency over the time. During last decade, the luminescence showed an

improvement from 1273 to 69,311 cd/m^2 (Fig. 2.6 (a)), EQE from 2.39% to 36.4% (Fig. 2.6 (b)), luminous efficiency from 2.6 to 93.2 lm/W (Fig. 2.6 (c)), and current efficiency from 24.8 to 85.6 cd/A (Fig. 2.6 (d)). As depicted in Fig. 2.6, the trend of the curves does not increase continuously because introduction of new materials, device architectures, or wavelength shifts often cause temporary drops until optimization is achieved.

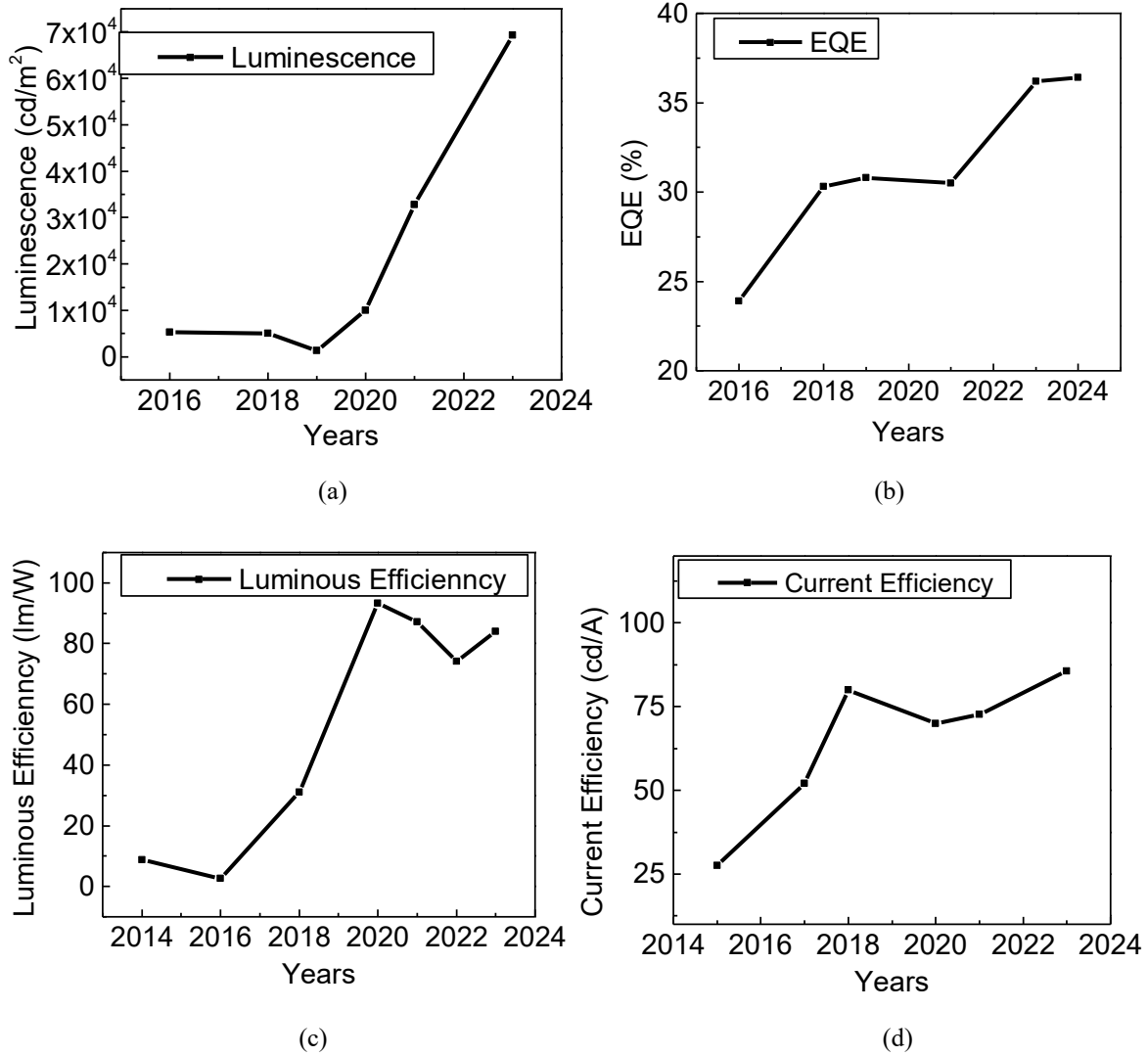


Fig. 2.6. Parametric improvement in OLEDs over the last decade in terms of (a) Luminescence, (b) EQE, (c) Luminous efficiency and (d) Current efficiency

Structural diversities and thin layers play a very crucial role in OLEDs. Selection of different layers with proper material for individual layer is of great concern and challenging. Basically, a multilayer OLED structure contains several thin layers; HIL/EIL, HTL/ETL, HBL and EML which are extensively employed during the last decade and discussed in detail in earlier sections. Each layer plays a vital role in charge transport and light emission. These layers have

their own pros and cons. The added layers can improve the efficiency and charge balance but with increased cost, interface defects and complexity.

Some advanced layers like spacer, mixed, and charge generation layers can also contribute for significant improvement in OLED device performance. Spacer layers are utilized in OLEDs between the functional layers. Unlike the conventional layers (HIL, HTL, ETL, HBL), the main purpose of this kind of layer is to provide excitonic/optical separation. These additional layers work great for exciton management, optical field control and energy level alignment. For example, a thin wide bandgap spacer can be placed between ETL and EML to block the exciton leakage. The spacer layer also helps in balancing electron/hole injection rate. The suitable materials for these layers are TAZ (3-(4-biphenyl)-4-phenyl-5-tert-butylphenyl-1,2,4-triazole), BCP (bathocuproine), UGH2 (ultra-wide bandgap host) etc.

Mixed interlayer is basically a thin intermediate layer which is composed of a mixture of two or more materials. These materials are opted for electron/hole transportation. Like spacer layer, these layers are also placed between functional layers like EML and ETL/HTL. The thickness for these layers can be kept from 2 to 10 nm as thicker layer may results in higher driving voltage due to decline in mobility. The MI layers improve exciton confinement, charge balance and interfacial stability. These layers help in matching the injection rate by blending *p* type and *n* type materials in the interlayer. These layers demonstrate some limitations as well like excess blending may lead to unwanted recombination zones. The suitable materials for electron transport in mixed interlayer are TPBi, Alq₃, and BPhen. However, NPB, TCTA, and TAPC materials show a good choice for hole transport.

Another important layer utilized for improving the device performance is charge generation layer which is the combination of two different layers which acts as electron generator and hole generator. This CGL layer enables proper stacking of electroluminescent units, resulting in noticeably improved charge balance and light extraction, which in turn leads to higher efficiency, enhanced brightness, and a significantly longer operational lifetime compared to single-unit OLED structures. The main purpose of CGL is to generate additional electrons and holes which further move into EML to accomplish more recombination. Subsequently, the overall efficiency of the device is improved. The suitable materials for hole generation in CGL are MoO₃, NiO, WO₃, V₂O₅, TAPC. Additionally, electron generation materials can be Cs₂CO₃, BPhen:Cs, Liq, and HAT-CN. Table 2.11 demonstrates the comparative analysis for spacer, mixed, and charge generation layer. As per the table, inclusion of CGL is more beneficial in comparison to spacer and mixed interlayer. CGLs contain dual functionality. Unlike spacer and

mixed interlayer, it significantly generates charge carriers and blocks exciton leakage. Additionally, using CGLs, high luminance can be achieved at low current density in tandem OLEDs. These layers contain better energy level tuning in comparison with the other two layers.

Table 2.11. Comparison of spacer, mixed interlayer, and charge generation layers across various aspects

Aspect	Spacer Layer	Mixed Interlayer	Charge Generation Layer
Primary role	Optically separates layers without active charge transport [25].	Balances exciton confinement and charge transport via mixed materials [23].	Generates new electron–hole concentration between stacked emissive units [24].
Charge transport	Very low or negligible: Layer is not considered for carrier transport.	Moderate: Depends on blend ratio and material mobility [16].	Strong: Generates and injects more electrons and holes into EML [26].
Energy level tuning	Weak: Minimal effect on energy levels [25].	Moderate: Blend permits limited tuning [23].	Strong: Tailored materials for near-zero injection barriers [26].
Exciton Management	Good: Restrict excitons, but does not significantly help recombination.	Good: Reduces exciton leakage at interfaces [60].	Excellent: Confines excitons in each sub-cell to block quenching [24].
Complexity	Low: Addition of simple layer [25].	Moderate: Demands composition optimization [67].	High: Requires appropriate material pairing and deposition control.
Application focus	Utilized in multilayered OLEDs for optical tuning and quenching avoidance [25].	Utilized for improved charge balance and stability [16].	Utilized in tandem OLEDs to attain brightness & long lifetime [24].
Advantages	Improves EQE and reduces roll-off.	Improves stability and optical efficiency [67].	Boosts brightness, efficiency, and lifetime.
Scalability	Few challenges in reproducibility.	Easy to fabricate.	Proven in commercial tandem OLEDs.

CGLs have outstanding charge transportation property than mixed interlayers as CGLs can directly generate and transport electrons and holes towards the EML. Moreover, these layers are extremely good in providing longer operating lifespan by reducing thermal and chemical degradation. CGLs are commercially utilized in high-end OLED displays such as TVs and smartphones. All these properties make CGLs the preferred choice for obtaining OLEDs with high brightness and long operational lifespan. In current OLED research, CGL is typically placed near or within the EML. Looking ahead, exploring alternative arrangements for placing the CGL; near the cathode/anode region and adjacent to the HTL/ETL may offer deeper insights.

2.2 STRUCTURAL DIVERSITY AND PARAMETERS FOR OTFT

This section focuses on the recent advancements for organic small molecule and polymer based organic thin film transistors. To better understand the conduction process and mapping of limiting factors, the structural variation between top and bottom contact organic TFTs is examined. As illustrated in Fig. 2.7, OTFT structure consists of four thin layers of source/drain, OSC, dielectric, and gate. The charge carriers are inserted and extracted from source and drain, respectively. Here, the source and drain are in contact with OSC layer and gate is separated by a gate dielectric layer to control the conductivity of the layer. The working mechanism of organic TFT is quite similar to the conventional TFTs. However, the method of channel formation is different.

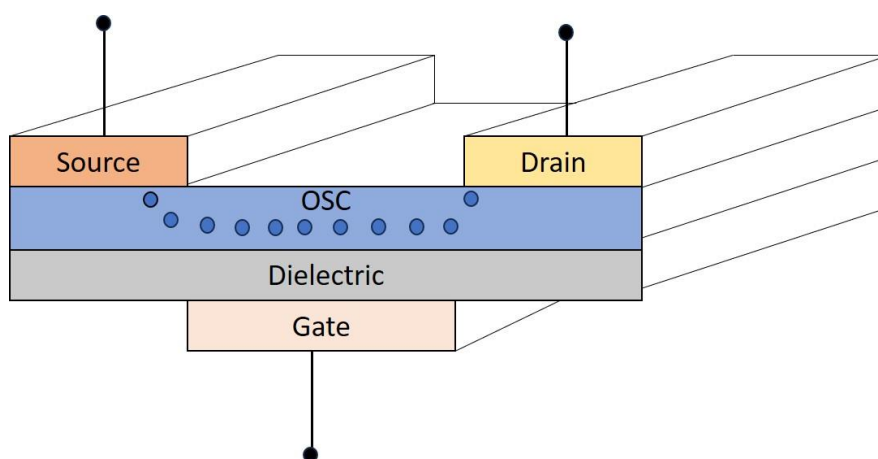


Fig. 2.7 Basic structure of OTFT

The channel formation in OTFT is due to the accumulation of the charges, on the other side, in case of inorganic transistors, it is because of the inversion process. On providing voltage between gate and source, the charge carriers are generated at the interface of the semiconductor/dielectric. After applying a suitable drain to source potential, current starts flowing between source and drain.

2.2.1 Performance Parameters for OTFTs

A TFT should possess a high value for I_{on}/I_{off} , transconductance and mobility. On the other hand, threshold voltage, contact resistance and sub-threshold swing (SS) should be low. The below sub-section illustrates all these mentioned parameters in detail.

a. Transconductance

Transconductance is defined by the change in drain current on modifying the gate voltage keeping the drain voltage constant. The higher transconductance is beneficial for various bio-

sensing applications in organic field. Various efforts have been made by many researchers to improve this. Klauk *et al.* [162] presented a BGTC (Bottom Gate Top Contact) structure which exhibited 4 μS transconductance at $V_{GS} = -3$ V. The drain voltage is kept constant at -1.5 V. Furthermore, an OTFT designed at $L=10$ nm by Lee *et al.* [163] showed noteworthy improvement in terms of transconductance and other electrical parameters. Additionally, a dual gate OTFT proposed by Ghosh *et al.* [164] showed a very high transconductance as 4.6 μS .

b. Mobility

The mobility refers to the property of charge carrier which shows that how efficiently carriers can move in the semiconductor. Higher mobility is preferable for high performance and fast switching applications. Xu *et al.* [165] designed a n type OTFT having the semiconductor material 6,13-bis((triisopropylsilyl)ethynyl)-5,7,12,14-tetraazapentacene. The device illustrated a high mobility of 11 $\text{cm}^2/\text{V.s}$. Further, Hasan *et al.* [166] proposed a device which obtained the mobility of 0.82 $\text{cm}^2/\text{V.s}$ at low input voltage (-3 V).

c. On/off current ratio

The ratio of current in accumulation and current in depletion mode is known as on/off current ratio. The device thickness and length of channel are the main parameters responsible for this ratio. The shorter the channel length, the higher on/off ratio is obtained [167]. Resendiz *et al.* [168] exhibited a refinement in the current on/off ratio as 10^9 by reducing poly(3-hexylthiophene) thickness from 160 nm to 20 nm. Furthermore, Kumar *et al.* [169] followed the same method for improving the current ratio by decreasing OSC layer by 130 nm.

d. Threshold voltage

A minimum amount of voltage required to create a channel at the interface of semiconductor and dielectric is called threshold voltage. The value of threshold voltage should be smaller for low power applications. Kano *et al.* [170] reported that short channel length and wide OSC layer result in lesser threshold voltage. Addition to this, threshold voltage was reduced to 5 V using electrode energy levels [171].

2.2.2 Classification of OTFT based on structural diversity

The geometry plays an important role in improving the performance of OTFTs. These transistors are categorised based on the number of gates as single gate and dual gate. The below section summarizes the work reported for single gate and dual gate transistors in terms of threshold voltage, drain current, sub-threshold swing and saturation mobility.

a. Single gate OTFTs

The single gate TFTs are classified in bottom gate and top gate structures. These devices are further divided in terms of their position of contacts. In bottom gate structures where contacts are placed below OSC layer are known as BGBC (Bottom Gate Bottom Contact). On the other hand, where contacts are placed above OSC layer is called as BGTC as shown in Fig. 2.8. Similarly, top gate TFTs are also divided into TGBC (Top Gate Bottom Contact) and TGTC (Top Gate Top Contact) structures.

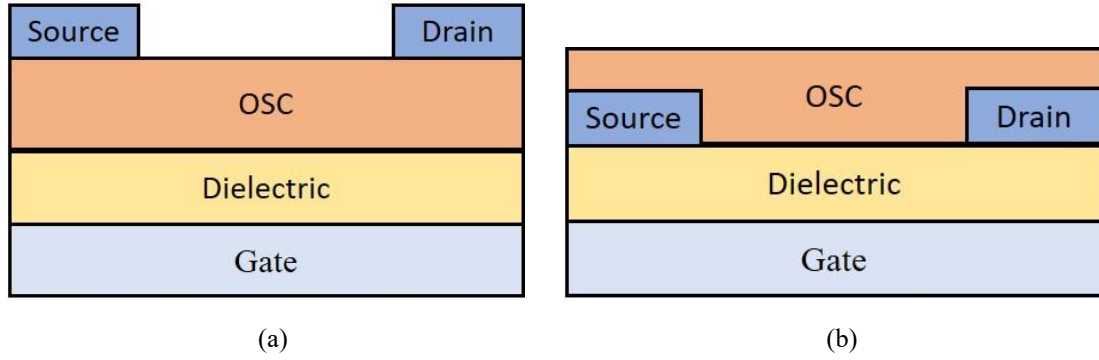


Fig. 2.8 Bottom gate OTFT with (a) Top contact (TC) and (b) Bottom contact (BC) structures.

Table 2.12. Comparison of performance parameters of different existing bottom gate top contact and bottom contact TFTs

Year	Ref.	Structure	Parameters				
			I_D (μA)	μ (cm^2/Vs)	V_t (V)	SS (V/dec)	I_{on}/I_{off}
2025	[172]	BC	-	11.39	1.2	64.10	1×10^7
2023	[173]	TC	60	0.135	1.3	0.591	10^5
		BC	59	0.0026	-1.6	1.219	10^3
2021	[174]	TC	-0.000133	0.0578	-0.601	0.291	3.7×10^4
		BC	-0.000146	0.0661	-0.666	0.284	4.1×10^4
2020	[175]	TC	-0.000057	NR	-0.52	0.347	10^4
		BC	-0.000061	NR	-0.594	0.341	1.1×10^4
2019	[176]	TC	-11	0.129	1.2	0.32	9.5×10^3
		BC	-12	0.14	1.1	0.26	1.9×10^4
2016	[177]	TC	30.63	0.13	32.78	NR	NR
		BC	-7.9	0.039	32.58	NR	NR
2014	[178]	TC	37	0.44	-14	NR	10^8
		BC	8	0.11	-15	NR	10^6
2010	[179]	TC	3.7	0.36	0.71	NR	NR
		BC	1.2	0.04	0.81	NR	NR
2009	[180]	TC	-12	0.085	-3.2	NR	NR
		BC	-0.4	0.002	-8.4	NR	NR

When both TC and BC structures are compared, top contact (TC) exhibits improved performance due to large charge injection area. Table 2.12 summarizes a comparison of the

structures in terms of V_t , I_D , I_{on}/I_{off} , μ and SS . Ye *et al.* [173] reported a comparison between TC and BC structures and it was observed that TC structure outperformed in terms of I_D , μ , V_t , SS , and I_{on}/I_{off} . Herein, the saturation mobility for TC device was 51.9 times enhanced in comparison with BC devices. Similar results were reported by Verma *et al.* [177] wherein, saturation mobility was improved by 3.3 times for TC structure than bottom contact.

b. Dual gate OTFTs

To refine the charge carrier injection, TFTs with two gates along with their dielectric are introduced. In these types of TFTs, biasing can be provided at both sides of gate terminals. Thereby, drain current is enhanced by creating two conducting channels between source and drain and thus helps in refining other performance parameters. Table 2.13 summarizes a review on different dual gate transistors during the last few years.

Table 2.13. Comparison of performance parameters of different existing single gate and dual gate TFTs

Year	Ref.	Structure	Parameters					
			I_D (μA)	μ (cm^2/Vs)	V_t (V)	SS (V/dec)	I_{on}/I_{off}	C_i (nF/cm ²)
2025	[181]	Dual Gate	-	-	-1.8	0.009	1×10^6	385
2024	[182]	Single Gate	-	0.18	-1.26	1.4	1.06×10^5	NR
		Dual Gate	-	2.42	0.70	0.259	6.8×10^5	NR
2022	[183]	Single Gate	-6.5×10^3	0.0810	-0.795	0.286	4.2×10^5	NR
		Dual Gate	-6.9×10^3	0.0812	-1.114	0.059	7.3×10^{12}	NR
2020	[184]	Single Gate	-0.071	0.03	0.58	0.14	106	5.4
		Dual Gate	1.8	0.37	0.23	0.098	107	10.88
2020	[164]	Single Gate	2.4E-05	4.84	1.37	0.69	3.9×10^3	NR
		Dual Gate	0.0075	19.3	2.41	0.75	5.27×10^4	NR
2019	[185]	Single Gate	-0.00095	0.129	2.2	0.32	4.5×10^3	NR
		Dual Gate	-0.001.0	0.315	2.22	0.09	1.6×10^8	NR
2018	[186]	Single Gate	-0.01	0.012	1.5	0.5	NR	NR
		Dual Gate	-0.24	0.05	0.42	0.3	NR	NR

Saini *et al.* [187] demonstrated a dual gate structure using pentacene as OSC. This transistor achieved 30% improvement in the mobility. The current ratio for dual gate is also improved by 6 times as compared to single gate TFT. Additionally, Seo *et al.* [182] analysed single and dual structures wherein, μ and SS was improved by 13.4 and 5.4 times, respectively.

c. Vertical TFT

The straightforward way to provide better transconductance is to reduce the channel length [188]. But, to obtain it, the channel needs few sophisticated and expensive patterning methods

such as; stencil mask patterning and electron-beam lithography [11], which is not applicable for low-cost fabrication processes. To obtain the short channel, a vertical channel transistor can be a good alternative [12-14]. In vertical TFTs, the source and drain are placed in a vertical manner unlike horizontal in planar TFTs. This makes a significant reduction in channel length and improves the performance. The performance of some vertical OTFTs is summarized in Table 2.14.

Table 2.14. Review of different existing vertical TFTs in terms of performance parameters

Year	Ref.	Aspect	Performance Analysis
2025	Kang <i>et al.</i> [189]	Proposed an ultra-thin VOTFT photosensor using Au based graphene.	Carrier mobility: 4.8 cm ² /V. s High switching ratio. Significant photosensitive synaptic response.
2024	Choi <i>et al.</i> [190]	Presented a VOTFT using interfacial oxidation.	Device found applicable for low power electronic applications.
2023	Sun <i>et al.</i> [191]	Proposed a short channel vertical TFT and its performance improvement.	Higher current as compared to planar TFTs. Suitable for sensing applications.
2021	Kneppe <i>et al.</i> [192]	Presented the first solution-processed VOFET (Vertical Organic Field-Effect Transistor) and compared it with vacuum-processed VOFETs.	Better on-state performance than vacuum-processed VOFETs. Charge carrier mobility: 4.8 cm ² /V. s
2019	Chen <i>et al.</i> [193]	Fabricated a novel VQLET (Vertical Quantum-Dot Light-Emitting Transistor) based on a vertical OTFT.	Integrated OTFT and quantum dot light-emitting diode into a single device. VQLET exhibited extremely high current density. The maximum current efficiency is obtained as 37 cd/A.
2018	Rathi <i>et al.</i> [194]	Compared the performance for single and dual gate Vertical Channel OTFT.	Performance of dual gate VOTFT is much enhanced with higher I_{on}/I_{off} ratio current.
2013	Kleemann <i>et al.</i> [195]	Presented high-performance vertical organic transistors comprising pentacene for <i>p</i> type operation and C ₆₀ for <i>n</i> type operation.	Exhibited very high on/off ratio of 10 ⁶ . High transconductance value > 50 μ S/mm. VOTFTs containing pentacene showed on-state current densities of \sim 50 mA/cm ² .
2007	Yang <i>et al.</i> [14]	Compared pentacene-based planar and vertical type OTFTs. Also, added HIL in VOTFT.	VOTFT exhibited a low-voltage operation of less than 5 V. Higher current I_{on}/I_{off} ratio.

In 2021, Kneppe *et al.* [192] proposed the first solution-processed vertical organic transistor and further compared with vacuum-processed VOFETs and solution-processed TFTs. It witnessed comparatively a higher performance for solution-processed vertical TFT. Furthermore, Sun *et al.* [191] demonstrated a higher current for VOTFT as compared to planar TFT. These vertical channel devices were also found suitable for sensing applications. In 2024,

an interfacial oxidation based ultra short channel VOTFT [190] was demonstrated with quite significant performance improvement. Recently, in 2025, Kang *et al.* [189] presented a vertical thin film transistor utilizing Au based graphene. In this research, carrier mobility was obtained as $4.8 \text{ cm}^2/\text{V} \cdot \text{s}$ along with high switching ratio and good photosensitive synaptic response.

2.2.3 Critical analysis for different OTFT structures

It is widely reported that the bottom gate arrangement is well suited for the single gate OTFTs pertaining to the thermal treatments that may be applied to improve the dielectric surface without any impairment in the OSC layer. A comparison is performed for top and bottom contact structures in terms of mobility over the span of years (Fig. 2.9). Here, TC and BC devices taken for comparison are realized using same materials and possible dimensions. A big difference can be seen in mobility values and TC devices have outperformed. Although the performance of BGTC structure is observed superior than the BGBC, nevertheless the contacts deposited on the semiconductor in TC structure consequences in some sort of defects in the active layer. Therefore, the S/D contacts are preferably prepared prior to the OSC layer, thereby proving BC structures more promising in the real production field. Additionally, the threshold voltage is found lower for BC transistor due to a closer proximity of contacts to the OSC-dielectric interface that enables the channel to be formed at the lower gate voltage [176, 177].

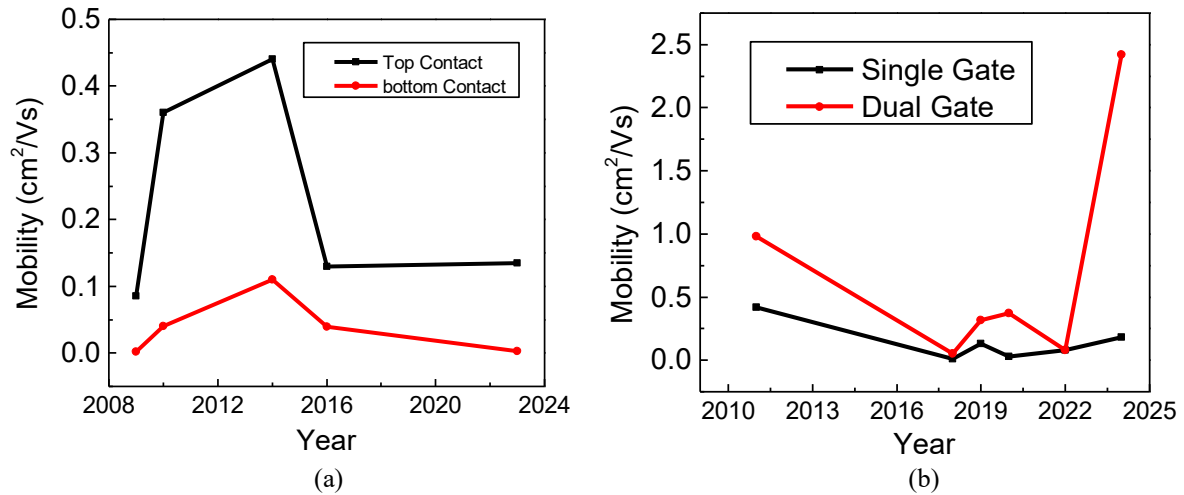


Fig. 2.9 Mobility variations in OTFTs based on (a) TC and BC structures and (b) Single and dual gate structures

Significant efforts have been devoted to achieve fully flexible transistors with all the thin layers comprising of organic materials and were realized by simple solution processing techniques, wherein most of the reported flexible OTFTs are based on the BC structural design [172]. On the contrary, these structures undergo some disorders and meager morphology of semiconductor that may arise due to pre-patterned source and drain contacts. This usually restricts the grains of semiconductor to be deposited well near the vertical edges of these

contacts leading to a low device mobility and output current as well [180]. Therefore, an inclusion of some modified TFT structures on the basis of fabrication feasibility complying with low cost is necessarily required that can be further used to realize high performance electronic circuits.

The performance of a single gate OTFT can be greatly enhanced with an additional gate and its respective dielectric [183, 184]. The dual gate structure provides low operational voltage, improved carrier mobility, strong channel control, and reduced subthreshold slope desirable for high-performance logic circuits, low-voltage electronics, and precision sensors [182, 196]. It is quite clear from Fig. 2.9 (b) that mobility for dual gate TFTs is higher than single gate and increased over the years. However, concerning to the fabrication feasibility, dual gate transistor may also result in the trap states in the semiconductor while preparing dielectric and second gate onto the active layer.

In this context, vertical channel structures can be considered. Unlike planar OTFTs, source and drain are placed in vertical manner in V-OTFTs resulting in a shorter channel length (only in nanometers). Subsequently, the operating voltage and switching speed can be improved due to lower capacitance and shorter channel length. These devices can be impactful in high-speed flexible electronics, high resolution OLED displays, integrated sensor-display systems, and compact wearable biomedical devices [197, 198]. The vertical structure provides strong electric field due to shorter channel which enables high transconductance. As a conclusion, V-OTFT can be a good choice over planar TFT to achieve a high performance that too with fabrication feasibility on to the flexible substrates.

2.3 ORGANIC PHOTO DIODE

Photodiodes based on silicon are very sensitive to a wide range of wavelengths (ultraviolet to in-red). However, organic semiconductor-based photodiodes can particularly identify a designated range of light wavelengths because of specific molecular design [30]. Materials used in OPDs can be altered chemically which leads to faster charge extraction and dynamic range adjustments. Photodiode is used to convert the light into current. Hence, the major application of photodiode is to detect the brightness [30]. In general, an OPD consists of the layers of cathode, anode, acceptor, donor, and substrate as demonstrated in Fig. 2.10.

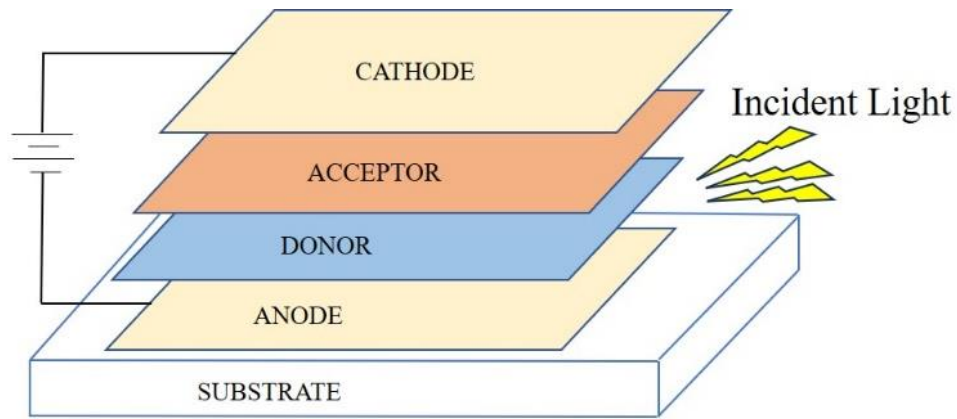


Fig. 2.10 Basic structure of organic photo diode

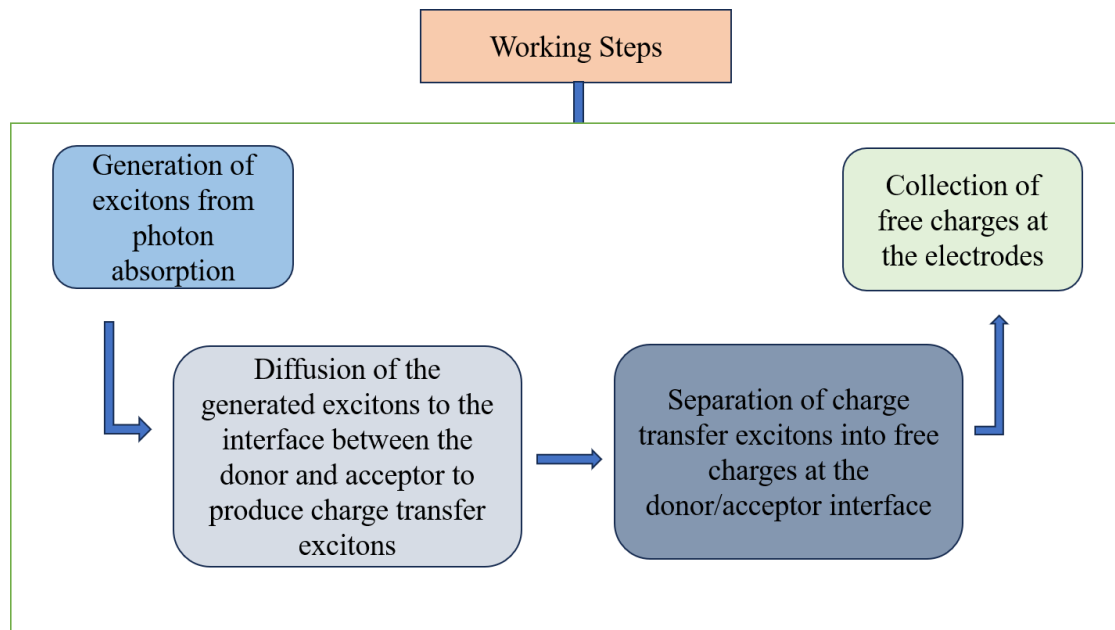


Fig. 2.11 The flow of working mechanism for organic photo diode

The photodiode operates in reverse bias by cathode connected to positive and anode to negative terminal of the battery. When the incident light falls on the active layer (combination of acceptor & donor), the bounded electrons and hole pairs inside the active layer gain some energy and thus free electrons and holes are generated. These free charge carriers are further collected at the electrodes and a photocurrent is produced. When there is no light incident on the active layer, a small amount of dark current flows [26]. The mentioned working mechanism are also depicted in Fig. 2.11.

2.3.1 Performance parameters and importance of dark current

The dark current of photodiode plays a vital role and should be minimum for low power consumption. This also improves the efficiency of detection by enhancing the photogenerated carriers.

Table 2.15. Review of different existing organic photo diode in terms of their performance

Reference	Aspect	Performance Analysis
Ng <i>et al.</i> [32]	Presented a BHJ (Bulk Heterojunction) photodiode on a flexible substrate using inkjet printing.	Efficient charge collection was reported with low dark current ($<1\text{ nA/cm}^2$).
Lee <i>et al.</i> [33]	Proposed a highly efficient fullerene-free BHJ OPD with the materials N,N-dimethyl quinacridone and dibutyl-substituted dicyanovinyl-terthiophene for donor and acceptor, respectively.	The device exhibited external quantum efficiency of about 67% at 540nm.
Deckman <i>et al.</i> [34]	Fabricated a fully printed OPD with the capability of RGB light separation.	Achieved EQE of $\sim 37\%$ at -4 V with the dark current of 0.5 nA/cm^2 .
Jang <i>et al.</i> [35]	Demonstrated a non-fullerene acceptor based OPD and compared it with fullerene acceptor based OPD.	The non-fullerene based OPD showed comparatively a faster time response and higher detectivity as $2.7\text{ }\mu\text{s}$ and $1.61 \times 10^{13}\text{ cm.Hz}^{1/2}/\text{W}$, respectively.
Titov <i>et al.</i> [38]	Proposed a high performance OPD for biomedical application.	The device showed the photocurrent and dark currents as 3.9 and 0.25 nA, respectively.
Tordera <i>et al.</i> [199]	Reported high-resolution slot-die-coated large-area BHJ OPD arrays.	Dark current density $\approx 10^{-7}\text{ mA/cm}^2$ at -2 V.
Baeg <i>et al.</i> [200]	Review on recent advancements of phototransistors and photodiodes.	Several applications based on OPDs were explored including opto-isolator, a photo-sensor, optically controlled phase shifter, image sensor and opto-electronic memory.

The researchers have reported different techniques to refine the performance parameters of photodiodes; photocurrent, dark current, responsivity and EQE as shown in the Table 2.15 [32-35]. Ng *et al.* [32] showed a bulk heterojunction photodiode on a flexible substrate using inkjet printing. In this work, an efficient charge collection was obtained with low dark current ($<1\text{ nA/cm}^2$). Additionally, Lee *et al.* [33] presented an efficient fullerene-free BHJ OPD with the materials N,N-dimethyl quinacridone and dibutyl-substituted dicyanovinyl-terthiophene for donor and acceptor, respectively. The device depicted a high EQE of 67% at 540 nm. Furthermore, Deckman *et al.* [34] proposed a fully printed photo diode with the capability of red-green-blue light separation. This OPD exhibited an EQE of $\sim 37\%$ at -4 V with the dark current of 0.5 nA/cm^2 . Additionally, Jang *et al.* [35] reported a non-fullerene acceptor based OPD which was compared with fullerene acceptor based OPD. The non-fullerene based OPD comparatively achieved a faster time response and higher detectivity as $2.7\text{ }\mu\text{s}$ and $1.61 \times 10^{13}\text{ cm.Hz}^{1/2}/\text{W}$, respectively.

2.3.2 Layer based analysis of different OPDs in recent time

The OPDs characteristics largely depends on the precise control of the functional layers and thereby the device structure. The active layer (consists of acceptor and donor) serves as the core, where light absorption, exciton generation, and charge separation take place. Surrounding this, ETL and HTL facilitate selective charge extraction, ensuring efficient carrier collection while suppressing recombination losses [201, 202]. To further optimize the device stability and minimize leakage, charge-blocking layers are often incorporated [203]. This prevents the unwanted flow of opposite carriers which reduces dark current.

In some advanced designs, the charge-trap generation layers are intentionally introduced to enable photomultiplication effects and thus enhanced the responsivity by leveraging trap-assisted carrier injection [204]. Additionally, the CGLs are also utilized in OPDs to facilitate efficient carrier generation and transport to design tandem architectures with broader absorption and enhanced performance.

Table 2.16. Performance improvement in existing OPDs in terms of layers

Year	Ref.	Layer	Materials	Thickness (nm)	Observations
2025	[201]	ETL	Polyethylenimine-functionalized Zinc Nanoparticles (PEI-Zn NP)	25	OPDs with PEI-Zn NP ETL showed stable detectivity (89%, 84%, 93%) under light, air, and heating with suppressed dark current. The proposed OPDs maintained high stability and low dark current under harsh environmental conditions, ensuring reliable performance.
2025	[202]	HTL	Cobalt(II) acetate	20	Cobalt(II) acetate HTL enabled OPD with low dark current (1.44×10^{-5} A/cm ²) and high detectivity (1.25×10^8 Jones). MoO ₃ material offered good stability and cost-effective scalability.
2024	[205]	Active Layer	Poly[N-9'-heptadecanyl-2,7-carbazole-alt-5,5-(4',7'-di-2-thienyl-2',1',3'-benzothiadiazole)]: [6,6]-Phenyl-C ₇₁ -butyric acid methyl ester (PCDTBT:PC71BM)		Optimized BHJ OPD (PCDTBT:PC71BM, 1:1) showed dark current 0.002 mA/cm ² , responsivity 114 mA/W, fast response (733/597 ms), and EQE as 29% for sensitive visible photodetection.
2021	[203]	HBL	Tin(IV) oxide	31 ± 7	OPDs with inkjet-printed SnO ₂ HBL achieved low dark current (5 nA/cm ²), high responsivity (>0.5 AW ⁻¹), fast bandwidth (>2 MHz),

					and detectivity (10^{11} Jones at 740 nm).
2021	[206]	HBL	Bathocuproine	-	OPDs with engineered carrier blocking layers effectively reduced the unwanted carriers. This leads to low dark current, enhanced efficiency which improves long-term stability benefits critical for high-performance flexible and large-area image sensors.
2021	[207]	Active Layer	TPD (N,N'-Bis(3-methylphenyl)-N,N'-diphenylbenzidine): Alq ₃	-	Self-powered TPD:Alq ₃ (1:2) OPD exhibited sensitivity as 1.76×10^3 , responsivity as 5.22×10^{-4} A/W, and detectivity as 3.11×10^{10} Jones at 365 nm under zero bias, which enabled efficient UV detection without external power.
2018	[34]	Single Active Layer	PVD4650:[6,6]-Phenyl-C ₇₀ -butyric acid methyl ester	-	Fully-printed OPD arrays with a single broadband active layer showed EQE ~37%, low dark current (0.5 nA/cm ²), and 98.5% RGB color detection and provided simplified fabrication of full-color imagers.
2018	[208]	ETL	Vanadium(V) oxide (V ₂ O ₅)	6	The addition of an ultrathin V ₂ O ₅ ETL further tuned the charge extraction, and enhanced the device response to a new range of ~13.2 mA/cm ² (OFF) and ~20.7 mA/cm ² (ON).
2018	[209]	Active Layer	Poly[(4,8-bis(2-ethylhexylthienyl)benzo[1,2-b:4,5-b']dithiophene)-alt-(thieno[3,4-c]pyrrole-4,6-dione)] (PBDTT-8tTPD)	1100	A thicker active layer was used to increase absorption of visible light (500–650 nm) due to PBDTT-8tTPD's high molar absorption coefficient.
2015	[210]	ETL	Amorphous Indium Gallium Zinc Oxide (a-IGZO)	7.5	OPDs with a-IGZO ETL achieved low dark current (10 nA/cm ² at -2 V) and high detectivity (3×10^{12} Jones at 550 nm). This resulted in enhanced reproducibility, and easier integration with IGZO backplanes.

As highlighted in Table 2.16, recent studies on OPDs emphasize the importance of interfacial and blocking layers engineering, active layer optimization, and scalable fabrication for achieving high performance. Advanced electron and hole blocking layers including PEI-Zn NP and inkjet-printed SnO₂, effectively reduce the dark current, enhance detectivity, and maintain stability under light, air, heating, or repeated bending cycles. Moreover, the use of a-IGZO material as the ETL provides very low dark current, high detectivity, and excellent

reproducibility as compared to TiOx. On the other hand, utilization of solution-processed Co(OAc)₂ HTL, reduces the noise current and improves the device stability due to thick active layers enabling stronger absorption without sacrificing transport due to high mobility.

In nutshell, these findings highlight that material innovation, blocking layer design, and printing-based scalable fabrication strategies are the keys for advancing OPDs with high detectivity, low dark current, mechanical flexibility, and operational stability for next-generation imaging, sensing, and portable optoelectronic applications. The OPDs have vastly designed and reported with HBL, HTL, ETL, and active layers (Table 2.16), but the CGLs are not explored up to that extent. Incorporating CGLs can enable more efficient charge separation and transport, reduction in dark current and improved detectivity beyond the conventional layers. This is particularly critical for biomedical applications, where detecting weak optical signals with high sensitivity and stability is essential. Therefore, exploring CGLs in OPDs may open new directions for high-performance, flexible, and ultra-sensitive biosensors.

2.4 SOLUTION PROCESSING FABRICATION TECHNIQUES FOR FLEXIBLE ELECTRONIC DEVICES

Some traditional fabrication techniques like physical vapor deposition and thermal evaporation have contributed in a large extent for manufacturing OLED devices. But the recent trend demands some versatile and low-cost techniques including inkjet printing, screen printing, and spin coating. Unlike vacuum deposition, screen printing process permits a reduction in use of materials as these are only needed for printed areas [211]. Some important solution processing techniques are discussed in the following sub-sections.

2.4.1 Spin coating

Soluble polymers can be deposited using spin coating in monochrome displays. A uniform deposition of emissive material in the form of drop occurs on the flat substrate and further it is rotated at a high-speed multiple times until it gets the desired thickness as shown in Fig. 2.12 (a). In this process, the carrier material is evaporated at a faster rate and this results in a uniform deposition of film. The parameters including spin time, fume extraction, speed of spin coater, temperature, fluids volatility and viscosity are greatly responsible for the thickness of film. The spin coating process has been opted by many researchers to improve the organic devices. In 2012, Hyun *et al.* [212] demonstrated a method for corrugated structure using spin coating process to improve the light extraction for organic LEDs. The performance parameters were

controlled by mixing ratio of solution of SiO_2 and TiO_x and varying the speed of spin-coating process.

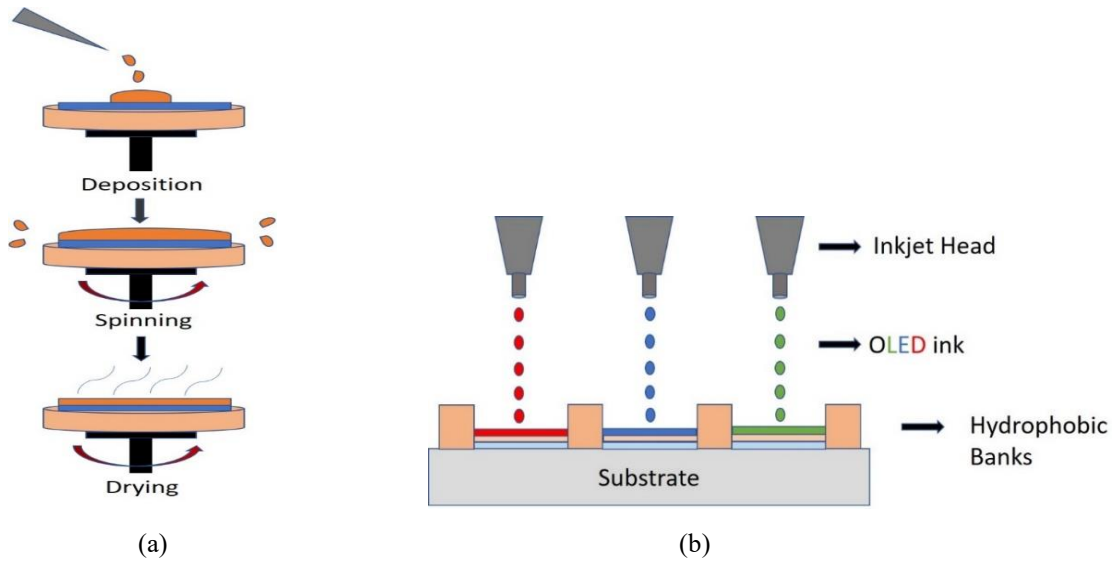


Fig. 2.12 (a) Processing steps for spin coating and (b) inkjet printing techniques

Yuan *et al.* [98] proposed a low-cost simple spin coating method to form a distributed embossed structure produced by Al_2O_3 nanospheres. The performance in terms of maximum current efficiency, power efficiency and EQE is achieved as 52.1 cd/A, 32.7 lm/W and 20.9%, respectively. Further, in 2020, Juhari *et al.* [213] analysed the electrical and structural properties of ITO/PEDOT:PSS doped polyethylenimine ethoxylated organic LED using spin coating technique.

2.4.2 Inkjet printing

OLED materials are sprayed out through inkjet head on the substrate in the similar manner as paper printing is done. This process is applicable for large devices as large films can be printed [214]. High resolution, easy multi layered deposition, cost effective process are the main advantages of this printing process. The figure 2.12 (b) highlights the flow for inkjet printing process. In 2019, Xing *et al.* [215] proposed a high luminance phosphorescent inkjet printing organic OLED with hole transporting material m-MTDATA (4,40,400-tris[3-methyl-phenyl(phenyl)amino]-triphenylamine). The OLED exhibited maximum luminance of 13240 cd/m^2 . Furthermore in 2020, Zheng *et al.* [18] proposed a highly efficient blue OLED based on inkjet printing having a novel host material mCP for the EML. In this device, the brightness was obtained as 92.7% which is good enough to realize a highly efficient large area display using inkjet printing. Additionally, Hu *et al.* [216] utilized inkjet printing to demonstrate a novel

display based on blue OLED and green and red quantum dots color conversion layers. The inkjet method in this report provided a cost-effective display for quantum dots applications.

2.4.3 Screen printing

In this process, a screen mask is utilized to squeeze the ink to get print patterns. The screen printing is widely applicable in commercial usage of printed circuit boards, active polymer layer and electrode printing. To avoid the screen blockage, particle size should be large enough. This process requires less use of materials as they are directed onto substrate at faster rate as compared to inkjet printing. In 2017, Preinfalk *et al.* [217] reported a cost-effective screen-printing method for the deposition of high refractive index scattering polymer: TiO₂-nanoparticle mixture onto a large area. In this research, luminous efficacy was increased up to 56%. Additionally, in 2019, Wan *et al.* [218] developed a printable mesoscopic perovskite solar cell containing triple layer scaffold of TiO₂/ Zirconium Dioxide/carbon. The screen-printing process was used for the deposition of scaffold which resulted in low- cost photovoltaics.

The fabrication process of organic layers depends on the type of materials whether it is small molecule [219] or conducting polymer [220]. Small molecule semiconductors, such as pentacene and oligothiophenes are widely employed owing to their high mobility, however, their inferior solubility makes them inappropriate for realizing through inexpensive printing methods. In contrast, conducting polymers, such as poly(3-hexylthiophene) and polythiophene exhibit low mobility but excellent solubility in a variety of organic solvents including chloroform and toluene [161], thereby promising for low cost and large area flexible devices. The main aim to explore different fabrication techniques and their advantages is to build an insight for selection of the soluble organic materials for different layers of the OTFT, OLED and OPD for possible realization of flexible devices.

2.5 DIFFERENT APPLICATIONS OF FLEXIBLE DEVICES

Organic electronics is a new technology that provides various applications in terms of OTFT driven OLED, sensors, biomedical, military, etc. It was a real challenge to replace inorganic devices by organic one. The properties including flexibility, large area fabrication, transparency, and wider viewing angle made organic devices suitable to compete with conventional devices. Some important applications of flexible devices are discussed here.

2.5.1 Bio-medical applications

The utilization of fluorescence detection for various bio-medical applications such as; oximeter sensor, cancer detection, monitor of protein-DNA interactions, heart stroke detection, etc. has

been on rise and firstly introduced by Heyduk and Lee in 1990 [221]. The integration of organic light emitting diode and organic photo diode well suits for these kinds of health-care applications and are illustrated in Table 2.17.

Table 2.17. Different bio-medical applications using OLED and OPD

Year	Reference	Improvement Technique	Observations
2025	Tiwari <i>et al.</i> [222]	Provided technique for cancer treatment using flexible LED and photodiode.	Various cancer such as; skin, ovarian, prostate and glioma were investigated. Suitable for non-invasive diagnostic application.
2024	Kim <i>et al.</i> [223]	Reported a wearable quantum dot-OLED for real time high power photomedicine.	Higher power density (23.28 mW/cm ²). Encapsulation performance 6×10^{-6} g/m ² day. Devices successfully detected PPG (Photoplethysmography) signals.
2022	Liu <i>et al.</i> [224]	Development of a fluorescence sensing platform for specific and sensitive detection of pathogenic bacteria in food samples.	Detected one strain of <i>S. aureus</i> , ATCC 29213. Limit of detection: 6 cfu/ mL
2022	Zhang <i>et al.</i> [225]	Established two kinds of test strips for RBD (Receptor Binding Domain) and N antigens of SARS-CoV-2 with high sensitivity and specificity.	Limit of detection: 6.9 ng/mL for RBD protein and 7.2 ng/mL for N protein. Test strip showed a high anti-interference capacity in complex bio-samples.
2021	Lee <i>et al.</i> [226]	Reported a compact, standalone device for the detection of COVID-19.	Developed system performed SARS-CoV-2 RNA detection within 20 min of sample loading. Limit of detection reached 3 copy/ μ L.
2021	Guo <i>et al.</i> [227]	Developed ultra-sensitive fluorescence sensor for proactive prognosis of COVID-19.	Detected spike protein with a detection of limit 1.6 ng/mL and nucleocapsid protein of limit 2.2 ng/mL.
2019	Khan <i>et al.</i> [228]	Demonstrated a reflectance oximeter sensor device using a light emitter, a detector and an optical barrier between emitter and detector.	Using this method, three sensor geometries; rectangular, bracket, and circular were designed.
2019	Negi <i>et al.</i> [229]	Reported organic LED based light sensor for detection of ovarian cancer.	Multi-layered OLED generated a current of 29 mA and 13 mA at an incident wavelength of 420 (not-detected) and 440 nm (detected) respectively.
2018	Lim <i>et al.</i> [40]	Presented an oxygen sensor device using the same OLED-OPD combination.	Simultaneous monitoring of TcPO ₂ (Transcutaneous Oxygen Pressure) is incorporated to sense oxygen level in the human body.

It is observed from the table that OLED-OPD device combination can be used as the bio-sensor for the detection of diseases. When light emitted from OLED passes through a sample (blood,

urine, saliva, etc.), then elements present in the sample alters the properties of light that may be intensity or wavelength. If this change can be detected and differentiate efficiently by an OPD, then it can be found whether the sample is infected by some virus/disease or not.

2.5.2 Sensors

Another important application of organic LED is to use as the sensor. In 2011, Kim *et al.* [230] reported a highly sensitive ultrathin active-matrix OLED device with the property of capacitive touch sensors. The touch sensor device of thickness 1.2 mm was developed to be operable at 200°C. Further, Watanabe and group [231] fabricated an 8.76-inch diagonal sized in-cell touch sensor using foldable OLED device. The properties of this display observed unaltered even after 105 folding operations. The display showed pixel size of 0.100 mm × 0.100 mm. Also, the aperture ratio, pixel density and number of effective pixels were obtained as 46%, 254 ppi, 1080 × RGBY (red-green-blue-yellow) × 1920, respectively. Additionally, Barre *et al.* [232] presented some OLED based applications for military including assistant gunner display, night vision goggles and vision enhancement system. The researchers Trakalo *et al.* [233] reported three display devices; OLED DDACT, OLED assistant gunner display and Polymer-OLED assistant gunner display to be useful for military.

2.5.3 OTFT driven OLED applications

OTFTs are widely used as the switching element to drive the OLED arrays for smart selection of pixel. Also, in some cases, if OTFT driven based OLED circuit is realized then using a high performance OTFT, the OLED can achieve the required current for light emission comparatively at lower voltage. In 2009, Katsuhara *et al.* [234] realized a full color AMOLED display (named C₁ for comparison purpose) on the flexible substrate and driven by pentacene semiconductor based OTFT (Fig. 2.13 (a)). This display showed a high electrical and environmental stability. In 2011, Noda *et al.* [235] reported an OTFT driven rollable and 80 μm thick AMOLED display (named C₂). The picture quality and initial properties of this display remained same even after 1000 cycles of roll up. The circuit arrangement of pixel panel is shown in Fig. 2.13 (b) that contains one capacitor and two organic transistors (one as a switch and other as driving source). This circuit operated at the frame rate of 60 Hz. The pixel size, display size, resolution, and peak luminescence for this display were obtained as 210 μm × 210 μm, 4.1 inch wide, 121 ppi, 100 cd/m², respectively.

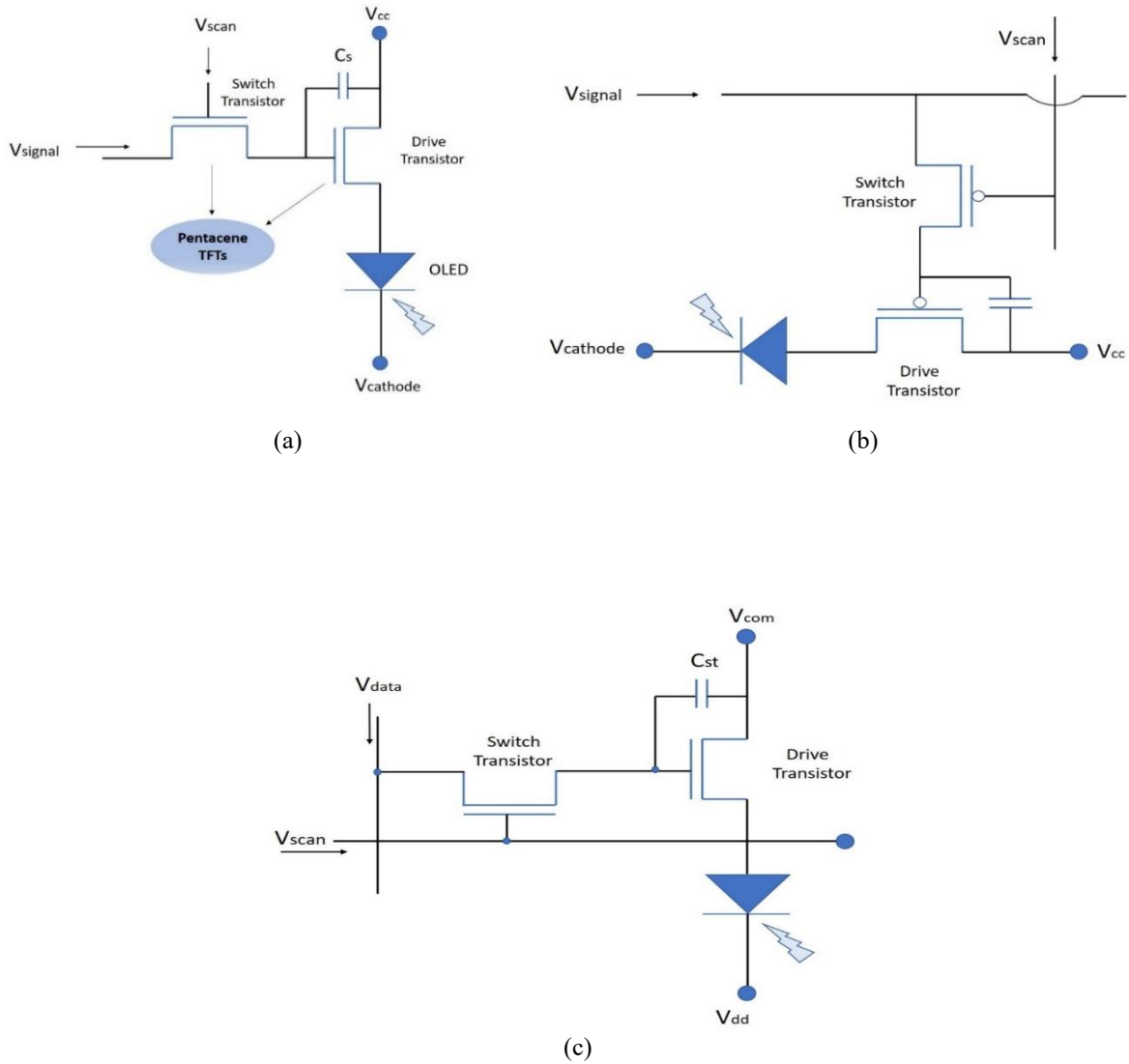


Fig. 2.13 Pixel circuits for OTFT driven AMOLED for (a) C_1 , (b) C_2 , and (c) C_3

Table 2.18. Performance comparison of three different displays based on OTFT driven AMOLEDs

Aspect	C_1 [234]	C_2 [235]	C_3 [236]
Pixel Size	$318 \mu\text{m} \times 318 \mu\text{m}$	$210 \mu\text{m} \times 210 \mu\text{m}$	$1.5 \text{ mm} \times 1.5 \text{ mm}$
Display Size	2.5 inch	4.1 inch	2.7 inch
Resolution	80 ppi	121 ppi	32×32
Peak Luminescence	150 cd/m^2	100 cd/m^2	$64,459 \text{ cd/m}^2$
Contrast Ratio	-	$>1000:1$	-
Scan Voltage	30 Vp-p	20 Vp-p	-
Signal Voltage	12 Vp-p	$<10 \text{ Vp-p}$	-
Thickness	$0.4 \mu\text{m}$	$80 \mu\text{m}$	$30 \mu\text{m}$

In 2016, Kim *et al.* [236] reported an AMOLED display (C_3) fabricated on polyethylene fabric substrate. A TIPS pentacene (6,13-bis(triisopropylsilyl)ethynyl)pentacene) based OTFT was utilized to drive the organic LED. A capacitor, OLED and two OTFTs are arranged as the pixel circuit (Fig. 2.13 (c)). Table 2.18 depicts the performance comparison of three different OTFT

driven active-matrix OLEDs; C_1 , C_2 and C_3 based on pixel size, display size, resolution, luminescence, contrast ratio, signal voltage and thickness.

The flexible electronic devices; OTFT, OLED, and OPD are observed promising for sensors and biomedical applications. Their properties including lightweight, mechanical flexibility, solution-processed low-cost fabrication, and usage of flexible economically viable substrates, make them suitable for wearable and implantable systems. OTFTs can enable real-time monitoring and efficient signal amplification in bio-medical circuits. The major requirement in OLED based display is to produce high luminance, low I_{off} and small V_{on} at low voltage operation that can be addressed using OTFT as the driving element.

2.6 RESEARCH GAPS

Productive research towards organic devices has ensured their potential use in the commercial applications and researchers have resolved various challenges related to organic devices. Undoubtedly, organic TFTs, OLEDs and OPDs have already been realized in applications requiring large area coverage, structural flexibility, and low cost. Nevertheless, some issues still need to be resolved for their robust and consistent use. Based on the all-embracing literature review, some gaps are identified and discussed in the following points:

- The performance of organic transistors is observed much dependent on the structural design even with same set of materials. Short channel length devices are preferred owing to their low operating voltage (leads to lower power consumption), faster switching, improved current and lower contact resistance. Vertical channel based TFTs can be a solution to achieve short channel length (nano-meters) based on the thickness of active layer. It is further imperative to understand the conduction mechanism in these TFTs so that some structural improvements can be made to further augment their performance.
- Researchers have devoted very hard efforts to improve the performance of flexible OLEDs by incorporating electron/hole transport, electron/hole injection, and hole blocking layers. These layers play an important role in improving charge transport, efficiency, luminescence and current. Further addition of some novel layers like charge generation, spacer and mixed interlayer can further lead to an improvement by efficient charge recombination. Inclusion of CGLs may lead to generate more electron-hole pairs and subsequently can result in better luminescence and current density. In fact, these layers can also improve the performance of OPDs.

- In recent times, OLEDs are realized in numerous worthwhile applications like large flexible displays, foldable displays, touch screen sensors, etc. A new dimension based on OLED-OPD integration for biomedical application is also explored. However, some more insight is required towards proposing OLED and OPD devices with similar structure and dimensions to realize on the single platform which can reduce complexity of fabrication process and may even lead the device realization at comparatively lower cost. Therefore, it is needed to select the material for layers of OLED and OPD wisely to perform a particular bio-medical application.
- The integration of OLED and OPD is a promising solution for biomedical diagnostics and sensing and several reports are available that focuses towards successful cancer detection. Some more applications including Covid-19 detection and heart rate monitoring can be further focused with potential use of OTFT, OLED and OPD devices. If these findings can be done at early stage, then these ailments can be cured and can improve the mortality rate.

CHAPTER-3

SHORT CHANNEL FLEXIBLE VERTICAL ORGANIC THIN FILM TRANSISTOR

3.1 INTRODUCTION

The organic thin film transistor is a category of field effect transistor that utilizes organic material for conduction instead of conventional semiconductors. These devices have many attractive features such as large area fabrication, mechanical flexibility, cost-effectiveness, and low temperature processing that makes these devices embracing unique characteristics and interesting for researchers. These devices contain a variety of structures including single gate, dual gate, vertical channel, and cylindrical.

Each of these structures has its own benefits and are therefore suitable for a varying range of applications. In a single gate structure, bottom gate configuration is preferred owing to an ease of surface smoothening at interfaces and processing with solution processing techniques. On the other hand, dual gate structure is utilized for higher current and lower threshold voltage requirements. Dual gate device provides better charge carrier injection due to dual biasing at gates. Apart from single and dual gate configurations, vertical structures of TFTs are reported, in which source and drain are placed in vertical arrangement. This vertical arrangement leads to achieve short channel OTFTs and thus liable for fast switching and operation at low voltage.

Even though significant progress has been made for enhancing the performance of organic TFTs, still a scope exists for improvement. During the recent decade, the researchers have devoted lot of efforts in refining the vital parameters of transistors with a major focus on charge carrier mobility. Few solution-processed organic materials such as; diF-TES-ADT (5,11-bis(triethylsilylethynyl)anthradithiophene), TIPS pentacene and C8-BTBT (2,7-dioctyl[1]benzothieno[3,2-b][1]benzothiophene) have reported higher mobilities [237, 238]. These materials exhibit adequate stability in air which is very important for industrial applications. Despite these features, the mobility still shows a big scope for improvement. Therefore, the performance of these organic material-based devices is not analogous to conventional transistors.

The mobility is not just a material related parameter and affected by device structure as well. Therefore, to resolve the issue pertaining to the device mobility, the devices containing short channel length (in nm) are quite beneficial and are analysed in this chapter. Subsequently, a

performance comparison is made for existing vertical channel structures. In addition to this, a novel vertical channel structure is proposed for possible performance enhancement. Therefore, following objective is framed here to obtain a high-performance short channel vertical OTFT:

“Design and structural analysis of high performance flexible vertical thin film transistor and comparison with existing OTFTs.”

To realize the desired objective, the methodology includes following steps:

- Validation of a planar BGTC transistor using Silvaco Atlas.
- Comparative analysis of planar and vertical TFTs in terms of performance parameters drain current, threshold voltage and mobility.
- Design a short channel flexible Vertical OTFT (VOTFT) and compare its performance against planar and other vertical TFTs.
- In-depth internal analysis of the proposed novel VOTFT using vertical and horizontal cutline to understand the device behaviour in terms of valance band, conduction band, potential, current density and hole concentration.

The chapter is aimed at improving the performance of OTFT through structural variation. A novel vertical channel OTFT structure is proposed in the present work. This proposed device is compared with other existing structures to investigate the impact of proposed architecture on different performance parameters including current, threshold voltage, mobility and I_{on}/I_{off} ratio. Additionally, devices internal device analysis is conducted on proposed device along with other devices. The internal analysis is intended to investigate the facts associated with better performance of the proposed device in terms of band energy, potential, current density, and hole/electron concentration.

This chapter is arranged in six sections including this introductory section numbered as 3.1. In Section 3.2, the performance analysis of an existing planar TFT is incorporated. Subsequently, in Section 3.3, this planar TFT is compared with a vertical OTFT structure and other vertical OTFTs are also analysed. In Section 3.4, the performance of proposed novel vertical TFT is analysed. Additionally, the proposed device is compared with existing devices in terms of threshold, mobility, drain current and on-off current ratio. Further, an in depth understanding of proposed VOTFT behaviour is shown using cut line analysis in Section 3.5. The summary of the complete research work of this chapter is highlighted in Section 3.6.

3.2 CHARACTERISTIC ANALYSIS AND PARAMETERS EXTRACTION OF SINGLE GATE PLANAR TRANSISTOR

In this section, a BGTC thin film transistor with C8-BTBT (2,7-dioctyl[1] benzothieno[3,2-b][1]benzothiophene) active layer material is simulated using Silvaco Atlas 2-D device simulator [238]. A high-k ultrathin polymer; pC1B5 (Phosphorus pentachloride) is used as the gate dielectric. The Au/MoO₃ bilayer electrodes with 70/20 nm thickness are used for source and drain electrodes. The layer of MoO₃ is placed between Au and C8-BTBT to enable smooth charge carrier injection [239] and helps in adhesion between the two layers. The device structure is shown in Fig. 3.1. The material and thickness of different layers; source, gate, drain, active layer and gate dielectric used in the device are summarized in the Table 3.1. The channel length and width are kept at 200 μm and 1000 μm , respectively.

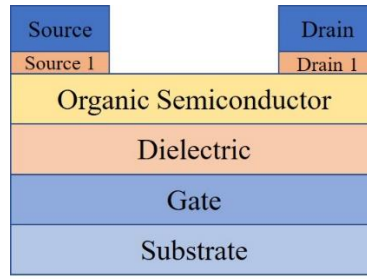


Fig. 3.1 Structure of BGTC planar TFT (D₁)

Table 3.1. Materials and thickness of different layers of D₁

Layer	Material	Thickness (nm)
Source/Drain	Gold	70
Source1/Drain1	MoO ₃	20
Active Layer	C8-BTBT	30
Gate Dielectric	pC1B5	29
Gate	Aluminium (Al)	50

Table 3.2. Material's specification for different layers of D₁

Parameter	Value
Band gap (C8-BTBT)	2.7 eV
Density of conduction band (C8-BTBT)	$1 \times 10^{21} \text{ cm}^{-3}$
Density of valence band (C8-BTBT)	$1 \times 10^{21} \text{ cm}^{-3}$
Acceptor doping concentration (C8-BTBT)	$6.5 \times 10^{17} \text{ cm}^{-3}$
Dielectric constant of C8-BTBT	5
Dielectric constant of pC1b5	7.5

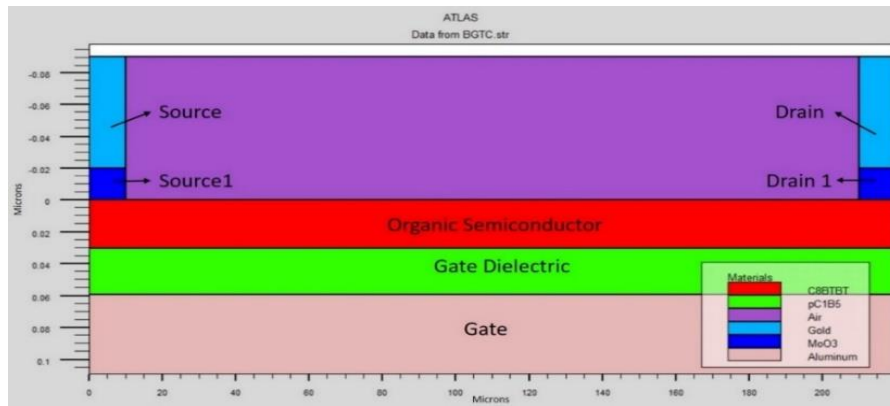
Table 3.2 highlights the properties of semiconductor and dielectric materials used in the device. The simulator predicts the electrical characteristics of the device by utilizing a set of differential equations derived from Maxwell's laws. These contain Poison's, transport, and continuity

equations. These equations are applied onto 2D/3D grid consisting of multiple grid points called nodes. The complete process is used to simulate the carrier's transportation in the device structure. Further, the device electrical performance can be modelled in DC, AC or transient modes of operation.

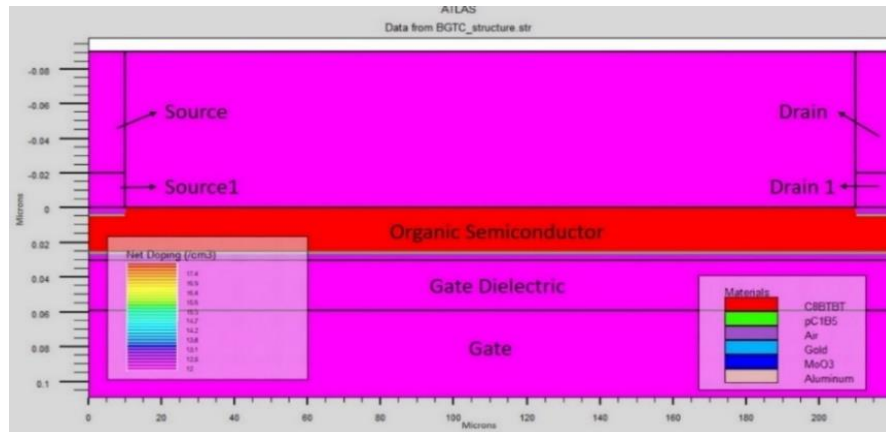
To simulate the organic device behaviour, Poole-Frenkel mobility model, proposed by Frenkel in 1938, is included to obtain the results under specified boundary conditions. This model is given as:

$$\mu(E) = \mu_0 e^{\left[-\frac{\Delta}{kT} + \left(\frac{\beta}{kT} - \gamma\right) \sqrt{|E|}\right]} \quad (3.1)$$

where μ , μ_0 and E are field dependent mobility, zero field mobility, and electric field, respectively. Additionally, the parameters Δ , k , T , β and γ represent activation energy at zero electric field, Boltzmann constant, effective temperature, hole Pool–Frenkel factor and fitting parameter, respectively.



(a)



(b)

Fig. 3.2 (a) Simulated device structure of BGTC (planar) transistor and (b) Representation of layers with current flow-lines from source to drain

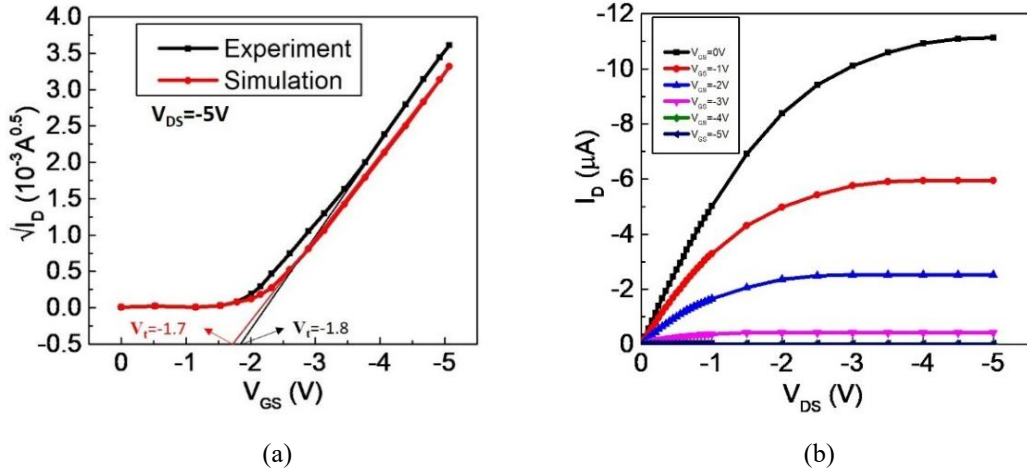


Fig. 3.3 (a) Transfer characteristics of experimental and simulated planar devices along with threshold voltage and (b) Drain characteristics of planar device

Figure 3.2 (a) demonstrates planar device structure with different regions obtained by using TollyPlot tool in Silvaco. Further, Fig. 3.2 (b) depicts the current flowlines in the structure. Here, it can be observed that the channel is formed just above the dielectric-semiconductor interface from source to drain contact in a horizontal manner. The transfer characteristics of simulated and experimental OTFTs are compared and show a close match [238], as shown in Fig. 3.3 (a). The threshold voltage is obtained by plotting a straight line on current-voltage characteristics and extended at x-axis as mentioned in the figure. The maximum drain current is obtained as 11 μA at gate voltage of -5 V (Fig. 3.3 (b)).

Table 3.3. Parametric comparison of simulated (D_1) and experimental device

Parameters	Experiment [238]	Simulation (D_1)
Threshold Voltage V_t (V)	-1.8	-1.7
Maximum Drain Current I_{Dmax} (μA)	12	11
I_{on}/I_{off}	$>10^6$	1×10^6
Saturation Mobility μ_{sat} ($cm^2/V.s$)	3.3	3.1

Further, the V_t , I_{Dmax} , I_{on}/I_{off} and μ_{sat} are also extracted and compared. These parameters are summarized in Table 3.3. The results highlight a close match between experimental and simulated transistors. The close match between the experimental and device D_1 reflects that the parameters and other aspects considered for the simulation match with the empirical fabrication conditions and thus set the boundaries for simulation of other devices.

3.3 PERFORMANCE COMPARISON OF VERTICAL AND PLANAR TRANSISTORS

The vertical channel device depicts better performance as compared to the planar device owing to their smaller channel length. To analyse the impact of vertical channel on the device

performance, this section compares the performance of planar and vertical TFTs keeping material and layer thickness same for both devices. Figure 3.4 outlines the structure of vertical device (named D₂) [192]. In D₂, vertical stacking of source and drain electrodes are incorporated. These electrodes are separated by an insulating spacer and a semiconductor layer. Table 3.4 summarizes the comparison of planar and vertical device in terms of performance parameters; V_t , I_{Dmax} , I_{on}/I_{off} and μ_{sat} . The table highlights a remarkable improvement for device D₂ as V_t , I_{Dmax} , and μ_{sat} are improved by 18, 2 and 9 times, respectively in comparison to D₁.

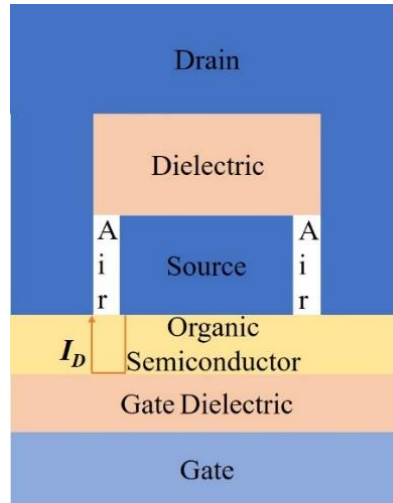


Fig. 3.4 Device structure for vertical thin film transistor (D₂)

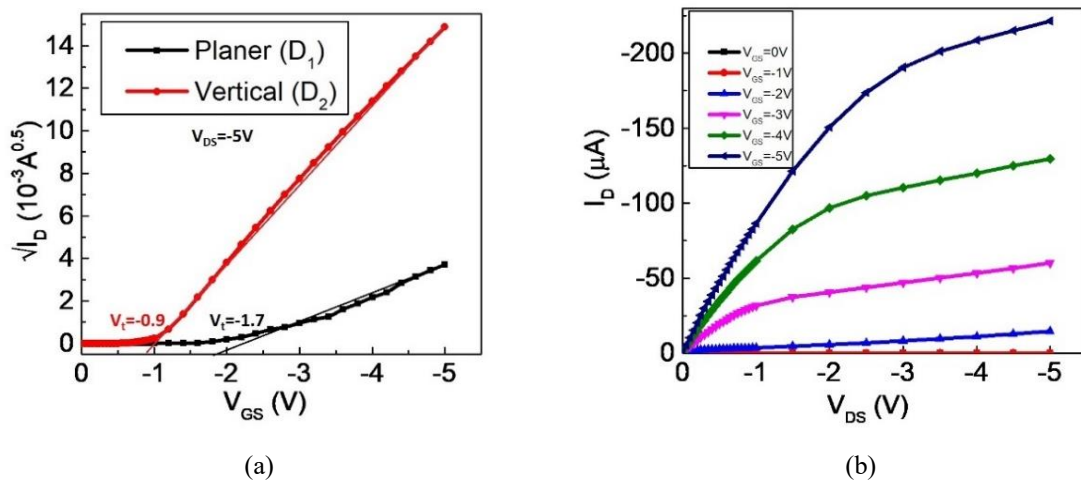
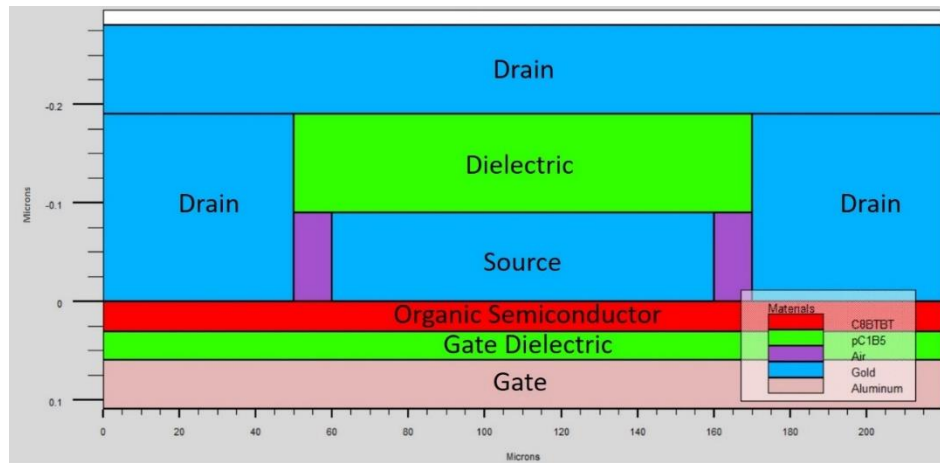


Fig. 3.5 (a) Comparison of transfer characteristics of D₁ (planar) and D₂ (vertical) devices along with threshold voltage and (b) Drain characteristics of D₂ device

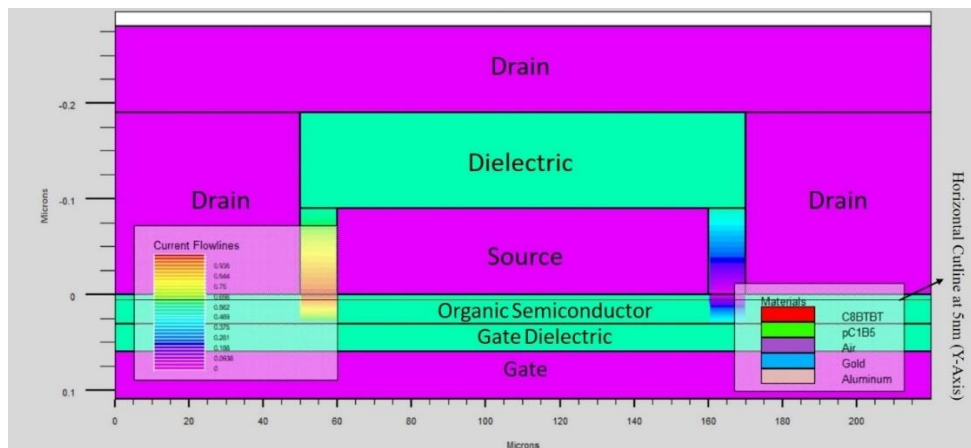
Table 3.4. Parametric comparison of planar (D₁) and vertical device (D₂)

Parameters	Planar Device (D ₁)	Vertical Device (D ₂)
Threshold Voltage V_t (V)	-1.8	-0.9
Maximum Drain Current I_{Dmax} (μA)	12	221
I_{on}/I_{off}	$>10^6$	2.3×10^{10}
Saturation Mobility μ_{sat} (cm ² /V.s)	3.3	30.2

Figure 3.5 (a) illustrates the comparison of transfer curves of D_1 and D_2 devices along with the threshold voltage. The figure highlights an enhancement in current for D_2 than that of D_1 on the same applied bias. Figure 3.5 (b) shows the drain characteristics of D_2 at different V_{GS} ranging from 0 to -5 V. The maximum drain current is obtained as 221 μA at $V_{GS} = -5$ V.



(a)



(b)

Fig. 3.6 (a) Simulated vertical device structure (D_2) and (b) Current flowlines inside the device

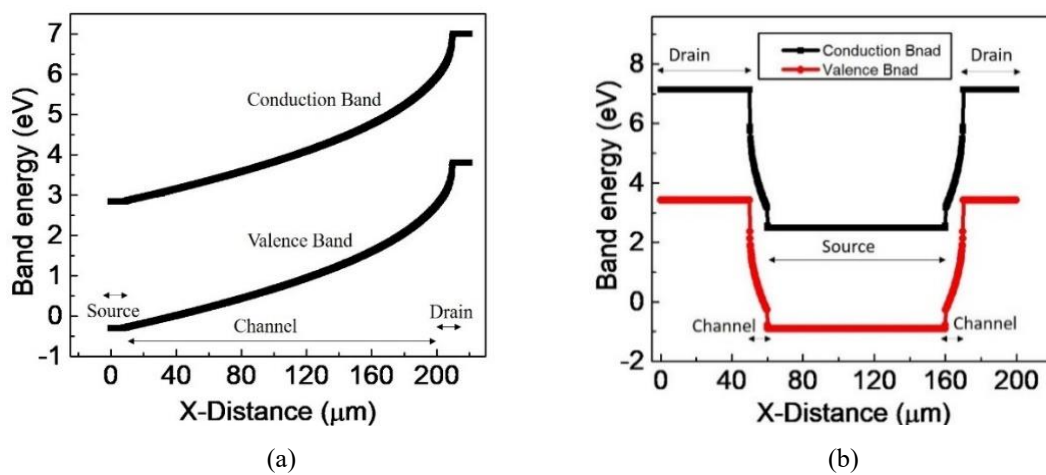
Further, the internal device analysis is performed in the TonyPlot tool of Silvaco. The device structure and current flowlines are shown in Figs. 3.6 (a) and (b) for device D_2 . In Fig. 3.6 (b), it is clearly observed that the channel is formed in a very small region (in nano-meter range) of active layer between source and drain and is in the vertical direction. Subsequently, the drain current and mobility, both are remarkably improved.

3.3.1 Cutline analysis for vertical and planar TFTs

In this section, internal analysis is performed for both D_1 and D_2 devices. This internal analysis examines the device behaviour in depth and thereby, helps in establishing the facts for the enhanced performance of device D_2 over D_1 . The internal analysis is conducted by drawing a

cutline in TonyPlot within the channel to examine the difference in various internal parameters. In device D_1 , a horizontal cutline is drawn at 1 nm (Y-axis) above the dielectric layer where the channel is formed. On the other hand, in device D_2 , horizontal cutline is drawn in the channel at 5 nm (Y-axis) as highlighted in Fig. 3.6 (b). In this device, the current is flowing across a U-shaped channel from source to drain. Hence, in this device, two different channels are developed due to the structural variation that too of short channel length (in nm). This results in significant enhancement in performance of D_2 .

Figure 3.7 shows band energies, potential and current densities for both planner and vertical channel devices. In these figures, X-distance is representing the total device length ($220\ \mu\text{m}$). Figures 3.7 (a) and (b) highlight the band energy profile of D_1 and D_2 in terms of valence and conduction band energies. In Fig. 3.7 (b), two different band are demonstrated as two channels are formed at both side of source electrode. Further, it is observed that the channel length in device D_2 is much smaller as compared to that in D_1 . Additionally, in vertical device two channels are formed, one on each side of the source, which directly results in higher carrier injection and a lower threshold voltage values. Further, the potential distribution in D_1 and D_2 devices are shown in Figs. 3.7 (c) and (d), respectively. In both figures, it is observed that drain is at highest potential and source is at lowest potential value. There is a steep change in potential for D_2 as compared to D_1 in the channel. This highlights a strong electric field in the channel region resulting in a higher carrier acceleration for D_2 . However, in D_1 the potential variation is comparatively gentle between the source and the drain terminals. This is the probable reason for higher mobility of carriers in D_2 .



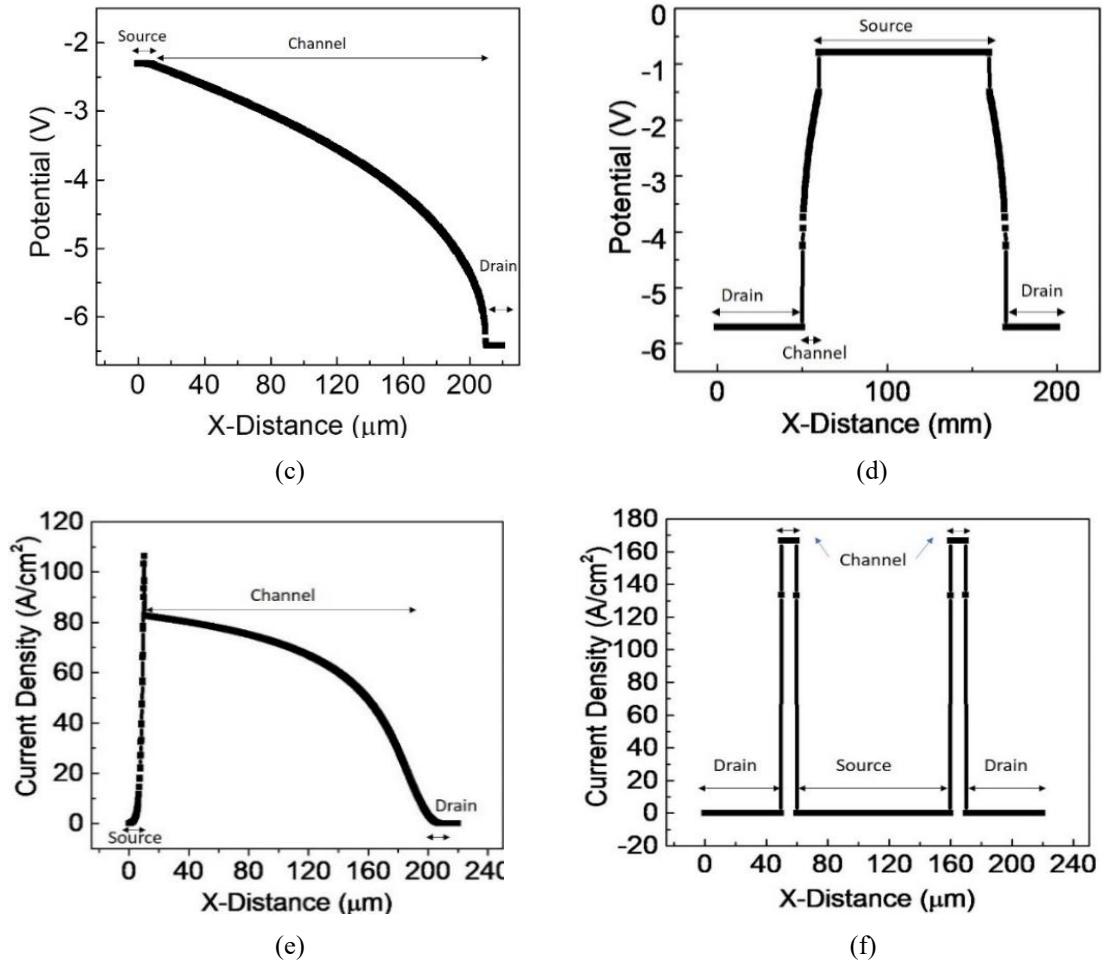


Fig. 3.7 Band energy for (a) D₁ and (b) D₂, Potential distribution for (c) D₁ and (d) D₂, current density for (e) D₁ and (f) D₂

Figures 3.7 (e) and (f) are representing the current density of D₁ and D₂, respectively. Device D₁ exhibits the maximum current density of 109 A/cm² at X= 10 nm. This value further keeps decreasing towards the drain electrode and becomes zero at X= 200 nm. As compared to this, it is noticed from the Fig. 3.7 (f) that current density for D₂ depicts a high value from 50 nm to 60 nm and again from 160 nm to 170 nm i.e. where the vertical channel formation takes place. Thus, the maximum current density is obtained as 169 A/cm², which is quite higher than that of D₁. All these figures suggest the presence of strong electric field in the channel region for D₂, resulting in higher carrier transfer and thus enhanced performance of the device.

3.3.2 Performance analysis of different vertical structures

The results in the previous section highlights the effectiveness of vertical structure in enhancing the performance of the organic transistors. Therefore, different arrangements of vertical transistors are analysed in the present section. Two other vertical structures D₃ [240] and D₄ [241] devices are considered for analysis. Device D₂ is now compared with these two vertical

devices D₃ and D₄. The materials of various regions in all three vertical TFT devices; D₂, D₃ and D₄ are kept same as in planar device with the same possible layer thickness.

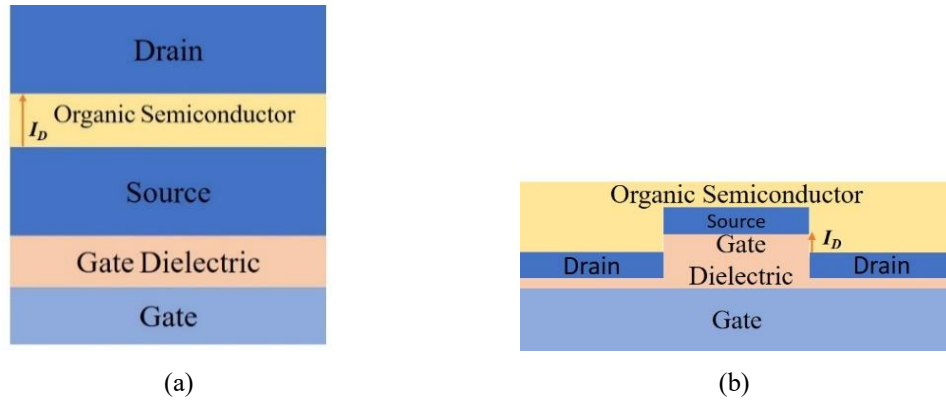


Fig. 3.8 Vertical structures of (a) D₃ and (c) D₄ devices

In the D₂ device, source and drain electrodes were placed vertically and separated by an insulating spacer and a semiconductor layer. On the other hand, in D₃ device, the source is placed above the dielectric and drain is placed above the OSC layer as depicted in Fig. 3.8 (a). As the channel is vertical and developed between source and drain, the channel length depends on the thickness of the active layer. Next, in device D₄, the source and drain electrodes are placed below the OSC layer in vertical manner. Here, the drain electrode is utilized in split form. The channel length is determined by the distance between source and drain. All D₂, D₃ and D₄ devices exhibit short channel which can counter the drawbacks of conventional organic TFTs.

Table 3.5. Materials and thickness of different regions in three vertical devices

Layer	Material	Thickness (nm)		
		D ₂	D ₃	D ₄
OSC	C8-BTBT	30	30	30
Source	Gold	90	90	10
Drain	Gold	90	90	10
Gate dielectric	pC1B5	29	29	29
Gate	Al	50	50	50

Table 3.6. Comparison of performance parameters of three vertical Devices

Parameters	D ₂	D ₃	D ₄
Threshold Voltage V_t (V)	-0.9	-1.7	-1.3
Maximum Drain Current I_{Dmax} (μA)	221	82.5	120
I_{on}/I_{off}	2.3×10^{10}	0.8×10^{10}	0.1×10^{11}
Saturation Mobility μ_{sat} ($cm^2/V.s$)	30.2	9.7	15.2

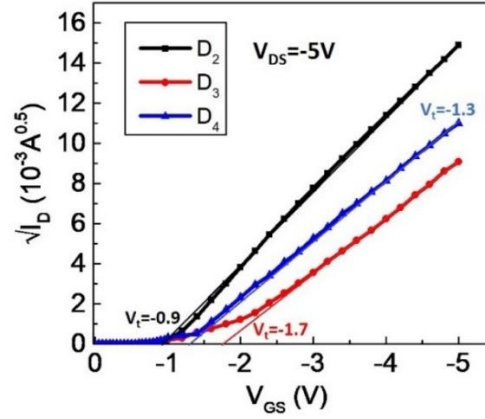


Fig. 3.9 Comparison of transfer curves of D₂, D₃ and D₄ along with the threshold voltages

The thickness of different layers for all vertical channel TFTs is summarized in Table 3.5. In device D₄, source and drain are considered of 10 nm thickness each due to the structural variation. However, change in electrode thickness does not affect the performance of the transistor. Table 3.6 highlights the performance parameters of D₂, D₃ and D₄ devices. The D₂ device outperforms all other devices and parameters; V_t , I_{Dmax} , μ_{sat} are improved by 0.5, 2.6, 3.1 times as compared to D₃ and 0.69, 1.8, 1.9 times than D₄ device. Figure 3.9 highlights the comparison of transfer characteristics for D₂, D₃ and D₄ along with extraction of threshold voltage. The maximum drain current at gate-source voltage (V_{GS}) and drain-source voltage (V_{DS}) both equal to -5 V is obtained as 221, 82.5, 120 μ A for D₂, D₃ and D₄, respectively. Addition to this, D₂ is operating at threshold voltage of -0.9 V which is smaller than D₃ and D₄. The facts for the better performance of device D₂ over D₃ can be attributed to the dual channel formation in D₂ configuration. On the other hand, D₂ is better in comparison to D₄ due to better gate control over the channel regions.

3.4 PROPOSED VERTICAL TFT

In the previous section, it is observed that the vertical channel is influential in ameliorating the device performance and even vertical channel-based devices show performance variation due to relative position of the layers and formation of the channel differently. Therefore, a novel vertical TFT (D₅) is designed and analysed (Fig. 3.10) in the present section, with an aim to further improve the device performance in terms of drain current and mobility parameters. The materials and thicknesses of D₅ are kept same as of D₂, D₃ and D₄ to make a fair comparison. The proposed vertical TFT exhibits a ditch in the dielectric filled with semiconductor.

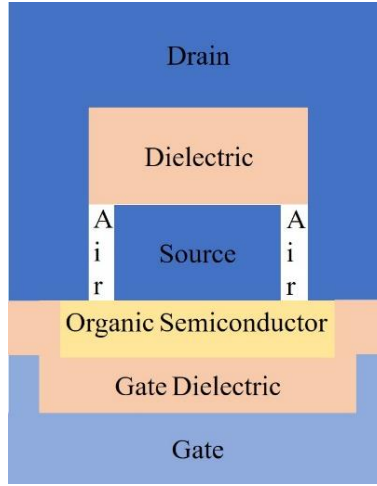
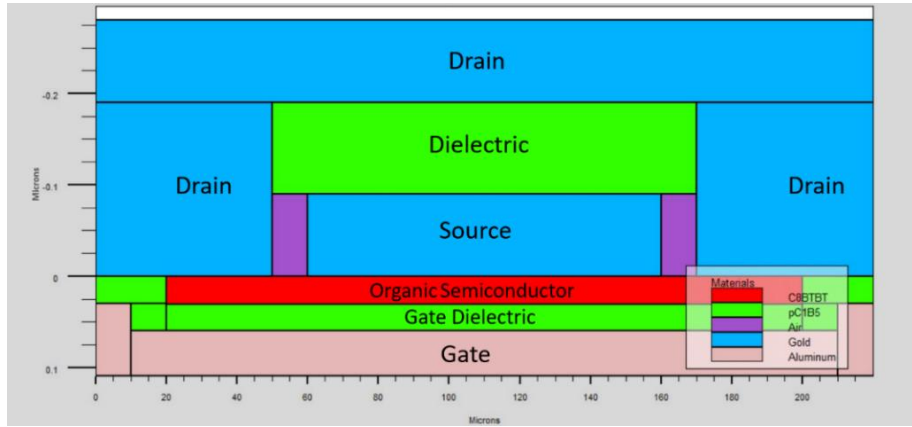
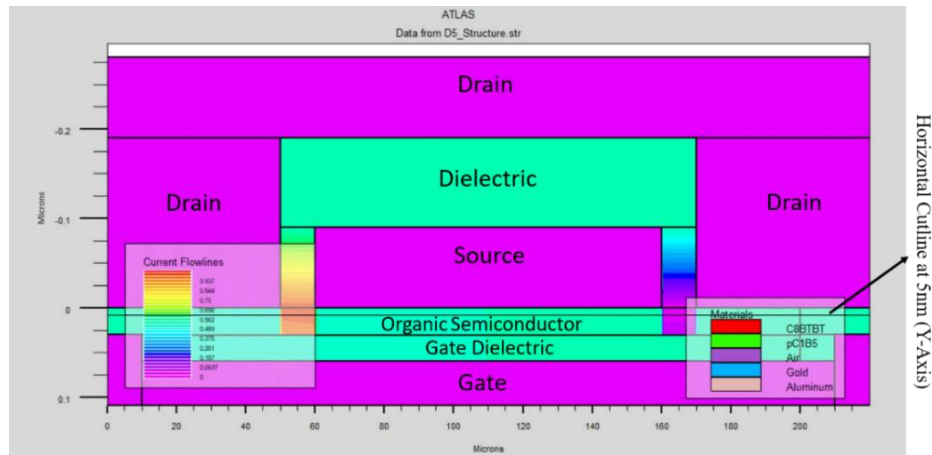


Fig. 3.10 Proposed vertical TFT structure (D₅) with a ditch in dielectric filled with organic semiconductor



(a)



(b)

Fig. 3.11 (a) Simulated structure of proposed device D₅ and (b) Current flowlines along with horizontal cutline

Table 3.7 consists of the materials and thickness of layers for D₂ and D₅ devices. Although, the thickness of gate dielectric is varied from 29 to 59 nm and gate from 50 to 80 nm due to the structural changes incorporated in D₅ device. Figures 3.11 (a) and (b) illustrate the device

structure and current flowlines in proposed VOTFT. It is evident from Fig. 3.11 (b), that the current density is much higher in case of device D₅ as compared with the D₂. The current voltage characteristics of device D₅ is shown in Fig. 3.12.

Table 3.7. Materials and thickness of different regions of D₂ and D₅

Layer	Material	Thickness (nm)	
		D ₂	D ₅
OSC	C8-BTBT	30	30
Source	Gold	90	90
Drain	Gold	90	90
Gate dielectric	pC1B5	29	59
Gate	Al	50	80

A comparison of the performance parameters of the two devices D₂ and D₅ is outlined in Table 3.8. It highlights that the proposed device exhibits I_{Dmax} and μ_{sat} as 528 μ A and 80.8 $\text{cm}^2/\text{V.s}$ which are higher by 2.38 and 2.67 times (approx.) than that of D₂ device. In the table, D₂* illustrates the performance of D₂ device wherein dielectric and gate layers are kept at 59 nm and 80 nm thickness, respectively. The dimensions of D₂* is similar to D₅ device. It is observed from the table that when both the devices have similar dimensions then performance of the proposed device D₅ is far better compared to the D₂*. Also, there is only slight variation in the performance of the device D₂* as compared with D₂.

Table 3.8. Parametric comparison for D₂ and D₅

Parameters	Device		D ₅ (Proposed)
	D ₂	D ₂ * (at gate= 80 nm, dielectric = 59 nm)	
Threshold Voltage V_t (V)	-0.9	-0.8	-1.5
Maximum Drain Current I_{Dmax} (μ A)	221	161	528
I_{on}/I_{off}	2.3×10^{10}	7.8×10^6	1.1×10^9
Saturation Mobility μ_{sat} ($\text{cm}^2/\text{V.s}$)	30.2	18.7	80.8

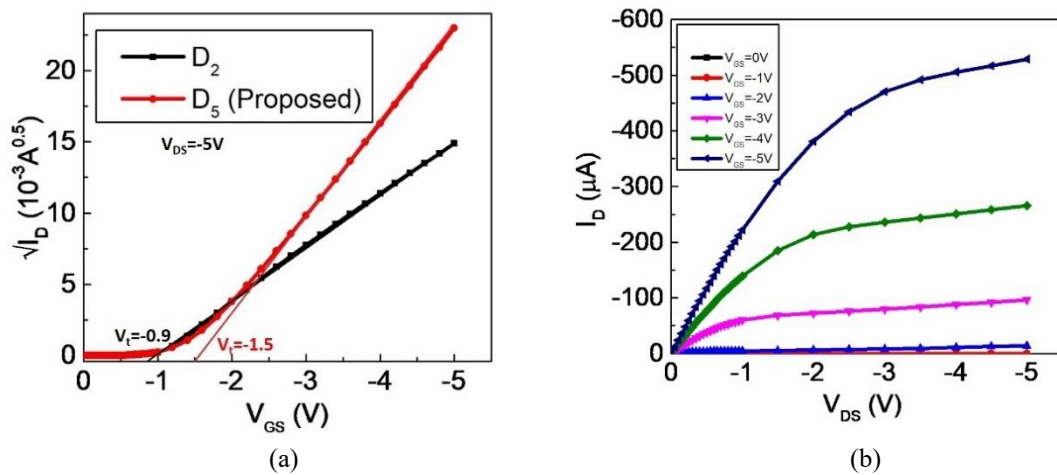


Fig. 3.12 (a) Comparison of transfer characteristics of D₂ and D₅ and (b) Drain characteristics of D₅ device

Figures 3.12 (a) and (b) show the transfer and drain characteristics of proposed device. Figure 3.12 (a) highlights a performance enhancement of device D₅ over D₂. The performance of the proposed novel structure (D₅) is significantly higher in comparison to other devices: D₁, D₂, D₃ and D₄ as shown in Fig. 3.12 (b). The higher performance of D₅ is probably owing to its ditch-based structure that leads to comparatively higher vertical electric field strength around the source contact resulting in a high charge carrier injection. In D₂, on applying negative potential at gate terminal, holes start accumulating towards the gate and the source side as their biasing is more negative compared to the drain. It can be seen in Fig. 3.4 that the complete channel is developing in both the directions (vertical and horizontal). Here, from source to OSC, the channel is strongly induced but it is comparatively weak as we move from OSC to drain due to the biasing. On the other hand, in case of D₅, the gate and the dielectric layers are twisted towards OSC which should result in additional charge carriers into the vertical channel created towards the drain side as well. This should enhance the current density and mobility of the proposed device. Two more vertical OTFTs; D₆ [242] and D₇ [243] are analysed to confirm the improved performance of proposed structure. Table 3.9 summarizes the performance of all six different vertical devices analysed with same materials and possible layer thickness.

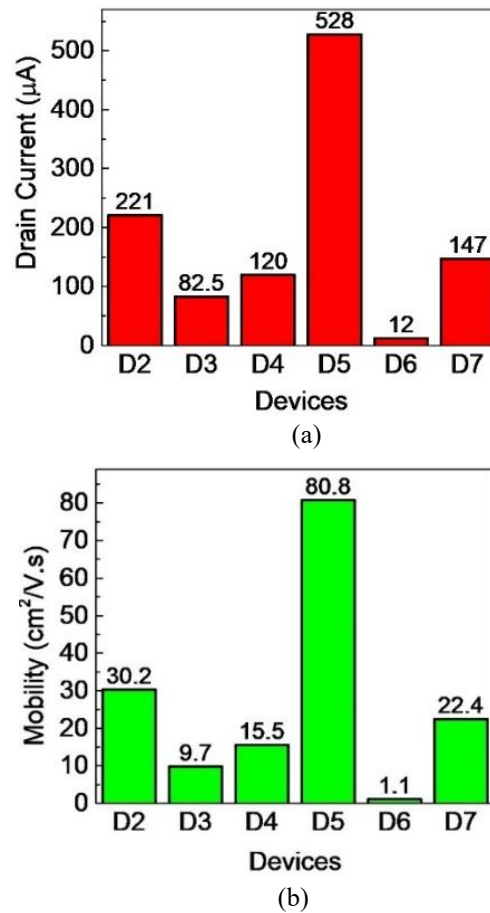
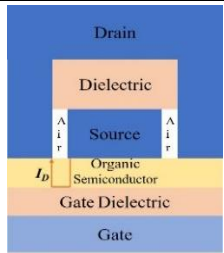
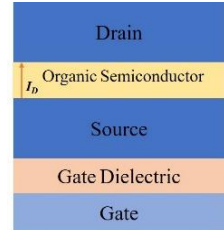
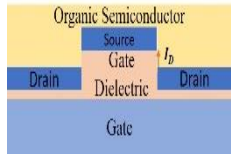
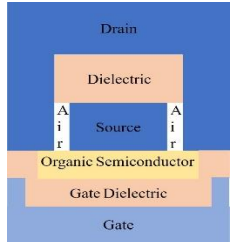
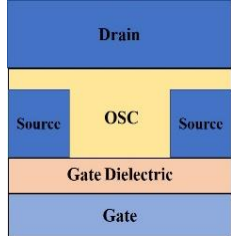
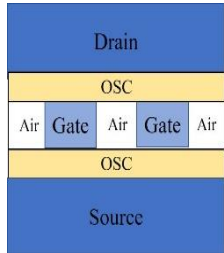


Fig. 3.13 Comparison of different vertical TFTs in terms of (a) Drain current and (b) Mobility

Table 3.9. Comparison of the proposed device D₅ with existing vertical devices (simulated at common platform)

Sr. No	Name	Different VOTFT Device Structures	Materials- (Source/Drain: Gold, Gate: Al, OSC: C8-BTBT, Gate Dielectric: pC1B5)			
			$V_{GS} = -5$ V and $V_{DS} = -5$ V			
			I_{Dmax} (μ A)	V_t (V)	μ_{sat} ($cm^2/V.s$)	I_{on}/I_{off}
1.	D ₂		221	-0.9	30.2	2.3×10^{10}
2.	D ₃		82.5	-1.7	9.7	0.8×10^{10}
3.	D ₄		120	-1.3	15.5	0.1×10^{11}
4.	D ₅		528	-1.5	80.8	1.1×10^9
5.	D ₆		12	-2.1	1.1	4.1×10^8
6.	D ₇		147	-1.6	22.4	3.4×10^7

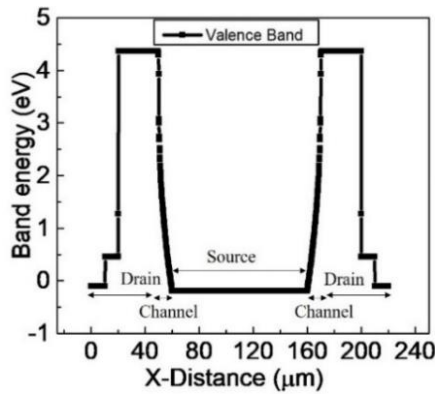
It can be observed from Table 3.9, that the proposed device exhibits the best performance as compared to the other vertical devices. To be precise, the drain current of the proposed device (D_5) is higher by 2.38, 6.4, 4.4, 44, 3.59 times on comparing with D_2 , D_3 , D_4 , D_6 and D_7 , respectively as depicted in Fig. 3.13 (a). Addition to this, the saturation mobility is 2.67, 8.32, 5.21, 73.45 and 3.6 times better than D_2 , D_3 , D_4 , D_6 and D_7 , respectively (Fig. 3.13 (b)).

3.5 INTERNAL CUTLINE ANALYSIS FOR THE PROPOSED DEVICE

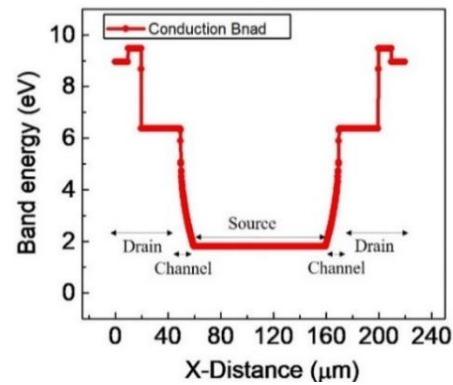
The present section discusses the internal analysis for device D_5 performed to better understand the device behaviour. The proposed TFT is analysed using horizontal and vertical cutlines to understand potential distribution inside the device, current density, band energy for conduction and valence band and hole concentration around the channel.

3.5.1 Horizontal cutline analysis

A horizontal cutline is undertaken at 5 nm below the source electrode where the channel formation takes place and maximum current density is observed as highlighted in Fig. 3.11 (b). All the parameters variation along the X axis are then observed. Figures 3.14 (a) and (b) depict the energies of valence and conduction band, respectively. A high variation in the energy levels of the conduction and valence band is observed in the channel regions. It is much higher as compared to the device D_2 as highlighted in Fig. 3.7 (b). This observation supports the previously derived assumption that there is a stronger gate control for the device D_5 owing to the ditch type gate structure. Additionally, it highlights a strong accumulation of charge carriers in the region towards the drain electrode as well, which was lower in case of D_2 . Owing to the strong gate control in the channel region, a high electric potential and current density is also observed in the region as highlighted in Figs. 3.14 (c) and (d), respectively.



(a)



(b)

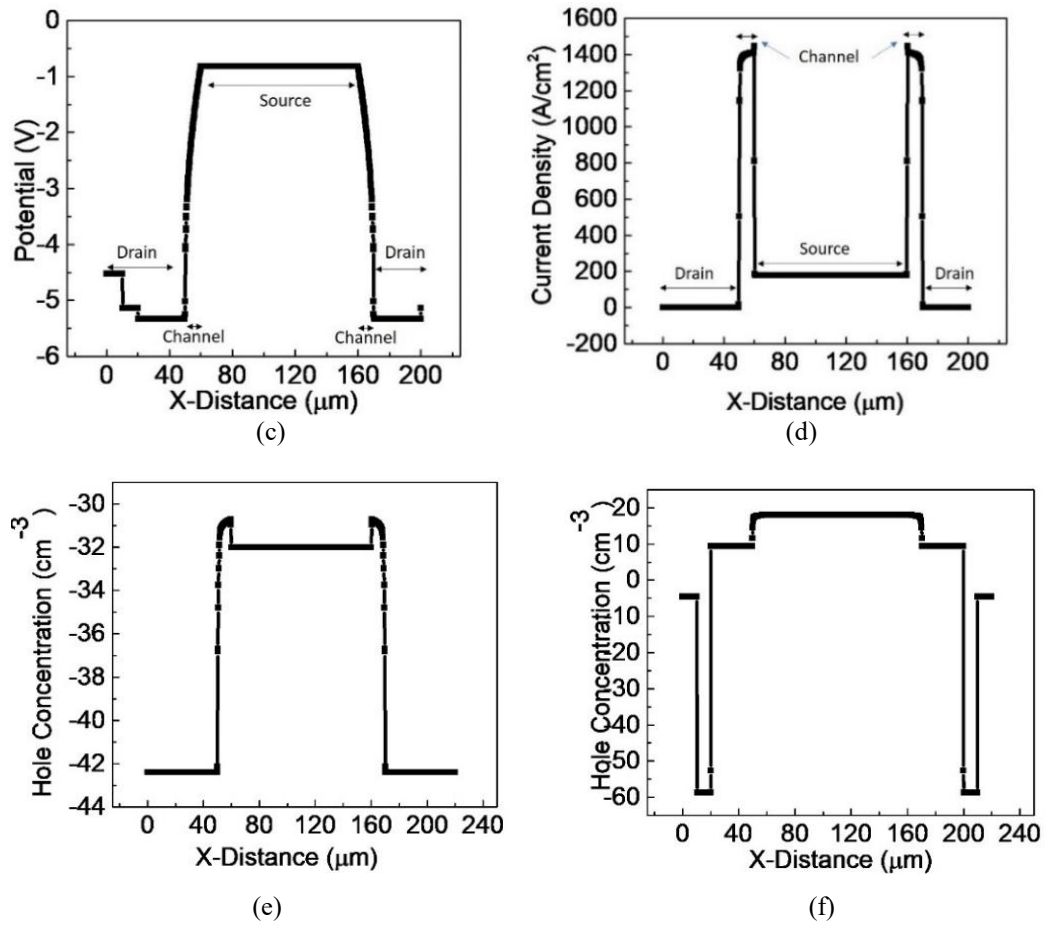


Fig. 3.14 Horizontal cutline analysis of (a) Valence band, (b) Conduction band, (c) Potential distribution (d) Current density of D₅ Device (e) Hole concentration of D₂ and (f) Hole concentration of D₅

It can be observed from the figure that potential is lower at source (-1 V) and is higher (~-5 V) at drain electrodes. The device has achieved the maximum current density at the channel with a value of 1451 A/cm². Furthermore, Figs. 3.14 (e) and (f) demonstrate the hole concentration in D₂ and D₅ devices, respectively. From the figures, it is clear that the ditch structure results in better accumulation of the charge carriers near the source. On the other hand, a steep fall in the hole concentration signifies that holes are being rapidly extracted due to the better channel formation near the drain region. Hence, it is clearly understood from the above figures that the proposed structure (D₅) is exhibiting reasonably good performance as compared with D₂ device. The reason behind this performance enhancement can be attributed to the presence of the ditches type structure of gate dielectric and gate in the proposed device which improved the gate control and respectively the charge injection.

3.5.2 Vertical cutline analysis

A horizontal cutline analysis helps to investigate the variation within the device about a specific point, and is usually undertaken around the channel region. On the other hand, a vertical cutline

analysis helps us assuage the variation of parameters through the different layers of the transistor. Therefore, a vertical cutline is drawn at $X=58 \mu\text{m}$. This cutline analysis explores the information pertaining to the parameters; band energy, potential graph and current density within the different layers. Figures 3.15 (a) and (b) illustrate the band energies in terms of valence and conduction band, respectively, while Fig. 3.15 (c) shows the potential distribution of the device in vertical manner.

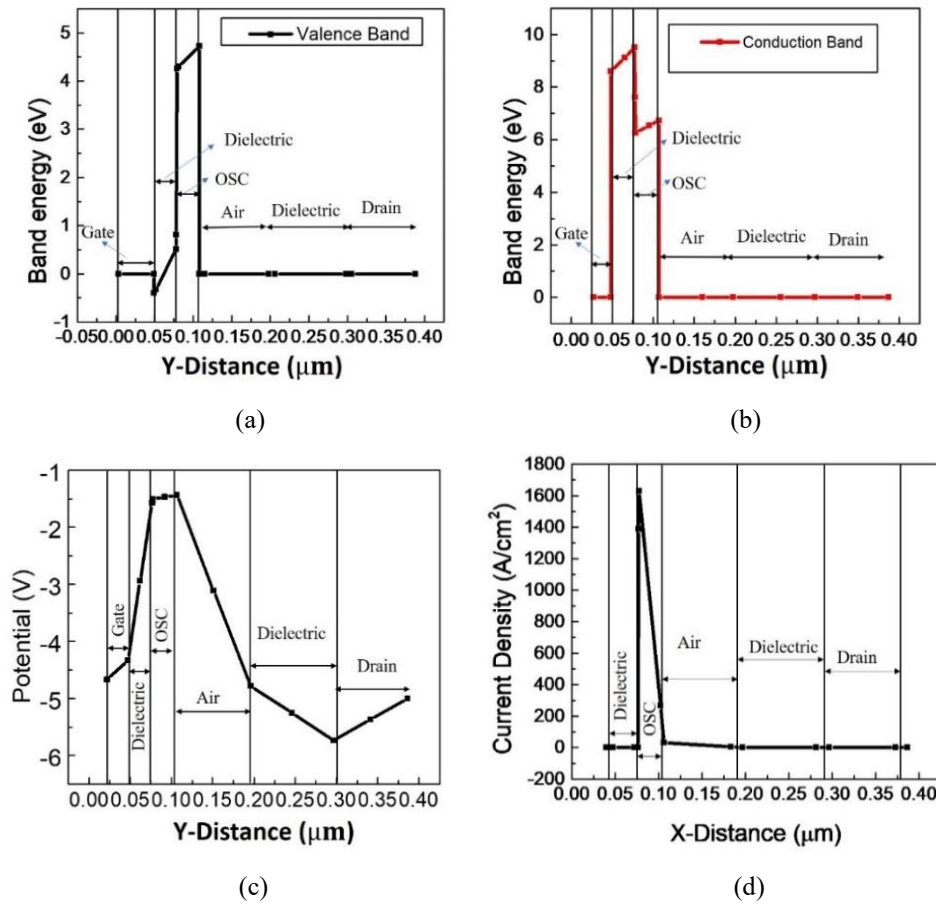


Fig. 3.15 Vertical cutline analysis of (a) Valence band, (b) Conduction band (c) Potential distribution and (d) Current density of D_5 Device

As already depicted through the horizontal cutline analysis, the vertical cutline analysis also highlights variation in band energy within the organic semiconductor layers where channel formation takes place (cutline at $X=58 \mu\text{m}$ is the channel region). Steep change in both valence and conduction bands is observed within the channel region. This results in higher gate control and thereby a high current density within the OSC as depicted in Fig. 3.15 (d). Almost negligible current density is observed in other layers, as current does not travel through dielectric layers. However, the potential varies throughout the different layers as highlighted in Fig. 3.15 (c). Maximum potential drop occurs at the dielectric region and a low potential is observed in all the other regions. Consequently, a stronger accumulation region is formed in

the vertical direction resulting in a stronger channel. Similar observations are taken from horizontal cutline analysis, wherein the results highlight ditch structure is creating a stronger channel.

3.6 SUMMARY OF THE RESULTS

The current chapter is focused on enhancing the performance of organic TFT by analysing the impact of the vertical channel structure and thereby proposing a novel vertical channel OTFT device. The different analysis results included herein highlights the role of vertical channel structure in improving the device performance. Further, the results highlight that the proposed vertical channel device D₅ depicts the improved performance owing to the better gate control over the channel region. Additionally, horizontal and vertical cut-line analysis is undertaken to better understand the device behaviour and facts for better performance. The results highlight that in vertical channel device; a short channel formation takes place. Additionally, two conducting channels are formed between source and drain contacts. This dual channel configuration results in higher charge carrier injection within the device which consequently reducing the threshold voltage. The important outcomes of the chapter are enlisted below.

- Firstly, a planar OTFT (D₁) is validated using Silvaco Atlas tool to set the boundary conditions and compared the performance with vertical channel OTFT (D₂). The I_{Dmax} , V_t and μ_{sat} are improved by 18, 2 and 9 times, respectively for D₂ in comparison to D₁.
- Internal device analysis is undertaken to understand the reasons for better performance. The results highlight that in vertical channel device D₂, small channel formation takes place. Additionally, owing to its structure, two channel are formed which results in higher charge carrier injection within the device and consequently reducing the threshold voltage.
- A novel vertical OTFT (D₅) is proposed and parameters; I_{Dmax} and μ_{sat} are obtained as 528 μA and 80.8 $cm^2/V.s$ which are higher by 2.38 and 2.67 times than D₂ device.
- Different vertical structures (D₃, D₄, D₆ and D₇) are analysed and compared with proposed device; D₅ to confirm the improved performance of proposed OTFT. The drain current of D₅ is higher by 2.38, 6.4, 4.4, 44, 3.59 times and mobility by 2.67, 8.32, 5.21, 73.45 and 3.6 times on comparing with D₂, D₃, D₄, D₆ and D₇, respectively.
- The proposed D₅ device exhibits reasonably good performance in terms of drain current and mobility as compared with other vertical devices. The reason behind this performance enhancement can be attributed to the presence of the ditch type structure of gate dielectric

and gate in the proposed device which improved the gate control and respectively the charge injection.

- The behaviour of the proposed device in terms of potential distribution inside the device, current density, band energy for conduction/valence band and hole concentration around the channel is explored using horizontal and vertical cutlines.
- Higher accumulation of charge carriers towards the drain region is observed in D₅ as compared with the D₂ device. Additionally, an increase in potential and current distribution is also seen within the device. This increment is all possible due to higher charge carrier accumulation in the proposed structure. This analysis highlights the role of ditch type gate & dielectric structure (device D₅) in forming a strong gate control on the vertical channel formation.

The present work depicts the performance improvement in the device in terms of I_{Dmax} and μ_{sat} with the utilization of vertical channel structure. However, mobility of TFT devices still is one parameter which requires more attention as it governs switching characteristics and circuit performance. Therefore, further focus can be towards exploring organic semiconductor materials that can illustrate a high mobility. Moreover, research can focus on device fabrication methodologies that can reduce the interfacial traps and injection barrier for the charge carriers. These aspects can significantly improve the mobility thereby improving the device performance.

CHAPTER-4

CHARACTERISTICS PERFORMANCE ANALYSIS OF IMPROVED MULTILAYERED OLED AND OPD DEVICES

4.1 INTRODUCTION

The OLEDs based full color displays with high resolution have been developed by many researchers [15, 16]. These organic materials-based displays have various attractive features specifically flexibility, light weight, fast response, easy fabrication, and wide viewing angle [17]. However, a scope of improvement for current density, luminescence and lifetime still exists. Similarly, researchers have done a lot of efforts in developing high performance wavelength detectors and thus OPDs (Organic Photo-Detectors) are widely explored [32-35]. These detectors depicted a significant performance improvement over the span of years, still there is the possibility to further augment their performance in terms of photo current and dark current.

OLED and OPD devices work on different principals and illustrate interaction with light in different manners, however, researchers have tried similar methodologies to enhance their performance. With an aim to use both these devices in cohesion for biomedical applications, the present chapter focuses on utilizing similar methodologies for enhancing the performance of these devices, specifically by improving current and luminance in OLEDs and optimizing dark current and photocurrent in OPDs. This aspect also helps in looking into the possibility of fabricating these devices on a single substrate, as well.

Recently, it has been observed that various researchers have investigated the display devices and improved them by adding additional layers; electron/hole transport layer, electron/hole injection layer, and hole blocking layer [126, 134]. Addition of these layers successfully addresses the basic issues of low charge injection and electrode quenching and thus are liable for improving the device performance significantly [18]. The role of these layers is limited to support the existing charge carrier in terms of their movement. The injection layer enhances the carrier injection by reducing the gap between their energy levels and work function of the electrode. However, the transport layers help in carrier movement. While the blocking layer prevents the charge carriers escaping from the emission layer. All these layers are influential in improving the device performance and thus researchers showed their interest in defining novel layers, such as; mixed interlayer and spacer layer [23, 25] that are utilized in OLEDs for further controlling the movement of charge carriers.

In a broad sense, mixed interlayer balances the mobility of electrons and holes, before the emission layer (EML) to enhance the recombination. On the other hand, spacer layer is used to slow down the charge carriers to prevent carrier quenching at the electrode. It is observed that performance enhancement in these devices cannot be addressed by only controlling the movement of charge carriers. Their generation and concentration within the device are equally important. Hence, charge generation layer is being investigated [24] for this purpose. In this chapter, the role of CGL is examined for the improvement of luminescence and current density in OLED and OPD devices. Thus, to design CGL based novel OLED and OPD, the following objective is framed:

“Investigation of charge generation layers and positional analysis for performance improvement of OLED and OPD devices.”

The following methodology is used to obtain above mentioned objective:

- Validation of a reference blue OLED using Silvaco Atlas simulator to set the boundary conditions for device in terms of materials, structure and layers' dimensions.
- Analyse the performance of OLED based on the position variation of CGL and further design a novel OLED structure for performance improvement.
- Cut-line analysis to understand its internal physics and comprehend the facts for change in device performance with respect to layers' materials and their variation.
- Validation of a reference OPD using Silvaco Atlas simulator and design an improved OPD based on similar methodology utilized for OLED performance enhancement.
- Analyse and compare different possible structures of OPD for the performance enhancement and explore the device internal physics.

The aim of this chapter is to enhance the performance of OLED and OPD devices to enable their potential use in biomedical applications. The primary focus is on enhancing the OLED emission which is the guiding factor in all light-based fluorescence detection and to design the OPD device to discriminate the wavelengths and produce the corresponding current. Additionally, it is preferable to develop both the devices on a single substrate. Therefore, in the present chapter a novel CGL based OLED is proposed for enhancing the device performance in terms of current and luminescence. Similarly, OPD structure is also changed to enhance its performance. However, same CGL based methodology is adopted for enhancing the OPD performance as that utilized for OLED. This opens the possibility of developing both the devices on a single substrate with minimum variation in fabrication methodologies.

This chapter is arranged in total nine sections. The introduction is included in Section 4.1, wherein basic discussion of OLED and OPD devices is provided with the introduction of work undertaken in the present chapter. In Section 4.2, a reference multi-layered OLED device is analysed to set the boundary conditions. This is followed by incorporating CGL in the OLED structure and its positional analysis in Section 4.3. Thereafter, in Section 4.4, a novel CGL based OLED device is proposed and its in-depth internal analysis is performed. Further, the thickness optimization for CGL layer is carried out in section 4.5. This is followed by validation of a reference OPD device is validated in Section 4.6. Afterwards, CGL based OPD is proposed in section 4.7. This section also compares the proposed OPD device with other OPD structures and conducts a thickness optimization for CGL layers. In section 4.8 an in-depth internal analysis is undertaken for the proposed OPD. Finally, concluding remarks of the work are enlisted in section 4.9.

4.2 CHARACTERISTIC ANALYSIS AND PARAMETERS EXTRACTION OF MULTILAYERED OLED

To analysis the performance of OLED, firstly, an experimentally fabricated device by Titov *et al.* [38], is validated using Silvaco Atlas simulator and named as device L₁. In this device, seven layers including cathode, anode, ETL, HTL and EML are used as shown in Fig. 4.1. The length and width of the device are of 400 and 1000 μm , respectively. The device consists of an anode followed by a 90 nm HTL of PEDOT:PSS. On top of this, a second HTL of NPB (60 nm) is placed. The emissive layer (20 nm) comprises DPVBi doped with 5% BCzVBi material for blue light emission. Above the EML, a 30 nm layer of BPhen (4,4'-Bis(9-ethyl-3-carbazovinylenes)-1,1'-biphenyl) material serves as both the HBL and ETL. Afterwards, a two layers cathode is formed with 1 nm of LiF (Lithium Fluoride) and 150 nm layer of Al. The materials along with thickness for this multilayered blue OLED are summarized in Table 4.1.

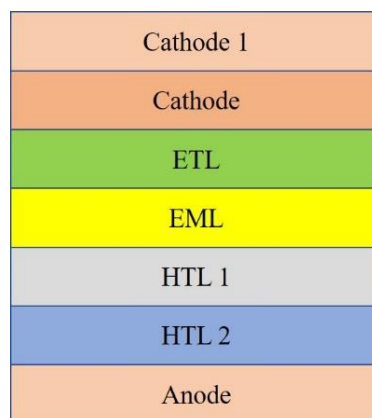


Fig. 4.1 Structure of multilayered OLED device (L₁)

Table 4.1. Materials along with their thickness for each layer used in L₁ device

Layer	Material	Thickness (nm)
Cathode1	Al	150
Cathode	LiF	1
ETL	BPhen	30
EML	DPVBi & BCzVBi	20
HTL1	NPB	60
HTL2	PEDOT:PSS	90
Anode	ITO	20

In OLED, the generation of light is achieved with two important processes: 1) formation of charge carriers, and 2) recombination of charge carriers. This is achieved by using Langevin recombination rate model in Silvaco Atlas 2-D device simulator for the validation of the reference device.

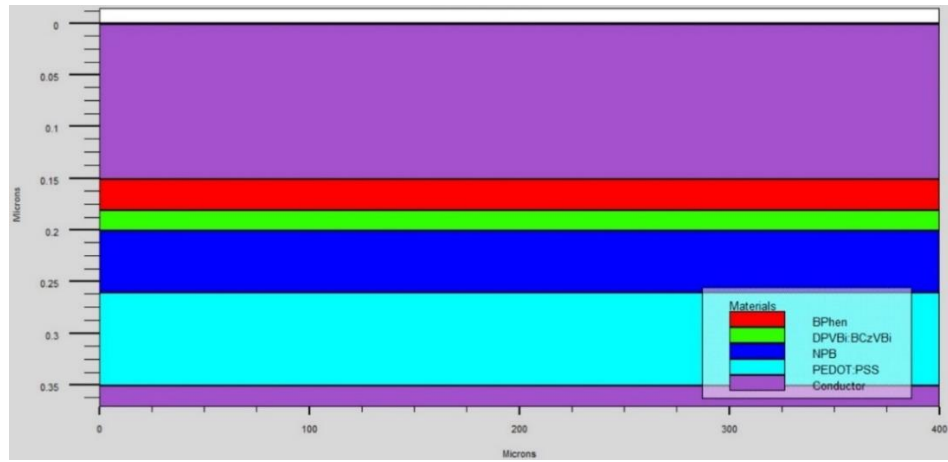


Fig. 4.2 Simulated structure of OLED L₁ showing the thickness of different materials used in the device

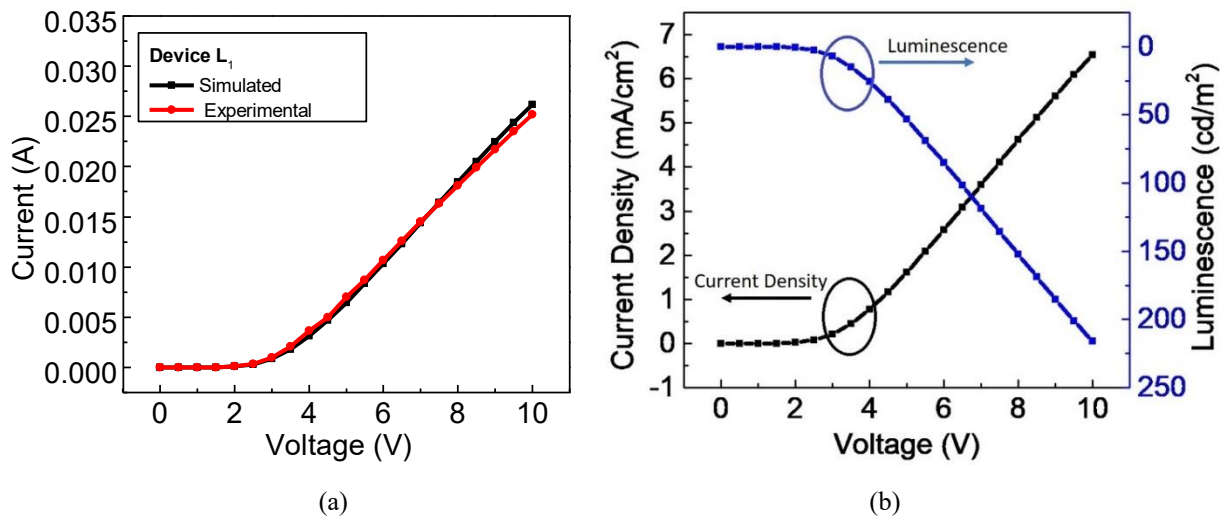


Fig. 4.3 (a) Comparison of current for existing experiment and simulated device and (b) Combined curves of current density and luminescence for L₁

The expression for the model is as follows:

$$R_L(n, p) = r_l(x, y, t) (np - n_i^2) \quad (4.1)$$

Here, r_l , n , p and n_i denote the recombination rate coefficient, electron concentration, hole concentration, and intrinsic concentration, respectively. In addition to this, to simulate the carrier's transportation in a device structure, Poole-Frenkel mobility model is used which was given by Frenkel in 1938. This model is discussed in detail in the previous chapter. The simulated device structure is depicted in Fig. 4.2.

The curves in Fig. 4.3 (a) illustrate the current characteristics of OLED device (L_1). The current values are observed as 0.025 A for existing experiment OLED and 0.026 A for simulated device with fairly a close match. This validation of results is necessary to set the boundaries for the simulation keeping empirical parameters into the consideration. Also, Fig. 4.3 (b) depicts the combined curves for luminiscence and current density for L_1 . The maximum luminescence and current density are obtained as 215 cd/m² and 6.5 mA/cm², respectively.

4.3 PERFORMANCE ANALYSIS WITH CGL AT DIFFERENT POSITION FOR OLED

The CGL is very useful for improving the concentration of charge carriers which can further enhance the luminescence properties and current of OLED device. Through the recombination process, the OLED can generate maximum of 30% efficiency, while rest carriers are lost due to different processes. Additionally, the generated photons do not always escape from the device and are lost due to optical losses and Plasmon [244]. With the utilization of CGL, the charge carrier generation is enhanced resulting in higher carrier density and thus higher output which further enhances the electro luminescence emission and efficiency [244] of the device.

In the present work, the used CGL is a combination of two different types of semiconducting layers; p type & n type, for injecting holes and electrons, respectively. These carriers get injected towards emissive layer where the photons are generated after the recombination. Here, TAPC (1,1-bis[(di-4-tolyamino)phenyl]cyclohexane) and HAT-CN (1,4,5,8,9,11-hexaazatriphenylene-hexacarbonitrile) materials are incorporated as top and bottom layers for CGL. These two layers are selected based on their HOMO and LUMO level aligning with the other layers of device L_1 . Further, the device is analysed based on placement of CGL at different positions while materials and thickness of the layers do not change. Here, four blue OLEDs L_2 ,

L₃, L₄ and L₅ are considered in which a CGL is incorporated at different positions as depicted in Figs. 4.4 (a), (b), (c) and (d), respectively.

The combined layer of HAT-CN and TAPC acts as the electron and hole injector, respectively, owing to the favorable alignment of their HOMO and LUMO energy levels with those of the adjacent layers in device L₁. In devices L₂ and L₃, CGL is placed below the cathode and above the anode, respectively. On the other hand, in device L₄, it is placed near both electrodes (above the anode and below the cathode). Furthermore, in device L₅, CGL is kept inside the emissive layer, as depicted in Fig. 4.4 (d). The thickness of EML in L₅ is taken as 40 nm, as CGL needs to be incorporated within the EML. All these four devices (L₂- L₅) are compared based on current density and luminescence with respect to reference device L₁.



Fig. 4.4 Different OLED structures based on positional variation of CGL (a) Below cathode (L₂), (b) Above anode (L₃), (c) Both sides of device (below cathode and above anode) (L₄), and (d) Inside emissive layer (L₅)

Figures 4.5 (a) & (b) demonstrate current and luminescence parameters of all these devices (L_1 - L_5). Both the figures depict the similar trends for these five devices. As shown in Fig. 4.5, device L_5 outperforms among these devices as CGL is placed inside of emissive layer which improves the recombination of charge carriers. In the device L_5 , the top layer of CGL (of TAPC) acts as hole injector and bottom layer (of HAT-CN) as electron injector. Now, holes in top layer of CGL get attracted towards cathode and reach to emissive layer. Similarly, electrons in bottom layer of CGL get attracted towards anode and reach to emissive layer as CGL in L_5 is surrounded by the emissive layer only. These charge carriers are mixed up with charge carriers which have travelled from cathode and anode side. This automatically enhances the recombination rate of the device. The maximum current and luminescence are obtained as 0.27 A and 2277.2 cd/m^2 , respectively as mentioned in Table 4.2.

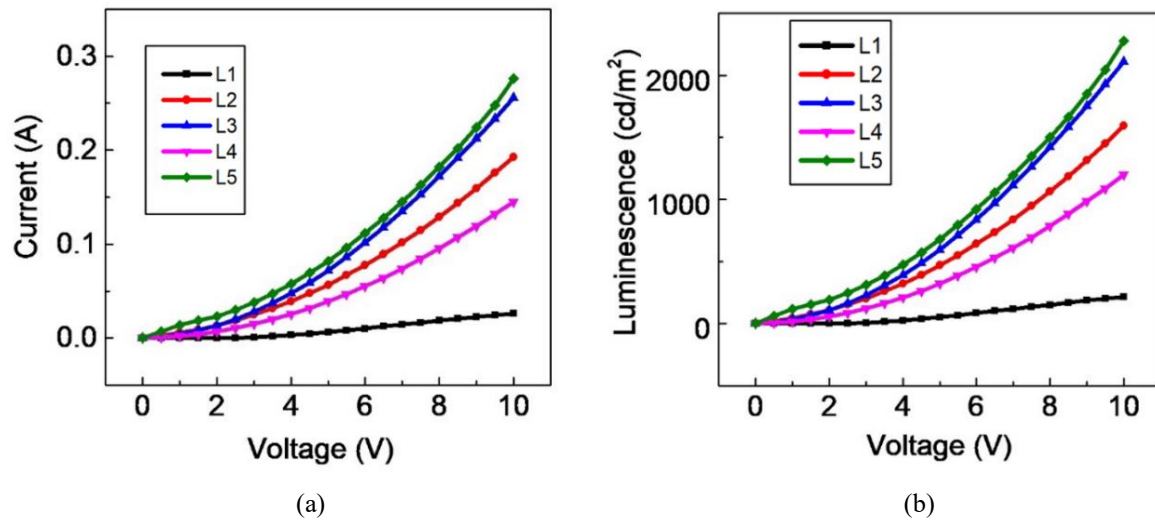


Fig. 4.5 Comparison of (a) Current and (b) Luminescence for L_1 - L_5 devices

Table 4.2. Comparison of current and luminescence for different OLEDs (L_1 - L_5)

Device	Current (A)	Luminescence (cd/m^2)
L_1	0.026	215.9
L_2	0.193	1592.3
L_3	0.256	2112.2
L_4	0.145	1198.4
L_5	0.276	2277.2

As compared to L_5 , other devices exhibit CGL on either side of emission layer. Therefore, on biasing, CGL can inject only one type of charge carrier in the EML. Also, the applied bias forces the other type of charge carrier towards the nearest electrode, and the observed effect is particularly pronounced in devices L_2 and L_3 . Still these devices illustrate satisfactory performance in terms of current and luminescence as compared to device L_4 . The performance of device L_4 is quite unexpected as CGL is used in two different positions. Therefore, a high

carrier concentration of both types was expected in the device. The possible reason for the lower performance of this device is probably increased device dimension [24]. Consequently, a longer distance is required to be covered by the charge carriers in reaching the emission layer leading to a lower performance.

4.4 PROPOSED NOVEL OLED DEVICE

In the previous section, it is shown that among all five devices (L_1 - L_5), the L_5 depicts reasonably good performance as shown in Fig. 4.5. This highlights the importance of CGL and its placement at an appropriate position for device performance enhancement. Therefore, in this section, a novel high-performance blue OLED is proposed, wherein the position of CGL and emissive layers is reversed to that of device L_5 as illustrated in Fig. 4.6. This device is named as L_6 and here the position of top and bottom CGL layers is also interchanged.

Now, the top layer of CGL is made of HAT-CN and bottom layer of TAPC materials. Thus, the electrons generated in top CGL layer are repelled by the cathode and are forced towards the emissive layer. In the similar manner, holes generated in bottom CGL layer will be repelled by anode and move towards the emissive layer. So, electron and hole concentrations are increased inside the emissive layer. The movement of charge carriers generated from the electrodes is supported by CGLs as the HOMO and LUMO levels of the adjacent layers are more properly aligned in the device.

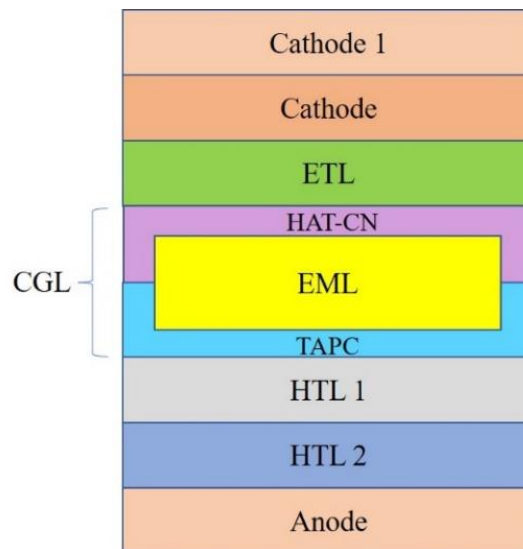


Fig. 4.6 CGL based proposed OLED device (L_6)

The addition of CGL enhances the charge carrier density of both type of carriers in the device. According to the Langevin's theory, recombination rate is directly proportional to the probability of charge carriers finding each other in organic materials. Hence, with increased

charge carrier concentration, the probability is highly increased. Therefore, this structure directly improves the recombination rate which significantly enhances the performance of L_6 in terms of current and luminescence. The simulated structure of L_6 is shown in Fig. 4.7. The thickness of EML is kept at 20 nm like reference device. The maximum current and luminescence of proposed device is obtained as 0.44 A and 3636.3 cd/m^2 . The device exhibits reasonably improved luminescence and higher by 16.8, 2.3, 1.7, 3.0 and 1.6 times than that of L_1 , L_2 , L_3 , L_4 and L_5 , respectively.

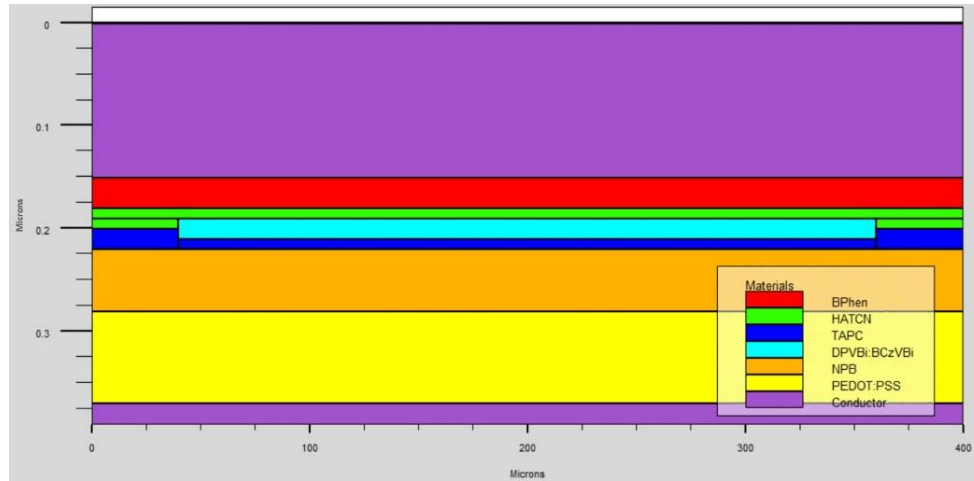


Fig. 4.7 Simulated structure of L_6 showing the thickness of different materials

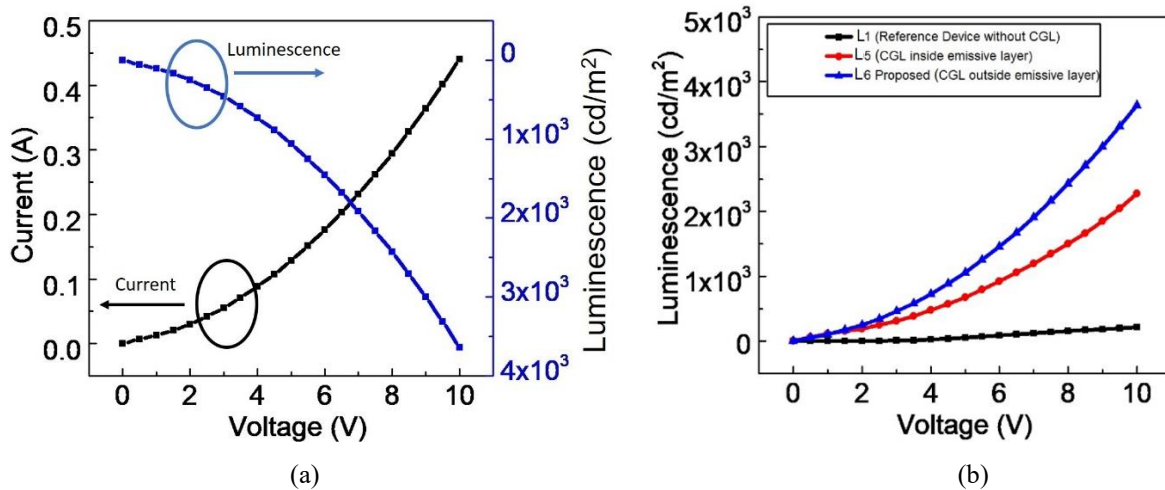


Fig. 4.8 (a) Combined curves of current and luminescence for proposed device (L_6) and (b) Variation of luminescence with respect to voltage for L_1 , L_5 and L_6

The figure 4.8 (a) illustrates current and luminescence for the device L_6 . These values are better than the preceding devices. A comparison between the reference device L_1 and CGL based devices L_5 and L_6 is also highlighted in Fig. 4.8 (b). The proposed device L_6 outperforms owing to the high electron and hole concentration within the device due to the better positioning of the CGL. Therefore, to validate the inference that optimized CGL positioning enhances charge

concentration and device performance, internal analysis is undertaken in the following subsections.

4.4.1 Internal analysis of OLED devices

In this section, all the mentioned OLED devices are analysed in-depth to better understand the device physics. This internal analysis is performed by drawing a cutline on the device in horizontal and vertical manner. All the devices are analysed in terms of different internal parameters including hole/electron concentration, recombination rate and electric field distribution within the device. The variation of these parameters in the devices will help in understanding the factors responsible for their respective performance.

a. Vertical Cutline Analysis

OLED is a device wherein different layers are stacked one over the other, therefore, it is more appropriate to conduct a vertical cutline analysis first. The vertical cutline so drawn passes through each layer and analyse the changes encountered in different parameters. Hence, in this sub-section, a vertical cutline is performed on the simulated structures of all the six devices at 200 μm as shown in Fig. 4.9. Here, different internal device parameters that are instrumental for OLED working are examined. These include hole concentration, electron concentration, total current density, Langevin recombination rate, conduction current density, and electron affinity.

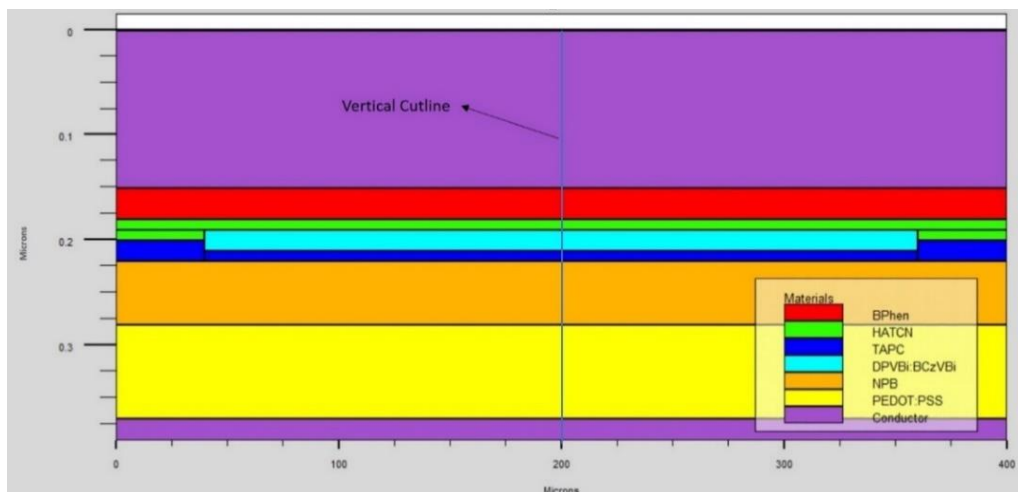


Fig. 4.9 Vertical cutline at 200 μm inside proposed device (L_6)

Figure 4.10 shows the graphs for charge carrier concentrations, current density, and Langevin recombination rate. Here, it is observed that the hole concentration is higher at bottom side of the devices between 0.18 μm - 0.36 μm . This region is towards the anode along with layers responsible for hole injection. Therefore, when holes travel from anode side towards the EML,

a high hole concentration is observed. Thereafter, the hole concentration falls drastically. Similar observations are made for the electron concentrations from Fig. 4.10 (b). Here, the electron concentration is higher towards the cathode side till the emission layer and thereafter, there is a steep fall. The most probable reason for the change in carrier concentration can be attributed to the recombination process taking place within the emission layer [23, 25].

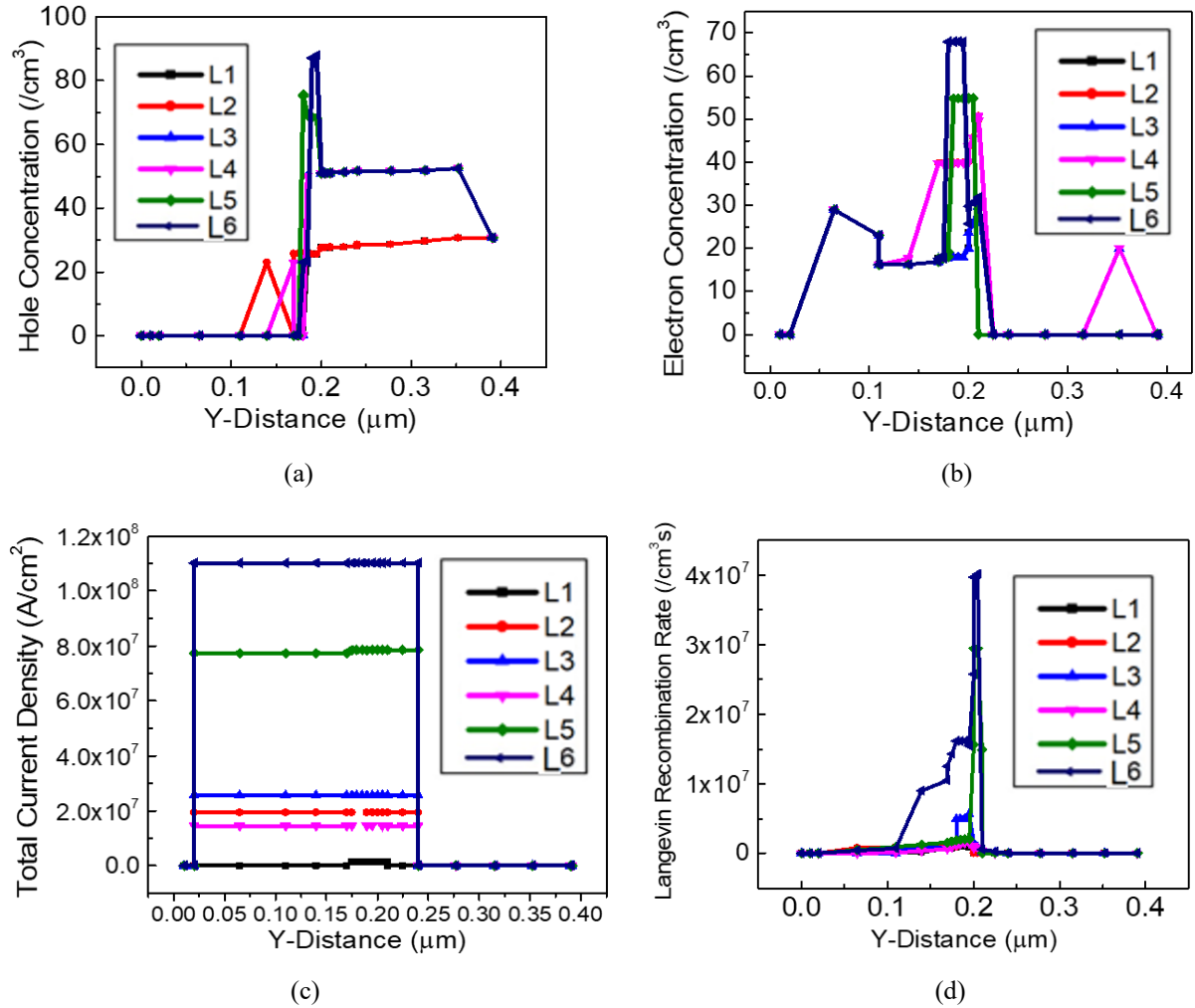


Fig. 4.10. Performance comparison of all six OLED devices (L₁-L₆) using vertical cutline in terms of (a) Hole concentration, (b) Electron concentration, (c) Total current density, and (d) Langevin recombination rate.

The minimum and maximum carrier concentration values for both types of charge carriers are exhibited by L₁ and L₆ devices, respectively as shown in Fig. 4.10 (a) and (b). In all the cases, it is maximum near the emissive layer where holes and electrons are accumulated eventually for the recombination process. Thereafter, a fall indicates that these carriers are recombining in the EML. The hole concentration of L₆ is obtained as three times higher than L₁ owing the incorporation of CGL outside the emissive layer. The small peaks around 0.1 to 0.2 μm at the cathode side for devices L₂ and L₄ highlight the presence of TAPC that acts as the hole

generation layer. Similar peak is observed for L₄ in terms electron concentration due to the presence of HAT-CN, an electron generation layer.

Further, on observing Figs. 4.10 (a) & (b)), it is seen that L₅ and L₆ represents the highest charge carrier concentration within the emission layer at nearly 0.2 μm . For other devices, such high charge carrier concentration is not observed around the EML. The primary reason for this is the presence of CGL within emission layer or right outside the EML in case of L₅ and L₆, respectively. Otherwise, even for both these devices, between the electrode and emission layer, the charge carrier concentration is similar to other devices. This proves the assumption that CGL is creating extra charge carriers and these are being effectively injected within the emission layer. Additionally, L₆ offers higher carrier concentration as compared to L₅, because in L₆, the applied biasing is helping CGL in injecting both types of carriers directly in EML, whereas in case of L₅, this is not the case.

Furthermore, Fig. 4.10 (c) shows the current density for the devices (L₁- L₆). The proposed device exhibits the highest current density which is almost 73, 5.7, 4.4, 7.8 and 1.4 times higher than L₁, L₂, L₃, L₄ and L₅, respectively. This is because of higher electron/hole concentration in L₆ as discussed above. The generation of additional charge carriers are responsible for higher recombination, but at the same time excess charge carriers are reaching the opposite electrode resulting in higher current density. The proposed device also depicts a high Langevin recombination rate as illustrated in Fig. 4.10 (d). In this figure, it is observed that recombination peaks are achieved around 0.2 μm as this area belongs to emissive layer. As per the Langevin theory, for the materials with low mobility, the recombination rate is governed by the probability of opposite carriers finding each other. The materials TAPC and HAT-CN inject the charge carrier (holes & electrons) directly from the outside of EML which automatically improves carrier concentration within the device and consequently improves the Langevin recombination rate of the proposed device.

Furthermore, Fig. 4.11 (a) shows the potential distribution of the proposed device (L₆). In this figure, the voltage is maximum at 0.4 μm i.e. towards anode and it keeps decreasing towards cathode and becomes zero. This represents that the entire applied voltage gets dropped effectively across the device and helps in the different processes within the device. Next, Figs. 4.11 (b), (c) and (d) depict a comparison in terms of conduction current density, electron affinity and acceptor trap ionized density for L₅ and L₆. The conduction current is higher in case of L₆ as a large amount of charge carriers are travelling from electrode towards the emission layer.

Additionally, when the charge carriers are injected from the CGL, a high concentration of electron and holes is present around the emission layer on the corresponding sides. The presence of these charge carriers also creates an inbuilt potential within the device, that further supports carrier injection from the respective electrodes. Additionally, a high electron affinity is observed for L₆ as compared to L₅ as depicted in Fig. 4.11 (c). The higher electron affinity further strengthens the fact that the inbuilt potential within the device due to accumulation of carriers injected by the CGL enhances the movement of electrons within the device.

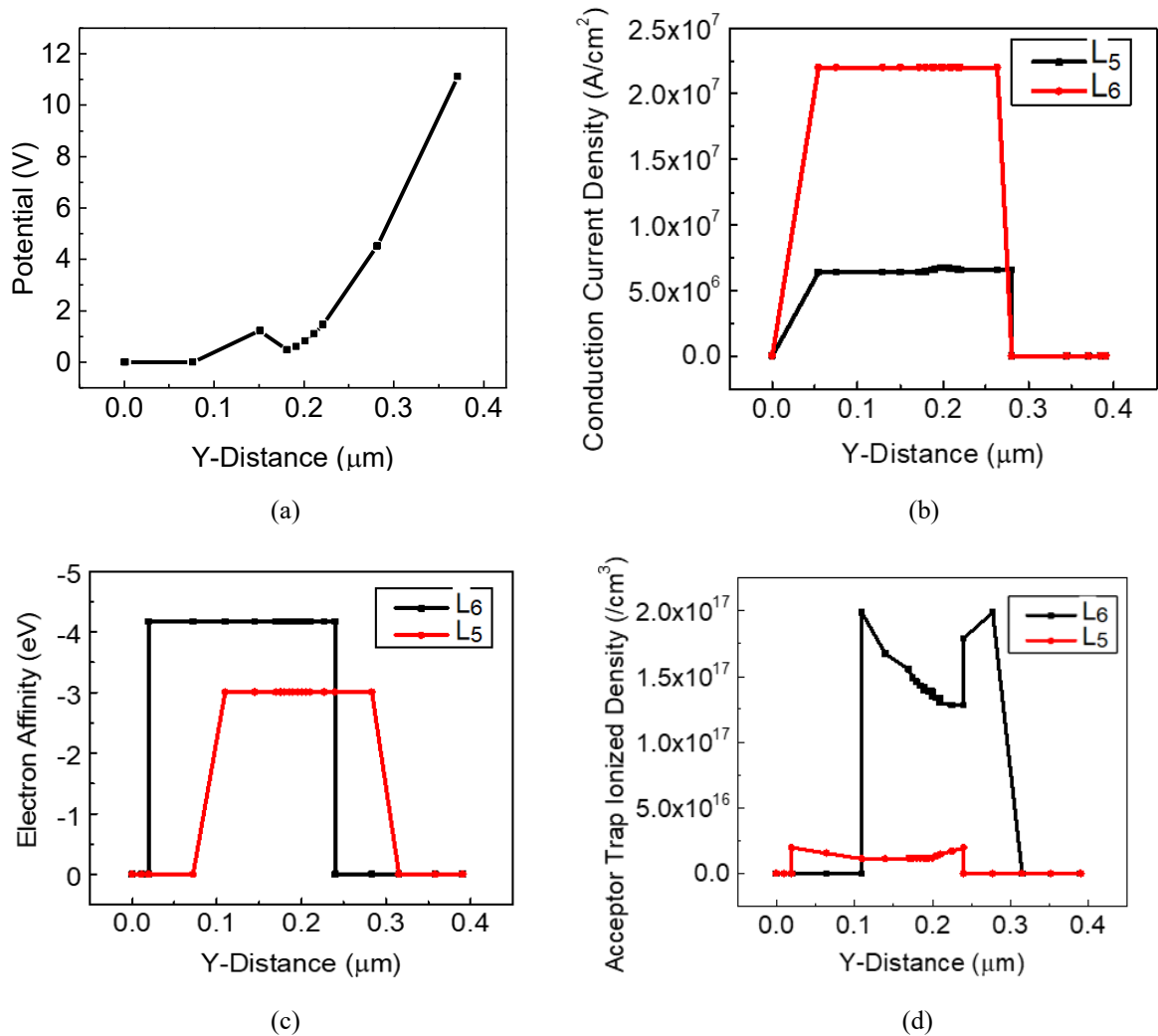


Fig. 4.11. (a) Potential distribution of the proposed device (L₆), Comparison of devices L₅ and L₆ based on (b) Conduction current density, (c) Electron affinity and (d) Acceptor trap ionized density.

b. Horizontal Cutline Analysis

Here, a comparison of the parameters is highlighted by performing a horizontal cutline inside the CGL towards cathode and anode.

Cutline analysis inside CGL towards cathode: In this case, a horizontal cutline is drawn at $0.195\ \mu\text{m}$ in both L_5 and L_6 devices as depicted in Fig. 4.12. The parameters; Langevin recombination rate, conduction current density, conduction band, valence band, and hole QFL (quasi-Fermi level) are examined to understand the performance comparison of L_5 and L_6 devices. The peak Langevin recombination rate for L_6 is improved by 10 times as compared to L_5 as depicted in Fig. 4.13 (a).

A high recombination rate is observed at the edges of emission layer for L_6 , highlighting that electrons entering from HAT-CN are readily combining with the holes in the emission layer. On the contrary, TAPC layer is present at this position in device L_5 and it is in the middle of emission layer. Similar observations are made but this time high recombination is observed at the interface of EML and TAPC in the middle rather than the corner. Additionally, the recombination rate is much lower in L_5 as compared to L_6 due to lower carrier concentration. Additionally, as holes are injected in the EML from TAPC, these get attracted towards the electrode due to applied bias.

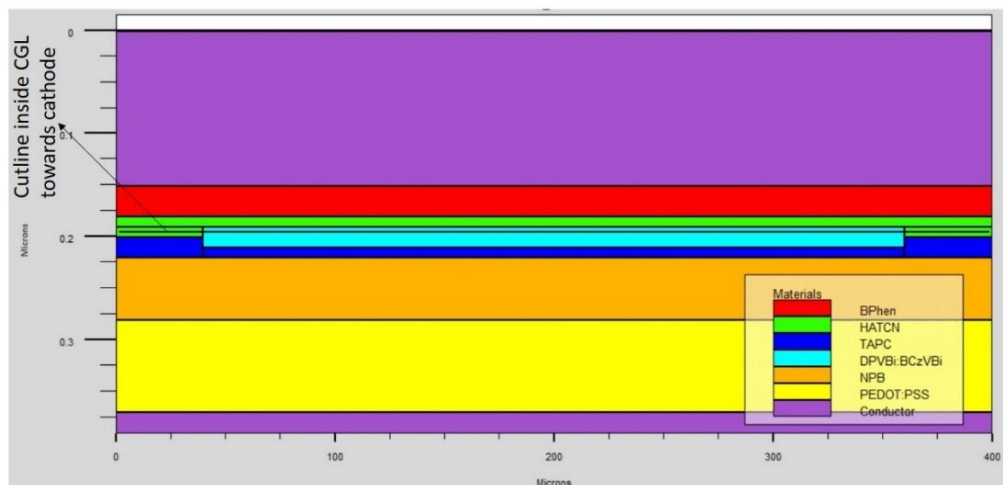


Fig. 4.12 Horizontal cutline drawn towards cathode at $0.195\ \mu\text{m}$ in proposed OLED device (L_6)

Similarly, the conduction current density of L_6 is enhanced by eight times than L_5 , as illustrated in Fig. 4.13 (b). This enhancement in current density is the direct consequence of higher charge carriers present in the device L_6 as compared to L_5 due to the reversal of CGL. Additionally, in device L_6 , charge carriers generated in CGL also help inject more charge carriers by creating an internal potential, thereby further increasing the current density in the device. Furthermore, band energies are also shown in Figs. 4.13 (c) and (d) for devices L_5 and L_6 , respectively. The band energies of L_5 are much lower as compared to device L_6 which helps in injection of holes in the device. However, the TAPC layer prevents a good electron injection due to higher LUMO

level, resulting in lower recombination. On the other hand, device L₆ shows a higher valance band energy, enabling further ease in hole injection. Thus, with the higher charge carrier concentration, a high recombination in the device is expected.

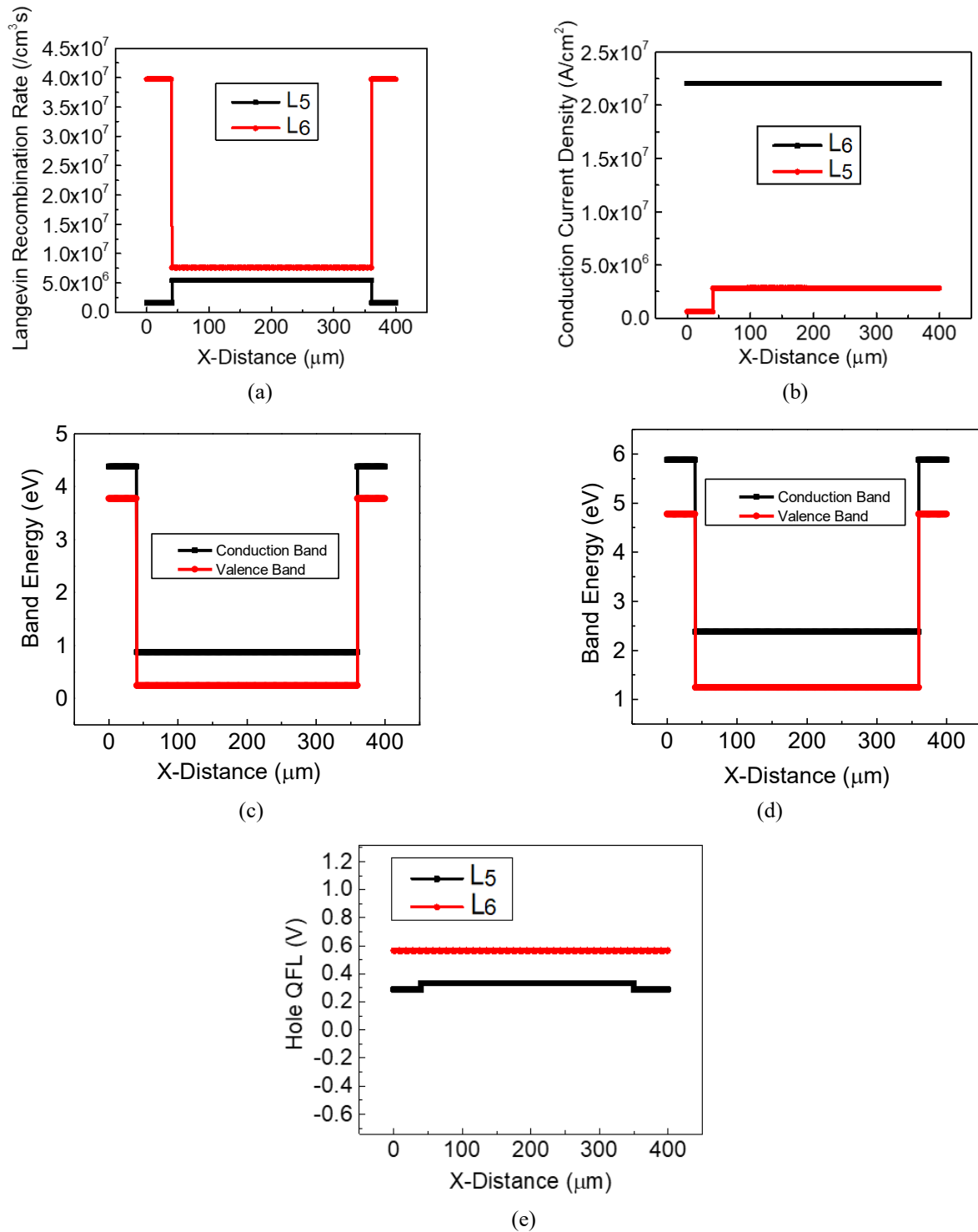


Fig. 4.13 Comparison of parameters for L₅ and L₆ based on horizontal cutiline in terms of (a) Langevin recombination rate, (b) Conduction current density, (c) Band energy of L₅, (d) Band energy of L₆, and (e) Hole QFL of L₅ & L₆

The figure 4.13 (e) illustrates hole QFL for both devices. The figure shows a higher QFL for L_6 as compared to L_5 . This shows a higher hole concentration in the emission layer. The higher hole concentration in L_6 is because of the holes injected from TAPC layer, which is at the anode side right outside the EML. This higher hole accumulation acts as a positive charge for electrons thereby enhancing their injection from the electrode as well.

Cutline analysis inside CGL layer towards anode: In this sub-section, a horizontal cutline is drawn at $0.215\ \mu\text{m}$ inside the TAPC layer of device L_6 as shown in Fig. 4.14. Herein, all six devices (L_1 - L_6) are analysed and compared in terms of hole mobility, electron mobility, Langevin recombination rate and hole QFL. It can be clearly observed from the Fig. 4.15 (a) that L_6 exhibits extremely high hole mobility; $100\ \text{cm}^2/\text{Vs}$ which is higher by 12, 6.4, 1.9, 8.1 and 1.6 times as compared to L_1 , L_2 , L_3 , L_4 and L_5 devices, respectively. Primarily, this high hole mobility is due to the better matching of energy levels of the adjacent layers that helps in hole injection [52].

In the same manner, electron mobility of L_6 is obtained as $51.2\ \text{cm}^2/\text{Vs}$ which is improved by 11, 5.2, 2, 6.2 and 1.9 times than that of L_1 , L_2 , L_3 , L_4 and L_5 , respectively (Fig. 4.15 (b)). A high electron mobility for L_6 can be attributed to the high hole concentration in the CGL of TAPC material which led to attract the electrons towards itself. This value is lower in case of L_5 , as CGL of HAT-CN material is placed towards anode side. HAT-CN material is responsible for injecting electrons in the EML but these electrons are attracted towards the anode due to its positive bias.

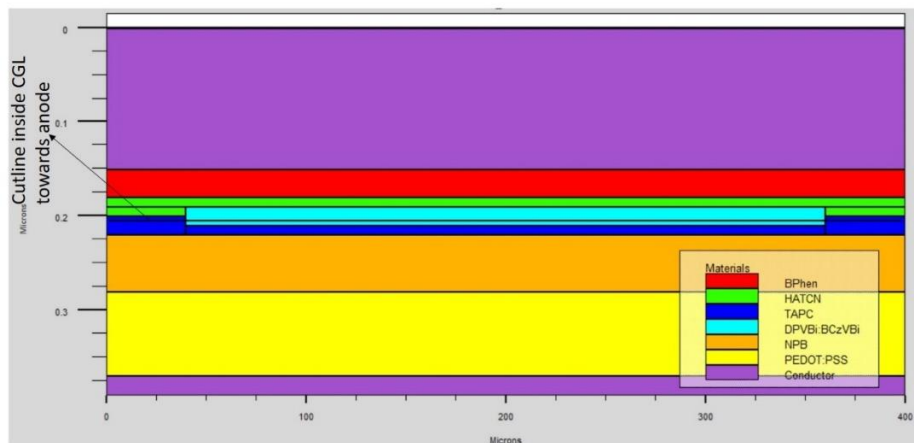


Fig. 4.14 Horizontal cutline drawn towards anode at $0.215\ \mu\text{m}$ in proposed OLED device (L_6)

Furthermore, Fig. 4.15 (c) shows the peak recombination rate for all the devices in graphical manner. The values of recombination rate are extremely high in case of L_6 as compared to other devices. The primary reason aligns with high charge carrier concentration in the EML due to

the well managed structure. Here, CGL is properly used and the applied bias helps CGL in injecting the charge carriers. This is reverse in case of L_5 wherein applied bias is opposing the carrier movement towards an effective recombination. Addition to this, the parameter hole QFL is also compared in all these devices as depicted in Fig. 4.15 (d).

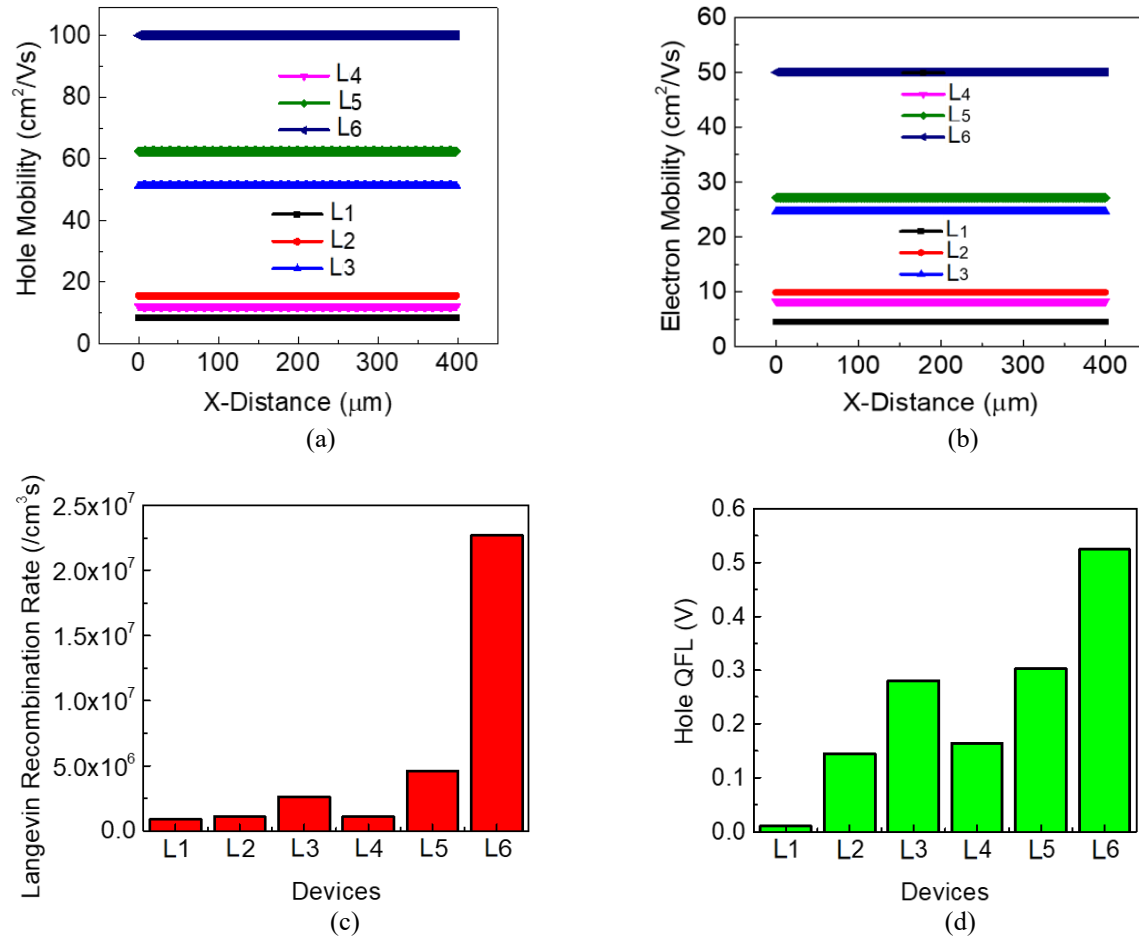
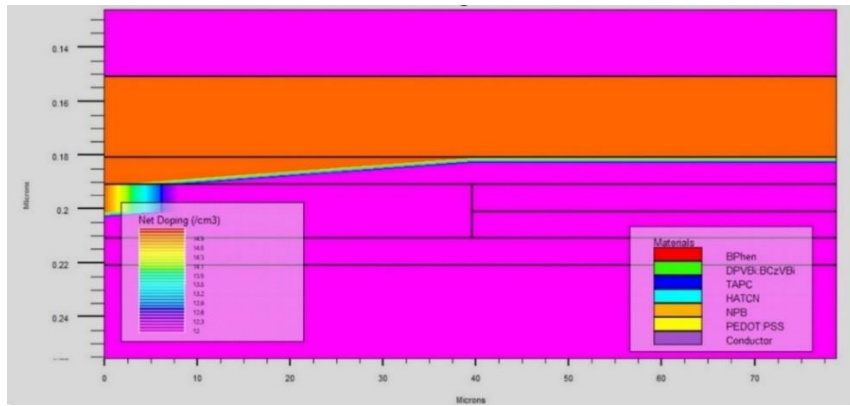


Fig. 4.15 Comparison of all six devices (L_1 - L_6) using horizontal cutline in terms of (a) Hole mobility and (b) Electron mobility and (c) Langevin recombination rate

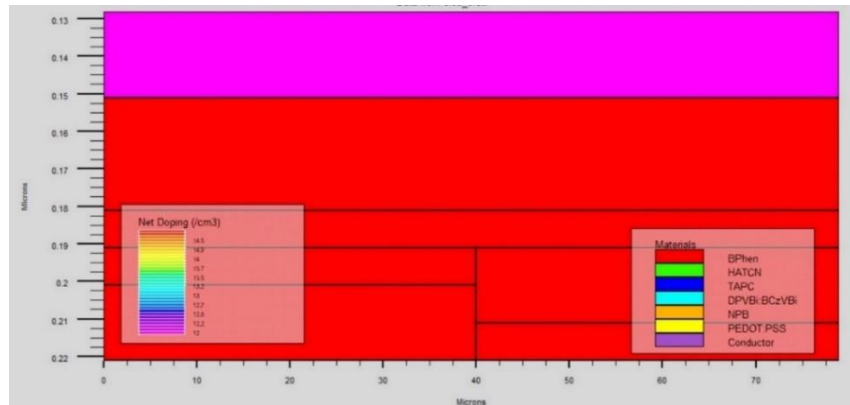
The higher hole QFL for L_6 highlights the similar results as in case of horizontal cutline analysis on cathode side. It is expected to be higher towards the anode as in L_6 charge carrier layers are well balanced for hole injection. Additionally, device L_6 exhibits a higher hole concentration. However, QFL levels are almost similar for L_3 and L_5 devices. HAT-CN layer is common on the anode for both these devices. So, there is some mismatch of energy levels for hole injection. However, due to the presence of TAPC layer in L_3 , this mismatch is minimized and thus resulting in a better injection. Subsequently, its QFL level is improved. Contrastingly, some injection barrier exists in device L_5 , still, its QFL is higher than L_3 because of higher hole injection continuously generated from TAPC layer on the opposite end.

c. Structural Internal Analysis

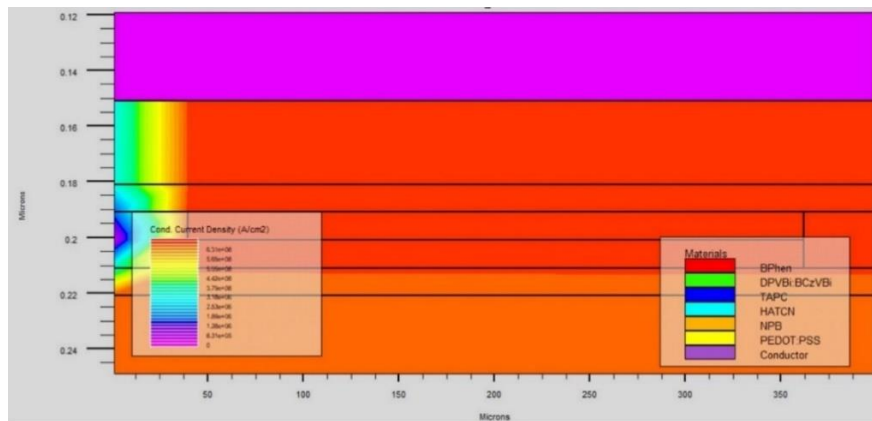
This section comprises of layer wise analysis for L₅ and L₆ devices as illustrated in Figs. 4.16 (a) to (d). Here, the parameters; net doping and current density are analysed more deeply by examining the affected regions mainly around the emissive layer. The figures show the zoomed in version with the focus on left side of the devices capturing the CGL and emission layers. Since organic devices generally do not use the concept of doping, therefore, the net doping in the figures refer to the carrier density profile in the biased device.



(a)



(b)



(c)

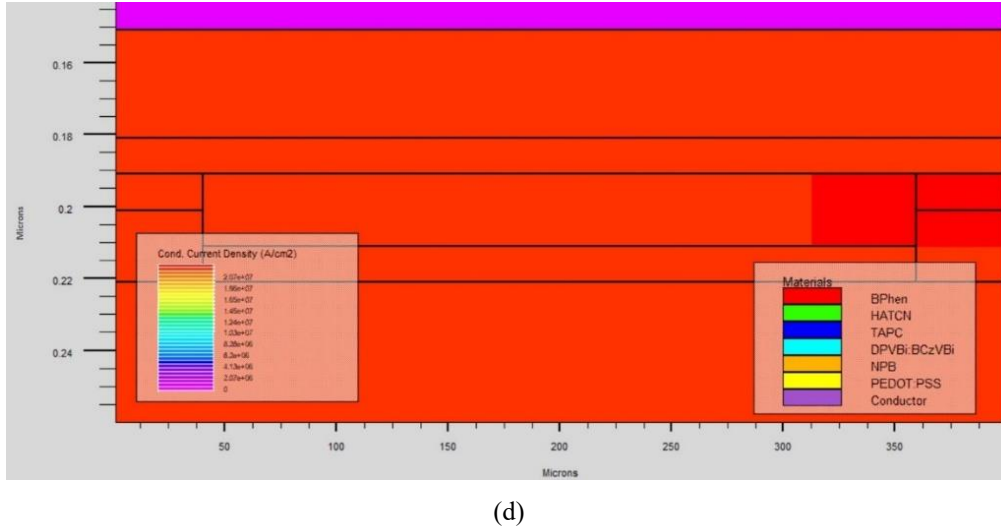


Fig. 4.16 Enlarged view of devices showing (a) Net doping of L_5 , (b) Net doping of L_6 , (c) Conduction current density of L_5 and (d) Conduction current density of L_6

Figures 4.16 (a) and (b) demonstrate the net doping for L_5 and L_6 , respectively. It is noticed that maximum net doping which is highlighted in red color is achieved in the wider region for device L_6 as compared to L_5 . In L_5 , it is only higher near the edge of the emissive layer. Here, the CGL is at the centre and EML is all around it. Thus, it shows that carriers generated from the CGL are entering the emission layer and thus depicts the variation in the doping levels and are getting recombined effectively. Hence, carrier doping decreases within the emission layer. However, in case of L_6 , the CGL is all round the emission layer. Now, electrode injects the charge carriers and these added to the carriers generated within CGL and finally injected in the EML. The charge carrier concentration is comparatively higher in case of L_6 thus even after recombination, there are enough carriers remaining within the device. These carriers are responsible for higher current density within the device [25]. Additionally, a large amount of these carriers is accumulated in L_6 , which acts as a supporting potential for carrier injection from the opposite electrode.

Additionally, Figs. 4.16 (c) and (d) demonstrate the current density of L_5 and L_6 , respectively. Herein, this parameter is the maximum in whole region of emissive layer for L_6 as shown in Fig. 4.16 (d) since the higher concentration charge carriers are present. All these charge carriers cannot recombine and result in the emission layer and therefore, resulting in generation of higher current within the device. However, for device L_5 , the conduction current density is lower at outside of CGL layer particularly at left side (which is the emission layer) as shown in Fig. 4.16 (c). This shows that the generated carriers are effectively recombining within the

emission layer. Further, in L₅, emission layer is thicker and thus resulting in more recombination and less current due to the flow of injected carriers from CGL.

4.5 THICKNESS OPTIMIZATION OF THE PROPOSED OLED

The results in the previous sections highlight that the CGL is influential in enhancing the performance of the device. However, the device thickness is also increased which can lead to adverse effects on the internal device working. The increment in device thickness is observed specially in the case of device L₄, wherein, CGL was used near both the electrodes. This configuration substantially increased the device dimensions and led to a decline in performance. Hence, this section aims to optimize the thickness of CGL in proposed novel device (L₆). The process is carried out in three ways; Case I- reduction of thickness in both layers of CGL evenly, Case II- fix the thickness of HAT-CN layer at 20 nm and reduce the thickness of TAPC layer and Case III- fix the thickness of TAPC layer at 20 nm and reduce the thickness of HAT-CN layer. This analysis also helps in understanding whether both the layers are influential for the device performance improvement or not. The thickness reduction is performed by reducing 2 nm thickness in each step and the corresponding results are as shown in Fig. 4.17. All the three cases are discussed below in details.

4.5.1 Case I: Thickness decrement in HAT-CN and TAPC layers

Initially, the total thickness of CGL was considered as 40 nm (20 nm each for HAT-CN and TAPC). In Case I, both layers of CGL are decreased in the step size of 2 nm (total variation of 4 nm in overall device dimension in each step), as shown in Fig 4.17 (a). Consequently, the total thickness of CGL is reduced to 24 nm which provides 1.3 times better luminescence. The luminescence is obtained as 3640 cd/m² and 4670 cd/m² at 40 and 24 nm, respectively and depicted in Fig 4.17 (b). The thickness of CGL is not reduced further, as this layer is responsible for generation and injection of excess charge carriers. A lower thickness may adversely affect the charge generation and degrade the device performance.

4.5.2 Case II: Thickness decrement in only TAPC layer

In this case, only layer of TAPC is varied from 20 nm to 12 nm, whereas; the layer of HAT-CN material is kept fixed at 20 nm. Here, the curves for luminescence are drawn at 20, 18, 16, 14 and 12 nm thickness, as shown in Fig. 4.17 (c). The maximum luminescence is observed as 4080 cd/m² and can be noticed from Fig 4.17 (d).

4.5.3 Case III: Thickness decrement in only HAT-CN layer

This case is reverse of case II. The thickness of HAT-CN material is varied from 20 nm to 12 nm in five steps and TAPC is constant at 20 nm as depicted in Fig. 4.17 (e). The peak luminescence is obtained as 4150 cd/m^2 (Fig. 4.17 (f)).

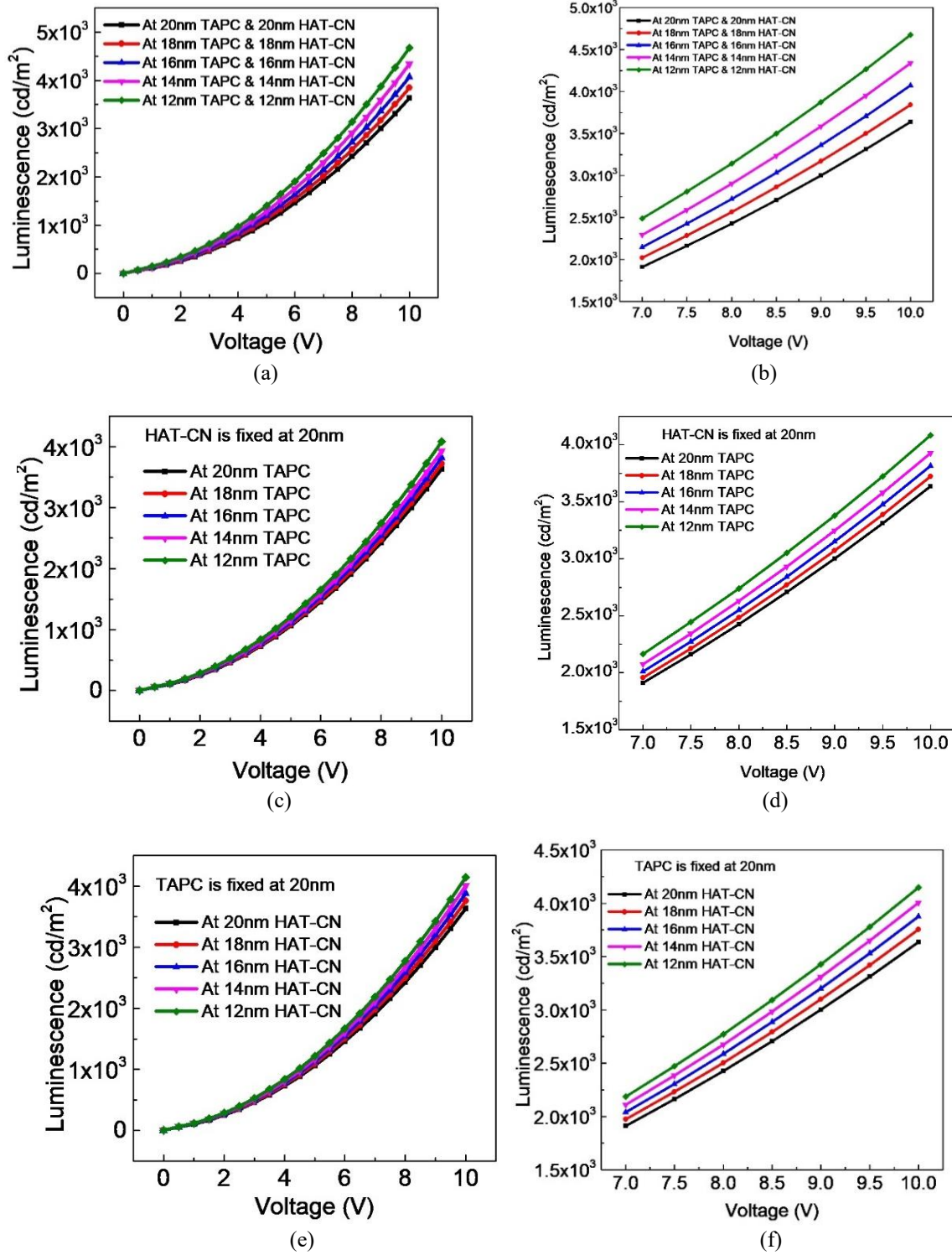


Fig. 4.17 (a) Luminescence comparison of Proposed OLED L_6 with thickness variation in (a) HAT-CN and TAPC both, (c) TAPC only and (e) HAT-CN only, with respective enlarged view in b, d and f.

In all the three cases, the maximum luminescence is obtained in Case I i.e. 4670 cd/m^2 at 24 nm thickness of CGL as highlighted in Table 4.3. This is improved by 78% as compared with the device (L_6) where thickness of CGL is kept at 40 nm. In case I, both the top and bottom layers are varied in similar way and thus on reduced thickness the carriers generated in the CGL need to travel less distance towards the EML from both sides owing to their proximity with EML. On the contrary, electrons and holes take more time to travel in Case II and Case III in comparison to Case I. The longer transit time directly affects the recombination of charge carriers. Hence, the peak luminescence values are less in both the cases.

Table 4.3. Different values of luminescence at different CGL thickness for proposed OLED (L_6)

Case	Thickness (nm)		Luminescence (cd/m^2)
	TAPC	HAT-CN	
I	20	20	3.64×10^3
	18	18	3.84×10^3
	16	16	4.07×10^3
	14	14	4.34×10^3
	12	12	4.67×10^3
II	18	20	3.72×10^3
	16		3.82×10^3
	14		3.93×10^3
	12		4.08×10^3
III	20	18	3.75×10^3
		16	3.88×10^3
		14	4.01×10^3
		12	4.15×10^3

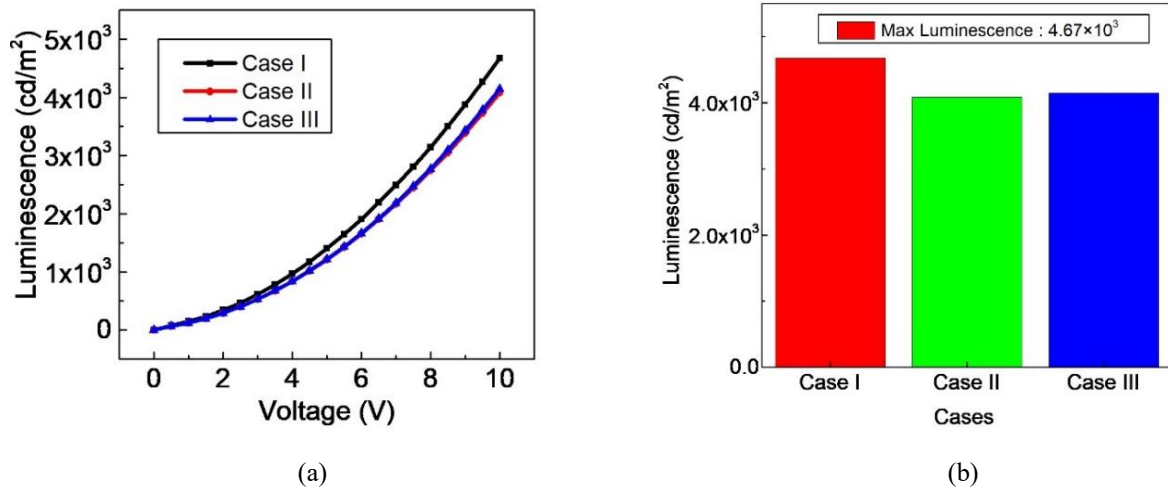


Fig. 4.18 (a) Comparison of luminescence of device L_6 at CGL thickness (in Case I both CGLs = 12nm, Case II bottom CGL = 12nm and Case III, top CGL = 12nm) and **(b)** Maximum luminescence for three cases

Further, Case III shows better results than Case II. In Case III, the layer of TAPC is fixed which generates holes. Here, the mobility of holes is better than electrons so holes can travel fast to

the emissive layer [245] which attributes to the better luminous characteristics in Case III as recombination is higher in this case. A comparison of maximum values for the luminescence in three cases (at 12 nm) is depicted in Fig. 4.18.

4.6 CHARACTERISTIC ANALYSIS AND PARAMETERS EXTRACTION OF OPD

OPD is a device that produces an electrical response to the light input. OPD can work as an effective light detector by producing a variation in the current for different wavelengths. Primarily, an experimental OPD (reference device) reported by Titov *et al.* [38], is analysed and validated using Silvaco Atlas 2-D device simulator to set the boundary conditions. The Langevin recombination and Poole Frenkel mobility models (explained in earlier sections) are used to characterise the performance. The reference device [38] named as P_1 is composed of seven layers as highlighted in Fig. 4.19. The simulated structure of P_1 is shown in Fig. 4.20.

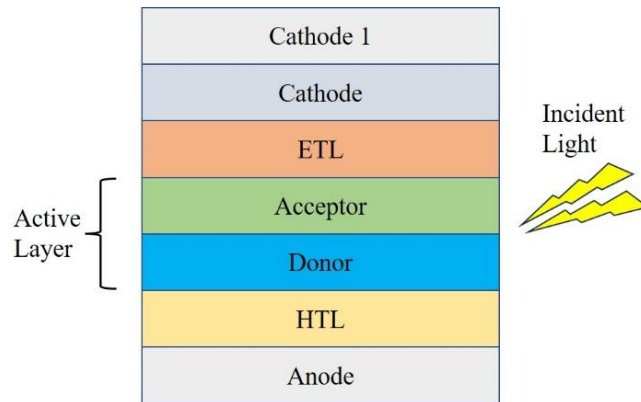


Fig. 4.19 Device structure for Multilayered OPD (P_1)

Table 4.4. Materials used and thickness of each layer for multilayered device P_1

Layer	Material	Thickness (nm)
Cathode 1	Al	150
Cathode	LiF	1
ETL	BPhen	12
Acceptor	C60	40
Donor	CuPc	20
HTL	PEDOT:PSS	90
Anode	ITO	20

Table 4.4 demonstrates the materials along with the thickness for each layer. The various layers of device are selected to establish a close structural match between the OLED and OPD. A close structural match in terms of different layers increases the possibility of fabricating both devices on a single substrate to realize some applications with this OLED-OPD integration.

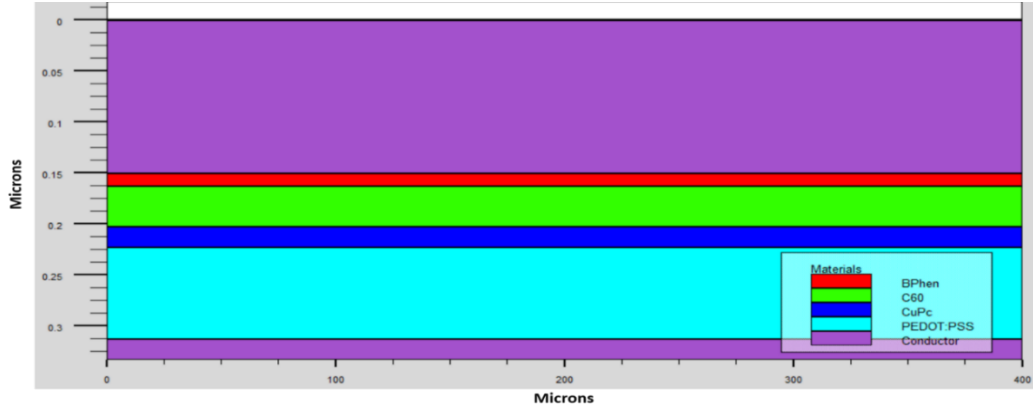


Fig. 4.20 Simulated structure of multilayered device P_1

Table 4.5. Parametric comparison of experimental results with multilayered device P_1

Parameters	Multilayered Device	Experimental results P_1
Dark Current (nA)	0.25	0.24
Photo Current (nA)	3.9	3.8

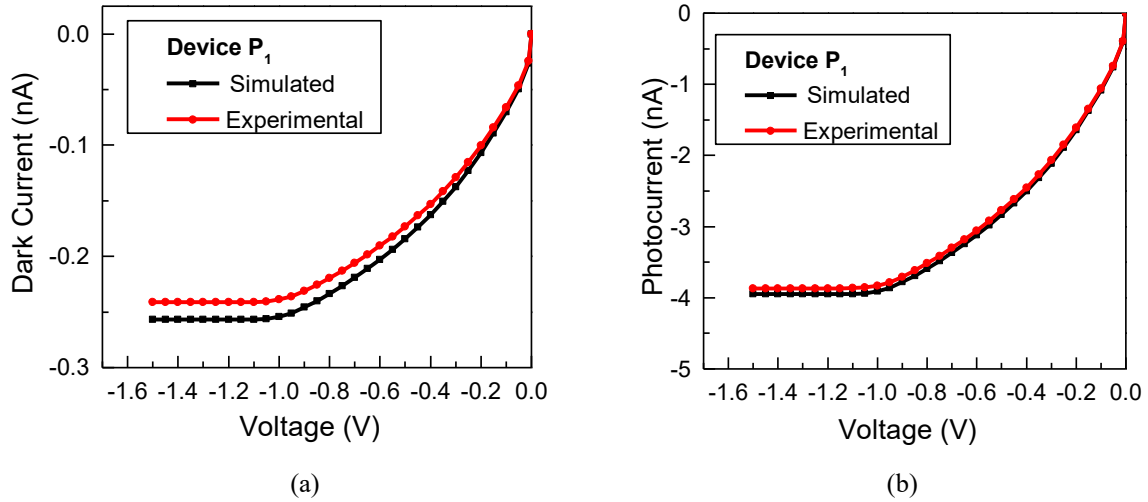


Fig. 4.21. Characteristics comparison for reported experiment and simulated OPDs (P_1) for (a) Dark current and (b) Photocurrent

Figures 4.21 (a) and (b) demonstrate the combined characteristic curves of dark current and photocurrent for reported experiment and simulated OPDs. These curves highlight a close match between the characteristics of simulated and experimental devices. Herein, the experimental reported values of photocurrent and dark current are -3.86 nA and -0.24 nA, respectively, which are very close to the results of simulated device (photocurrent= -3.9 nA, dark current= -0.25 nA) as shown in Table 4.5.

4.7 PROPOSED OPD DEVICE

In this section, a CGL based multilayer OPD is proposed with the aim to improve the performance of OPD (P_1). This improved structure is analysed with the same boundary

conditions as taken for device P₁ in terms of materials and layer thickness. The proposed novel structure contains an additional CGL (80 nm) of TAPC and HAT-CN materials similar to OLED structure. As illustrated in Fig. 4.22, the CGL is a combination of HAT-CN (50 nm) and TAPC (30 nm) materials which are placed at the side of acceptor and donor layers, respectively.

HAT-CN and TAPC are used to generate free electrons and holes, respectively on interacting these layers with excitons. The OPD works in reverse bias condition (cathode connected to positive and anode to negative terminal of the battery) and thereby a depletion region is developed. The depletion region is devoid of all the charge carriers. Now, when light falls on the acceptor-donor layer, excitons are generated and the interaction of these excitons with the acceptor and donor layers results in electron-hole pairs generation.

The CGL layers are very close to these acceptor-donor layers, therefore, exciton interacts with them as well. The HAT-CN layer generates large number of electrons that travel towards cathode and similarly, TAPC generates large number of free holes travelling towards anode. These free charge carriers get mixed-up with the carriers generated inside the active layer and produced significant large amount of photocurrent. This clearly indicates that the CGL plays a vital role in enhancing OPD performance in terms of photocurrent, as it facilitates efficient charge separation and transport.

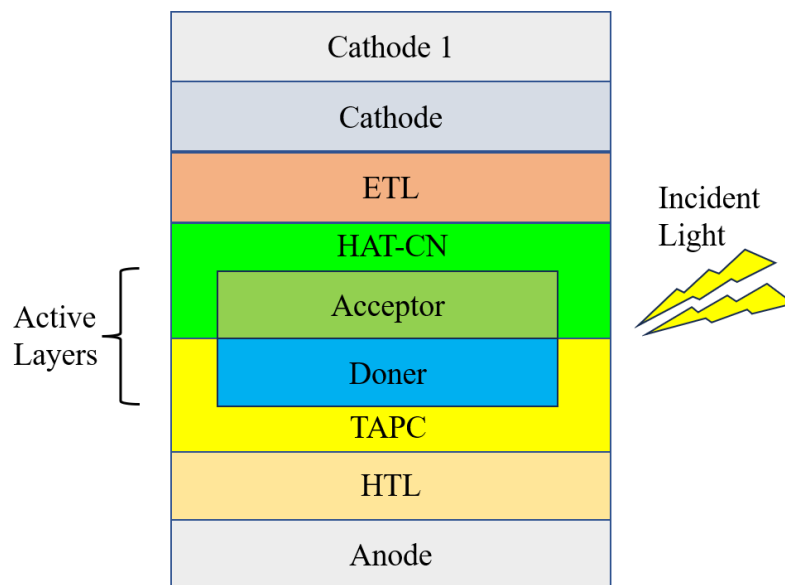


Fig. 4.22. Device structure for proposed CGL based OPD device (P₂)

The simulated structure of the proposed device (P₂) is shown in Fig. 4.23 (a). Additionally, Fig. 4.23 (b) highlights the potential distribution within the device. The potential distribution highlights a good potential across the HAT-CN layer, whereas it is reasonable within the acceptor-donor layers and TAPC layer. This potential distribution highlights a excitons

dissociation within these layers. Additionally, it is highlighting that potential drop is higher towards the cathode as compared to anode. This drop is probably due to the mismatch in energy levels of ETL with the work-function of cathode. The cathode has a higher work-function as compared to ETL LUMO level which is good for electron injection, as these carriers must move from a higher energy level to lower energy level in case of OLED. At the same time, this higher work- function may act as barrier in case of OPD, wherein charge separation is required.

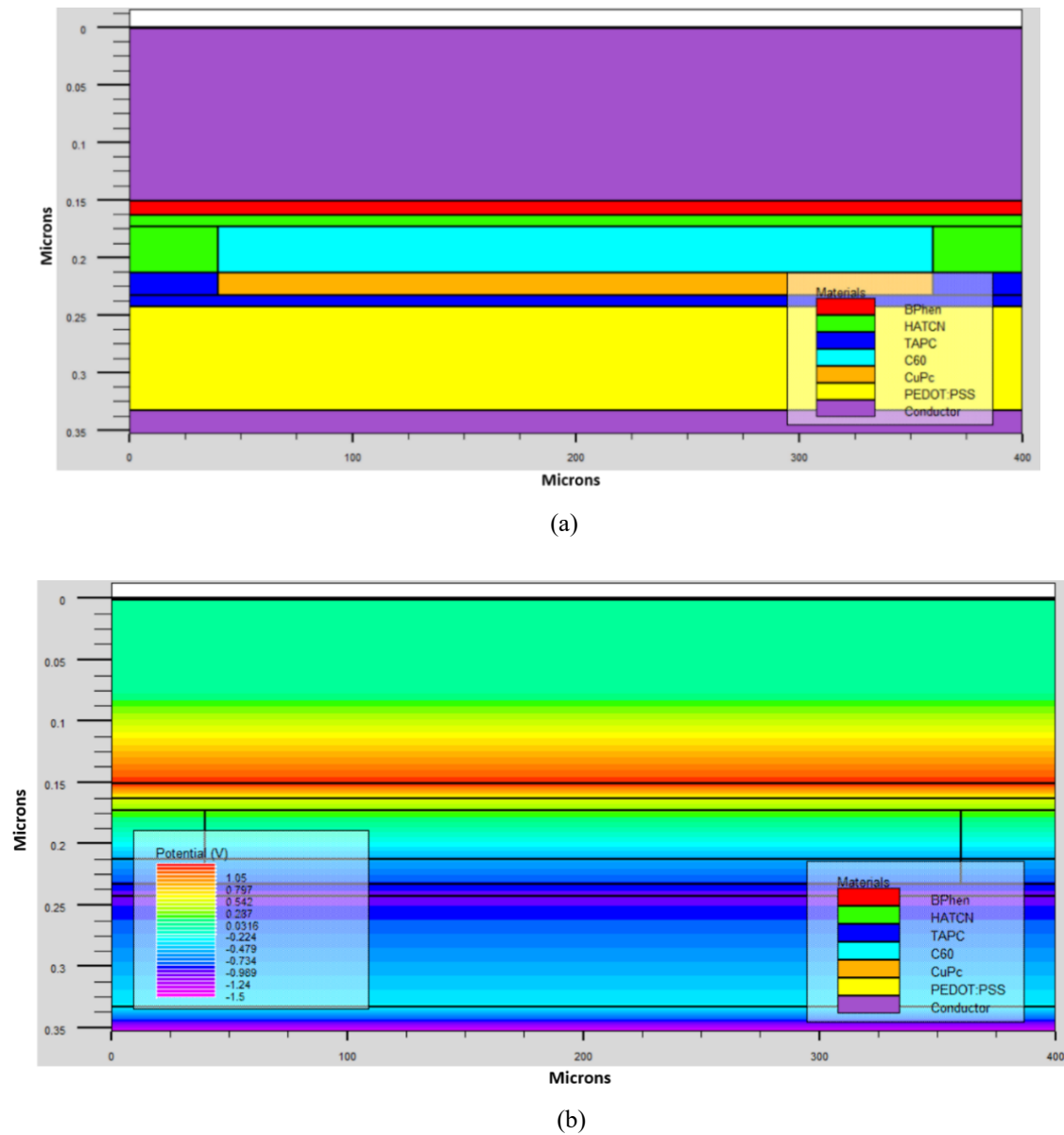


Fig. 4.23. (a) Simulated structure of proposed device (P_2) and (b) Potential distribution inside P_2

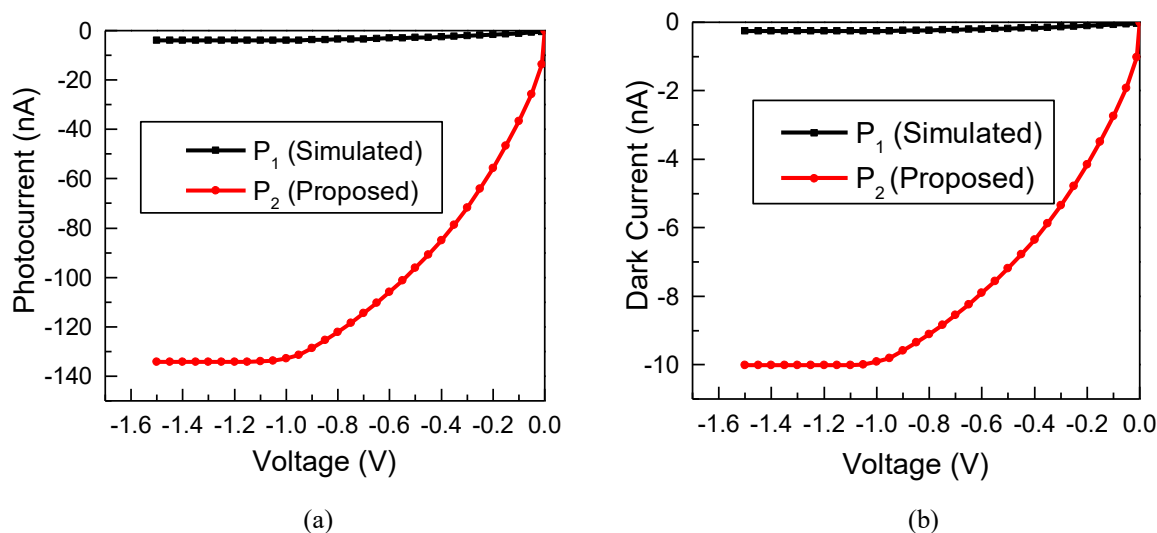
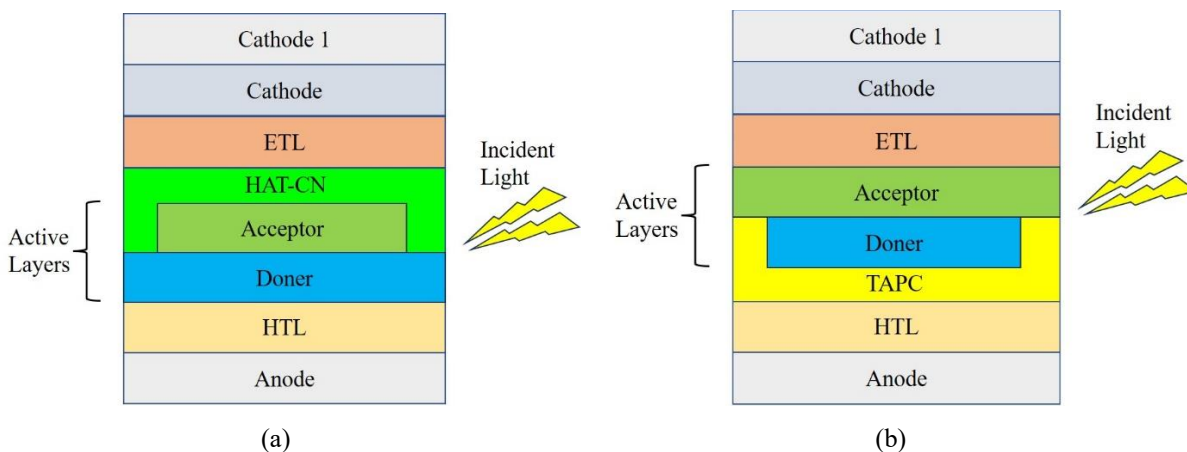


Fig. 4.24 Comparison of multilayered device (P_1) and proposed device (P_2) based on (a) Photocurrents and (b) Dark currents

Figure 4.24 demonstrates the results pertaining to the photocurrent and dark current within the device P_2 . The device exhibits photocurrent of 134.2 nA which is about 34 times higher on comparing with P_1 . The dark current of P_2 (10.2 nA) is also higher than that of P_1 (0.25 nA) probably due to the inclusion of CGL.

4.7.1 Analysis of proposed device with positional variations of CGL

Here, the proposed device (P_2) is analysed on different position of CGL (devices named as P_3 , P_4 and P_5). The device P_3 (Fig. 4.25 (a)) contains only electron generator layer of HAT-CN near the acceptor layer. However, device P_4 exhibits only hole generator layer of TAPC near donor layer (Fig. 4.25 (b)). Furthermore, device P_5 (Fig. 4.25 (c)) is the reverse form of the proposed device P_2 wherein both the layers of CGL are incorporated. The concentration of electrons and holes is higher in P_3 and P_4 , respectively. Hence, P_4 exhibits better results in comparison with P_3 due to higher mobility of holes than electrons for organic materials.



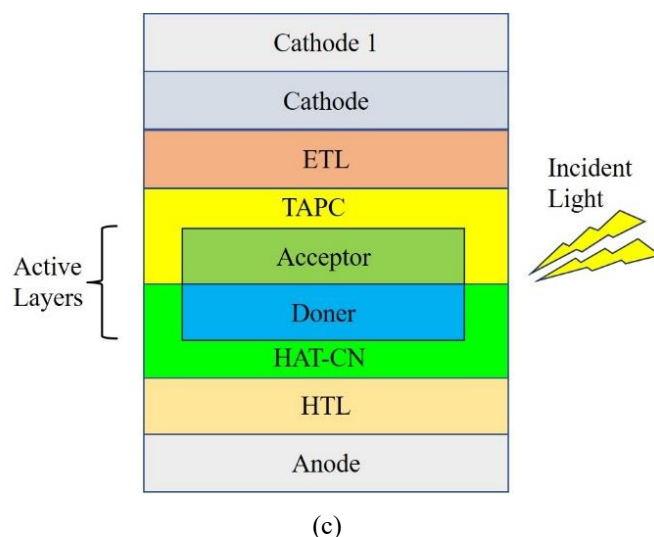


Fig. 4.25 Different OPD structures (a) P_3 with only HAT-CN, (b) P_4 with only TAPC and (c) P_5 with TAPC at top and HAT-CN at bottom

In case of P_5 , both HAT-CN and TAPC layers are utilized but in the reverse manner of the proposed device P_2 . So, the electrons and hole in P_5 will be pushed towards the active layer because of the applied bias and these carriers need to cross it to reach the respective electrode. Therefore, such movement might interfere with the generation process. Additionally, the charge carriers have to cross the additional distance, therefore, the contribution to photocurrent generation will not be significant. On the contrary, in case of P_2 , all the generated holes and electrons from the CGL are completely attracted towards the nearer electrodes and added up with charge carriers of the active layer and large amount of photocurrent is produced. As a result, device P_2 outperforms among all four devices.

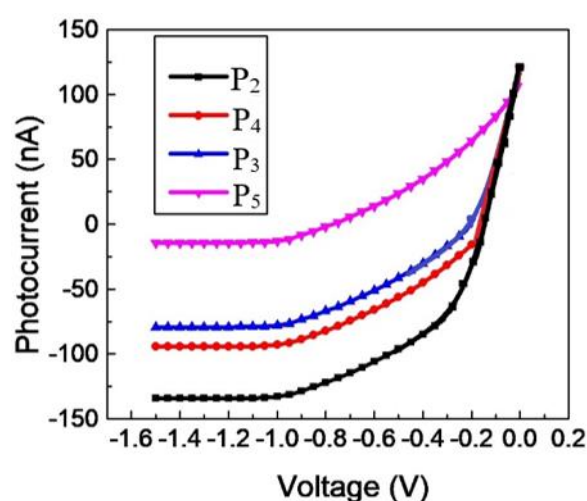


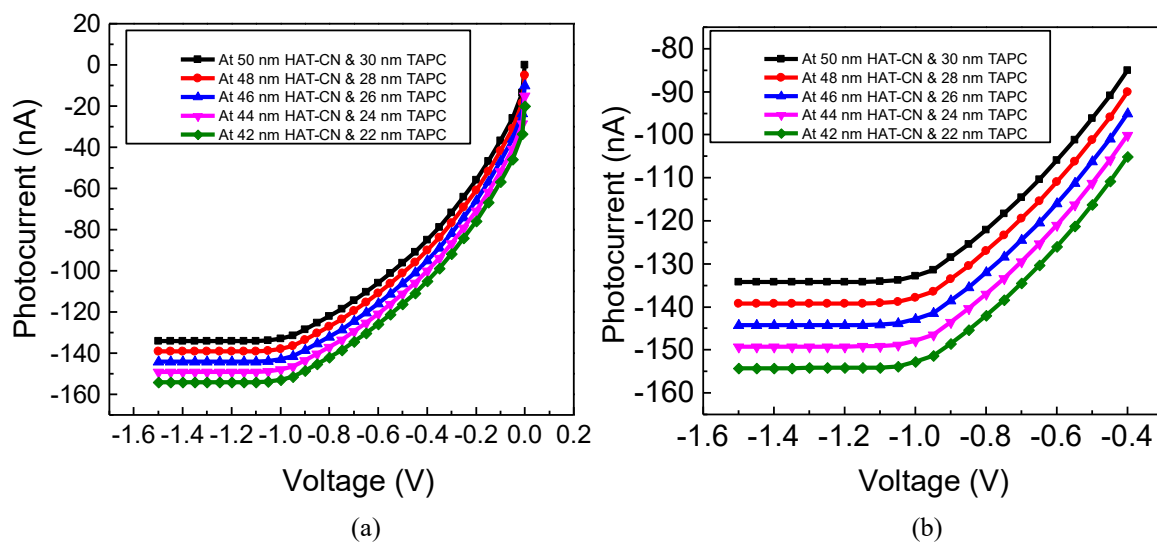
Fig. 4.26 Photocurrent characteristics for P_2 , P_3 , P_4 and P_5 devices

All the four devices (P₂-P₅) are compared in terms of their photocurrent characteristics as plotted in Fig. 4.26. The proposed device P₂ attains the maximum photocurrent of 134 nA which is improved by 1.6, 1.4 and 9 times in comparison to P₃, P₄ and P₅, respectively. Moreover, it is observed that device P₅ with the reverse position of CGLs exhibits the lowest photocurrent. The reasons for poor performance of this P₅ device are already discussed above.

4.7.2 Thickness optimization of proposed OPD

Herein, the performance of proposed device (P₂) is optimized by reducing the thickness of the CGL layer. The total thickness of CGL is 80 nm where 50 nm is for HAT-CN and 30 nm for TAPC. The thickness is optimized using three ways. In case I (Fig. 4.27 (a)), both layers of CGL are considered for the thickness reduction (step size of 2 nm). The performance is analysed for HAT-CN from 50 to 42 nm towards acceptor layer and TAPC from 30 to 22 nm towards donor layer. However, HAT-CN is fixed at 50 nm and TAPC is reduced from 30 to 22 nm (Fig. 4.27 (c)) for case II. Further, in case III, TAPC is fixed at 30 nm and HAT-CN is reduced from 50 to 42 nm (Fig. 4.27 (e)).

After comparing all the cases, it is concluded that the device performs better on reducing the thickness. In case I, the maximum photocurrent of 154.2 nA is obtained (Table 4.6). The reason is very obvious here as in case I the CGL thickness is minimum. As a result, the recombination losses are less in these layers. Additionally, the charge carriers reach the respective electrode faster due to the reduced distance between their generation and the electrode. For the other two cases, the case II exhibits better results.



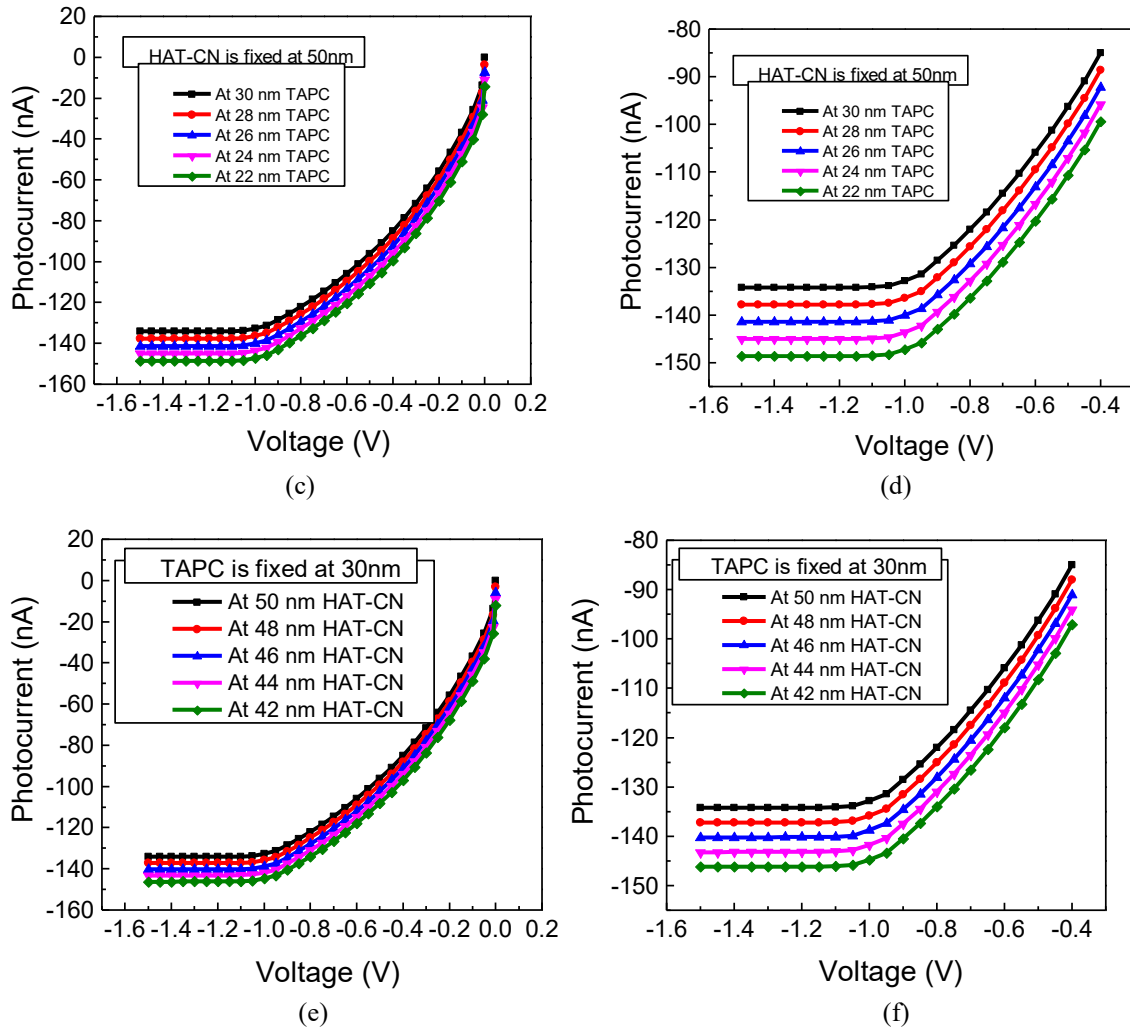


Fig. 4.27 Proposed OPD Performance with thickness variation (a) HAT-CN and TAPC both, (c) TAPC only and (e) HAT-CN only with respective enlarged view in b, d and f.

Table 4.6. Photocurrent at different thicknesses of HAT-CN and TAPC for proposed OPD (P₂)

Cases	Thickness (nm)		Photocurrent (nA)
	HAT-CN	TAPC	
Case I	50	30	134.2
	48	28	139.2
	46	26	144.2
	44	24	149.2
	42	22	154.2
Case II	50	30	134.2
		28	137.8
		26	141.4
		24	145.1
		22	148.6
Case III	50	30	134.2
	48		137.2
	46		140.3
	44		143.2
	42		146.3

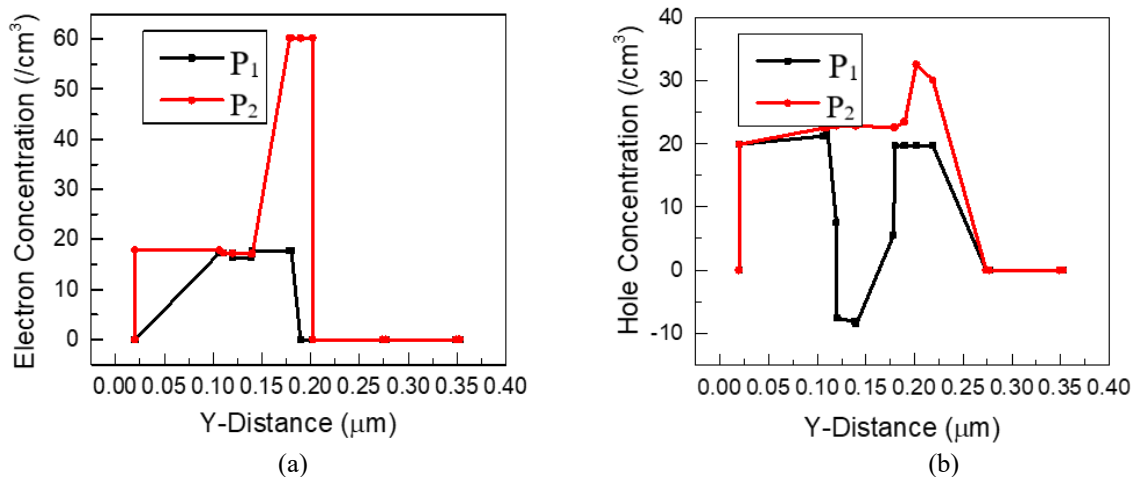
It has been observed in the previous section through internal analysis that HAT-CN is more influential in generating charge carriers with exciton interaction. Therefore, the photocurrent obtained in the corresponding configuration is higher. Figures 4.27 (b), (d) and (f) are the enlarged view of Figs. 4.27 (a), (c) and (e), respectively to depict the clear variation of photocurrents. Table 4.6 summarizes photocurrent values for all the three cases. Herein, the maximum and minimum values are obtained as 154.2 nA (case I) and 146.3 nA (case II), respectively.

4.8 INTERNAL ANALYSIS OF REFERENCE AND PROPOSED OPD

Herein, reference device (P_1) and the proposed device (P_2) are compared based on internal device parameters; electron/hole concentration, electron current density, potential distribution, band energies, and electron QFL to better comprehend the device behaviour and related facts. This internal analysis is done using both vertical and horizontal cutline in the TonyPlot.

4.8.1 Vertical cutline analysis

Here, a vertical cutline is drawn at the centre of device crossing all the layers. As discussed in the previous sections, device P_2 contains CGL layer which generates free electrons and holes. As the CGL is near the active layer, hence, the exciton interacts with these layers and generated charge carriers are swept towards electrodes and added up with charge carriers created in the active layer. This enhanced generation of the electrons and holes can be clearly observed in Figs. 4.28 (a) and (b). Herein, these figures depict that the P_2 contains much higher concentration of electron and hole as compared with P_1 . This higher concentration of charge carriers improves the current density (photocurrent per unit area). The electron current density of P_2 is much higher than P_1 as illustrated in Fig. 4.28 (c). It is specifically higher near the cathode region because of higher concentration of the electrons.



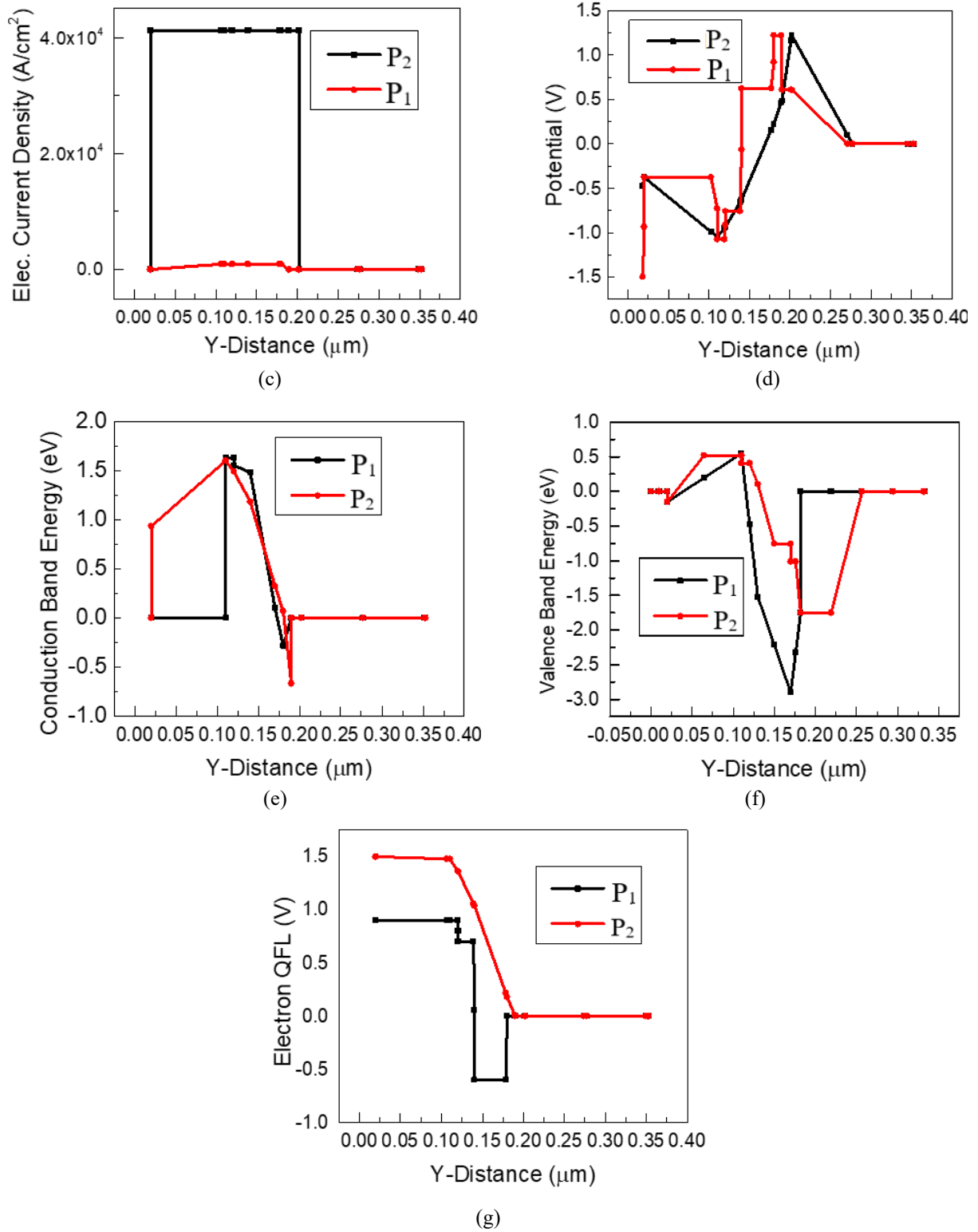


Fig. 4.28 Vertical cutline analysis of P₁ and P₂ in terms of (a) Electron concentration, (b) Hole concentration, (c) Electron current density, (d) Potential, (e) Conduction band energy, (f) Valence band energy and (g) QFL

Next, Fig. 4.28 (d) outlines the potential distribution of the proposed device P₂, wherein the potential is observed maximum at the interface of acceptor-donor layers. However, for device P₁, potential is falling on each side in a step graph manner which represents the mismatch of

energy levels at different positions in the reference device. On the other hand, the potential drop is smooth for P_2 and thus illustrating a better matching of energy levels that also helps in smooth conduction of charge carriers.

Further, the conduction band and valence band energy plots for P_1 and P_2 are depicted in Figs. 4.28 (e) and (f), respectively. The conduction and valence band energy declines in the acceptor donor layer range for novel device P_2 . However, the conduction band bends steeply towards the anode for P_1 which interprets that in device P_2 , the potential energy is being used in and near acceptor-donor layers for the purpose of hole pair generation through the exciton. Additionally, there is a low injection barrier for the charge carriers near the electrodes. On the contrary, P_1 shows a steep slope near the electrodes highlighting mismatch in the energy levels, thus, creating higher resistance for the carrier flow which results in higher current for the proposed novel device P_2 .

These assumptions for the charge carrier generation and flow are also supported through the electron QFL plot. Figure 4.28 (g) depicts the electron QFL plot for both the devices. The QFL value of P_2 is much improved due to the addition of CGL. It shows a smooth QFL throughout the device, whereas, for P_1 , the QFL level is stepped and even goes below zero value. This variation again depicts a high injection barrier for the charge carriers at the electrode resulting in contact limited carrier extraction. After examining all these parameters, it is very clear that the proposed OPD shows a significant improvement in the performance.

4.8.2 Horizontal cutline analysis

To understand the impact of structure, a horizontal cutline is drawn inside the active layer of P_1 and P_2 . Figure 4.29 (a) depicts the conduction band and valence band energies of the P_2 . The figure illustrates straight and smooth band within the active layer. Further, the potential distribution of P_1 and P_2 is shown in Fig. 4.29 (b) and a slight variation in potential is observed for between the two devices due to CGL. This variation highlights a better exciton dissociation in P_2 within the active layer. Afterwards, Fig. 4.29 (c) depicts a higher current density for device P_2 than that of P_1 . A high current density within the active layer means more effective separation of charge carriers in the active layer and their movement towards the respective electrodes.

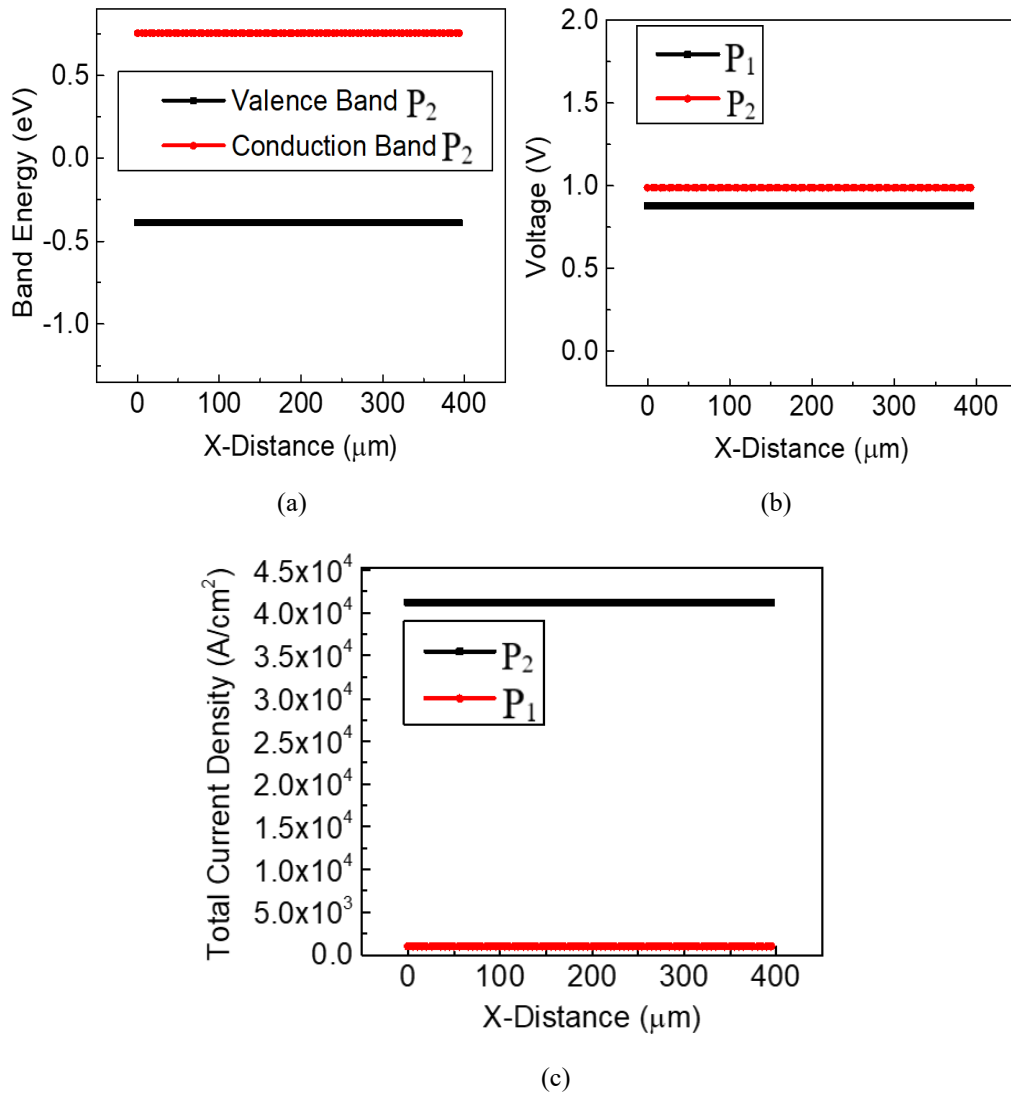


Fig. 4.29 Horizontal cutline analysis for (a) Band energies, (b) Potential distribution, and (c) Current density

The cutline analysis brings forth that the CGL is impactful in enhancing the device performance. The CGL helps in exciton dissociation in active layer and in themselves. Such behavior is inferred through the high charge carrier density and potential energies observed in these layers and their vicinity. Additionally, the band diagrams and QFL plot show that CGL improves the energy level alignment within the device and thus resulting in an easier transfer of charge carriers from the device towards the electrodes. Consequently, the current density in the device is much improved.

4.9 SUMMARY OF THE RESULTS

The present chapter is focused on investigating the impact of charge generation layers on the performance of OLED and OPD devices. An in-depth analysis is conducted on the position and thickness of these layers and the consequent impact on the device performance is observed. A

novel OLED device (L_6) is proposed, wherein, the CGL encapsulates the emission layer and results in the best performance. Similarly, a novel OPD structure (P_2) is also proposed with CGL on both sides of the active layer. Achieving the best performance from both the OLED and OPD devices with similar architecture, opens the possibility of fabricating both the devices on the single substrate. The important outcomes of the analysis performed in this chapter are enlisted below.

- The performance of a reported (fabricated device) blue reference OLED (L_1) is analysed and validated using Silvaco Atlas tool.
- A CGL based novel structure of OLED (L_6) is proposed. The CGL consists of hole (TAPC) and electron (HAT-CN) injector layers. Additionally, the CGL is placed at different positions (L_2 , L_3 , L_4 and L_5) to observe the performance variation in terms of current density and luminescence. The outcomes depict that the OLED with CGL at outside of emissive layer (in device L_6) exhibit the best results. The enhanced performance of the proposed device L_6 can be attributed to increased electron and hole concentrations arising from the optimized placement of the CGL.
- The current density and luminescence of proposed device (L_6) is obtained as 0.44 A and 3636.3 cd/m². The device exhibits an improvement in luminescence by 16.8, 2.3, 1.7, 3.0 and 1.6 times and in current density by 73.0, 5.7, 4.4, 7.8 and 1.4 times than that of L_1 , L_2 , L_3 , L_4 and L_5 , respectively.
- Furthermore, vertical and horizontal cutline analysis is performed to understand the internal device behaviour and the facts associated with the device performance. The results of internal analysis depict that CGL layers are influential in enhancing the electron and hole concentration within the device L_6 which results in higher carrier recombination as per the Langevin's theory of recombination for slow moving charge carriers.
- Since, CGL generates these charge carriers in huge number, therefore, maximum of these combines in the emission layer. However, for the charge carriers that do not combine move towards the electrode and results in higher current density in device L_6 .
- A reference OPD device (P_1) is validated with less than 5% deviation for photo current and dark current characteristics. This validation is performed to set the boundary conditions in terms of materials, thickness, and structure to propose a novel device.
- CGL is incorporated in the OPD (P_2) to enhance its performance in terms of dark current and photocurrent. The P_2 device exhibited a photocurrent of 134.2 nA which is about

34 times higher on comparing with P_1 . The dark current of P_2 (10.2 nA) is also higher than the P_1 (0.25 nA) probably due to the inclusion of CGL.

- The proposed device (P_2) is further compared with three other CGL based devices named as P_3 , P_4 and P_5 . In case of P_2 , the holes and electrons generated from the CGL are efficiently attracted toward the electrodes and contribute to the charge carriers in the active layer, resulting in enhanced current and higher photocurrent generation. Consequently, device P_2 exhibits the best performance among all four devices. The photocurrent of P_2 is increased by 1.6, 1.4 and 9 times in comparison to P_3 , P_4 and P_5 , respectively.
- Additionally, internal analysis is performed on the proposed and reference OPD using horizontal and vertical cutlines at different positions of the structures. This analysis highlights that the CGL layers used in the device also interact with the excitons produced due to the light interaction within the active layer. Thus, the CGLs generate extra electron and holes in the device enhancing the photocurrent. Also, the energy levels are better aligned in device P_2 as compared to P_1 . Therefore, the charge extraction is easier in P_2 as can be observed by its higher photocurrent values.

Present work focuses on the enhancement of OLED and OPD performance using charge generation layers. Both the devices have depicted an improved performance. However, both devices have scope for improvement, particularly the OPD, for which dark current is critical. The significance arises from the fact that the detectivity of the device depends on its value and so does the device power consumption. This parameter should be given due attention while designing the OPD by using novel methodologies. It is observed that CGLs can improve device performance, similarly, more advanced layers such as cathode interlayers can be investigated to reduce the dark current in the device. Additionally, synthesizing new materials can enhance charge separation and boost device performance.

CHAPTER-5

COVID-19 DISEASE DETECTION USING PROPOSED FLEXIBLE DEVICES

5.1 INTRODUCTION

The light-based disease detection has been prominent in the field of medical science for almost a century now. Scientists and researchers have been using basic spectroscopy-based study of bio-molecules for even a longer duration. These studies are often based on interaction of biological molecules with light and change its properties, most often with respect to wavelength. This process is based on fluorescence mechanism. When a light of some wavelength falls on a sample, it interacts with it and re-emits a light of different wavelength and this change in wavelength further helps in detection.

In the modern medical science, fluorescence detection is being used for an assorted range of bio-medical applications, such as oximeter sensor, cancer detection, monitoring protein-DNA interactions, heart stroke detection, etc. This smart detection methodology was first introduced by Heyduk and Lee in 1990. With the advancement in the science and technology, ultra-thin and flexible sensors have emerged as a highly promising field for such health-care applications. The integration of organic light emitting diode and organic photo diode presents themselves as a well-suited methodology for these kinds of health-care applications.

Therefore, in the present chapter the OLED and OPD devices, investigated in the previous chapters, are utilized to work in unison for biomedical application. A light-based sensor requires two major aspects, one is a light source wherein OLED can be used, and the other is a light detector for which OPD is well suited. Focusing on this aspect, the present chapter proposes a methodology for Covid-19 detection. The procedure consists of proposed blue OLED and OPD devices (discussed in chapter 4) that analyses the human saliva sample and determine whether the person is infected with SARS-COV-2 or not.

The basic detection is based on methodology proposed by Lee *et al.* [226]. Using a simplified procedure, a saliva assay was so developed that the N1 and N2 genes pertaining to SARS CoV-2 RNA were extracted [226]. These genes further interact with light in the presence of proposed probe [226] and made it possible to detect Covid-19. Additionally, research has shown that the procedure is highly accurate as normal Covid does not test positive for this arrangement. Herein, for simplification, the developed saliva system for gene extraction is called as saliva

sample. The work is focused only on the interaction of light with the system and since OLED and OPD are more sensitive to light therefore, it is expected that utilizing these devices help the entire system in achieving a higher accuracy. An in-depth analysis is being performed on both the OLED and OPD devices to make these devices work in unison for the detection of SARS-COV-2 virus inside human saliva sample.

This work also compares the proposed methodology with some other researcher's work. The proposed OLED-OPD integration may be utilized for other sensing applications such as environmental monitoring, multispectral sensing, optical sensing and IoT devices. Here, following objective is formulated to realize suitable OLED and OPD devices for Covid-19 detection:

“Covid-19 disease detection using proposed OLED, OPD and OTFT devices”

The following methodology is used to obtain desired objective: -

- Design and analysis of CGL based OLED which emits light of the required wavelength for Covid-19 detection.
- Characteristics analysis of CGL based OPD to detect and differentiate between the 490 nm and 525 nm wavelength for Covid-19 detection.
- Analyse the proposed methodology for multiple persons.

The objective of the present chapter is to propose a novel OLED and OPD based portable sensor on a single substrate for detection of Covid-19. The methodology based on OLED and OPD is a novel one as previously researchers have not used the two devices for similar application. Moreover, OTFT has been utilized in the present work for possibility of driving the present OLED device to emit the desired wavelength of light. Additionally, an analysis has been undertaken for the utilizing the proposed methodology for detection of Covid-19 in different people wherein their saliva sample attributes can vary.

The complete chapter is arranged in five sections including introduction in Section 5.1. Afterwards, the methodology for Covid-19 detection as used by various researchers is showcased in Section 5.2. Further, the OLED and OPD devices are analysed for Covid-19 detection in Section 5.3 followed by OLED driving circuit. Thereafter, in Section 5.4, Covid-19 detection is performed using suitable OLED and OPD devices. Furthermore, to validate the detection arrangement, methodology is applied on multiple persons. The summary of this work is incorporated in Section 5.5.

5.2 METHODOLOGY FOR DETECTION OF COVID-19

In 2019, coronavirus pandemic forced us to think the importance of rapid and accurate point of care diagnostic tests using flexible portable devices. Many researchers have proposed different Covid-19 methodologies focused on light-based detection. Wang *et al.* [246] in 2020, proposed a sensitive and rapid detection of Covid-19 using CRISPR/Cas12a (CRISPR-associated protein 12a (Cas12a) endonuclease)-based assay. It was suitable for reliable and simple diagnosis in 45 minutes. Thereafter, in 2020, Ding *et al.* [247] proposed dual CRISPR/Cas12a assay for ultrasensitive and visual Covid-19 detection. The assay was applied on corona virus swab samples and provided consistent results when compared with RT-PCR assay.

Further, in 2021, Lee *et al.* [226] designed a compact Covid-19 test device which detected the presence of SARS-CoV-2 and produced the rapid results within 20 mins of sample loading. Furthermore in 2022, Lian *et al.* [248] presented antibody detection method by using an OLED based on fluorescence-linked immunosorbent assay. In 2022, Zhang *et al.* [249] developed a wearable flexible test strips for corona virus rapid detection. In this research, two highly sensitive test strips were designed for RBD and N antigens of SARS-CoV-2.

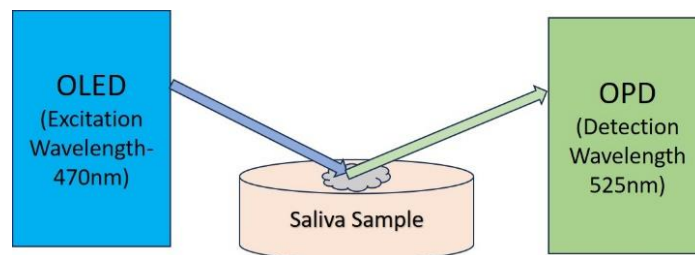


Fig. 5.1. Covid-19 detection using OLED and OPD devices

The methodology for Covid-19 detection used here is depicted in Fig. 5.1. Herein, OLED is utilized as light emitter whereas, OPD is utilized as light detector based on their basic properties. First, light from OLED falls on the saliva sample which excites the saliva sample (i.e. the SARS-CoV-2 genes in the presence of CRISPR probe) and further the fluorescence emission takes place. This fluorescence emission is further detected by the OPD. If the fluorescence emission occurs in the range of 525 nm, OPD produces 63.5 mA of current. Emission of this wavelength depicts the presence of Covid-19 RNA. On the other hand, the emission wavelength of 490 nm range produces a current of 37.2 mA and thus the person is declared healthy. The peak emission and detection wavelengths of OLED and OPD is 470 nm and 525 nm, respectively.

5.3 ORGANIC LED AND PHOTO DIODE UTILIZATION FOR COVID-19 DETECTION

The present section explores the possibility of using organic devices for Covid-19 detection. The OLED (L_6) and OPD (P_2) devices proposed and analysed previously (depicted in Fig. 5.2 again for reference) are examined to check the possibility of Covid-19 detection with their usage. The proposed OLED is suitable to produce blue color light and the designed OPD is capable to detect green light emission. These characteristic specifications for both devices are based on the reports available in literature [246-248] to diagnose the Covid -19 disease. The researchers have investigated different light-based methodologies for Covid-19 detection and few of these works specifically on light-based detection are enlisted in Table 5.1.

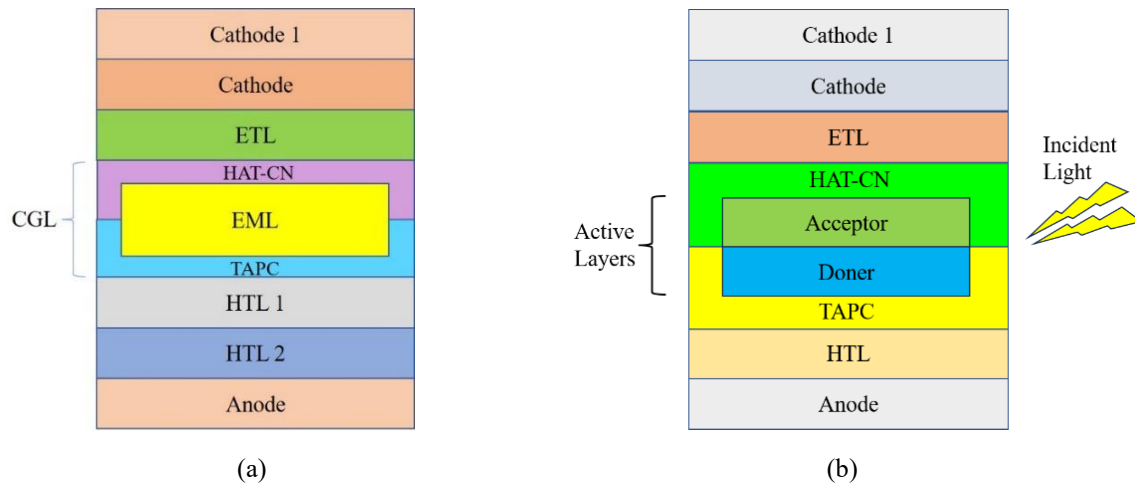


Fig. 5.2. Utilized (a) OLED and (b) OPD devices for Covid-19 detection

Table 5.1. Comparison of existing research work with proposed work in terms of wavelength

Ref.	Excitation Wavelength (nm)	Detection Wavelength (nm)	Sample	Virus detected
[249]	365	550	Saliva	SARS-CoV-2
[246]	485	520	Saliva	SARS-CoV-2
[248]	495	570	Saliva	SARS-CoV-2
[247]	470	550	Saliva	SARS-CoV-2
[226]	470	525	Saliva	SARS-CoV-2
Prop.	470	525	Saliva	SARS-CoV-2

It is observed from the table that almost 90% of the researchers have used the detection emission wavelength in the range of 450-495 nm for excitation of the samples. This wavelength range provides blue light which matches the emission spectra of the proposed OLED device L_6 . On the other hand, the fluorescence emission from the sample is detected in the range of 520-570

nm that is the regime of green wavelength. Hence, the OPD device P_2 is capable to detect the wavelengths in this range and can produce corresponding current values.

Therefore, based on the data provided in Table 5.1, the proposed devices are effectively utilized to efficiently detect the SARS-CoV-2 virus. Additionally, the structures of proposed devices are similar and based on CGL layers which can lead to realize both devices on same platform more efficiently. Therefore, in this work, the proposed blue OLED and OPD are integrated to check whether a person is infected by Covid-19 or not. The excitation and detection wavelengths are considered as 470 and 525 nm, respectively.

5.3.1 OLED driver circuit

The detection methodology discussed earlier needs an effective emission from the OLED with a good luminescence and intensity characteristics. This emission should be of a particular wavelength that can further acquire a fair enough wavelength difference on reflection from the sample for a healthy person and a patient suffering from corona virus. To accomplish the emission on a particular wavelength, the current should be high enough for the OLED, which can be achieved at a high voltage. Sometimes, a driving element can be helpful to acquire the sufficient voltage to generate a significant intensity of light from the OLED. In recent times, OTFTs are reported as a good switching element to drive the OLED based arrays owing to their very high on-off current ratio [250, 251]. In some cases, OTFT based amplifiers can also be used to raise the signal strength of the detector, if it is low and not differentiable.

Here, to drive the OLED (L_6) device, voltage-controlled vertical OTFT can be used but with inclusion of some high mobility materials to attain a high driving current. These high mobility materials can be DNNT, diF-TES-ADT, C8-BTBT, etc. [252-254]. Vertical channel based OTFTs consist of a low channel length and thus attain high current values at low V_{DS} and V_{GS} . The structure of vertical TFT (proposed in Chapter 3) consists a ditch like structure filled with organic semiconductor and observed capable enough to generate high current values. The device resistance of vertical channel transistor also observed lower than that of planar OTFTs that leads to a lower voltage drop across the transistor while it is operated in full conduction mode.

It can be understood from the Fig. 5.3, where the driver V-OTFT is connected in series with the OLED device. The current in OTFT can be controlled by the gate voltage (V_{Gate}) and supply voltage V_{DD} . Here, the gate voltage is kept at zero to attain a high V_{GS} (here -5V) and to enable a high current in the transistor. A small variation in gate voltage (subsequently in V_{GS}) can lead

to a significant change in the current and thus the luminescence of OLED too. The curve between anode voltage (node 3) with respect to V_{DD} (node 1) is plotted in Fig. 5.4 (a). Here, it is evident that a very less voltage drop occurs across the V-OTFT and it can deliver maximum voltage to the OLED.

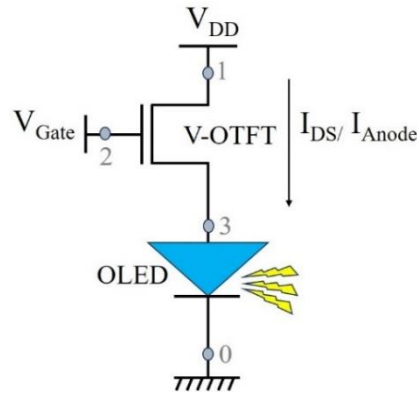


Fig. 5.3. OLED driver circuit using V-OTFT

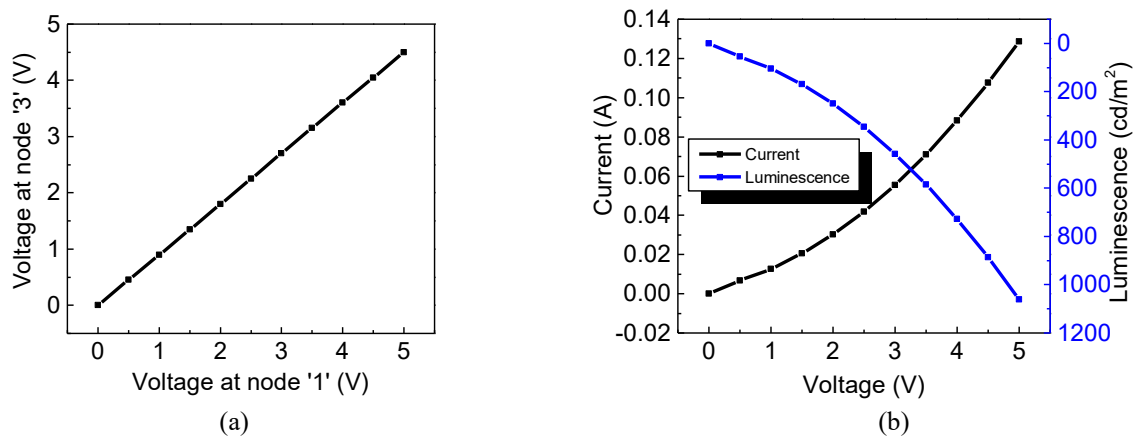


Fig. 5.4. (a) Variation of anode voltage at node 3, and (b) Current and luminescence curves of OLED

Further, Fig. 5.4 (b) outlines the current vs voltage at node 1 (V_{DD}) curve. The OLED is producing 0.128 A of current and maximum luminescence of 1061 cd/m^2 at terminal voltage of 5 V. It can be concluded that anode voltage of the OLED is controlled by the V_{DD} , which further regulates the luminescence of the light emitting diode.

5.4 COVID-19 FLUORESCENCE DETECTION USING OLED AND OPD DEVICES

The present section provides the results pertaining to the Covid-19 detection using OLED and OPD devices. The detection methodology is basically based on the emission of wavelength from OLED and detection of wavelengths at OPD. A light beam of 470 nm emitted from OLED falls on a human saliva sample and excites the sample. Now, fluorescence from saliva sample

is detected by OPD and respectively a current is produced. When the sample contains SARS-COV-2 virus, the RNA gene sequence forces the emission in 525 nm range. Corresponding to this wavelength, the OPD produces a current of 63.5 mA.

On the contrary, if the SARS-COV-2 gene is not present, the emission wavelength from the sample is 490 nm. Corresponding to 490 nm, the current produced by the OPD is 37.2 mA. The difference of two currents is quite high and thus the currents can be differentiated to determine a person healthy or infected by Covid-19. The complete information related to excitation wavelength and resultant fluorescence emission wavelength is summarized in the Table 5.2. The table also shows the current obtained in the two cases and possible interpretation of results.

Table 5.2. Excitation and emission wavelengths with current for Covid-19 detection using OLED and OPD

Excitation Wavelength	Peak Fluorescence Emission	Current corresponding to Fluorescence Emission	Outcome
470 nm	525 nm	63.5 mA	Person is infected by Covid-19
470 nm	490 nm	37.2 mA	Person is healthy

Herein, Fig. 5.5 depicts the current produced by the OPD on the basis of received wavelengths. It is clearly seen from the figure that a higher current of about 63.5 mA is produced at 525 nm wavelength. However, the current is 37.2 mA for a wavelength of 490 nm. This observation shows that the OPD is capable of differentiating between these two wavelengths. Furthermore, Figs. 5.6 (a) and (b) illustrate the comparison of the proposed work with other researcher's work in terms of peak intensities of OLED and detection wavelengths at OPD, respectively. It is observed from Fig. 5.6 (a) that even at different peak intensities, light output from the OLED is similar for same wavelengths. Additionally, when light of different wavelength falls on OPD, the different current values are achieved.

The proposed Covid-19 detection methodology is applicable for different persons. It takes into account the individuality of the person as different people may have varying attributes. Herein, ten values of luminescence (L_1 - L_{10}) at different voltages (0-5 V) are considered from the output of the proposed OLED device as depicted in Table 5.3. This table highlights that at different voltages, the luminescence values will be different and these luminescence values are named as L_1 - L_{10} . When the light of these different luminescence values from the OLED falls on saliva sample, the output fluorescence values are received in the form of beam. Different beam emission values (B_1 - B_{10}) from saliva sample corresponds to the different luminescence values (L_1 - L_{10}), respectively.

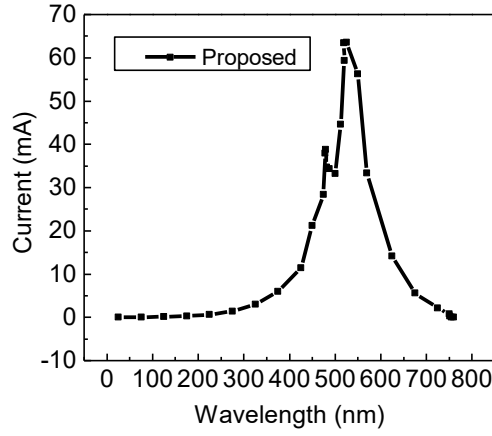


Fig. 5.5. Current with respect to wavelength variation for OPD

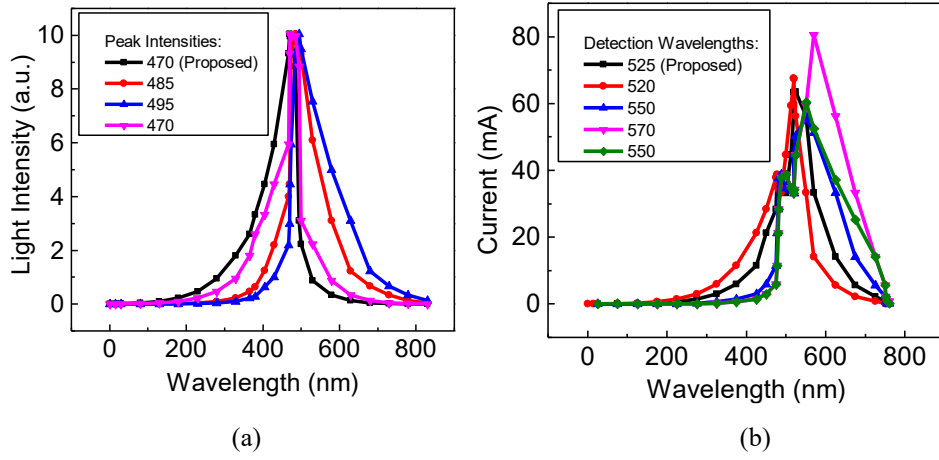


Fig. 5.6. Comparison of the proposed work with others in terms of (a) Peak intensities, and (b) Output current produced by OPD

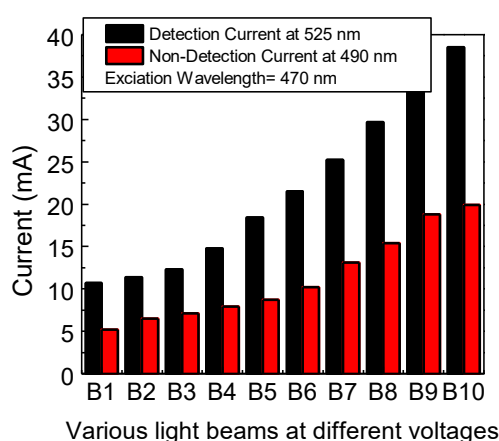
Table 5.3. Luminescence values of OLED (L_6) at different voltages (0-5 V) for wavelength 470 nm

Voltage (V)	Luminescence (cd/m ²)
0.5	$L_1=54.34$
1	$L_2=104.26$
1.5	$L_3=169.11$
2	$L_4=249.68$
2.5	$L_5=345.94$
3	$L_6=457.86$
3.5	$L_7=585.40$
4	$L_8=728.51$
4.5	$L_9=887.12$
5	$L_{10}=1061.17$

Corresponding to each beam a current value is generated by the OPD for both cases, one when the patient is suffering from Covid-19 and second when person is a healthy one. These values are shown in Table 5.4. Corresponding current values for healthy person (490 nm wavelength) and a Covid-19 patient (525 nm wavelength) for each beam is also depicted in Fig. 5.7.

Table 5.4. Current variations in OPD at different light beams from OLED for Covid-19 detection

Light beams fall on OPD with different luminous values at different voltages (emission wavelength=470 nm)	Currents (mA) obtained at detector corresponding to B ₁ -B ₁₀	
	Wavelength for Disease Detection=525 nm	Wavelength for No Disease = 490 nm
B ₁	10.7	5.2
B ₂	11.4	6.5
B ₃	12.3	7.1
B ₄	14.8	7.9
B ₅	18.4	8.7
B ₆	21.5	10.2
B ₇	25.2	13.1
B ₈	29.7	15.4
B ₉	34.1	18.8
B ₁₀	38.5	19.9

**Fig. 5.7.** Currents variations in OPD at different light beams

When the light beams (B₁-B₁₀) with these different luminous values having same excitation wavelength (470 nm) fall on the photo diode, it produces different values of currents at 525 nm and 490 nm for Covid-19 detection and non-detection, respectively (Table 5.4). Because all the light beams contain different intensity and luminescence, but same wavelength. This proposed idea can be compared with the real time situations where saliva samples may vary for different persons even if it does not contain any Covid-19 virus. In that case, the luminescence and intensity can be altered as per the discussed logic but the current values corresponding to the wavelengths 525 nm and 490 nm may be only slightly varied. Thereby, it can be concluded that the proposed methodology for the Covid-19 detection is suitable for various persons.

5.5 SUMMARY OF THE RESULTS

In the present chapter, it is depicted that the combination of organic devices: OLED, OPD and OTFT can be used successfully for the detection of Covid-19. The novelty of the detection lies

in the fact that OLED and OPD devices are used first time for such a biomedical application. Additionally, the V-OTFT is utilized for driving the OLED so that the emission wavelength can be controlled effectively. Finally, it is illustrated that the present methodology can be successfully implemented for the detection of Covid-19 using a portable sensor based on the above-mentioned organic devices. The important outcomes of the chapter are highlighted below.

- This chapter explores the flexible devices: OLED, OPD and OTFT in order to design a flexible bio-medical sensor for Covid-19 detection. The work discusses a fluorescence-based method for the detection of SARS-COV-2 virus present in a human saliva sample.
- Two high performance OLED and OPD devices designed and analysed previously are used for the detection. The OLED excites the sample at 470 nm.
- The Covid-19 gene present in the saliva sample changes the property of light. Thereby the wavelength is altered as 525 nm for the detection of Covid-19 and 490 nm for a healthy person. Further, the OPD provides the current variations corresponding to these two different emission wavelengths from the saliva sample.
- The OPD generates a current of 63.5 mA corresponding to 525 nm wavelength, which shows the presence of corona virus in the saliva sample. Conversely, for a healthy person, the current generated by OPD is 37.2 mA corresponding to 490 nm wavelength.
- Furthermore, it is also shown that the proposed detection technique is applicable for detecting SARS-CoV-2 in different persons. Analysis results show that by providing different voltages to the OLED, varying luminescence is achieved. Respectively, emission beam varies and the OPD still provides different current values for Covid-19 patient and healthy person.

Here, the detection of Covid-19 is focused by integrating OLED, OPD and OTFT devices. This method presents the possibility of developing portable sensor for multiple biomedical applications. These devices should be developed with the focus on specific applications that requires intensive investigation of materials and device structure. Therefore, the focus should be on obtaining specific colour outputs from the OLED as per the requirement of the application while developing these devices. Additionally, the output should be stable for longer duration. Therefore, the materials fabrication and development techniques should be focused in this aspect.

CHAPTER-6

HEART RATE MONITORING AND OVARIAN CANCER DETECTION USING OLED AND OPD DEVICES

6.1 INTRODUCTION

The Covid-19 pandemic of 2020 has made people more cautious about their wellbeing. Consequently, people are becoming more aware about their health and its regular monitoring which has led to the rapid advancements in the field of sensors with the focus on biomedical applications. As discussed previously, light-based detection methodologies are at the frontrunner in most of these sensors. The primary reason is the non-invasive nature of these methods. Sensory devices based on this approach are being explored not only for disease detection but also for the continuous monitoring of various critical health related parameters.

LED's and photodiodes are the primary choice for these light-based fluorescence devices. These devices have been used for designing various sensors including PPG, pulse oximeter, spectrophotometer, optical coherence tomography (OCT). However, with the focus on portability, affordability and low-cost, recently, OLED and OPD devices have been explored for similar applications. Based on these devices, researchers have proposed methodologies for detection of ovarian cancer [229], heart stroke, and SARS-COV-2 [248]. Additionally, due to high sensitivity towards light, organic devices have proved to be more accurate.

Incorporation of these flexible organic LED and photo-diode provides compact and ultra-flexible sensors. Various researchers have used these devices for a range of sensory applications. A combination of OLED and OPD was investigated by Titov *et al.* [38] to design a cost-effective optical detector. Additionally, quantitative detection of inositol phosphoglycans antibodies was presented by Katchman *et al.* [39] using human serum by using these organic devices. Further, Lim *et al.* [40] proposed an oxygen sensor Utilizing OLED and OPD. In this research, the detection of oxygen concentration was performed by the simultaneous monitoring of $TcPO_2$.

Furthermore, Lochner *et al.* [255] proposed a low-cost methodology to design a pulse oximeter using both OLED and OPD. The fabricated novel design showed good results with an error of 1% and 2% only while measuring the pulse rate and oxygen, respectively. Moreover, a reflectance oximeter sensing device was proposed with integration of these two optoelectronic devices. With this method, three sensor geometries: circular, rectangular and bracket were

illustrated. Afterwards, Lee *et al.* [226] fabricated an organic LED and photodiode-based sensor for the detection of corona virus i.e. SARS-CoV-2. The proposed device could detect the virus within 20 minutes using fluorescence emission.

This chapter focuses on two different methodologies: one for monitoring the heart rate and the other for detecting ovarian cancer using OLED-OPD integration. The following objective is framed to accomplish the work:

“Characteristic analysis of proposed OLED and OPD devices with selected materials and their utilization for heart rate monitoring and detection of ovarian cancer”

The following methodology is followed to achieve above mentioned objective: -

- Design and analysis of Polymer SPG-01T (Spiro-copolymer) (EML) based green color OLED incorporating suitable CGLs for heart rate monitoring.
- Design and analysis of QAD (4-(5,6-dimethoxy-1-benzothiophen-2-yl)-4-oxobutanoic acid) (EML) and CGLs based OLED for ovarian cancer detection.
- Analysing OPD device with modified layers as light detector to monitor heart rate and detect ovarian cancer in cohesion with proposed OLED.

The present chapter continues the work in the preceding chapter wherein combination of organic devices was used for detection of Covid-19. However, herein the focus lies in monitoring of heart rate. Therefore, using the novel proposed architecture, OPD device is designed to emit green light specific to heart rate monitoring. Similarly, green OPD device is also developed for the detection purpose. Combination of these devices makes it possible for monitoring of heart rate. Additionally, OLED and OPD devices are also used for detection of ovarian cancer. Researchers have tried detection of ovarian cancer through fluorescence detection; however, OLED-OPD integration is used for the first time for this application. Moreover, the results depict successfully non-invasive methodologies for monitoring of heart rate and detection of ovarian cancer.

This chapter is arranged in eight different sections, wherein, Section 6.1 is about introducing different sensing application using OLED and OPD. The methodology for heart rate detection is illustrated in Section 6.2. and accordingly, some layers of OLED and OPD devices are modified in order to measure the heart rate in human in Section 6.3. Subsequent results are discussed in Section 6.4. Similarly, ovarian cancer detection methodology is discussed in Section 6.5 along with a comparison of reported researchers' work with the proposed work. Afterwards, the devices are modified on the basis of need for the cancer detection and

discussed in Section 6.6 with subsequent results in Section 6.7. Further, Section 6.8 summarized the work presented in this chapter.

6.2 DETECTION MECHANISM FOR HEART RATE MONITORING

The photoplethysmography (PPG) is very popular medical technology to measure heart rate and blood oxygen in real time [256, 199]. This device was most widely used during the 2020 pandemic to measure these two vital health parameters. The working principle follows the light detection methodology which contains a LED and a photo-diode as depicted in Fig. 6.1. A target light beam of green color falls from the LED on the blood tissue. The blood has the property to absorb this green light. Therefore, a portion of the light is absorbed and rest is reflected depending upon the amount of blood volume flowing in the vessels. The photo-diode senses the reflected light and converts it into an electrical signal.

Various researchers have devoted efforts in designing a highly efficient, motion tolerant low noise PPG sensor. Kim *et al.* [257] proposed an ‘All in one sensor’ by integrating OLED and OPD aimed to detect heart rate, blood pressure and heart rate variability. Moreover, Lochner *et al.* [255] reported all organic optoelectronic sensor to measure the human pulse rate using green and red OLEDs and single flexible OPD. The device exhibits only 1% error in the pulse rate measurement.

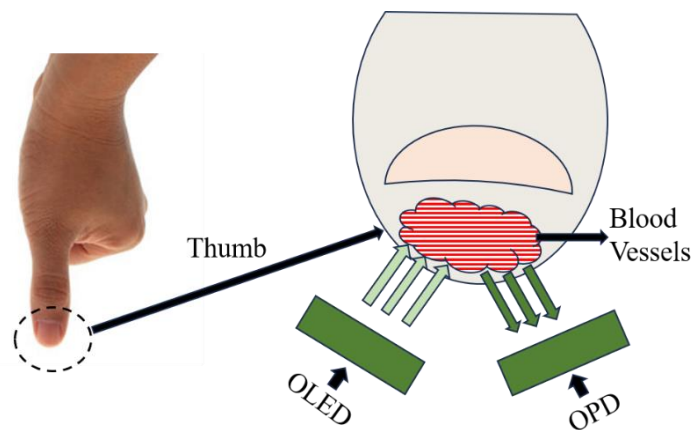


Fig. 6.1 Heart rate detection methodology using OLED and OPD devices

Pandey *et al.* [258] also designed an OLED-OPD based flexible sensor in which heart rate is measured with 96% accuracy. In addition to this, the ideas for flexible and wearable devices for pulse oximetry sensor are discussed by Dcosta *et al.* [259]. This research was focused on the geometry, design, processing technique, and encapsulation of the oximetry sensor. Furthermore, Jhuma *et al.* [260] presented a review which is focused on the growth of PPG sensors in terms of their flexibility.

Moreover, Simone *et al.* [261] proposed an organic reflectance PPG array using 16×16 OPD pixel. The pixel device exhibits the sensitivity up to 950 nm and low dark current as 10^{-6} mA/cm². Additionally, Bilgaiyan *et al.* [262] investigated the OPD performance for refining the sensing ability of PPG sensor. The review presented here highlights that researchers are more focused on utilizing the OPD for the detection of heart rate and use of OLED is not that prominent. Mostly, the OLED has been explored for sensor displays. However, the few researchers who have used the combination of OLED and OPD for heart rate monitoring have achieved better results. Therefore, the present work focuses on the combination of these two devices for heart rate monitoring.

6.3 DEVICE MODIFICATION IN TERMS OF WAVELENGTH FOR HEART RATE MONITORING

The proposed work incorporates OLED and OPD devices for heart rate monitoring. The devices designed in the previous chapters are based on blue color wavelength and thus needs some modifications to apply for heart rate monitoring. Therefore, in this section, two devices OLED (H₁) and OPD (H₂) are designed and analysed specifically focused on the requirements of a heart rate monitor. The device structure is same as the proposed devices; however, the material of the emission layer is changed with the focus of green light emission. Accordingly, the CGL layers are selected to have a close energy matching with the adjacent layers. As per the methodology, the light emitter device should able to produce a desired green wavelength and the light detector must be capable of detecting the reflected wavelength. Both devices H₁ and H₂ are discussed in the following sections in detail.

6.3.1 Modified green OLED (H₁) for heart rate monitoring

Herein, a modified OLED structure (H₁) is presented as shown in Fig. 6.2 (a) wherein the proposed device shown in Fig. 4.6 is altered with respect to the layers to achieve desired green wavelength emission. The reference device for this structure is validated previously in chapter 4. Figure 6.2 (b) outlines the simulated structure of the OLED device (H₁). The device contains eight different layers detailed in the Table 6.1 along with materials and thicknesses. The results are obtained using Langevin recombination rate model that is applied in the 2-D device simulator for the study of recombination rate. Further, Poole-Frenkel mobility model is applied to understand the carrier's transportation in the device.

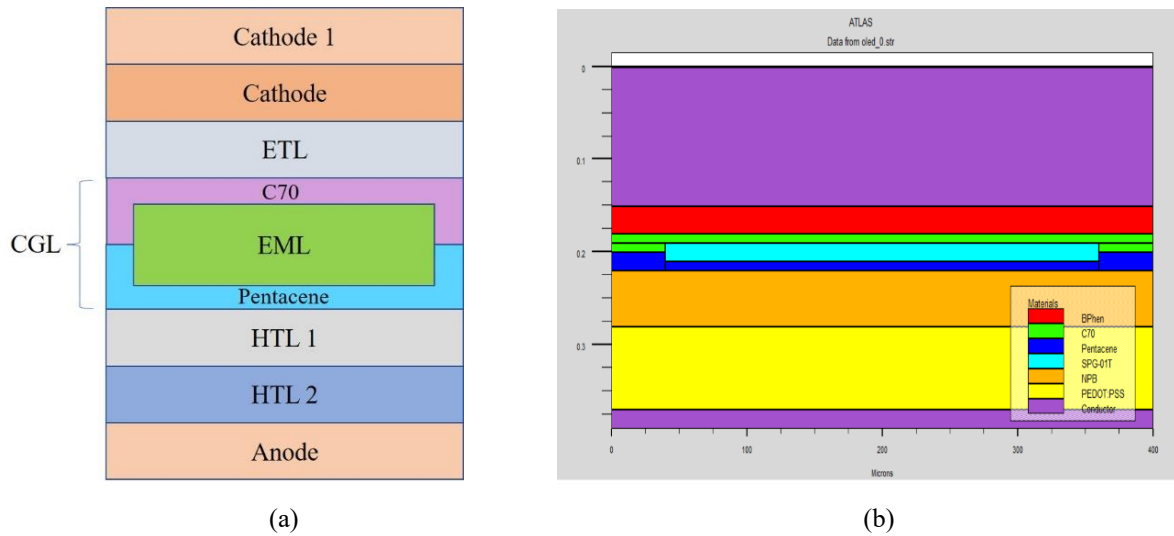


Fig. 6.2 (a) Structure of Green OLED device H₁ and (b) Simulated structure of device H₁

Table 6.1 Different materials used in OLED (H₁) along with the thickness of each layer

Layer	Material and dimensions for Proposed Device (H ₁)	
	Material	Thickness (nm)
Cathode 1	Al	150
Cathode	LiF	1
ETL	BPhen	30
CGL (Electron generator)	C70	20
EML	Polymer green SPG-01T	20
CGL (Hole generator)	Pentacene	20
HTL1	NPB	60
HTL2	PEDOT:PSS	90
Anode	ITO	20

a. Need of CGL in OLED H₁

The charge generation layer has proven influential in enhancing the device performance as demonstrated previously. Therefore, the present device H₁ also consists of the CGL layers. The selection of CGL is based on the matching of the energy levels with the adjacent layers. In the present work, CGL layers (Pentacene and C70 (Fullerene-70)) are placed between the HTL layer NPB and the ETL layer BPhen. The Pentacene material meant for hole generation, is placed close to NPB, which leads to a good match in their corresponding energy levels of 5 eV and 5.4 eV. Similarly, BPhen and C70 (for electron generation), depicting LUMO levels 3.2eV and 4.0eV respectively, are placed next to each other. The small energy gap between these adjacent layers results in better injection of the charge carriers from electrodes towards the EML. Additionally, these layers generate the charge carriers, which are further provided to the EML.

The CGL is placed on each side the EML (Fig. 6.2 (a)) in the modified device. Inclusion of CGL in organic LED contributed significant improvement in charge carrier injection. Thereby, the device exhibits higher current density and enhanced luminous properties [25-28]. Thus, generated excess electrons and holes are directly moving to the EML which automatically results in an enhanced recombination rate in H₁ as based on the Langevin's theory.

b. Wavelength calculation for H₁

Every light wave has its own specific wavelength which is dependent on the energy band gap of the materials used for emission layer. Herein, the calculation of wavelength for the modified green OLED H₁ is mentioned. As shown in Table 6.1, the material for EML is SPG-01T which contains the energy band gap of 2.5 eV [263].

$$\text{The energy gap } (E_g) = h\nu \quad (6.1)$$

$$\text{where, } \nu = \frac{c}{\lambda} \quad (6.2)$$

$$\text{Hence, } E_g = \frac{hc}{\lambda} \text{ (in Joule),} \quad (6.3)$$

$$\text{and } \lambda = \frac{hc}{E_g} \text{ (in meters)} \quad (6.4)$$

In equation 6.4, the parameters h , λ and c represents Planck's constant, wavelength and speed of light, respectively.

After incorporating all the values in equation 6.4,

$$\lambda = \frac{6.626 \times 10^{-34} \times 3 \times 10^8}{2.5 \times 1.6 \times 10^{-19}}$$

$$\lambda = 497\text{nm}$$

It is clear from the value of λ that OLED (H₁) exhibits green color wavelength as the green light ranges from 495 nm to 570 nm.

6.3.2 Modified OPD (H₂) for the detection of wavelengths

The OPD device required for the detection of heart rate, should detect green wavelength and must be able to produce corresponding current output based on even a small variation. Therefore, in the present sub-section, the proposed OPD device (Fig. 4.22) is modified with respect to active layers and CGLs. The CGLs (Pentacene and C70) used herein are same as that of OLED device H₁ which opens the prospect of fabricating both the devices on a single substrate. The active layer utilized herein are C60 and CuPc as acceptor and donor layers, respectively. These active layers are sensitive to green light thereby, enhancing the device sensitivity. This OPD device is named as H₂.

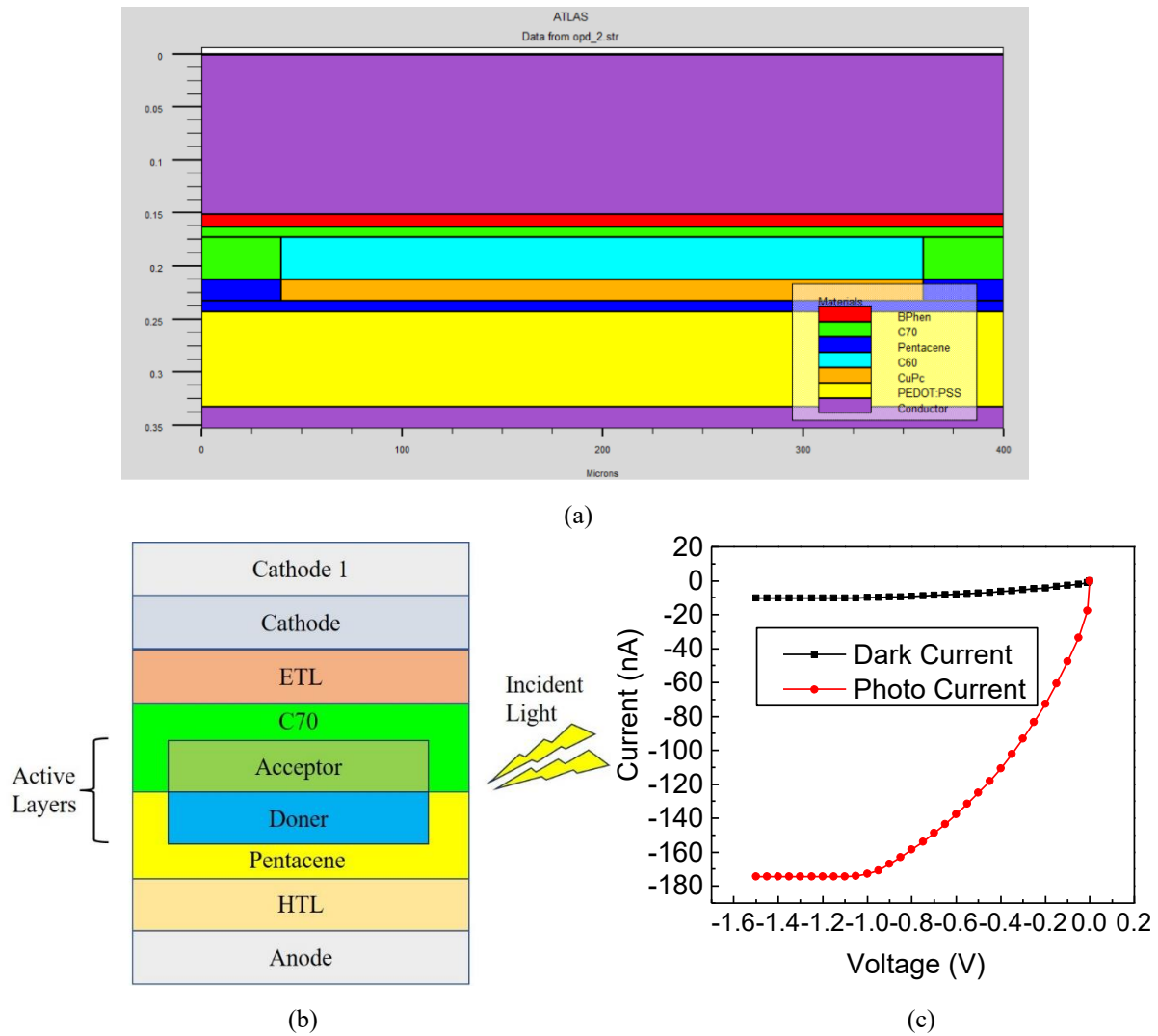


Fig. 6.3 (a) Simulated structure of OPD (H₂), (b) Proposed structure of the device OPD (H₂), and (c) Results for dark current and photo current of H₂

Table 6.2 Enlisting of the materials along with their thickness values for each layer of OPD (H₂)

Layer	Material and dimensions for H ₂	
	Material	Thickness (nm)
Cathode 1	LiF	1
Cathode	Al	150
ETL	BPhen	12
CGL (Electron generator)	C70	50
Acceptor	C60	40
Donor	CuPc	20
CGL (Hole generator)	Pentacene	30
HTL1	PEDOT:PSS	90
Anode	ITO	20

Table 6.2 shows all the incorporated materials used in H₂ along with the thickness for each layer. Figure 6.3 (a) depicts the simulated structure of H₂ device. Similar to the proposed device, CGLs of C70 and Pentacene are used such that acceptor and donor materials should remain

between these two layers. Herein, Pentacene (the hole generator layer) is used towards the donor layer - CuPc and C70 (the electron generator layer) is used on the acceptor layer side (C₆₀). The respective thickness of these two CGL layers are 30 nm and 50 nm. The device is operated in reversed bias mode.

When the light falls on the acceptor donor layer interface, the process of exciton dissociation takes place resulting in generation of electrons and holes. Additionally, the excitons also interact with the nearby CGL, which results in the generation of additional charge carriers. Since, Pentacene is a hole injector therefore, on interaction with excitons it generates additional holes. Similarly, C70 generates additional electrons. Thus, these extra charge carriers get added with the carriers generated in acceptor and donor layers and help in conduction within the device. Consequently, a huge amount of photocurrent is observed in the device, as depicted in Fig. 6.3 (c). The maximum values of photocurrent generated is 174.5 nA.

6.4 HEART RATE MONITORING USING MODIFIED OLED AND OPD

The present section explores the utilization of OLED (H₁) and OPD (H₂) devices for monitoring heart rate and investigates the present methodology for persons with varying traits. The entire research is a step towards flexible heart rate sensor. The green OLED is selected for this application as skin has a high coefficient of absorption for this wavelength and a better contrast signal is received [264]. The effectiveness of using green emission is also illustrated by multiple researchers in their work, as shown in Table 6.3, which highlights that the green wavelength is prevalent across all these works.

Table 6.3. Comparison of existing work with the proposed work for heart rate detection in terms of wavelength

Ref.	OLED Color	Wavelength (nm)	Sample	Detection
[265]	Green	527	Blood cells	Heart Rate
[255]	Green	532	Blood cells	Heart Rate
[258]	Green	530	Blood cells	Heart Rate
[259]	Green	530	Blood cells	Heart Rate
Prop.	Green	497	Blood cells	Heart Rate

The detection is achieved when a target light beam of 497 nm from the OLED falls on the human blood tissue. Depending upon the blood flow, a part of this light is absorbed, whereas the rest is reflected back. This reflected light is detected by the OPD and a corresponding current is produced. During the systole, amount of blood in the vessels is high, therefore, a higher amount of light is absorbed. On the other hand, for the diastole cycle, the blood flow is low and a higher amount of light is reflected. Accordingly, the current is produced by the OPD.

If the heart rate is high, then frequent systole cycles lead to less amount of light to be reflected, thereby, the current produced by the OPD is low. On the contrary, during the normal heart rate, systole cycles are more balanced and good amount of light gets reflected which prompts the OPD to produce a higher amount of current during lower heart rate. Thereby, it can be concluded that a high current is achieved when lower blood volume flows in the tissue. Contrary to this, a lower current is achieved during high blood flow in the tissue (Table 6.4).

Table 6.4. Methodology for heart rate detection based on dedicated OLED wavelength values for excitation and corresponding current values generated by the OPD

Excitation Wavelength (nm)	Detection Wavelength (nm)	Blood Volume	Output Current	Heart Rate
497	497	High	Low	High
		Low	High	Low

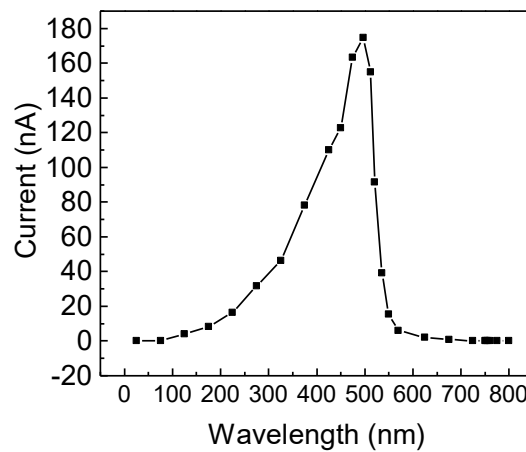


Fig. 6.4 Current values of OPD (H₂) at different wavelengths

The current values generated by OPD at different wavelength are shown in Fig 6.4 which implies that at different wavelengths, OPD produces different current values. However, in the above methodology, it is observed that the variation in current is because of the intensity of the light and not due to the variation in wavelength. The same thing is highlighted in Table 6.4. Therefore, analysis is conducted to investigate the performance of the organic photodiode at different light intensities having same wavelength. Herein, it is shown that the proposed photo diode (H₂) is capable of producing the different current values at different light intensities.

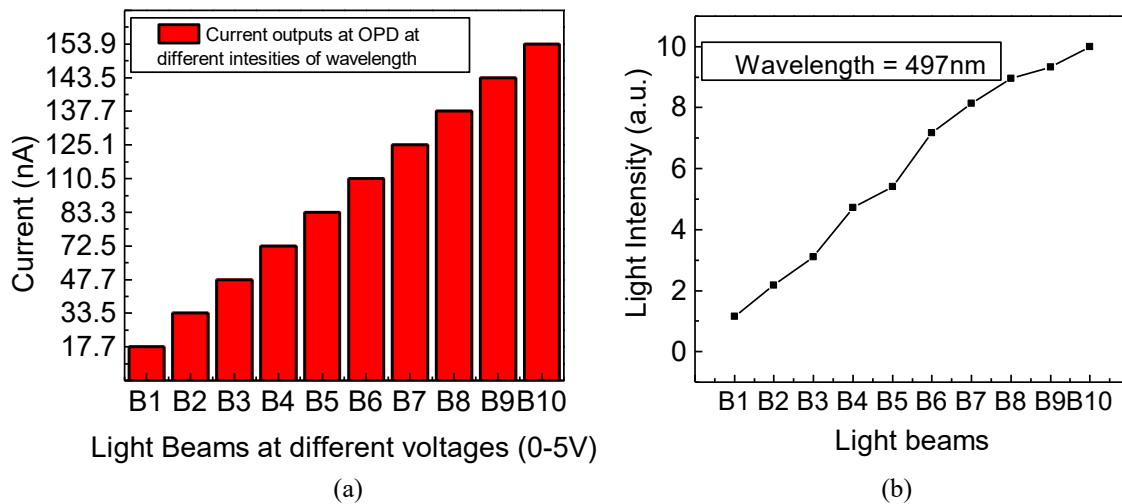
The voltage at the anode of the OLED is varied from 0 – 5 V in a step size of 0.5 V which results in varying values of luminescence output from the device. These ten voltage levels provide ten different light beams (L₁-L₁₀) as shown in Table 6.5. When these light beams fall on the blood tissue, some of this light is absorbed by the blood and the rest is reflected. The different reflected light beams are represented by (B₁-B₁₀) also have varying intensities. These are detected by the OPD.

Table 6.5. Luminescence values of OLED (H₁) at different voltages (0-5 V)

Voltage (V)	Luminescence (cd/m ²)
0.5	L ₁ = 124.9
1	L ₂ = 239.8
1.5	L ₃ = 388.9
2	L ₄ = 574.5
2.5	L ₅ = 795.6
3	L ₆ = 1053.1
3.5	L ₇ =1346.4
4	L ₈ =1675.5
4.5	L ₉ =2040.4
5	L ₁₀ = 2440.6

Table 6.6. Different current values generated by OPD (H₂) at different light beams (B₁-B₁₀) for heart rate monitoring

Light beams fall on OPD with different luminous values at different voltages (emission wavelength= 497 nm)	Currents (nA) obtained at detector corresponding to B ₁ -B ₁₀
B ₁	17.7
B ₂	33.5
B ₃	47.7
B ₄	72.5
B ₅	83.3
B ₆	110.5
B ₇	125.1
B ₈	137.7
B ₉	143.5
B ₁₀	153.9

**Fig. 6.5** (a) Current values of OPD at different light beams, and (b) Light intensity at different beams

The light beams falling on the OPD are of the same wavelength, however, their intensity varies. The OPD device (H₂) is capable of differentiating these beams of different intensity and respectively produces different current values at the same wavelength. The current values

produced by the OPD for different intensities are summarized in Table 6.6. Additionally, the variation in different current values is shown in the bar graph in Fig. 6.5 (a). Further, the intensity of each beam is plotted in Fig. 6.5 (b). The figure clearly depicts a variation in the intensities of corresponding light beams. Thus, at these different light intensities, OPD is capable of generating different current values as shown in the figure which enables accurate detection of heart rate even if operating conditions are varying.

6.5 DETECTION MECHANISM FOR OVARIAN CANCER

The urine sample can provide a substantial information regarding the health and physiological condition of a human. The human urine sample shows a strong interaction with light and alters the characteristics of light in accordance with the health conditions of a human being. This concept is proposed and validated by a number of researchers. To analyse the different chemical component of urine, the first fluorescence emission was studied by Leiner *et al.* [266]. Similarly, Ahmed *et al.* [267] discussed the use of Infrared spectroscopy to examine the presence of urea in human urine. The study depicted a relation between the concentration of urea and the absorption spectra of urine. The examination showed that the absorption got improved with increment of the urea concentration.

The biggest advantage of using the light dependent analysis is its non-invasive nature. The methodology is successfully used for detecting even fatal diseases: cancer and heart stroke. Following light based detection, Masilamani *et al.* [268] demonstrated a non-invasive technique to examine various kind of cancers using urine fluorescence properties. Herein, cancer in many human organs including cervix, liver, breast, bladder was investigated. Similarly, Zavarik *et al.* [269] proposed a fluorescence-based methodology for the detection of ovarian cancer. They showed that if a light beam of 330-370 nm wavelength is used to excite the urine sample, it is possible to detect ovarian cancer. The patient of ovarian cancer shows the presence of pteridines in high amount as compared to a normal person which leads to the fluorescence emission wavelength as 440 nm for the ovarian cancer patient. Whereas, for a normal person this emission value is recorded as 420 nm.

Table 6.7. Comparison of the proposed work with other researchers' work in terms of excitation and detection wavelength for ovarian cancer detection

Ref.	Excitation Wavelength (nm)	Detection Wavelength (nm)	Sample	Disease
[229]	330	440	Urine	Ovarian Cancer
[269]	300-400	420	Urine	Ovarian Cancer
[270]	280	400	Urine	Ovarian Cancer
Proposed	350	440	Urine	Ovarian Cancer

Furthermore, based on the methodology of Zavarik, Negi *et al.* [229] proposed the detection of ovarian cancer using OLED device only. In their work, similar wavelengths were used for the emission. However, the light detection was also proposed by using the OLED device. The light wavelength used in these research work along with the proposed work is summarized in Table 6.7. The table highlights that the detection wavelength in all these cases lies in the region of green color.

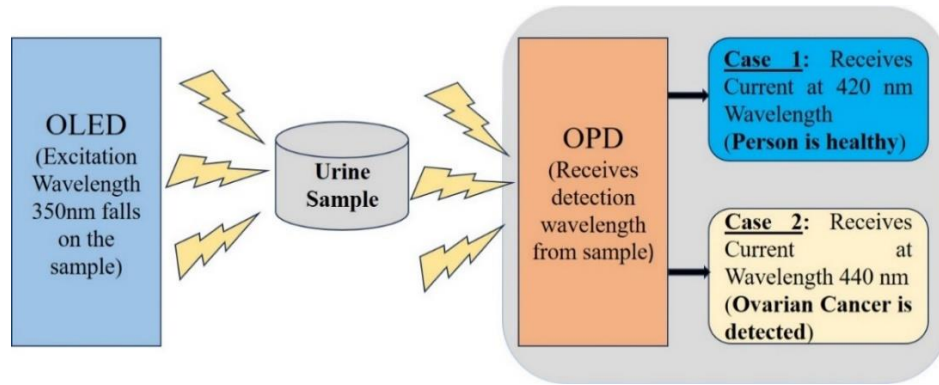


Fig. 6.6 Ovarian cancer detection methodology

Thus, in the proposed work, the excitation wavelength for the sample is selected as 350 nm. The OLED device is modified such that the desired wavelength is achieved. Similarly for the detection purpose, OPD device should be capable of detecting the emission by green OLED. Since, the OPD modified in the previous section is capable for detection of this wavelength, therefore, same OPD (H₂) is utilized for this application as well. The complete methodology for the detection of ovarian cancer used in the present work is highlighted in Fig. 6.6. Herein, the OLED excites the urine sample with the light beam of 350 nm. This beam emits the urine sample and corresponding fluorescence is observed. If the person is suffering from ovarian cancer, then due to the presence of pteridine, the emission is in 440 nm range which is detected by the OPD and corresponding current is generated.

6.6 OLED MODIFICATION IN TERMS OF MATERIALS FOR OVARIAN CANCER DETECTION

The previous section highlights that the excitation wavelength for the detection of ovarian cancer is near to 350 nm. Therefore, in this section, the proposed OLED device is modified to achieve this emission wavelength. The device is modified with respect to the materials used for CGLs and emission layer. The CGL layers are composed of m-MTDATA and Alq₃ materials for charge generation. Whereas, QAD is chosen for the emission layer owing to its superior green color emission. The present OLED device is named as O₁ and it can produce the light

output in 300-400 nm range which is the required excitation wavelength for the detection of ovarian cancer. The structure of the device (O_1) is shown in Fig. 6.7 (a) and Table 6.8 provides the dimensions of different layers used in the device. The simulated structure of the device is shown in Fig. 6.7 (b).

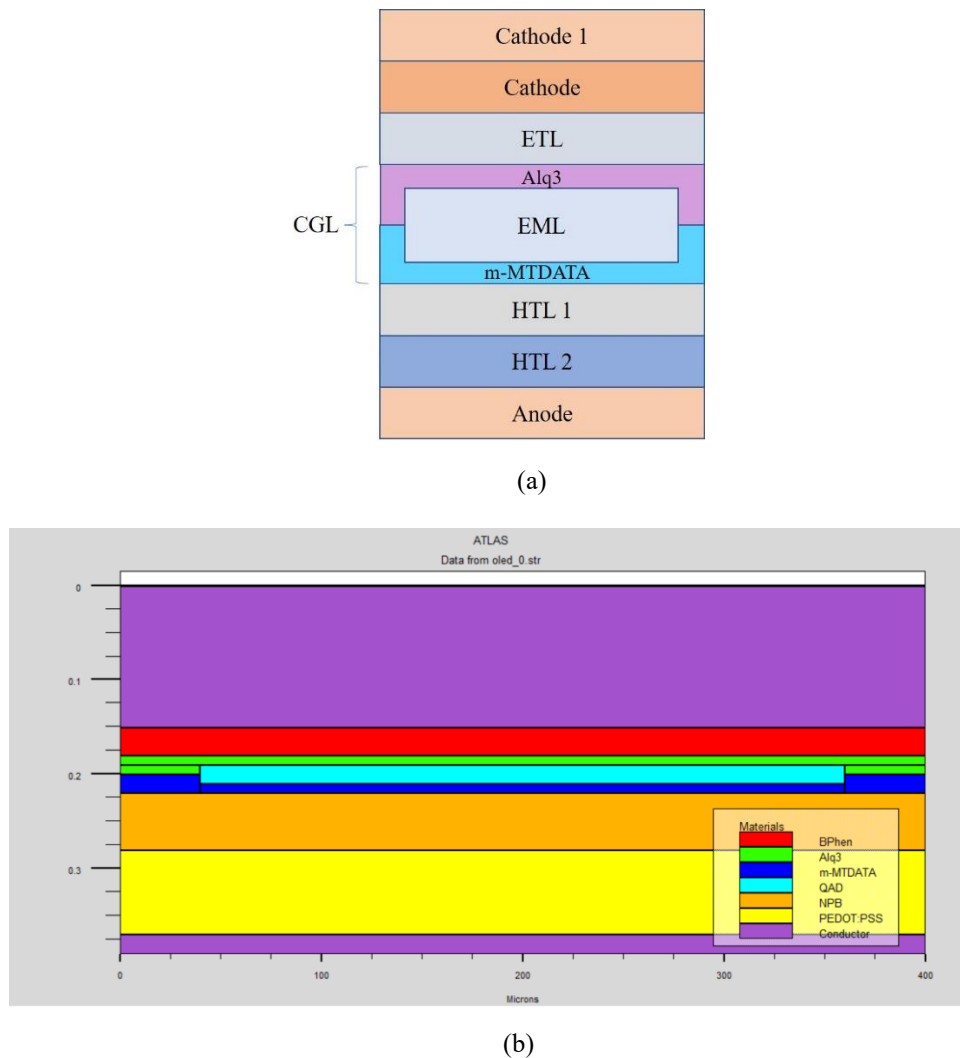


Fig. 6.7 (a) Modified structure of OLED Device (O_1), and (b) Simulated structure of modified OLED device (O_1) for ovarian cancer detection

As discussed in Chapter 4, the use of CGLs outside the emission layer enhances the charge carrier concentration within the device which leads to an enhanced recombination rate, leading to higher luminescence and current density. Once the OLED excites the urine sample, the fluorescence emission takes place and the emitted light needs to be detected. The wavelength of the emitted light is in the range of 400-500 nm. The OPD device (H_2) analysed in the previous section can detect this wavelength and produces relative current.

Table 6.8. Materials and thickness for OLED (O₁)

Layer	Material and dimensions for Modified Proposed Device (O ₁)	
	Material	Thickness (nm)
Cathode 1	Al	150
Cathode	LiF	1
ETL	BPhen	30
CGL (Electron generator)	Alq ₃	20
EML	QAD	20
CGL (Hole generator)	m-MTDATA	20
HTL2	NPB	60
HTL1	PEDOT:PSS	90
Anode	ITO	20

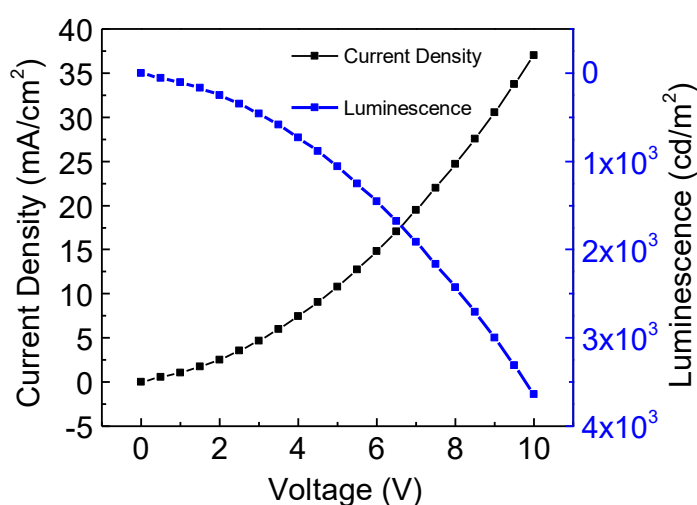


Fig. 6.8 Parametric analysis of OLED (O₁) in terms of current density and luminescence

The characteristics of the modified OLED (O₁) is analysed and are shown in Fig. 6.8. The graph illustrates both the current as well as luminescence characteristics. The maximum observed current density is 37.02 mA/cm². Additionally, the luminescence for the device is observed as 3638 cd/m².

6.7 OVARIAN CANCER DETECTION USING MODIFIED DEVICES OLED O1 AND OPD H2

The detection of ovarian cancer is achieved when a light beam from OLED O₁ falls on the urine sample and its fluorescence emission is analysed through the OPD H₂. The excitation wavelength from O₁ is 350 nm. Once this beam falls on the urine sample, the various components present in it causes a fluorescence emission which is different from the excitation wavelength. With respect to the present input wavelength, the emission wavelength for a healthy person is 420 nm. However, for an ovarian cancer patient, due to the presence of

pteridine, the emission is observed at 440 nm. Device H₂ produces two different current values 31.2 nA and 47 nA with respect to 420 nm and 440 nm wavelengths and thus two wavelengths are clearly differentiable.

If the current achieved is 31.2 nA, it corresponds to 420 nm wavelength and it can be inferred that the person is healthy. However, if the output of the OPD is 47 nA, corresponding to 440 nm, the person is declared suffering from ovarian cancer. These results are mentioned in the Table 6.9. However, it is to be noted that in a practical scenario, situation can vary with respect to the device operating voltages and the urine sample which varies from person to person.

Table 6.9. Technique for ovarian cancer detection using OLED and OPD

Excitation Wavelength (nm)	Peak Fluorescence Emission (nm)	Current corresponding to Fluorescence Emission (nA)	Result
350	420	31.2	Woman is healthy
350	440	47	Ovarian Cancer is detected

The device O₁ produces the required wavelength of 350 nm which is a material related parameter. However, depending on different scenarios, the luminescence of the device can vary. The color and density of the urine sample vary from person to person, which can impact the luminescence intensity of the output light. Therefore, a possibility is analysed wherein the present device combination can detect ovarian cancer under different attributes and conditions.

Herein, ten different light beams of varying luminescence output (L₁₁-L₂₀) from the OLED are considered corresponding to different operating voltages as shown in Table 6.10. The emission wavelength for all these ten beams will be same. When these beams fall on urine sample, the emission will be either in 420 nm or 440 nm range depending on whether sample is of a healthy person or an ovarian cancer patient. Now, since the input luminescence is different with same wavelength, therefore, output current generated by the device H₂ will vary.

Table 6.10. Luminescence values of OLED (O₁) at various voltage from 0-5 V

Voltage (V)	Luminescence (cd/m ²)
0.5	L ₁₁ =54.2
1	L ₁₂ =103.9
1.5	L ₁₃ =168.9
2	L ₁₄ = 250
2.5	L ₁₅ =346
3	L ₁₆ =458
3.5	L ₁₇ =586
4	L ₁₈ =729.1
4.5	L ₁₉ =886.9
5	L ₂₀ =1058.2

Table 6.11. Current variations in OPD at different light beams

Light beams fall on OPD with different luminous values at different voltages (emission wavelength=350 nm)	Currents (nA) obtained at detector corresponding to B1-B10	
	Wavelength of detection=440 nm	Wavelength of non-detection = 420 nm
B ₁₁	5.2	2.9
B ₁₂	6.3	3.7
B ₁₃	7.5	5.2
B ₁₄	8.0	6.8
B ₁₅	8.9	7.2
B ₁₆	10.2	8.9
B ₁₇	13.2	9.8
B ₁₈	15.6	10.7
B ₁₉	21.2	12.8
B ₂₀	23.1	14.9

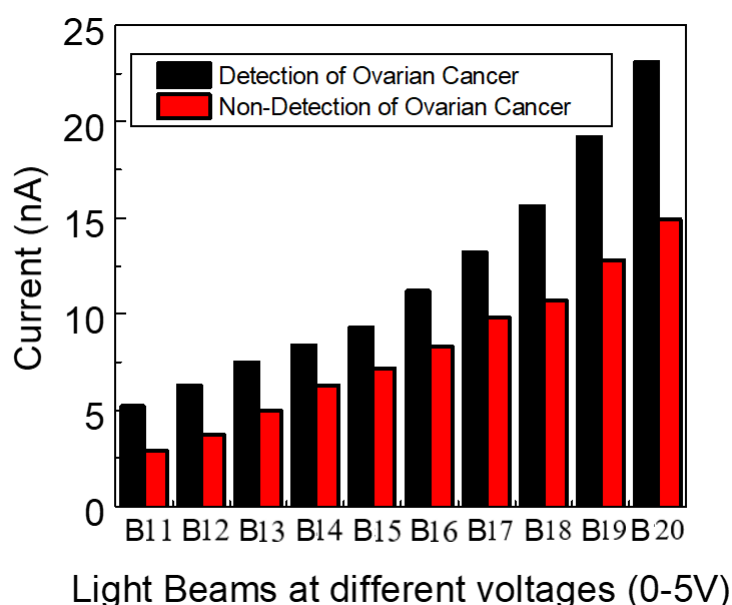
**Fig. 6.9** Different Current values generated by OPD at different light beams

Table 6.11 shows the current values corresponding to the different light beams. The emission corresponding to these different beams at 420 nm and 440 nm results in different current values as depicted in the table. Thus, it can be inferred that if different people are analysed with different attributes, the OPD device can still detect whether the emission is at 420 nm and 440 nm even at different luminescence values.

Figure 6.9 shows the comparison of current values obtained at wavelengths 440 nm and 420 nm for different fluorescence beams B₁₁-B₂₀. It is observed that the current values for all luminescence values are higher for 440 nm. Additionally, the current values obtained at these two different wavelengths are sufficiently far and can be easily differentiated. Thus, the proposed methodology is comparable with the real time implementation where urine samples

may differ for multiple persons even if it does not have any cancer component. In that case, the excitation wavelength will be altered as per the discussed technique but the current values corresponding to the wavelengths 440 nm and 420 nm may easily be differentiated. Thereby, it can be concluded that the presented methodology is suitable for various persons for the ovarian cancer detection.

6.8 SUMMARY OF THE RESULTS

The present work is focused on utilization of the organic devices, namely OLED and OPD for measuring the heart rate and detection of ovarian cancer. It is depicted that using the proposed architecture of CGL based OLED and OPD devices heart rate monitoring is achieved. Herein OLED (H_1) and OPD (H_2) devices are designed that can emit and detect the green color light (497 nm wavelength), respectively. Additionally, it is evident that the methodology for the measuring heart rate is possible for people with varying traits. Thereafter, novel methodology for detection of ovarian cancer is also illustrated. Herein, OLED and OPD devices are used for the first time to realize the proposed mechanism. The emission from the OLED (O_1) is in the range of 350 nm whereas for the detection, urine sample alters the wavelength in the range of 420-440 nm which can be successfully detected by the OPD. Thus, the work shows that the integration of the OLED and OPD devices can be used successfully for a range of biomedical applications. The important results pertaining to the present chapter are highlighted below.

- This work showcases the methodologies for heart rate monitoring and ovarian cancer detection using CGL based OLED and OPD devices.
- For heart rate monitoring, a green OLED (H_1) is opted for the light source which emits the light with wavelength of 497 nm. Herein, the current density and luminescence are obtained as 0.92 A and 8363.6 cd/m², respectively.
- The organic photo-diode is modified with respect to the requirements for heart rate detection and it produces a peak photocurrent and dark current of 10.2 and 174.5 nA, respectively.
- The methodology of heart rate detection depicts that during the diastole, a higher current is produced by the OPD as blood cell absorbs less green light. However, a lesser current is witnessed in the case of systole due to less absorption of the green light by presented blood cells in the blood vessels.
- In both the proposed OLED and OPD, an additional layer of CGL is incorporated to obtain the significant improvement in the device performances. The utilized novel

OLED exhibits the luminescence and current density as 3636.38 cd/m² and 37.02 mA/cm², respectively. While, the OPD registers 10.2 nA and 174.5 nA as the dark and photo current, respectively.

- Furthermore, a detection methodology for ovarian cancer using combined arrangement of OLED and OPD is presented. The OLED is developed to emit a light of 350 nm wavelength and falls on the urine sample. Afterwards, the property of light is altered by the component (pteridine associated with ovarian cancer patient) presents inside the sample and thus the OPD may receive the light of two different wavelengths: 420 and 440 nm depending upon the condition of person.
- Thus, the OPD produces two different photo currents 31.2 nA and 47 nA corresponding to 420 nm and 440 nm wavelengths, respectively. These current values are easily distinguishable and thus a clear differentiation for a healthy or suffering person can be achieved.

This chapter shows the heart rate monitoring and detection of ovarian cancer using OLED and OPD devices. The OLED and OPD devices are modified in terms of materials to achieve specific application, i.e. green OLED and OPD for heart rate monitoring and blue OLED and OPD for ovarian cancer detection. Such differentiation highlights an important aspect that must be addressed from the perspective of OLED design and functionality. Blue OLED emitter materials need focus as their development is still lagging. Blue emitter materials degrade rapidly and often depict lower performance. Thus, it is needed to develop blue emitters with an improved performance. Novel methodologies such as insertion of phosphorescent materials and activated delayer fluorescence methodologies can be given due consideration which will enhance the development of displays and other applications as well wherein RGB emission is important.

CHAPTER - 7

CONCLUSIONS AND FUTURE SCOPE

The present research work is focused on the design and analysis of different organic electronic devices: OTFT, OLED and OPD based on structural modifications and suitable material combinations for different layers. These proposed devices are further utilized to detect Covid-19 virus and cancer. Also, these devices showcased their potential use in heart rate monitoring. This chapter summarizes the important results of the proposed work. Conjointly, it also presents some specific directions for future research work.

7.1 CONCLUSIONS

The present work is focused on investigating the utilization of organic optoelectronic devices: OLED and OPD for biomedical applications with the OTFT as a driving element. All the three devices are composed of organic polymeric materials that results in portable, low cost and flexible devices. Additionally, the optoelectronic devices have structured with a prospect of fabricating these devices on a single substrate. Each of the three mentioned devices are analysed with respect to their respective structure and its impact on their corresponding performance. Novel structure for each device is proposed with an aim of enhancing the performance of these devices.

Organic thin film transistor is explored first. The analysis of planar structure of OTFT illustrated satisfactory performance, however, it is observed that a shorter channel can enhance the device performance. Subsequently, a vertical channel based TFT with novel ditch structure (D_5) is designed and compared with the planar transistor (D_1) of same materials. Additionally, three other vertical channel devices (D_2 - D_4) are analysed keeping the same materials and dimensions as the planar device. A performance improvement is observed for vertical device with respect to threshold voltage and drain current.

The proposed device (D_5) exhibited threshold voltage of -1.5 V, with the high current value of 528 μ A, and the saturation mobility of 80.8 cm^2/Vs . The current and mobility values are higher by 2.5 times than the basic vertical device D_2 . Additionally, in comparison to other vertical OTFT devices analysed in the work, the improvement in current values is 6.4, 4.4, 44 and 3.59 times with respect to devices D_3 , D_4 , D_6 and D_7 . Similarly, a high saturation mobility is achieved for device D_5 which is higher by 2.67, 8.32, 5.21, 73.45 and 3.60 times in comparison to D_2 , D_3 , D_4 , D_6 and D_7 .

An internal device analysis is undertaken to understand the facts associated with the device performance improvement. Higher energies are observed for the conduction and valance band in device D₅ in comparison to other devices. The results depict that the proposed device has a better gate control over the channel as compared to the device D₂. Due to this better gate control, a higher accumulation of holes is seen in the gate region. Additionally, the value of charge carrier changes rapidly depicting enhanced extraction of the charge carriers. The presence of ditch structure led to the formation of broader channel that improved the current conduction. A high current density of 1451 A/cm² is observed in the device. The proposed device D₅ illustrates an improvement of 44 times in drain current and 24 times in saturation mobility than that of planar TFT.

The main goal of the research is to explore the utilization of organic LED and photodiode for biomedical application. Therefore, OLED device is analysed next. The OLED's performance is very sensitive to the structural modifications as highlighted by several researchers. Through the literature review, it is inferred that by using the traditional layers, device performance enhancement is not possible up to great extent. Therefore, the work analysed the utilization of CGLs and impact of their performance on the device performance. After analyzing different OLED devices (L₁-L₅) with and without the CGLs, a novel device structure is proposed (L₆).

The proposed device exhibited high luminescence and current values of 3636.3 cd/cm² and 0.44 A, respectively. The luminescence is improved by 16.8, 2.3, 1.7, 3 and 1.6 times as compared to L₁, L₂, L₃, L₄ and L₅, respectively. Also, the internal device analysis utilizing both vertical and horizontal cutlines is undertaken to understand the facts for the performance enhancement. Internal device parameters: hole/electron concentration, recombination rate of charge carriers, electron affinity, conduction current rate, band energies, hole QFL, acceptor trap ionized density, net doping and hole/electron mobility are analysed.

The results of internal analysis show that the presence of CGLs enhances the charge carrier concentration within the device. These charge carriers are responsible for enhancement for luminescence and current density. Additionally, these CGLs are well aligned with the adjacent layers which supports the carrier injection from the electrodes as well. Thus, device L₆ depicts the best performance. The internal analysis illustrates a higher electron and hole concentration within the emission layer in the device. Therefore, as per the Langevin's theory for the low mobility semiconductors, the recombination will be higher if the probability of charge carriers finding each other is higher. This probability is significantly increased due to higher carrier concentration, consequently resulting in higher recombination rate and thereby a higher

luminescence. Since the entire research work is focused on amalgamation of OLED and OPD for the biomedical application, therefore, OPD device is analysed with similar structure as of the OLED, i.e. utilizing the CGLs. The CGL layer based OPD structure (P₂) is designed and positional analysis is undertaken to better understand the device behaviour.

The results highlight that the proposed OPD P₂ illustrates an improved photocurrent which is higher by 34 times as compared to reference device P₁. On comparing with other OPD devices incorporating CGLs at different positions (P₃, P₄ and P₅), the proposed device depicts 1.6, 1.4 and 9 times better output current, respectively. Here as well, an internal device analysis is conducted for reasoning out the results observed for P₂. Herein, various important parameters: electron/hole concentration, electron current density, potential, conduction/valence band energy and electron QFL are analysed and compared.

The result of internal analysis highlights that a higher charge carrier concentration is observed for proposed device P₂ due to the presence of CGL. This observation shows that the exciton interact not only with the active layer but with the CGLs as well. Similarly, the incorporation of CGL also results in a better matching of the energy levels which is observed in potential distribution, wherein the potential drop is smooth for the proposed device as compared with the reference device. Similar observations are made for band energies as well and the conduction/valence band energies get decreased in the acceptor and donor layers for P₂. However, a sharp bending is observed towards the electrodes for reference device P₁. Thus, the potential energy for P₂ is used for the generation of electron-hole pairs which is contrary to P₁ wherein potential energy is utilized for overcoming the mismatch of energy levels. Thus, the proposed device shows better results in comparison to all other devices.

The proposed devices are further examined for the biomedical applications. First, combination of organic LED and photodiode is utilized for the detection of Covid-19. Saliva sample is excited using the OLED at 470 nm wavelength. The detection of SARS-CoV-2 RNA results in fluorescence emission at 525 nm, whereas for a normal person the emission is at 490 nm. The OPD successfully detects these different wavelengths and produces current values as 63.5 mA and 37.2 mA corresponding to Covid patient and for a normal person. The OTFT is used herein as the driving element for OLED. Additionally, an analysis is conducted pertaining to differentiate the results under varying attributes of saliva sample from different people. Here also the proposed methodology is successful in differentiating Covid-19 patients from a healthy person.

Further, OLED and OPD devices are utilized to monitor the heart rate. Both the devices are modified as per the requirements. Herein the OLED emission is required at 497 nm. Therefore, using the proposed architecture, materials of layers are changed to achieve this emission using SPG-01T polymer and subsequently the modified OLED device is named as H₁. Similarly, OPD device is also upgraded to detect the emission wavelength and named as H₂. Here, OPD is required to detect reflected green light from the blood vessels. Thus, OPD here detects the variation in intensity of the reflected light and not the change in wavelength. The analysis depicts that the OPD can successfully undertake this task. For a higher blood flow representing higher number of beats, less amount of light is reflected and thus lower current is generated by the OPD. However, the OPD generates a high current for lower heart beat as more light is reflected. This simple methodology is successfully implemented by combination of these two devices.

Finally, the combination of these organic devices is also used for the detection of Ovarian cancer. This detection is made possible by using fluorescence emission-based methodology. If the urine sample is excited with a light of 350 nm wavelength and the reflected light shows emission at 440 nm, then the observation directs towards ovarian cancer patient. However, this reflected light shows emission at 420 nm for a healthy person. OPD produces different current for these wavelengths resulting in successful detection. The current values corresponding to these wavelengths are 47 mA and 31.2 mA, respectively. Additionally, it is shown that same methodology is possible for varying patient wherein their urine sample varies in characteristics. To conclude, it is shown that the organic devices: LED, photodiode and transistor can be successfully used for a range of biomedical applications which will open the dimensions in the field of sensors and result in low-cost portable devices. Additionally, these organic material-based devices will greatly improve the performance of these portable bio-medical diagnose system.

7.2 FUTURE SCOPE

The present research depicts the performance analysis and structural modification to achieve improved OLED, OPD and OTFT device and their further realization in biomedical applications. This work addresses some aspects related to flexible electronic devices and builds an approach to cater some performance limitations. However, there are multiple aspects related to these devices that still need attention for further enhancing the performance of these devices to enable their realization in more diversified practical applications.

The future scope of OTFTs lies in attaining lower threshold voltage, higher charge carrier mobility, and improved operational stability. The vertical channel structure has significantly improved the device performance and it is understood that device structure and selection of materials are the prime attributes. Therefore, a further focus can be towards making dual gate vertical channel-based transistors. In the proposed work, it is observed that vertical channel leads to high conduction due to effective vertical electric field component. Therefore, some novel structures are needed, where the carrier transportation starts within the thickness of active layer means the channel formation is vertical. It also provides a solution to achieve a small channel length device. So, in future, such structures where electrodes are elevated can be a solution to augment the performance of OTFTs.

In addition to this, the cylindrical structure also leads to achieve small channel length devices. These structures are feasible from fabrication point of view, however got less attention. Some hybrid structure featuring the benefits of vertical and cylindrical structure may create some horizons for high performance OTFTs. Moreover, the future prospect can be towards the development and optimization of OSC materials with high carrier mobility, environmental stability and compatibility with respect to novel architectures. Fabrication techniques can be focused on minimizing the contact resistance which arises due to poor electrodes-OSC interface. Biopolymeric materials can also be explored in the aspect of enhancing the device performance.

Mobility is the biggest barrier in the case of the OTFT. Higher mobility allows faster switching and enhanced circuit performance. The mobility is generally limited by disorders, traps, and poor molecular packing. Therefore, there is a need to develop new OSCs with reduced traps. Innovative methodologies including defect healing can also be used to ameliorate mobility and reduce trap density.

In the proposed work, it is observed that addition of layer with proper material is a worthwhile approach to achieve good luminescence and current density for the OLED device. Thus, the performance of OLED can be improved by structural redesigning. The incorporation of CGL witnessed surprisingly an augmented performance. Further, the use of mixed interlayer and graded emissive layer can be explored to improve the charge balance and more efficient recombination which may lead to brighter and more stable devices. The OPDs are very promising for flexible imaging, optical communication, and health monitoring. Redesigning of structures using electron/hole blocking layers can be focused to decrease the dark current and

improve the charge collection efficiency. Optimizing interfacial layers can further minimize the trap states and boost the performance.

The primary challenge is to boost the luminescence efficiency, operational lifetime, and maintaining mechanical stability under bending or stretching conditions. Although OLEDs are already widely used in flexible displays, but further optimization is required to enhance color stability, and reduce power consumption. Additionally, a significant potential lies in the systematic optimization of CGL materials and their interface properties to ensure efficient charge separation and transport. Advancements in low-temperature and solution-based fabrication techniques such as spin coating, inkjet printing, and roll-to-roll processing can facilitate cost-effective and large-area device fabrication.

All these organic devices should be developed for application specific purposes. The materials used in these layers can be developed keeping in mind the specificity and importance of the applications. The biomedical applications require specific color output from the OLED. Thus, focusing on the light output, materials should be developed to achieve specific color with high luminescence. Specific color limitations should be taken into consideration with special focus needed for blue color emitters which are most challenging. These emitter materials degrade much faster and depicts lower efficiency. For these materials, chemical bonds degrade much quickly over time and causes chemical instability. Therefore, novel material designing methodologies and other stabilizing techniques need to be explored. Some techniques such as insertion of thin phosphorescent materials have shown some improvement with respect to enhancing the device operation lifetime.

In the case of OPD, the dark current is of great importance. It can alter detectivity of OPD, which is very important for biomedical applications. The design of the OPD itself is the primary consideration for reducing the dark current. In the present work, CGL were utilized, similarly cathode interlayers have shown promising results by reducing dark current and improving the charge transfer. Therefore, future work can be focused on improving the device structures. Additionally, materials used in these layers can play a major role. Thus, material development with lower trap states and fabrication methodologies with the focus on reducing the interface disorders should be given more attention. Organic devices are made of carbon-based compounds that are naturally degradable. Further, these devices should investigate the utilization of biopolymers as a way towards fully biodegradable nature friendly devices. Research should focus on using biopolymers in electronic devices and improve their performance. This may lead to low-cost environmentally friendly devices.

REFERENCES

- [1] X. Guo and A. Facchetti, “The journey of conducting polymers from discovery to application”, *Nat. Mater.*, vol. 19, no. 9, pp. 922–928, 2020.
- [2] M. C. Tang, M. Y. Chan, and V. W. W. Yam, “Molecular design of luminescent gold(III) emitters as thermally evaporable and solution-processable organic light emitting device (OLED) materials: Focus review”, *Chem. Rev.*, vol. 121, no. 13, pp. 7249–7279, 2021.
- [3] P. Mittal, S. Yadav, and S. Negi, “Advancements for organic thin film transistors: Structures, materials, performance parameters, influencing factors, models, fabrication, reliability and applications,” *Mater. Sci. Semicond. Process.*, vol. 133, p. 105975, 2021.
- [4] H. Klauk, “Organic thin-film transistors,” *Chem. Soc. Rev.*, vol. 39, no. 9, pp. 2643–2666, 2010.
- [5] H. N. Raval, S. P. Tiwari, R. R. Navan, S. G. Mhaisalkar, and V. R. Rao, “Solution-processed bootstrapped organic inverters based on P3HT with a high-k gate dielectric material,” *IEEE Electron Device Lett.*, vol. 30, no. 5, pp. 484, 2009.
- [6] F. Shunpei, S. Shaari, S. Naka, and H. Okada, “Organic thin-film transistors with bilayer of rubbed and evaporated hydrocarbon-based acene as active layer,” *Mater. Sci. Semicond. Process.*, vol. 60, pp. 1–4, 2017.
- [7] D. Li and L. J. Guo, “Organic thin film transistors and polymer light-emitting diodes patterned by polymer inking and stamping,” *J. Phys. D: Appl. Phys.*, vol. 41, no. 10, p. 105115, 2008.
- [8] S. I. Qashou, “Effect of UV irradiation on the linear and nonlinear optical properties of Erbium (III)-Tris (8-hydroxyquinolinato) thin films: optoelectronic performance,” *Phys. Scr.*, vol. 97, no. 5, p. 055803, 2022.
- [9] A. Mahmood, A. Nadeem, Q. Raza, T. M. Khan, M. Mehmood, M. M. Hassan, et al., “Effect of thermal annealing on the structural and optical properties of ZnO thin films deposited by the reactive e-beam evaporation technique,” *Phys. Scr.*, vol. 82, no. 6, p. 065801, 2010.
- [10] N. W. Emanetoglu, C. Gorla, Y. Liu, S. Liang, and Y. Lu, “Epitaxial ZnO piezoelectric thin films for SAW filters,” *Mater. Sci. Semicond. Process.*, vol. 2, no. 3, p. 247, 1992.

- [11] J. Lenz, F. Del Giudice, F. R. Geisenhof, F. Winterer, and R. T. Weitz, "Vertical, electrolyte-gated organic transistors show continuous operation in the MA cm⁻² regime and artificial synaptic behaviour," *Nat. Nanotechnol.*, vol. 14, no. 6, p. 579, 2019.
- [12] H. Kleemann, K. Krechan, A. Fischer, and K. Leo, "A review of vertical organic transistors," *Adv. Funct. Mater.*, vol. 30, no. 20, p. 1907113, 2020.
- [13] Y. Chen, and I. Shih, "Fabrication of vertical channel top contact organic thin film transistors," *Org. Electron.*, vol. 8, no. 6, p. 655-661, 2007.
- [14] C. Y. Yang, S. S. Cheng, T. M. Ou, M. C. Wu, C. H. Wu, C. H. Chao, et al., "Pentacene-based planar-and vertical-type organic thin-film transistor," *IEEE Trans. Electron Devices*, vol. 54, no. 7, pp. 1633-1636, 2007.
- [15] S. Negi, P. Mittal, and B. Kumar, "Characteristic performance of OLED based on hole injection, transport and blocking layers," *Recent Pat. Electr. Electron. Eng.*, vol. 14, no. 3, p. 373, 2020.
- [16] E. Angioni, M. Chapran, K. Ivaniuk, N. Kostiv, V. Cherpak, P. Stakhira, et al., "A single emitting layer white OLED based on exciplex interface emission," *J. Mater. Chem. C*, vol. 4, p. 3851, 2016.
- [17] H. Lee, "Phosphorescent white organic light-emitting diodes with stable white color depending on luminance," *Curr. Appl. Phys.*, vol. 21, no. 3, pp. 116-120, 2021.
- [18] X. Zheng, Y. Liu, Y. Zhu, F. Ma, C. Feng, Y. Yu, et al., "Efficient inkjet-printed blue OLED with boosted charge transport using host doping for application in pixelated display," *Opt.*, vol. 101, p. 109755, 2020.
- [19] G. Tan, J. H. Lee, S. C. Lin, R. Zhu, S. H. Choi, S. T. Wu, et al., "Analysis and optimization on the angular color shift of RGB OLED displays," *Opt. Express*, vol. 25, no. 26, pp. 33629–33642, 2017.
- [20] N. Ide, H. Tsuji, N. Ito, Y. Matsuhisa, S. Houzumi, and T. Nishimori, "White OLED devices and processes for lighting applications," in *Organic Photonics IV*, vol. 7722, pp. 11–18, SPIE, 2010.
- [21] S. Krotkus, D. Kasemann, S. Lenk, K. Leo, and S. Reineke, "Adjustable white-light emission from a photo-structured micro-OLED array," *Light Sci. Appl.*, vol. 5, p. e16121, 2016.
- [22] S. Negi, P. Mittal, and B. Kumar, "Impact of different layers on performance of OLED," *Microsyst. Technol.*, vol. 24, no. 12, pp. 4981–4989, 2018.
- [23] C. H. Gao, X. B. Shi, D. Y. Zhou, L. Zhang, Z. K. Wang, and L. S. Liao, "Highly efficient white organic light-emitting diodes with controllable excitons behaviour by a

- mixed interlayer between fluorescence blue and phosphorescence yellow-emitting layers,” *Int. J. Photoenergy*, vol. 2013, no. 1, p. 831765, 2013.
- [24] Y. Chen, J. Chen, D. Ma, D. Yan, L. Wang, F. Zhu, “High power efficiency tandem organic light-emitting diodes based on bulk heterojunction organic bipolar charge generation layer,” *Appl. Phys. Lett.*, vol. 98, no. 24, p. 114, 2011.
- [25] Y. M. Kim, J. W. Lee, J. H. Jung, K. K. Paek, M. Y. Sung, J. K. Kim, et al., “Enhanced brightness and efficiency of organic light-emitting diodes with an LiF in the Alq₃,” *IEEE Electron Device Lett.*, vol. 27, no. 7, pp. 558-560, 2006.
- [26] D. Zhao, H. Liu, Y. Miao, H. Wang, B. Zhao, Y. Hao, et al., “A red tandem organic light-emitting diode based on organic photovoltaic-type charge generation layer,” *Org. Electron.*, vol. 32, pp. 1-6, 2016.
- [27] L. Lu, T. Zheng, Q. Wu, A. M. Schneider, D. Zhao, and L. Yu, “Recent advances in bulk heterojunction polymer solar cells,” *Chem. Rev.*, vol. 115, no. 23, pp. 12666-12731, 2015.
- [28] P. Chamola, and P. Mittal, “Flexible organic solar cell to power modern cardiac pacemakers: Versatile for all age groups, skin types and genders,” *Phys. Scr.*, vol. 98, no. 3, p. 035018, 2023.
- [29] H. Zhang, S. Jenatsch, J. De Jonghe, F. Nüesch, R. Steim, A. C. Véron, et al., “Transparent organic photodetector using a near-infrared absorbing cyanine dye,” *Sci. Rep.*, vol. 5, p. 9439, 2015.
- [30] S. Dong, K. Zhang, B. Xie, J. Xiao, H. L. Yip, and Y. Cao, “High-performance large-area organic solar cells enabled by sequential bilayer processing via nonhalogenated solvents,” *Adv. Energy Mater.*, vol. 9, no. 1, p. 1802832, 2019.
- [31] P. Chamola, and P. Mittal, “Impact of ZnTe, SbZnTe and SnZnTe absorber materials for multi-layered solar cell: parametric extraction and layer wise internal analysis,” *Optik*, vol. 224, p. 165626, 2020.
- [32] T. N. Ng, W. S. Wong, M. L. Chabinyc, S. Sambandan, and R. A. Street, “Flexible image sensor array with bulk heterojunction organic photodiode,” *Appl. Phys. Lett.*, vol. 92, no. 21, p. 213303, 2008.
- [33] K. H. Lee, D. S. Leem, S. Sul, K. B. Park, S. J. Lim, H. Han, et al., “A high performance green-sensitive organic photodiode comprising a bulk heterojunction of dimethyl-quinacridone and dicyanovinyl terthiophene,” *J. Mater. Chem. C*, vol. 1, no. 15, p. 2666, 2013.

- [34] I. Deckman, P. B. Lechêne, A. Pierre, and A. C. Arias, "All-printed full-color pixel organic photodiode array with a single active layer," *Org. Electron.*, vol. 56, pp. 139-145, 2018.
- [35] W. Jang, S. Rasool, B. G. Kim, J. Kim, J. Yoon, S. Manzhos, et al., "Superior noise suppression, response time, and device stability of non-fullerene system over fullerene counterpart in organic photodiode," *Adv. Funct. Mater.*, vol. 30, no. 45, p. 2001402, 2020.
- [36] Kenry, J. C. Yeo, and C. T. Lim, "Emerging flexible and wearable physical sensing platforms for healthcare and biomedical applications," *Microsyst. Nanoeng.*, vol. 2, no. 1, p. 16043, 2016.
- [37] T. Mayr, T. Abel, E. Kraker, S. Köstler, A. Haase, C. Konrad, et al., "An optical sensor array on a flexible substrate with integrated organic opto-electric devices," *Procedia Eng.*, vol. 5, pp. 1005–1008, 2010.
- [38] I. Titov, M. Köpke, N. C. Schneidewind, J. Buhl, Y. Murat, and M. Gerken, "OLED-OPD matrix for sensing on a single flexible substrate," *IEEE Sens. J.*, vol. 20, no. 14, pp. 7540–7547, 2020.
- [39] A. B. Katchman, J. T. Smith, U. Obahiagbon, S. Kesiraju, Y. K. Lee, B. O'Brien, et al., "Application of flat panel OLED display technology for the point-of-care detection of circulating cancer biomarkers," *Sci. Rep.*, vol. 6, p. 29057, 2016.
- [40] C. J. Lim, S. Lee, J. H. Kim, H. J. Kil, Y. C. Kim, and J. W. Park, "Wearable, luminescent oxygen sensor for transcutaneous oxygen monitoring," *ACS Appl. Mater. Interfaces*, vol. 10, no. 48, pp. 41026–41034, 2018.
- [41] C. Zhu, "OLED Technology Research Progress and Prospects for Future Application," *IJERT*, vol. 181, p. 2278, 2019.
- [42] A. Ghosh, "OLED historical development," *Inf. Display*, vol. 28, no. 7–8, pp. 26–27, 2012.
- [43] W. Helfrich and W. G. Schneider, "Recombination radiation in anthracene crystals," *Phys. Rev. Lett.*, vol. 14, no. 7, pp. 229–231, 1965.
- [44] C. W. Tang and S. A. VanSlyke, "Organic electroluminescent diodes," *Appl. Phys. Lett.*, vol. 51, no. 12, pp. 913–915, 1987.
- [45] B. N. Patel, and M. M. Prajapati, "Malignant Mesenteric Perivascular Epithelioid Cell Neoplasm Presenting as an Intra-Abdominal Fistula in a 49-Year-Old Female," *Int. J. Sci. Res. Publ.*, vol. 4, p. 1, 2014.

- [46] B. Geffroy, P. Le Roy, and C. Prat, "Organic light-emitting diode (OLED) technology: materials, devices and display technologies," *Polym. Int.*, vol. 55, no. 6, pp. 572–582, 2006.
- [47] G. G. Malliaras, and J. C. Scott, "Numerical simulations of the electrical characteristics and the efficiencies of single-layer organic light emitting diodes," *J. Appl. Phys.*, vol. 85, no. 10, p. 7426, 1999.
- [48] D. Gupta, M. Katiyar, and D. Gupta, "An analysis of the difference in behavior of top and bottom contact organic thin film transistors using device simulation," *Org. Electron.*, vol. 10, no. 5, pp. 775–784, 2009.
- [49] A. Dodabalapur, "Organic light emitting diodes," *Solid State Commun.*, vol. 102, no. 2–3, pp. 259–267, 1997.
- [50] S. Negi, P. Mittal, and B. Kumar, "Modeling and analysis of high-performance triple hole block layer organic LED based light sensor for detection of ovarian cancer," *IEEE Trans. Circuits Syst. I: Regul. Pap.*, vol. 68, no. 8, pp. 3254–3264, 2021.
- [51] H. Fujikawa, M. Ishii, S. Tokito, and Y. Taga, "Organic light-emitting diodes using triphenylamine based hole transporting materials," *MRS Online Proc. Libr.*, vol. 621, pp. Q3.-1, 2000.
- [52] A. P. Kulkarni, C. J. Tonzola, A. Babel, and S. A. Jenekhe, "Electron transport materials for organic light-emitting diodes," *Chem. Mater.*, vol. 16, no. 23, pp. 4556–4573, 2004.
- [53] D. Ammermann, A. Böhler, S. Dirr, H. H. Johannes, and W. Kowalsky, "Multilayer organic light emitting diodes for flat panel displays," *Int. J. Electron. Commun.*, vol. 50, pp. 327–333, 1996.
- [54] L. S. Hung, C. W. Tang, M. G. Mason, P. Raychaudhuri, and J. Madathil, "Application of an ultrathin LiF/Al bilayer in organic surface-emitting diodes," *Appl. Phys. Lett.*, vol. 78, no. 4, pp. 544–546, 2001.
- [55] S. Negi, P. Mittal, and B. Kumar, "In-depth analysis of structures, materials, models, parameters, and applications of organic light-emitting diodes," *J. Electron. Mater.*, vol. 49, pp. 4610–4636, 2020.
- [56] Z. Wu, H. Guo, and J. Wang, "Highly efficient green top-emitting organic light-emitting devices with metal electrode structure," *Microelectron. J.*, vol. 38, no. 6-7, pp. 686–689, 2007.
- [57] Y. Pareek and S. Kumar, "Optical light emitting diodes," *Int. J. Eng. Res. Technol. (IJERT)*, vol. 6, no. 17, 2018.

- [58] C. Dong, X. Fu, S. Amoah, A. Rozelle, D.-H. Shin, A. Salehi, et al., “Eliminate angular color shift in top-emitting OLEDs through cavity design,” *J. Soc. Inf. Display*, vol. 27, no. 8, pp. 469–479, 2019.
- [59] Y. Qu, C. Coburn, D. Fan, and S. R. Forrest, “Elimination of plasmon losses and enhanced light extraction of top-emitting organic light-emitting devices using a reflective subelectrode grid,” *ACS Photonics*, vol. 4, no. 2, pp. 363–368, 2017.
- [60] Y. Liu, X. Wei, Z. Li, J. Liu, R. Wang, X. Hu, et al., “Highly efficient, solution-processed organic light-emitting diodes based on thermally activated delayed-fluorescence emitter with a mixed polymer interlayer,” *ACS Appl. Energy Mater.*, vol. 1, no. 2, pp. 543–551, 2018.
- [61] K. Takahashi, T. Sato, R. Yamamoto, H. Shishido, T. Isa, S. Eguchi, et al., “13.3-inch 8k4k 664-ppi Foldable OLED Display Using Crystalline Oxide Semiconductor FETs,” *Dig. Tech. Pap. - SID Int. Symp.*, vol. 46, p. 250, 2015.
- [62] K. Watanabe, Y. Iwaki, Y. Uchida, D. Nakamura, H. Ikeda, H. Miyake, et al., “18.3: An 8.67-in. Foldable OLED Display with an In-cell Touch Sensor,” *Dig. Tech. Pap. - SID Int. Symp.*, vol. 46, p. 246, 2015.
- [63] S. Idojiri, M. Ohno, K. Takeshima, S. Yasumoto, M. Sato, and N. Sakamoto, “4.1: Distinguished paper: Apparatus for manufacturing flexible OLED displays: Adoption of transfer technology,” *Dig. Tech. Pap. - SID Int. Symp.*, vol. 46, p. 8, 2015.
- [64] J. de Dieu, B. Mugiraneza, T. Maruyama, T. Yamamoto, and Y. Sugita, “44-3: 3D piezo-capacitive touch with capability to distinguish conductive and non-conductive touch objects for on-screen organic user interface in LCD and foldable OLED display application,” *Dig. Tech. Pap. - SID Int. Symp.*, vol. 50, no. 1, pp. 608–611, 2019.
- [65] B. Zhang, P. Qi, Z. Yang, Z. Lai, Z. Wang, S. Li, et al., “P-124: A 17.3-inch WQHD Top-Emission Foldable AMOLED Display with Outstanding Optical Performance and Visual Effects,” *Dig. Tech. Pap. - SID Int. Symp.*, vol. 51, p. 1836, 2020.
- [66] Z. Qin, Y. W. Yeh, Y. H. Tsai, W. Y. Cheng, Y. P. Huang, and H. P. D. Shieh, “31-2: See-through image blurring of transparent OLED display: diffraction analysis and oled pixel optimization,” *SID Symp. Dig. Tech. Pap.*, vol. 47, no. 1, pp. 393–396, 2016.
- [67] Z. Shu, E. Beckert, R. Eberhardt, and A. Tünnermann, “ITO-free, inkjet-printed transparent organic light-emitting diodes with a single inkjet-printed Al:ZnO:PEI interlayer for sensing applications,” *J. Mater. Chem. C*, vol. 5, no. 44, pp. 11590–11597, 2017.

- [68] Y. H. Tsai, Y. L. Wu, W. T. Liou, Y. R. Kung, Y. H. Huang, and K. C. Lee, “P-202: a flexible transparent OLED display with FlexUPTM technology,” *Dig. Tech. Pap. - SID Int. Symp.*, vol. 48, no. 1, p. 2021, 2017.
- [69] M. G. Song, K. S. Kim, H. I. Yang, S. K. Kim, J. H. Kim, C. W. Han, et al., “Highly reliable and transparent Al doped Ag cathode fabricated using thermal evaporation for transparent OLED applications,” *Org. Electron.*, vol. 76, p. 105418, 2020.
- [70] L. Chen, Y. Jiang, H. Nie, R. Hu, H. S. Kwok, F. Huang, et al., “Rational design of aggregation-induced emission luminogen with weak electron donor–acceptor interaction to achieve highly efficient undoped bilayer OLEDs,” *ACS Appl. Mater. Interfaces*, vol. 6, no. 19, pp. 17215–17225, 2014.
- [71] E. F. Gomez and A. J. Steckl, “Improved performance of OLEDs on cellulose/epoxy substrate using adenine as a hole injection layer,” *ACS Photonics*, vol. 2, no. 3, pp. 439–445, 2015.
- [72] N. Zhou, S. Wang, Y. Xiao, and X. Li, “Double light-emitting layer implementing three-color emission: Using DCJTb lightly doping in Alq3 as red-green emitting layer and APEAn1N as blue-green emitting layer,” *J. Lumin.*, vol. 196, pp. 40–49, 2018.
- [73] M. Klein, N. Rau, M. Wende, J. Sundermeyer, G. Cheng, C. M. Che, et al., “Cu (I) and Ag (I) complexes with a new type of rigid tridentate N, P, P-ligand for thermally activated delayed fluorescence and OLEDs with high external quantum efficiency,” *Chem. Mater.*, vol. 32, no. 24, pp. 10365–10382, 2020.
- [74] X. Zheng, Y. Liu, Y. Zhu, F. Ma, C. Feng, Y. Yu, et al., “Efficient inkjet-printed blue OLED with boosted charge transport using host doping for application in pixelated display,” *Opt. Mater.*, vol. 101, p. 109755, 2020.
- [75] H. Park, J. Lee, I. Kang, H. Y. Chu, J. I. Lee, S. K. Kwon, et al., “Highly rigid and twisted anthracene derivatives: a strategy for deep blue OLED materials with theoretical limit efficiency,” *J. Mater. Chem.*, vol. 22, no. 6, pp. 2695–2700, 2012.
- [76] P. Rajamalli, N. Senthilkumar, P. Gandeepan, C. C. Ren-Wu, H. W. Lin, and C. H. Cheng, “A method for reducing the singlet–triplet energy gaps of TADF materials for improving the blue OLED efficiency,” *ACS Appl. Mater. Interfaces.*, vol. 8, no. 40, pp. 27026–27034, 2016.
- [77] K. H. Han, K. Kim, Y. Han, Y. D. Kim, H. Lim, and D. Huh, et al., “Highly Efficient Tandem White OLED Using a Hollow Structure,” *Adv. Mater. Interfaces*, vol. 7, p. 1901509, 2020.

- [78] M. Xie, X. Chao, C. Ma, T. Li, X. Wang, Y. Zhou, et al., “Deep red/near-infrared electro-fluorescence material with nearly 10% external quantum efficiency based on hybridized local and charge-transfer,” *Chem. Eng. J.*, vol. 489, p. 151481, 2024.
- [79] P. Han, C. Lin, E. Xia, J. Cheng, Q. Xia, D. Yang, et al., “Non-Doped Blue AIEgen-Based OLED with EQE Approaching 10.3%,” *Angew. Chem.*, vol. 135, no. 43, p. e202310388, 2023.
- [80] K. K. Kesavan, J. Jayakumar, M. Lee, C. Hexin, S. S. Swayamprabha, D. K. Dubey, et al., “Achieving a 32% EQE solution-processed simple structure OLED via exciplex system,” *Chem. Eng. J.*, vol. 435, p. 134879, 2022.
- [81] Y. Yu, H. Xing, D. Liu, M. Zhao, H.-Y. Sung, I. D. Williams, et al., “Solution-processed AIEgen NIR OLEDs with EQE Approaching 15%,” *Angew. Chem.*, vol. 134, no. 26, p. e202204279, 2022.
- [82] H. Lee, “Phosphorescent white organic light-emitting diodes with stable white color depending on luminance,” *Curr. Appl. Phys.*, vol. 21, no. 1, pp. 116–120, 2021.
- [83] G. Lu, Z. G. Wu, R. Wu, X. Cao, L. Zhou, Y. X. Zheng, et al., “Semitransparent circularly polarized phosphorescent organic light-emitting diodes with external quantum efficiency over 30% and dissymmetry factor close to 10^{−2},” *Adv. Funct. Mater.*, vol. 31, no. 36, p. 2102898, 2021.
- [84] D. Cui, S. Wang, S. Li, Y. Liu, H. Du, Q. Du, et al., “Enhanced performance of OLED based on molecular orientation of emission layer by optimized substrate temperature,” *Journal of Materials Science: J. Mater. Sci. Mater. Electron.*, vol. 32, no. 9, pp. 12075–12083, 2021.
- [85] Y. F. Wang, M. Li, J. M. Teng, H. Y. Zhou, and C. F. Chen, “High-performance solution-processed non-doped circularly polarized OLEDs with chiral triptycene scaffold-based TADF emitters realizing over 20% external quantum efficiency,” *Adv. Funct. Mater.*, vol. 31, no. 49, p. 2106418, 2021.
- [86] C. Huang, Y. Zhang, J. Zhou, S. Sun, W. Luo, W. He, et al., “Hybrid tandem white OLED with long lifetime and 150 Lm W^{−1} in luminous efficacy based on TADF blue emitter stabilized with phosphorescent red emitter,” *Adv. Opt. Mater.*, vol. 8, no. 18, p. 2000727, 2020.
- [87] Y. Luo, S. Li, Y. Zhao, C. Li, Z. Pang, Y. Huang, et al., “An ultraviolet thermally activated delayed fluorescence OLED with total external quantum efficiency over 9%,” *Adv. Mater.*, vol. 32, no. 32, p. 2001248, 2020.

- [88] X. Zheng, R. Huang, C. Zhong, G. Xie, W. Ning, M. Huang, et al., “Achieving 21% external quantum efficiency for non-doped solution-processed sky-blue thermally activated delayed fluorescence OLEDs by means of multi-(donor/acceptor) emitter with through-space/-bond charge transfer,” *Adv. Sci.*, vol. 7, no. 7, p. 1902087, 2020.
- [89] T. Yang, B. Liang, Z. Cheng, C. Li, G. Lu, and Y. Wang, “Construction of efficient deep-red/near-infrared emitter based on a large π -conjugated acceptor and delayed fluorescence OLEDs with external quantum efficiency of over 20%,” *J. Phys. Chem. C*, vol. 123, no. 30, pp. 18585–18592, 2019.
- [90] K. Albrecht, K. Matsuoka, D. Yokoyama, Y. Sakai, A. Nakayama, K. Fujita, et al., “Thermally activated delayed fluorescence OLEDs with fully solution processed organic layers exhibiting nearly 10% external quantum efficiency,” *Chem. Commun.*, vol. 53, no. 16, pp. 2439–2442, 2017.
- [91] K. Guo, J. Zhang, T. Xu, X. Gao, and B. Wei, “High-efficiency near ultraviolet and blue organic light-emitting diodes using star-shaped material as emissive and hosting molecules,” *J. Disp. Technol.*, vol. 10, no. 8, pp. 642–646, 2014.
- [92] C. Ou, Y. C. Qiu, C. Cao, H. Zhang, J. Qin, Z. L. Tu, et al., “Modulating the peripheral large steric hindrance of iridium complexes for achieving narrowband emission and pure red OLEDs with an EQE up to 32.0%,” *Inorg. Chem. Front.*, vol. 10, pp. 1018–1026, 2023.
- [93] Z. Hao, N. Li, J. Miao, Z. Huang, X. Lv, and X. Cao, “Chiral sulfoximine-based TADF emitter for circularly polarized luminescence and highly efficient OLEDs,” *Chem. Eng. J.*, vol. 454, p. 140070, 2023.
- [94] M. Hengge, K. Livanov, N. Zamoshchik, F. Hermerschmidt, and E. J. List-Kratochvil, “ITO-free OLEDs utilizing inkjet-printed and low temperature plasma-sintered Ag electrodes,” *Flex. Print. Electron.*, vol. 6, no. 1, p. 015009, 2021.
- [95] V. Mohan, A. K. Gautam, S. D. Choudhary, M. M. Bee, R. Puvirasi, S. Saranya, et al., “Enhanced performance organic light emitting diode with CuI: CuPC composite hole transport layer,” *IEEE Trans. Nanotechnol.*, vol. 19, pp. 699–703, 2020.
- [96] M. Singh, J. H. Jou, S. Sahoo, Z. K. He, G. Krucaite, S. Grigalevicius, et al., “High light-quality OLEDs with a wet-processed single emissive layer,” *Sci. Rep.*, vol. 8, no. 1, pp. 1–9, 2018.
- [97] D. H. Cho, O. E. Kwon, Y. S. Park, B. G. Yu, J. Lee, et al., “Flexible integrated OLED substrates prepared by printing and plating process,” *Org. Electron.*, vol. 50, pp. 170–176, 2017.

- [98] S. Yuan, Y. Hao, Y. Miao, Q. Sun, Z. Li, Y. Cui, et al., “Enhanced light out-coupling efficiency and reduced efficiency roll-off in phosphorescent OLEDs with a spontaneously distributed embossed structure formed by a spin-coating method,” *RSC Adv.*, vol. 7, no. 69, pp. 43987–43993, 2017.
- [99] S. I. Yoo, J. A. Yoon, N. H. Kim, J. W. Kim, J. S. Kang, C. B. Moon, et al., “Improvement of efficiency roll-off in blue phosphorescence OLED using double dopants emissive layer,” *J. Lumin.*, vol. 160, pp. 346–350, 2015.
- [100] Z. Xi, B. Zhao, L. Chen, W. Li, H. Wang, X. Liu, et al., “Demonstration of highly efficient orange EL device and warm white OLED,” *Org. Electron.*, vol. 57, pp. 21–27, 2018.
- [101] S. H. Han, J. H. Jeong, J. W. Yoo, and J. Y. Lee, “Ideal blue thermally activated delayed fluorescence emission assisted by a thermally activated delayed fluorescence assistant dopant through a fast reverse intersystem crossing mediated cascade energy transfer process,” *Mater. Chem. C*, vol. 7, no. 10, pp. 3082–3089, 2019.
- [102] J. Qi, W. Ding, Q. Zhang, Y. Wang, H. Chen, and S. Y. Chou, “Significant Light Extraction and Power Efficiency Enhancement of Organic Light Emitting Diodes by Subwavelength Dielectric-Nanomesh Using Large-area Nanoimprint,” *arXiv preprint arXiv:2302.00044*, 2023.
- [103] M. Vasilopoulou, M. Yusoff, M. Daboczi, J. Conforto, A. E. X. Gavim, and W. J. da Silva, “High efficiency blue organic light-emitting diodes with below-bandgap electroluminescence,” *Nat. Commun.*, vol. 12, p. 4868, 2021.
- [104] D. Cui, S. Wang, S. Li, Y. Liu, H. Du, and Q. Du, et al., “Enhanced performance of OLED based on molecular orientation of emission layer by optimized substrate temperature,” *J. Mater. Sci.: Mater. Electron.*, vol. 32, no. 9, pp. 12075–12083, 2021.
- [105] M. Wang, W. Zhu, Z. Yin, L. Huang, and J. Li, “Synergistic effects of Li-doped NiOx film prepared by low-temperature combustion as hole-injection layer for high performance OLED devices,” *Org. Electron.*, vol. 85, p. 105823, 2020.
- [106] Q. Yang, Y. Hao, Z. Wang, Y. Li, H. Wang, and B. Xu, “Double-emission-layer green phosphorescent OLED based on LiF-doped TPBi as electron transport layer for improving efficiency and operational lifetime,” *Synth. Met.*, vol. 162, pp. 398–401, 2012.
- [107] Y. F. Chang, C. H. Yu, S. C. Yang, I. H. Hong, S. C. Jiang, H. F. Meng, et al., “Great improvement of operation-lifetime for all-solution OLEDs with mixed hosts by blade coating,” *Org. Electron.*, vol. 42, pp. 75–86, 2017.

- [108] T. N. Le, E. Y. Park, V. Thangaraji, and M. C. Suh, “Operational lifetime improvement of solution-processed OLEDs: Effect of exciton formation region and degradation analysis by impedance spectroscopy,” *Org. Electron.*, vol. 99, p. 106346, 2021.
- [109] K. Guo, C. Lin, Y. Wu, S. Xiao, X. Qiao, D. Yang, et al., “Understanding of Degradation Mechanism by Exciton Dynamics and Enhancement of Operational Lifetime by Exciton Management in Blue Fluorescent OLEDs Based on Hybridized Local and Charge-Transfer Molecule,” *Adv. Opt. Mater.*, vol. 11, p. 2202988, 2023.
- [110] C. Y. Wong, S. L. Lai, M. Y. Leung, M. C. Tang, L. K. Li, M. Y. Chan, et al., “Realization of Long Operational Lifetimes in Vacuum-Deposited Organic Light-Emitting Devices Based on para-Substituted Pyridine Carbazolylgold (III) C⁺ C⁺ N Complexes,” *J. Am. Chem. Soc.*, vol. 145, no. 4, pp. 1998–2012, 2023.
- [111] S. Aasha, D. Emerald, and S. Prince, “Maximising OLED performance: Unleashing the power of stacking transport, injection and blocking layers along with different emissive materials,” *Pramana*, vol. 98, no. 4, p. 141, 2024.
- [112] J. Luo, Y. Wu, C. Lin, S. Xiao, X. Qiao, D. Yang, et al., “Influence of host materials on degradation of phosphorescent organic light-emitting diodes under electrical stress,” *J. Mater. Chem. C*, vol. 11, no. 10, pp. 3596–3605, 2023.
- [113] W. Zhu, K. Ding, C. Yi, R. Chen, B. Wei, L. Huang, et al., “Use of Hybrid PEDOT: PSS/Metal Sulfide Quantum Dots for a Hole Injection Layer in Highly Efficient Green Phosphorescent Organic Light-Emitting Diodes,” *Front. Chem.*, vol. 9, p. 1, 2021.
- [114] K. W. Tsai, M. K. Hung, Y. H. Mao, and S. A. Chen, “Solution-processed thermally activated delayed fluorescent OLED with high EQE as 31% using high triplet energy crosslinkable hole transport materials,” *Adv. Funct. Mater.*, vol. 15, p. 1901025, 2019.
- [115] Q. Zheng, D. Qu, Y. Zhang, W. Li, J. Xiong, P. Cai, et al., “Facile solution-processed aqueous MoO_x for feasible application in organic light-emitting diode,” *Opt Laser Technol.*, vol. 101, p. 85, 2018.
- [116] D. Dong, Y. Wang, I. L., D. Feng, H. Wang, and G. He, “Novel Solution-Processed ZnO-Based Electron Injection Layer for Organic Light-Emitting Diodes,” *Phys. Status Solidi A*, vol. 12, p. 1700583, 2017.
- [117] Q. Zheng, F. You, J. Xu, J. Xiong, X. Xue, P. Cai, et al., “Solution-processed aqueous composite hole injection layer of PEDOT: PSS+ MoO_x for efficient ultraviolet organic light-emitting diode,” *Org. Electron.*, vol. 46, p. 7, 2017.

- [118] S. Stolz, Y. Zhang, U. Lemmer, G. Hernandez-Sosa, and H. Aziz, "Degradation mechanisms in organic light-emitting diodes with polyethylenimine as a solution-processed electron injection layer," *ACS Appl. Mater. Interfaces*, vol. 3, p. 2776, 2017.
- [119] H. Fujimoto, M. Yahiro, S. Yukiwaki, K. Kusuhara, N. Nakamura, T. Suekane, et al., "Influence of material impurities in the hole-blocking layer on the lifetime of organic light-emitting diodes," *Appl. Phys. Lett.*, vol. 24, p. 243302, 2016.
- [120] Z. Zhong, Z. Hu, Z. Jiang, J. Wang, Y. Chen, C. Song, et al., "Hole-Trapping Effect of the Aliphatic-Amine Based Electron Injection Materials in the Operation of OLEDs to Facilitate the Electron Injection," *Adv. Electron. Mater.*, vol. 3, p. 1400014, 2015.
- [121] S. Y. Lu, S. Mukhopadhyay, R. Froese, and P. M. Zimmerman, "Virtual screening of hole transport, electron transport, and host layers for effective OLED design," *J. Chem. Inf. Model.*, vol. 12, p. 2440, 2018.
- [122] J. Liu, J. Chen, J. Wang, T. Peng, B. Wang, Y. Zhou, et al., "Discovery of a resonant high-level reverse intersystem crossing of hot exciton from conventional TTPA fluorescent semiconductor and an attempt on high-efficiency TTPA-based OLEDs," *Adv. Opt. Mater.*, vol. 13, no. 11, p. 2403105, 2025.
- [123] M. R. Nagar, Shahnawaz, R. A. K. Yadav, J. T. Lin, and J. H. Jou, "Nanocomposite electron-transport layer incorporated highly efficient OLED. ACS Applied Electronic Materials," *ACS Appl. Electron. Mater.*, vol. 2, p. 1545, 2020.
- [124] F. Huang, H. Liu, W. Sun, X. Li, and S. Wang, "Hole transport layer-free deep-blue OLEDs with outstanding colour purity and high efficiency," *J. Mater. Chem. C*, vol. 8, p. 9184, 2020.
- [125] J. Zhang, X. Zhang, H. Feng, Z. Yu, J. Zhang, S. Liu, et al., "An efficient and stable hybrid organic light-emitting device based on an inorganic metal oxide hole transport layer and an electron transport layer," *J. Mater. Chem. C*, vol. 7, p. 1991, 2019.
- [126] W. H. Lee, D. H. Kim, P. J. Jesuraj, H. Hafeez, J. C. Lee, D. K. Choi, et al., "Improvement of charge balance, recombination zone confinement, and low efficiency roll-off in green phosphorescent OLEDs by altering electron transport layer thickness," *Mater. Res. Express*, vol. 5, p. 076201, 2018.
- [127] C. H. Chen, N. T. Tierce, M. K. Leung, T. L. Chiu, C. F. Lin, C. J. Bardeen, et al., "Efficient Triplet–Triplet Annihilation Upconversion in an Electroluminescence Device with a Fluorescent Sensitizer and a Triplet-Diffusion Singlet-Blocking Layer," *Adv. Mater.*, vol. 30, p. 1804850, 2018.

- [128] C. Yun, H. Cho, T. W. Koh, J. H. Kim, J. W. Kim, Y. Park, et al., “Doping-free inverted top-emitting organic light-emitting diodes with high power efficiency and near-ideal emission characteristics,” *IEEE Trans. Electron Devices*, vol. 59, p. 159, 2011.
- [129] X. W. Zhang, L. M. Liu, J. Li, L. Zhang, X. Y. Jiang, Z. L. Zhang, et al., “The Feasibility of Using Cu as Reflective Anode in Top-Emitting Organic Light-Emitting Diodes,” *JDT*, vol. 7, p. 515, 2011.
- [130] L. Lu, J. N. Yu, L. Long, F. F. Yu, J. H. Zhang, H. Zhang, et al., “Low-voltage and high-stability p-type doped blue organic light-emitting diodes with bilayer hole injection layers,” *Phys. Status Solidi A*, vol. 208, p. 2321, 2010.
- [131] S. J. Kim, Y. Zhang, C. Zuniga, S. Barlow, S. R. Marder, and B. Kippelen, “Efficient green OLED devices with an emissive layer comprised of phosphor-doped carbazole/bis-oxadiazole side-chain polymer blends,” *Org. Electron.*, vol. 12, p. 492, 2011.
- [132] Y. Zhao, L. Zhu, J. Chen, and D. Ma, “Improving color stability of blue/orange complementary white OLEDs by using single-host double-emissive layer structure: comprehensive experimental investigation into the device working mechanism,” *Org. Electron.*, vol. 13, p. 1340, 2012.
- [133] N. C. Erickson and R. J. Holmes, “Investigating the Role of Emissive Layer Architecture on the Exciton Recombination Zone in Organic Light-Emitting Devices,” *Adv. Funct. Mater.*, vol. 23, p. 5190, 2013.
- [134] A. Bachelet, M. Chabot, A. Ablat, K. Takimiya, L. Hirsch, and M. Abbas, “Low voltage operating organic light emitting transistors with efficient charge blocking layer,” *Org. Electron.*, vol. 88, p. 106024, 2021.
- [135] A. Sharma and T. D. Das, “Highly efficient OLED device based on the double emissive layer with an EQE about 39%” *Optik*, vol. 221, p. 165350, 2020.
- [136] D. Nayak and R. B. Choudhary, “Augmented optical and electrical properties of PMMA-ZnS nanocomposites as emissive layer for OLED applications,” *Opt. Mater.*, vol. 91, p. 470, 2019.
- [137] S. Olivier, E. Ishow, S. M. Della-Gatta, and T. Maindron, “Inkjet deposition of a hole-transporting small molecule to realize a hybrid solution-evaporation green top-emitting OLED,” *Org. Electron.*, vol. 49, p. 24, 2017.
- [138] J. W. Huh, J. Moon, J. W. Lee, D. H. Cho, J. W. Shin, J. H. Han, et al., “The optical effects of capping layers on the performance of transparent organic light-emitting diodes,” *IEEE Photonics J.*, vol. 4, p. 39, 2011.

- [139] Z. Li, L. Zhang, H. Xue, H. Yang, Y. Yu, L. Xu, et al., "Improving thermal stability of TEOLED by introducing Yb as cathode blocking layer," *Org. Electron.*, vol. 103, p. 106468, 2022.
- [140] A. Soman and K. N. Unni, "Enhancement in electron transport and exciton confinement in OLEDs: role of n-type doping and electron blocking layers," *EPJ Appl. Phys.*, vol. 86, p. 10201, 2019.
- [141] S. Jang, S. H. Han, J. Y. Lee, and Y. Lee, "Pyrimidine based hole-blocking materials with high triplet energy and glass transition temperature for blue phosphorescent OLEDs," *Synth. Met.*, vol. 239, p. 43, 2018.
- [142] X. F. Wei, W. Y. Tan, J. H. Zou, Q. X. Guo, D. Y. Gao, D. G. Ma, et al., "High T g small-molecule phenanthroline derivatives as a potential universal hole-blocking layer for high power-efficiency and stable organic light-emitting diodes," *J. Mater. Chem. C*, vol. 5, p. 2329, 2017.
- [143] W. Y. Tan, J. H. Zou, D. Y. Gao, J. Z. Liu, N. N. Chen, and X. H. Zhu, "Promising Operational Stability of Potentially High Power Efficiency Organic Light-Emitting Diodes Utilizing a Simple and Versatile Electron-Transport/Hole-Blocking Layer," *Adv. Electron. Mater.*, vol. 2, p. 1600101, 2016.
- [144] J. A. Seo, S. K. Jeon, M. S. Gong, J. Y. Lee, C. H. Noh, and S. H. Kim, "Long lifetime blue phosphorescent organic light-emitting diodes with an exciton blocking layer," *J. Mater. Chem. C*, vol. 3, p. 4640, 2015.
- [145] D. Wahyuningrum and A. Alni, "Study on the Nitration Reaction of N, N-diphenylamine Compounds and Its Characterization as Organic Light Emitting Diode (OLED) Material," *Procedia Chem.*, vol. 16, p. 586, 2015.
- [146] E. R. Triboni, M. R. Fernandes, J. R. Garcia, M. C. Carreira, R. G. D. S. Berlinck, P. B. Filho, et al., "Naphthalimide-derivative with blue electroluminescence for OLED applications," *Univ. Sci.*, vol. 9, p. 579, 2015.
- [147] W. Yuan, Q. Jin, M. Du, L. Duan, and Y. Zhang, "Tailoring ultra-narrowband tetraborylated multiple resonance emitter for high-performance blue OLED," *Adv. Mater.*, vol. 36, no. 48, p. 2410096, 2024.
- [148] D. Park, S. Kang, C. H. Ryoo, B. H. Jhun, S. Jung, T. N. Le, M. C. Suh, et al., "High-performance blue OLED using multiresonance thermally activated delayed fluorescence host materials containing silicon atoms," *Nat. Commun.*, vol. 14, no. 1, p. 5589, 2023.

- [149] S. Tasaki, K. Nishimura, H. Toyoshima, T. Masuda, M. Nakamura, and Y. Nakano, et al., “Realization of ultra-high-efficient fluorescent blue OLED,” *J. Soc. Inf. Disp.*, vol. 30, no. 5, pp. 441-451, 2022.
- [150] B. Wei, H. Xu, N. Zhao, X. Gao, Y. Ye, Y. Wang, et al., “Deep-blue organic light-emitting diodes based on multi-tert-butyl modified naphthylene,” *J. Ind. Eng. Chem.*, vol. 102, pp. 44–50, 2021.
- [151] C. Y. Chan, M. Tanaka, Y. T. Lee, Y. W. Wong, H. Nakanotani, and T. Hatakeyama, et al., “Stable pure-blue hyperfluorescence organic light-emitting diodes with high-efficiency and narrow emission,” *Nat. Photonics*, vol. 15, no. 3, pp. 203–207, 2021.
- [152] M. Han, Y. Chen, Y. Xie, F. Zhang, X. Li, A. Huang, et al., “1.42-fold enhancement of blue OLED device performance by simply changing alkyl groups on the acridine ring,” *Cell Rep. Phys. Sci.*, vol. 1, no. 11, p. 100252, 2020.
- [153] X. Zheng, Y. Liu, Y. Zhu, F. Ma, C. Feng, and Y. Yu, et al., “Efficient inkjet-printed blue OLED with boosted charge transport using host doping for application in pixelated display,” *Opt. Mater.*, vol. 101, p. 109755, 2020.
- [154] J. Yang, Q. Guo, J. Wang, Z. Ren, J. Chen, Q. Peng, et al., “Rational molecular design for efficient exciton harvesting, and deep-blue OLED application,” *Adv. Opt. Mater.*, vol. 6, no. 15, p. 1800342, 2018.
- [155] K. Nakao, H. Sasabe, R. Komatsu, Y. Hayasaka, T. Ohsawa, and J. Kido, “Significant enhancement of blue OLED performances through molecular engineering of pyrimidine-based emitter,” *Adv. Opt. Mater.*, vol. 5, p. 1600843, 2017.
- [156] T. Wang, X. Song, Z. Huang, J. Miao, Z. Chen, Y. Cheng, et al., “Color-tunable TADF conjugated polymers toward voltage-regulating white OLEDs for intelligent lighting,” *Adv. Opt. Mater.*, vol. 12, no. 15, p. 2303067, 2024.
- [157] S. J. Lee, C. M. Kang, J. W. Shin, D. H. Ahn, C. W. Joo, H. Cho, et al., “Three-wavelength white organic light-emitting diodes on silicon for high luminance and color gamut microdisplays,” *J. Ind. Eng. Chem.*, vol. 105, pp. 132–137, 2022.
- [158] S. H. Yang and T. L. Huang, “High fluorescence efficiency of dual-wavelength white OLED with NPB emission and triplet annihilation,” *Opt. Mater.*, vol. 111, p. 110725, 2021.
- [159] H. J. Kim, M. H. Shin, H. G. Hong, B. S. Song, S. K. Kim, W. H. Koo, et al., “Enhancement of optical efficiency in white OLED display using the patterned

- photoresist film dispersed with quantum dot nanocrystals,” *J. Disp. Technol.*, vol. 12, no. 6, pp. 526-531, 2015.
- [160] Y. Chen, J. Wang, Z. Zhong, Z. Jiang, C. Song, Z. Hu, et al., “Fabricating large-area white OLED lighting panels via dip-coating,” *Org. Electron.*, vol. 37, p. 458, 2016.
- [161] P. P. Lima, F. A. A. Paz, C. D. S. Brites, W. G. Quirino, C. Legnani, M. C. e Silva, et al., “Ferreira RAS, Júnior SA, Malta OL, Cremona M, Carlos LD (2014) White OLED based on a temperature sensitive $\text{Eu}^{3+}/\text{Tb}^{3+}$ β -diketonate complex,” *Org. Electron.*, vol. 15, p. 798, 2014.
- [162] H. Klauk, U. Zschieschang, and M. Halik, “Low voltage organic thin film transistors with large transconductance,” *J. Appl. Phys.*, vol. 102, no. 7, p. 074514, 2007.
- [163] J. B. Lee, P. C. Chang, J. A. Liddle, and V. Subramanian, “10-nm channel length pentacene transistors,” *IEEE Trans. Electron Devices*, vol. 52, no. 8, pp. 1874-1879, 2005.
- [164] S. Ghosh and L. Rajan, “In 2020 International Conference on Innovative Trends in Information Technology (ICITIIT),” in *Proc. 2020 Int. Conf. Innov. Trends Inf. Technol. (ICITIIT)*, IEEE, 2020, p. 1, 2020.
- [165] X. Xu, Y. Yao, B. Shan, X. Gu, D. Liu, J. Liu, et al., “Electron mobility exceeding $10 \text{ cm}^2 \text{ V}^{-1} \text{ s}^{-1}$ and band-like charge transport in solution-processed n-channel organic thin-film transistors,” *Adv. Mater.*, vol. 28, p. 5276, 2016.
- [166] M. M. Hasan, M. M. Islam, X. Li, M. He, R. Manley, J. Chang, et al., “Interface engineering with polystyrene for high-performance, low-voltage driven organic thin film transistor,” *IEEE Trans. Electron Devices*, vol. 67, no. 4, p. 1751-1756, 2020.
- [167] Y. Sun, Y. Liu, and D. Zhu, “Advances in organic field-effect transistors,” *J. Mater. Chem.*, vol. 15, p. 53, 2005.
- [168] L. Resendiz, M. Estrada, A. Cerdeira, B. Iniguez, and M. J. Deen, “Effect of active layer thickness on the electrical characteristics of polymer thin film transistors,” *Org. Electron.*, vol. 11, no. 12, pp. 1920-1927, 2010.
- [169] B. Kumar, B. K. Kaushik, and Y. S. Negi, “Analysis of electrical parameters of organic thin film transistors based on thickness variation in semiconducting and dielectric layers,” *IET Circuits Devices Syst.*, vol. 8, p. 131, 2014.
- [170] M. Kano, T. Minari, K. Tsukagoshi, and H. Maeda, “Control of device parameters by active layer thickness in organic thin film transistors,” *Appl. Phys. Lett.*, vol. 98, p. 073307, 2011.

- [171] R. N. Bennett, A. D. Hendsbee, J. H. Ngai, A. Ganguly, Y. Li, and T. L. Kelly, "Bisisoindigo–benzothiadiazole copolymers: Materials for ambipolar and n-channel OTFTs with low threshold voltages," *ACS Appl. Electron. Mater.*, vol. 2, p. 2039, 2020.
- [172] A. Bilgaiyan, M. Abiko, K. Watanabe, and M. Mizukami, "Critical impact of source/drain surface modification treatment on the performance of 4H-21DNTT OTFT," *ACS Appl. Electron. Mater.*, vol. 7, no. 6, pp. 2583–2592, 2025.
- [173] K. Ye, Y. Di, Z. Gan, C. Liu, F. Xing, and P. Zhang, "A study of bottom-contact organic thin-film transistors based on source/drain tunneling structure," *J. Phys.: Conf. Ser.*, vol. 2613, no. 1, p. 012004, 2023.
- [174] S. Gupta and M. K. Singh, "Effect of variation in channel length and thickness of organic semiconductor in the bottom-gate configuration of OTFT," *IOP Conf. Ser.: Mater. Sci. Eng.*, vol. 1119, no. 1, p. 012012, 2021.
- [175] A. Singh and M. K. Singh, "TCAD based study of parameters affecting the electrical performance of organic thin-film transistors," *J. Phys.: Conf. Ser.*, vol. 1706, p. 012074, 2020.
- [176] P. Kumari and A. D. D. Dwivedi, "Numerical simulation and characterization of pentacene based organic thin film transistors with top and bottom gate configurations," *Global J. Res. Eng.*, vol. 19, no. 3, p. 7-12, 2019.
- [177] A. Verma and P. Mittal, "Characterization and depth analysis of organic thin film transistor," *J. Graph. Era Univ.*, vol. 4, p. 22, 2016.
- [178] S. K. Kim, C. H. Shim, T. Edura, C. Adachi, and R. Hattori, "Improved organic thin film transistor characteristics using an elevated-electrode structure," *Jpn. J. Appl. Phys.*, vol. 53, no. 11, p. 111601, 2014.
- [179] Y. Xu, T. Minari, K. Tsukagoshi, J. Chroboczek, and G. Ghibaudo, "Direct evaluation of low-field mobility and access resistance in pentacene field-effect transistors," *J. Appl. Phys.*, vol. 107, no. 11, p. 114507, 2010.
- [180] D. Gupta, M. Katiyar, and D. Gupta, "An analysis of the difference in behavior of top and bottom contact organic thin film transistors using device simulation," *Org. Electron.*, vol. 10, no. 5, pp. 775–784, 2009.
- [181] S. Roy, M. M. Islam, A. Ali, J. K. Saha, H. Lee, A. Tooshil, et al., "High memory window, dual-gate amorphous InGaZnO thin-film transistor with ferroelectric gate insulator," *Phys. Status Solidi A*, vol. 222, no. 4, p. 2400638, 2025.

- [182] J. Seo, C. H. Kim, and H. Yoo, "Dual-gate operation and configurable logic from solution pattern-based zinc tin oxide thin-film transistors," *IEEE Trans. Electron Devices*, vol. 71, no. 5, pp. 3020-3025, 2024.
- [183] S. Gupta and M. K. Singh, "Key aspects affecting the performances of high-K dielectrics based single-gate and dual-gate OTFTs," *Mater. Today: Proc.*, vol. 50, pp. 231–237, 2022.
- [184] S. Singh, Y. Takeda, H. Matsui, and S. Tokito, "Flexible inkjet-printed dual-gate organic thin film transistors and PMOS inverters: Noise margin control by top gate," *Org. Electron.*, vol. 85, p. 105847, 2020.
- [185] A. D. D. Dwivedi and P. Kumari, "TCAD simulation and performance analysis of single and dual gate OTFTs," *Surf. Rev. Lett.*, vol. 27, p. 1950145, 2020.
- [186] R. Shiwaku, M. Tamura, H. Matsui, Y. Takeda, T. Murase, and S. Tokito, "Charge carrier distribution in low-voltage dual-gate organic thin-film transistors," *Appl. Sci.*, vol. 8, no. 8, p. 1341, 2018.
- [187] D. Saini and B. K. Kaushik, in *Proc. 2015 Natl. Conf. Recent Advances Electron. Comput. Eng. (RAECE)*, IEEE, p. 196, 2015.
- [188] H. Klauk, "Will we see gigahertz organic transistors?" *Adv. Electron. Mater.*, vol. 4, p. 1700474, 2018.
- [189] T. Kang, A. Rani, W. Ren, M. J. Sultan, N. E. Lee, and T.G. Kim, "Ultra-thin vertical TFT photosensor and photosynapse based on Au-doped-graphene under transition metal selenide reaction," *J. Mater. Sci. Technol.*, vol. 183, pp. 215–222, 2024.
- [190] S. Choi, B. S. Hwang, S. H. Hwang, S. H. Hwang, S. J. Moon, and B. S. Bae, "Development of vertical structured TFT using interfacial oxidation," *Electrochem. Soc. Meeting Abstracts*, vol. MA2024-02, no. 34, pp. 2397–2397, 2024.
- [191] B. Sun, H. Huang, P. Wen, M. Xu, C. Peng, and L. Chen, "Research progress of vertical channel thin film transistor device," *Sensors*, vol. 23, no. 14, p. 6623, 2023.
- [192] D. Knepe, F. Talnack, B. K. Boroujeni, C. T. da Rocha, M. Höppner, and A. Tahn, "Solution-processed pseudo-vertical organic transistors based on TIPS-pentacene," *Mater. Today Energy*, vol. 21, p. 100697, 2021.
- [193] Q. Chen, Y. Yan, X. Wu, S. Lan, D. Hu, and Y. Fang, "High-performance quantum-dot light-emitting transistors based on vertical organic thin-film transistors," *ACS Appl. Mater. Interfaces*, vol. 11, pp. 35888–35895, 2019.

- [194] R. Rathi, R. Ahmad, S. Negi, and V. Panwar, "Performance Analysis of Single and Dual Gate Vertical Channel Organic Thin Film Transistor," in Proc. 2018 IEEE UPCON, pp. 1-4, 2018.
- [195] H. Kleemann, A. A. Günther, K. Leo, and B. Lüssem, "High-Performance Vertical Organic Transistors," *Small*, vol. 9, pp. 3670–3677, 2013.
- [196] H. Zheng, Z. Ye, B. Liu, M. Wang, L. Zhang, and C. Liu, "Dual-gate metal-oxide-semiconductor transistors: Nanoscale channel length scaling and performance optimization," *Electronics*, vol. 14, no. 7, p. 1257, 2025.
- [197] S. Y. Yang, J. B. Kim, J. H. Cho, Y. Jang, T. Lee, and C. N. Kim, "Highly flexible vertical organic thin film transistors," *ACS Nano*, vol. 8, no. 10, pp. 9594-9602, 2014.
- [198] Y. H. Kim, B. Kang, K. Cho, T. Lee, and C. N. Kim, "High-performance organic vertical thin film transistor using graphene as a tunable contact," *ACS Nano*, vol. 9, no. 11, pp. 10453-10460, 2015.
- [199] D. Tordera, B. Peeters, H. B. Akkerman, A. J. van Breemen, J. S. Maas, and S. Shanmugam, "A high-resolution thin-film fingerprint sensor using a printed organic photodetector," *Adv. Mater. Technol.*, vol. 4, no. 11, p. 1900651, 2019.
- [200] K. J. Baeg, M. Binda, D. Natali, M. Caironi, and Y. Y. Noh, "Organic light detectors: photodiodes and phototransistors," *Adv. Mater.*, vol. 25, no. 31, pp. 4267–4295, 2013.
- [201] T. J. Wijaya, S. Xiong, K. Sasaki, Y. Kato, K. Mori, M. Koizumi, et al., "A highly stable organic–inorganic hybrid electron transport layer for ultra flexible organic photodiodes," *Adv. Mater.*, vol. 37, no. 21, p. 2501951, 2025.
- [202] J. K. Wu, P. Y. Chen, G. Suthar, Y. Y. Su, C. W. Chu, F. C. Chen, et al., "Cost-effective cobalt (II) acetate as an efficient and stable hole transport layer in inverted organic photodetectors," *ACS Appl. Electron. Mater.*, vol. 7, no. 4, pp. 1579-1589, 2025.
- [203] P. Krebsbach, S. Schliske, N. Strobel, M. Seiberlich, L. A. Ruiz-Preciado, C. Rainer, et al., "Inkjet-printed tin oxide hole-blocking layers for organic photodiodes," *ACS Appl. Electron. Mater.*, vol. 3, no. 11, pp. 4959-4966, 2021.
- [204] N. Li, Z. Lan, Y. S. Lau, J. Xie, D. Zhao, and F. Zhu, "Tuning the charge blocking layer to enhance photomultiplication in organic shortwave infrared photodetectors," *J. Mater. Chem. C*, vol. 8, no. 5, pp. 1585–1592, 2020.
- [205] S. A. Roslan, A. A. M. Sabri, N. A. Roslan, T. M. Bawazeer, M. S. Alsoufi, F. Aziz, et al., "Equal proportion of donor/acceptor active layer for reduced dark current in visible organic photodiode," *Opt. Mater.*, vol. 147, p. 114781, 2024.

- [206] Y. Li, H. Chen, and J. Zhang, "Carrier blocking layer materials and application in organic photodetectors," *Nanomaterials*, vol. 11, no. 6, p. 1404, 2021.
- [207] A. Basir, H. Alzahrani, K. Sulaiman, F. F. Muhammadsharif, S. M. Abdullah, A. Y. Mahmoud, et al., "A novel self-powered photodiode based on solution-processed organic TPD:Alq3 active layer," *Mater. Sci. Semicond. Process.*, vol. 131, p. 105886, 2021.
- [208] S. M. Abdullah, S. Rafique, M. I. Azmer, A. Jilani, V. K. Sajith, and A. Supangat, "Modified photo-current response of an organic photodiode by using V_2O_5 in both hole and electron transport layers," *Sens. Actuators A: Phys.*, vol. 272, pp. 334–340, 2018.
- [209] B. Park, J. W. Ha, S. C. Yoon, C. Lee, I. H. Jung, and D. H. Hwang, "Visible-light-responsive high-detectivity organic photodetectors with a 1 μm thick active layer," *ACS Appl. Mater. Interfaces*, vol. 10, no. 44, pp. 38294–38301, 2018.
- [210] H. Arora, P. E. Malinowski, A. Chasin, D. Cheyns, S. Steudel, S. Schols, et al., "Amorphous indium-gallium-zinc-oxide as electron transport layer in organic photodetectors," *Appl. Phys. Lett.*, vol. 106, no. 14, p. 143301, 2015.
- [211] N. T. Kalyani and S. J. Dhoble, "Novel materials for fabrication and encapsulation of OLEDs," *Renew. Sustain. Energy Rev.*, vol. 44, p. 319, 2015.
- [212] W. J. Hyun, S. H. Im, O. O. Park, and B. D. Chin, "Corrugated structure through a spin-coating process for enhanced light extraction from organic light-emitting diodes," *Organic Electronics*, vol. 13, no. 4, pp. 579–585, 2012.
- [213] N. Juhari, N. I. A. Shukri, N. Sabani, S. Shaari, M. F. Ahmad, and N. F. Zakaria, "The structural and electrical characterization of PEDOT: PSS/MEH-PPV doped with PEIE OLED fabricated using spin coating technique," in *AIP Conference Proceedings*, vol. 2203, p. 020046, 2020.
- [214] H. C. Chen, C. P. Kung, W. G. Houn, Y. R. Peng, Y. M. Hsien, C. C. Chou, et al., "Polymer inverter fabricated by inkjet printing and realized by transistors arrays on flexible substrates," *IEEE/OSA J. Display Technol.*, vol. 5, p. 216, 2009.
- [215] X. Xing, T. Lin, Y. X. Hu, Y. L. Sun, W. Y. Mu, Z. Z. Du, et al., "Inkjet printing high luminance phosphorescent OLED based on m-MTDATA: TPBi host," *Mod. Phys. Lett. B*, vol. 33, p. 1950149, 2019.
- [216] Z. Hu, Y. Yin, M. U. Ali, W. Peng, S. Zhang, and D. Li, et al., "Inkjet printed uniform quantum dots as color conversion layers for full-color OLED displays," *Nanoscale*, vol. 12, p. 2103, 2020.

- [217] J. B. Preinfalk, T. Eiselt, T. Wehlus, V. Rohnacher, T. Hanemann, and G. Gomard, et al., "Large-area screen-printed internal extraction layers for organic light-emitting diodes," *ACS Photonics*, vol. 4, p. 928, 2017.
- [218] Z. Wan, M. Xu, Z. Fu, D. Li, A. Mei, Y. Hu, et al., "Screen printing process control for coating high throughput titanium dioxide films toward printable mesoscopic perovskite solar cells," *Front. Optoelectron.*, vol. 12, p. 344, 2019.
- [219] L. Derue, S. Olivier, D. Tondelier, T. Maindron, B. Geffroy, and E. Ishow, "All-solution-processed organic light-emitting diodes based on photostable photo-cross-linkable fluorescent small molecules," *ACS Appl. Mater.*, vol. 8, p. 16207, 2016.
- [220] Y. Yoshioka and G. E. Jabbour, "Desktop inkjet printer as a tool to print conducting polymers," *Synthetic Metals*, vol. 156, no. 11–13, pp. 779–783, 2006.
- [221] V. J. LiCata and A. J. Wowor, "Applications of fluorescence anisotropy to the study of protein–DNA interactions," *Methods Cell Biol.*, vol. 84, pp. 243–262, 2008.
- [222] R. K. Tiwari, R. Mishra, S. K. Sharma, N. Prabhu, M. R. Nagar, and S. Grigalevicius, "Advancing cancer treatment and diagnosis: A review on photodynamic therapy using OLED technology," *Molecules*, vol. 30, no. 6, p. 1305, 2025.
- [223] Y. W. Kim, J. H. Kwon, H. R. Choi, J. G. Choi, O. K. Kwon, K. H. Kim, et al., "Wearable quantum dots organic light-emitting diodes patch for high-power near infra-red photomedicine with real-time wavelength control," *Chem. Eng. J.*, vol. 499, p. 156121, 2024.
- [224] R. Liu, S. A. Haruna, S. Ali, J. Xu, Y. Zhang, P. Lü, et al., "A sensitive and accurate fluorescent genosensor for *Staphylococcus aureus* detection," *Sens. Actuators B Chem.*, vol. 355, p. 131311, 2022.
- [225] M. Zhang, H. Wang, E. R. Foster, Z. L. Nikolov, S. D. Fernando, and M. D. King, "Binding behavior of spike protein and receptor binding domain of the SARS-CoV-2 virus at different environmental conditions," *Sci. Rep.*, vol. 12, no. 1, p. 789, 2022.
- [226] C. Y. Lee, I. Degani, J. Cheong, J. H. Lee, H. J. Choi, J. Cheon, et al., "Fluorescence polarization system for rapid COVID-19 diagnosis," *Biosens. Bioelectron.*, vol. 178, p. 113049, 2021.
- [227] J. Guo, S. Chen, S. Tian, K. Liu, J. Ni, M. Zhao, et al., "5G-enabled ultra-sensitive fluorescence sensor for proactive prognosis of COVID-19," *Biosens. Bioelectron.*, vol. 181, p. 113160, 2021.

- [228] Y. Khan, D. Han, J. Ting, M. Ahmed, R. Nagisetty, and A. C. Arias, "Organic multi-channel optoelectronic sensors for wearable health monitoring," *IEEE Access*, vol. 7, pp. 128114–128124, 2019.
- [229] S. Negi, P. Mittal, B. Kumar, and P. K. Juneja, "Organic LED based light sensor for detection of ovarian cancer," *Microelectron. Eng.*, vol. 218, p. 111154, 2019.
- [230] S. Kim, W. Choi, W. Rim, Y. Chun, H. Shim, H. Kwon, et al., "A highly sensitive capacitive touch sensor integrated on a thin-film-encapsulated active-matrix OLED for ultrathin displays," *IEEE Trans. Electron Devices*, vol. 58, no. 10, pp. 3609-3615, 2011.
- [231] K. Watanabe, Y. Iwaki, Y. Uchida, D. Nakamura, H. Ikeda, H. Miyake, et al., "An 8.67-in. Foldable OLED Display with an In-cell Touch Sensor," *Dig. Tech. Pap. - SID Int. Symp.*, vol. 46, no. 1, pp. 246-249, 2011.
- [232] F. Barre, A. Chiquard, S. Faure, L. Landais, and P. Patry, "In Building European OLED Infrastructure," *Proc. Int. Soc. Opt. Photon.*, vol. 5961, p. 596109, 2005.
- [233] M. Trakalo and S. Lorimer, "In Display Technologies and Applications for Defense, Security, and Avionics II," *Proc. Int. Soc. Opt. Photon.*, vol. 6956, p. 69560, 2008.
- [234] M. Katsuhara, I. Yagi, A. Yumoto, M. Noda, N. Hirai, R. Yasuda, et al., "In Organic Field-Effect Transistors VIII," *Proc. Int. Soc. Opt. Photon.*, vol. 7417, p. 74170, 2009.
- [235] M. Noda, N. Obayashi, M. Katsuhara, A. Yumoto, S. Ushikura, R. Yasuda, et al., "An OTFT-driven rollable OLED display," *J. Soc. Inf. Disp.*, vol. 19, p. 316, 2011.
- [236] J. S. Kim and C. K. Song, "AMOLED panel driven by OTFTs on polyethylene fabric substrate," *Org. Electron.*, vol. 30, p. 45, 2016.
- [237] C. H. Kim, "Bias-stress effects in diF-TES-ADT field-effect transistors," *Solid-State Electron.*, vol. 153, pp. 23–26, 2019.
- [238] Choi, J. Kang, C. Lee, K. Jeong, and S.G. Im, "Heavily crosslinked, high-k ultrathin polymer dielectrics for flexible, low-power organic thin-film transistors (OTFTs)," *Adv. Electron. Mater.*, vol. 6, p. 2000314, 2020.
- [239] Y. Bai, X. Liu, L. Chen, M. A. Khan, W. Q. Zhu, X. Y. Jiang, et al., "Organic thin-film field-effect transistors with MoO₃/Al electrode and OTS/SiO₂ bilayer gate insulator," *Microelectron. J.*, vol. 38, p. 1185, 2007.
- [240] N. A. Roslan, S. M. Abdullah, M. Z. M. Halizan, T. M. Bawazeer, N. Alsenany, M. S. Alsoufi, et al., "VTP as an active layer in a vertical organic field effect transistor," *J. Electron. Mater.*, vol. 47, p. 2184, 2018.

- [241] H. Naruse, S. Naka, and H. Okada, “Dual self-aligned vertical multichannel organic transistors,” *Appl. Phys. Express*, vol. 1, p. 011801, 2007.
- [242] H. W. Zan and K. H. Yen, “Vertical-channel organic thin-film transistors with meshed electrode and low leakage current,” *Jpn. J. Appl. Phys.*, vol. 46, p. 3315, 2007.
- [243] S. Y. Oh and J. Y. Lee, “Characteristics of vertical type organic transistor using n-type material and its application for OLED,” *Mol. Cryst. Liq. Cryst.*, vol. 444, no. 1, p. 211-218, 2006.
- [244] A. Jetly and R. Mehra, “Design of tandem organic light emitting diode using efficient charge generation layer,” *Opt. Mater.*, vol. 88, p. 304, 2019.
- [245] Y. P. Wang, Q. Liang, J. Huang, D. Ma, and Y. Jiao, “Investigation of the hole transport characterization and mechanisms in co-evaporated organic semiconductor mixtures,” *RSC Adv.*, vol. 7, pp. 28494-28498, 2017.
- [246] X. Wang, M. Zhong, Y. Liu, P. Ma, L. Dang, and Q. Meng, et al., “Rapid and sensitive detection of COVID-19 using CRISPR/Cas12a-based detection with naked eye readout, CRISPR/Cas12a-NER,” *Sci. Bull.*, vol. 65, no. 17, p. 1436, 2020.
- [247] X. Ding, K. Yin, Z. Li, R. V. Lalla, E. Ballesteros, M. M. Sfeir, et al., “Ultrasensitive and visual detection of SARS-CoV-2 using all-in-one dual CRISPR-Cas12a assay,” *Nat. Commun.*, vol. 11, no. 1, p. 4711, 2020.
- [248] C. Lian, D. Young, R. E. Randall, and I. D. W. Samuel, “Organic light-emitting diode based fluorescence-linked immunosorbent assay for SARS-CoV-2 antibody detection,” *Biosensors*, vol. 12, no. 12, p. 1125, 2022.
- [249] G. Q. Zhang, Z. Gao, J. Zhang, H. Ou, H. Gao, R. T. K. Kwok, et al., “A wearable AIEgen-based lateral flow test strip for rapid detection of SARS-CoV-2 RBD protein and N protein,” *Cell Rep. Phys. Sci.*, vol. 3, no. 2, 2022.
- [250] T. Yagi, T. Kawase, S. Minami, H. Koike, and T. Someya, “Flexible full-color AMOLED displays driven by organic thin-film transistors,” *J. Soc. Inf. Display*, vol. 16, no. 12, pp. 1053–1060, 2008.
- [251] C. Liu, H. Kang, and S. Lee, “Voltage driving pixel circuits using organic thin-film transistors for efficient OLED display operation,” *Org. Electron.*, vol. 10, no. 4, pp. 715–722, 2009.
- [252] M. E. Gershenson, V. Podzorov, and A. F. Morpurgo, “Colloquium: Electronic transport in single-crystal organic transistors,” *Rev. Mod. Phys.*, vol. 78, no. 3, pp. 973–989, 2006

- [253] S. K. Park, D. A. Mourey, S. Subramanian, J. E. Anthony, and T. N. Jackson, “High-mobility spin-cast organic thin film transistors,” *Appl. Phys. Lett.*, vol. 93, no. 4, p. 043301, 2008.
- [254] K. Sakanoue, H. Tsukagoshi, and T. Someya, “Solution-processed C8-BTBT OTFTs with hole mobilities up to $6.50 \text{ cm}^2/\text{V}\cdot\text{s}$ via interface engineering,” *J. Mater. Chem. C*, vol. 5, pp. 9123–9129, 2017.
- [255] C. M. Lochner, Y. Khan, A. Pierre, and A. C. Arias, “All-organic optoelectronic sensor for pulse oximetry,” *Nat. Commun.*, vol. 5, no. 1, p. 5745, 2014.
- [256] Y. Lee, J. W. Chung, G. H. Lee, H. Kang, J. Y. Kim, C. Bae, et al., “Standalone real-time health monitoring patch based on a stretchable organic optoelectronic system,” *Sci. Adv.*, vol. 7, p. eabg9180, 2021.
- [257] C. Kim, K. S. Bae, G. Kim, D. Y. Lee, G. Moon, D. Yang, et al., “Sensor organic light-emitting diode display, combining fingerprint and biomarker capturing,” *Commun. Eng.*, vol. 3, no. 1, p. 92, 2024.
- [258] R. K. Pandey and P. C. P. Chao, “A dual-channel PPG readout system with motion-tolerant adaptability for OLED-OPD sensors,” *IEEE Trans. Biomed. Circuits Syst.*, vol. 16, no. 1, pp. 36-51, 2021.
- [259] J. V. Dcosta, D. Ochoa, and S. Sanaur, “Recent progress in flexible and wearable all organic photoplethysmography sensors for SpO₂ monitoring,” *Adv. Sci.*, vol. 10, no. 31, p. 2302752, 2023.
- [260] F. A. Jhuma and R. Hattori, “Application of organic photodetectors (OPD) in photoplethysmography (PPG) sensors: A small review,” *IEICES*, vol. 8, pp. 246-252, 2022.
- [261] G. Simone, D. Tordera, E. Delvitto, B. Peeters, A. J. van Breemen, S. C. Meskers, et al., “High-accuracy photoplethysmography array using near-infrared organic photodiodes with ultralow dark current,” *Adv. Opt. Mater.*, vol. 8, no. 10, p. 1901989, 2020.
- [262] A. Bilgaiyan, F. Elsamnah, H. Ishidai, C. H. Shim, M. A. B. Misran, C. Adachi, et al., “Enhancing small-molecule organic photodetector performance for reflectance-mode photoplethysmography sensor applications,” *ACS Appl. Electron. Mater.*, vol. 2, no. 5, pp. 1280-1288, 2020.
- [263] K. Papadopoulos, D. Tselekidou, A. Zachariadis, A. Laskarakis, S. Logothetidis, and M. Gioti, “The influence of thickness and spectral properties of green color-emitting

- polymer thin films on their implementation in wearable PLED applications,” *Nanomaterials*, vol. 14, no. 19, p. 1608, 2024.
- [264] A. N. Bashkatov, E. A. Genina, V. I. Kochubey, and V. V. Tuchin, “Optical properties of human skin, subcutaneous and mucous tissues in the wavelength range from 400 to 2000 nm,” *J. Phys. D: Appl. Phys.*, vol. 38, p. 2543, 2005.
 - [265] C. Murawski and M. C. Gather, “Emerging biomedical applications of organic light-emitting diodes,” *Adv. Opt. Mater.*, vol. 9, no. 14, p. 2100269, 2021.
 - [266] M. J. Leiner, M. R. Hubmann, and O. S. Wolfbeis, “The total fluorescence of human urine,” *Anal. Chim. Acta*, vol. 198, pp. 13-23, 1987.
 - [267] S. I. Ahmad, I. A. Syed, R. P. Prasad, and A. Ahmad, “Quantitation of urea in urine by Fourier transforms infrared spectroscopy,” *Der. Pharma. Chemica*, vol. 6, pp. 90-96, 2014.
 - [268] V. Masilamani, V. Trinku, M. Al Salhi, K. Govindaraj, A. P. V. Raghavan, and B. Antonisamy, “Cancer detection by native fluorescence of urine,” *J. Biomed. Opt.*, vol. 15, no. 5, p. 057003, 2010.
 - [269] M. Zvarik, D. Martinicky, L. Hunakova, I. Lajdova, and L. Sikurova, “Fluorescence characteristics of human urine from normal individuals and ovarian cancer patients,” *Neoplasma*, vol. 60, no. 5, pp. 533-537, 2013.
 - [270] T.W. Rockett, M. Almahyawi, M.L. Ghimire, A. Jonnalagadda, V. Tagliaferro, S.J. Seashols-Williams, M.F. Bertino, G.A. Caputo, and J.E. Reiner, “Cluster-enhanced nanopore sensing of ovarian cancer marker peptides in urine,” *ACS Sensors*, vol. 9, no. 2, pp. 860–869, 2024.

LIST OF PUBLICATIONS

SCI/SCIE Indexed Journal Papers Published

1. Sugandha Yadav, Poornima Mittal, and Shubham Negi. "Recent advancements over a decade for organic light-emitting diodes: from structural diversity, role of layers, colour emission, material classification, performance improvement, fabrication to applications." **Bulletin of Materials Science**, vol. 45, no. 3, p. 109, 2022. (IF:1.9, Springer)
2. Sugandha Yadav, Poornima Mittal, and Shubham Negi. "Architectural design, fabrication techniques, characteristics parameters and different applications for OLED along with some OTFT driven OLEDs: A review." **Main Group Chemistry**, vol. 23, no. 1, pp. 1-16, 2023. (IF: 1.5, IOS Press).
3. Sugandha Yadav, Poornima Mittal, and Shubham Negi. "Advancements and Perspectives of Organic LED: In Depth Analysis of Architectural Design, Characteristics Parameters, Fabrication Techniques, and Applications." **ECS Journal of Solid-State Science and Technology**, vol. 12, no. 4, p. 046004, 2023. (IF: 2.48, IOP Science).
4. Sugandha Yadav, Poornima Mittal, and Shubham Negi. "High-k dielectric based high performance vertical organic thin film transistor for flexible low power applications." **Physica Scripta**, vol. 99, no. 2, p. 025940, 2024. (IF: 3.08, IOP Science)
5. Sugandha Yadav, Poornima Mittal, and Shubham Negi. "Characteristic performance and analysis of the positional variation of the charge generation layer to enhance the performance of OLEDs." **Journal of Computational Electronics**, vol. 22, no. 6, pp. 1696-1705, 2023. (IF: 1.98, Springer)
6. Sugandha Yadav, Poornima Mittal, and Shubham Negi. "An In-Depth Analysis of Variation in Characteristic Performance of OLED with Respect to Position of Charge Generation Layer." **ECS Journal of Solid-State Science and Technology**, vol. 12, no. 10, p. 106001, 2023. (IF: 2.48, IOP Science)
7. Sugandha Yadav, Poornima Mittal, and Shubham Negi. "Impact of Varying Position and Ratio of Charge Generation Layer on Performance Parameters of Organic Photodiode." **ECS Journal of Solid-State Science and Technology**, vol. 13, no. 2, p. 026001, 2024. (IF: 2.48, IOP Science)

8. Sugandha Yadav, Poornima Mittal, and Shubham Negi. "Covid-19 Detection using Organic LED and Photo Diode based sensor device." **IEEE Sensors Journal**, vol. 24, no. 24, pp. 40678-40684, 2024. (IF: 4.32, IEEE)
9. Sugandha Yadav, Poornima Mittal, and Shubham Negi. "Parametric Analysis of Organic LED and Photo-Diode based Sensor for Heart Rate Detection." **Advanced Theory and Simulation**, p. 250037, 2025. (IF: 2.9, Wiley)

Paper Under-Process for Submission in SCI/SCIE International Journal

1. Sugandha Yadav, Poornima Mittal, and Shubham Negi. "Parametric Analysis of CGL based OLED-OPD Integration for Ovarian Cancer Detection." **Sensors and Actuators B: Chemical**, 2025. (IF: 4.9, Elsevier)

Scopus Indexed International Conference Papers

1. Sugandha Yadav, Poornima Mittal, and Shubham Negi. "Analysis and comparison of a high-K dielectric vertical channel based organic thin film transistor." **IIT Roorkee, International Conference on Electrical, Electronics, Communication and Computers (ELEXCOM)**, 23 held on 26-27 August, 2023.
2. Sugandha Yadav, Poornima Mittal, and Shubham Negi. "Positional Analysis and Comparison of Different Charge Layer based Blue OLEDs." **Graphic Era, 2nd IEEE International Conference on Device Intelligence, Computing and Communication Technologies (DICCT)**, 24 held on 15-16 March, 2024.

Paper Under-Process for Submission in Scopus Indexed International Conference

1. Sugandha Yadav, Poornima Mittal, and Shubham Negi. "Impact of CGL on OPDs and optimization techniques for performance improvement." (Under Process)



Recent advancements over a decade for organic light-emitting diodes: from structural diversity, role of layers, colour emission, material classification, performance improvement, fabrication to applications

SUGANDHA YADAV¹, POORNIMA MITTAL^{1,*}  and SHUBHAM NEGI²

¹Department of Electronic and Communication Engineering, Delhi Technological University, New Delhi 110042, India

²Department of Electronics and Communication Engineering, Tula's Institute, Dehradun 248197, India

*Author for correspondence (poornimamittal@dtu.ac.in)

MS received 11 October 2021; accepted 24 January 2022

Abstract. Organic light-emitting diode (OLED) is an emerging technology of organic electronics that exhibits an assortment of salient and attractive features like self-emitting ability, great flexibility, true dark tone, transparency and many more. Along with display applications, OLEDs are prudent for light detection-based applications. Enormous research work has been reported to refine the OLED technology in terms of structures, materials, performance parameters, lifetime and applications. There is a vast scope for developing white OLED devices for utilization in solid-state lighting applications. This review paper summarizes recent advancements in different aspects for OLEDs over the last decade. The main focus is to diversify different multilayer structures of OLEDs highlighting the role and significance of charge injection, charge transport, emission and blocking layers. Also, a timeline analysis for characteristics parameters, layer-wise materials and fabrication techniques is presented. Further, different performance improvement techniques based on layers, parameters and colour emission are demonstrated. This article also illustrates prudent applications based on organic thin-film transistor-driven OLED, sensors, military and healthcare. Some challenges and reliability issues are also discussed with a scope for future work for OLED.

Keywords. Active-matrix OLED (AMOLED); healthcare; military; organic light-emitting diode (OLED); sensors.

1. Introduction

In inorganic electronics, the integrated circuits can be made only on single crystals of semiconductors using high-temperature processing steps. Monolithic integration of components on other substrates like plastic, glass, etc. is not possible [1]. On the other hand, the properties of organic semiconductors are driven by the properties of molecules [2]. There is always a major scope of amending the properties of semiconductors by altering the molecular structure.

In 1950, electroluminescence was first observed in organic materials by giving high voltage in the air to acridine orange [3]. Further, the need for electrode contact was explained by Martin Pope in NY University in 1960 [4]. They developed the Ohmic dark-injecting electrode. First DC electroluminescence under vacuum was noticed on the crystal of anthracene in 1965. Therefore, electroluminescence in anthracene was observed through hole and electron double injection recombination in Canada [3]. They discussed about electron excitation between graphite molecules and anthracene particles at contacts. The first polymer light-emitting diode was reported in 1987 using a novel

two-layer structure having electron and hole transporting layers for the recombination. This resulted in light emission between organic layers. Thereafter in 1990, a green light-emitting polymer device was produced at the Cavendish Laboratory, Cambridge [3].

Organic semiconductors are molecular in nature where molecules are carried together by weak Van der Waals forces. Because of this property, semiconductors can be vaporized at very low temperatures to develop thin films. Additional to small molecules (SMs), polymers also belong to the organic semiconductors class, as these are soluble in common solvents such as xylene or chloroform and their films can be formed by simple spin-coating techniques. The organic semiconductors are not crystalline in nature and can be fabricated at very low temperatures. Due to this nature, organic devices like OLED, transistors, solar cells, etc. can be fabricated not only on inexpensive glass but also paper, plastic and fabric as these devices contain great flexibility.

Organic light-emitting diode (OLED) has been considered as one of the most promising techniques in display technology, as it is providing a new dimension to the display technology. There are many advantages of OLED over

Architectural design, fabrication techniques, characteristics parameters and different applications for OLED along with some OTFT driven OLEDs: A review

Sugandha Yadav^a, Poornima Mittal^{a,*} and Shubham Negi^b

^a*Department of Electronics and Communication Engineering, Delhi Technological University, New Delhi, India*

^b*Department of Electronics and Communication Engineering, Chandigarh University, Mohali, Punjab, India*

Abstract. In consumer electronics, Organic LED (OLED) has become mainstream display technology. Using organic materials, opto-electronics devices have become extensively desirable for various reasons. One of the fundamental properties i.e., flexibility permits to fabricate electronic circuits on flexible substrates to make these devices bendable and stretchable. This paper provides a review on various terms of OLED like fabrication methods, operation of OLED, its categorization, few OTFT driven OLEDs, stability issues of white OLED and various applications of OLED based on sensors, display, and lighting. Different lighting devices like incandescent bulb, tube light, CFL, LED and OLED are compared on the basis of their efficiency and lifetime. The comparison highlights that the LED provides good lifetime, however, for OLED it depends on the organic semiconducting materials responsible for emission. Different layers such as charge injection layers, transport layers and blocking layer to refine the properties of organic LEDs are also studied and compared. Addition to this, a low-cost methodology is also incorporated for the fabrication of flexible devices.

Keywords: HOMO, Light Emitting Diode, Luminescence, LUMO, multi-layered OLED structures

1. Introduction

The Organic LED is a carbon-based nascent technology in the field of displays, wherein thin films of specific light emitting organic materials are utilized. Owing to its high performance with respect to image quality, large fabrication area [1], flexibility [2, 3], low power [4] and design cost these devices have been successfully inducted for displays applications. Fabrication of OLED includes deposition of various organic semiconducting materials between the electrodes, each of these materials being used for a specific purpose. With the application of suitable voltage, a bright light is emitted by the device. Luminescence is one of the deciding factors to achieve uniform light output. The significant improvement in the performance of these devices is a direct result of developing novel methodologies

*Corresponding author: Poornima Mittal, Department of Electronics and Communication Engineering, Delhi Technological University, New Delhi, 110042, India. E-mail: poornimamittal@dtu.ac.in.

Review—Advancements and Perspectives of Organic LED: In Depth Analysis of Architectural Design, Characteristics Parameters, Fabrication Techniques and Applications

Sugandha Yadav,¹ Poornima Mittal,^{1,z} and Shubham Negi²

¹Department of Electronics and Communication Engineering, Delhi Technological University, Delhi-110042 (India)

²Department of Electronics and Communication Engineering, Chandigarh University, Mohali, Punjab-140413 (India)

^zE-mail: poornimamittal@dtu.ac.in

Abstract

This article presents a review on various aspect of Organic LED, such as its working, various categorization, impact of fabrication methodologies (organic vapor phase deposition, vacuum thermal evaporation, inkjet printing etc.) that are low-cost and its applications in serval domains like medical, sensor, display, lighting etc. Three categorizations of OLED are discussed with respect to circuit, architecture, and color of emission. Different layers of multi-layered structures such as injection layer, transport layer, block layers are also reviewed and their impacts are analyzed and compared. Moreover, an experimental fabrication technique for flexible substrate is reviewed that highlights low-cost fabrication method. In this technique, dynamic viscosity and contact angle are measured using rotational viscometer and contact angle meter, respectively. The result illustrates sheet resistance and effective opening ratio of 3.8 ohms per square and 82.5%, correspondingly. Additionally, various performance parameters like luminescence, external quantum efficiency and current efficiency are compared. The paper also incorporates recent advancement in organic thin film transistors along with some OTFT driven OLED devices.

1. Introduction

Organic light emitting diode (OLED) is a modern display technology which is made from organic thin films of light emissive materials. It has become successfully commercialized device in mobile and television display. This technology comes up with unparalleled image quality, flexible [1,2] and transparent display, large area fabrication [3], low power consumption [4], low-cost designs etc. The parameters like luminescence, current density and methodologies such as transport and block layers play important role for improving the performance of OLED. This paper provides a review on these parameters. Organic LEDs are



PAPER

High-k dielectric based high performance vertical organic thin film transistor for flexible low power applications

RECEIVED
31 January 2023REVISED
9 September 2023ACCEPTED FOR PUBLICATION
2 January 2024PUBLISHED
15 January 2024Sugandha Yadav^{1,*}, Poornima Mittal^{1,*}  and Shubham Negi²¹ Department of Electronics & Communication Engineering, Delhi Technological University, New Delhi, 110042, India² Department of Electronics and Communication Engineering, Chandigarh University, Mohali Punjab, 140413 India

* Author to whom any correspondence should be addressed.

E-mail: sugandhayadav555@gmail.com, poornimamittal@dtu.ac.in and shubhamnegi0192@gmail.com**Keywords:** organic semiconductors, organic thin film transistor (OTFT), vertical OTFT**Abstract**

The basic performance parameters such as threshold voltage, drain current and saturation mobility play an important role for any transistor-based devices. The planar organic TFT provides a good performance but it is still not satisfactory. Therefore, in this paper, a vertical channel TFT (D_5) is proposed that exhibits a significant improvement for threshold voltage V_t , drain current I_{Dmax} and saturation mobility μ_{sat} in comparison to planar devices. The proposed vertical device (D_5) is 44 and 24 times enhanced in comparison with planar device D_1 in terms of I_{Dmax} and μ_{sat} , correspondingly. Furthermore, this paper compares five different vertical-channel device architectures (D_2 , D_3 , D_4 , D_5 , D_6 & D_7). Out of these structures, our proposed novel structure (D_5) shows remarkable performance in terms of drain current (528 μA) and saturation mobility (80.8 $cm^2/V.s$). As compared to the best mentioned vertical devices D_2 , D_3 and D_7 , the proposed device exhibits 41.8 %, 15.6 % and 27.8 %, increment in drain current, respectively. Additionally, the proposed device exhibits about 2.7, 5.2 and 3.5 times improvement in comparison with D_2 , D_3 and D_7 correspondingly. The reasons for this better performance of the proposed device have been explained by vertical and horizontal cutline analysis.

1. Introduction

In the last decade, the performance of thin film transistors (OTFTs) has been enhanced remarkably [1, 2]. Various deposition techniques, in-depth analysis of physical structure and novel materials have played major role in this significant progress. In conventional OTFTs overlapping of capacitances and higher threshold voltage restrict the performance of device. Also, need of charge carrier injection and shorter channel length [3–7] has been highlighted. Therefore, researchers have made several efforts in scaling down the dimensions of TFTs by keeping the electric field constant [8, 9]. Even so, these methods are not enough to make significant improvement in cut-off frequency and transconductance of conventional horizontal organic TFTs. On the other hand, by incorporating additional injection layer and decreasing the parasitic capacitances the fabrication process becomes complex [10, 11]. The straightforward solution to improve the TFT transconductance is to decrease the channel length to the submicron regime [12]. However, submicron channels require sophisticated and often expensive patterning techniques such as electron-beam lithography or stencil mask patterning [13], which cannot be adopted to a possible low-cost fabrication process on flexible substrates. An alternative device concept, offering submicron channel lengths but without the compromise of using complex patterning techniques, is the vertical organic thin film transistor (VOTFT) [14–16].

In vertical TFTs, gate electrode, source electrode, organic semiconductor and drain electrode are arranged vertically which lead to a vertical channel instead of horizontal. The major difference between common lateral TFTs and vertical TFTs is the distance between source and drain. This distance is usually defined as the length of channel. This length is provided by the thickness of layer and so, ultra-short channel ($<1 \mu m$) can be easily achieved in VOTFTs. Many researchers have suggested various structures where vertical channels are incorporated. In 2008, Kim *et al* [17] fabricated a VOTFT using tris-(8-hydroxyquinoline) aluminium (Alq3) as



Characteristic performance and analysis of the positional variation of the charge generation layer to enhance the performance of OLEDs

Sugandha Yadav¹ · Poornima Mittal¹ · Shubham Negi²

Received: 3 June 2023 / Accepted: 22 September 2023 / Published online: 24 October 2023
© Springer Science+Business Media, LLC, part of Springer Nature 2023

Abstract

In this paper, a highly efficient charge generation layer (CGL)-based blue organic light-emitting diode is proposed. The proposed device contains a CGL composed of two materials, 1,1-bis[(di-4-tolylamino)phenyl]cyclohexane (TAPC) and 1,4,5,8,9,11-hexaazatriphenylene-hexacarbonitrile (HAT-CN), which act as hole and electron injectors, respectively. The CGL in the proposed device is placed outside the emissive layer, which provides better luminescence and current as compared with four other CGL-based devices D₂, D₃, D₄ and D₅ where CGL is utilized below the cathode, above the anode, near both electrodes (cathode and anode) and inside the emissive layer, respectively. The proposed device exhibits noteworthy results, achieving peak current and luminescence values of 0.44 A and 3636.3 cd/m², respectively. The luminescence obtained is improved by about 16.8, 2.3, 1.7, 3, and 1.6 times compared with D₁, D₂, D₃, D₄ and D₅. Thickness optimization of the proposed device is also outlined. The optimized device shows maximum luminescence of 4670 cd/m².

Keywords Organic light-emitting diode (OLED) · Charge generation layer (CGL) · Luminescence · Recombination rate of charge carriers

1 Introduction

Over the past few years, researchers have shown enormous interest in developing full-colour high-resolution displays which also achieve a longer lifetime [1–3]. These organic material-based displays possess very attractive properties such as ultra-thin thickness, flexibility, easy fabrication, light weight, wide viewing angle and fast response [4–7]. With these salient features, light-emitting diodes (OLEDs) have established their unique place in the display market and are garnering increasing attention among consumers. Despite the many attractive features of these devices, however, there is still a need for improved performance in terms of

luminescence, current density and lifetime [8]. Researchers have incorporated many additional layers in OLEDs including hole/electron injection layer, hole/electron transport layer and blocking layer, which have contributed greatly to enhancing their performance [9, 10]. But, nowadays, novel advanced layers including mixed interlayer [11], charge generation layer [12], and spacer layers [13] have come into the picture to further refine OLED performance. These layers are now widely utilized by researchers.

Maurya et al. [14] discussed an OLED device on which the positional analysis of a mixed interlayer was performed. In this study, it was noted that luminescence and current density were improved by changing the position of the layer towards the cathode. Peak luminescence and maximum current density of 17,139 cd/m² and 84.6 mA/cm², respectively, were obtained. Liu et al. [15] inserted a mixed interlayer of poly(9-vinylcarbazole) (PVK) and poly[(9,9-dioctylfluorenyl-2,7-diyl)-co-(4,4'-(N-(4-s-butylphenyl)diphenylamine))] (TFB) between the emissive layer and PEDOT:PSS layer. The proposed device exhibited maximum power efficiency of 47.2 lm/W and external quantum efficiency (EQE) of 18.86%. On the other hand, Ying et al. [16] utilized a spacer layer with the materials 1-bis[4-[N,N-di(4-tolyl)amino]

✉ Poornima Mittal
poornimamittal@dtu.ac.in

Sugandha Yadav
sugandhayadav555@gmail.com

Shubham Negi
shubhamnegi0192@gmail.com

¹ Department of Electronics and Communication Engineering,
Delhi Technological University, New Delhi 110042, India

² Department of Electronics and Communication Engineering,
Chandigarh University, Mohali, Punjab 140413, India

An In-Depth Analysis of Variation in Characteristic Performance of OLED with Respect to Position of Charge Generation Layer

Sugandha Yadav,¹ Poornima Mittal,^{1,z} and Shubham Negi²

¹Department of Electronics & Communication Engineering, Delhi Technological University, New Delhi, 110042, India

²Department of Electronics and Communication Engineering, Chandigarh University, Mohali Punjab, 140413 India

^zE-mail: poornimamittal@dtu.ac.in

Abstract

In this paper, a high performance blue organic light emitting diode having a charge generation layer (CGL) is proposed and compared with the other five CGL and non-CGL based devices. The utilized CGL layer in the different structure consists of two materials; HAT-CN (hexaazatriphenylene-hexacarbonitrile) and TAPC (1,1-bis[(di-4-tolylamino)phenyl]cyclohexane,) for electrons and holes generation, correspondingly. In the proposed novel structure, the CGL layer is incorporated outside of the emissive layer (EML) which significantly enhances the device performance in terms of current and luminescence. The device exhibits luminescence and current values as 3636.3 cd/m² and 0.44 A, respectively. Furthermore, this paper represents in-depth internal analysis of the six devices (D₁-D₆). This analysis is provided by drawing horizontal and vertical cutlines inside the devices. The proposed device is analysed and compared with other mentioned devices in terms of several parameters such as Langevin recombination rate, electron concentration, hole concentration, band energy, total current density, electron affinity, hole QFL (quasi-Fermi level), conduction current density, potential distribution and electron/hole mobility. In comparison with D₁, D₂, D₃, D₄ and D₅, the current of the proposed device (D₆) is about 16.9, 2.2, 1.7, 3 and 1.6 times improved, correspondingly. Moreover, structural analysis is also included to understand the performance of the devices more precisely.



Impact of Varying Position and Ratio of Charge Generation Layer on Performance Parameters of Organic Photodiode

Sugandha Yadav,^{1,z} Poornima Mittal,^{1,z}  and Shubham Negi^{2,z}

¹Department of Electronics and Communication Engineering, Delhi Technological University, Delhi-110042, India

²Department of Electronics and Communication Engineering, Chandigarh University, Mohali, Punjab-140413, India

Organic photodiodes have emerged as the best alternative to inorganic devices during the last decade. Herein, a highly efficient organic photodiode having charge generation layer (CGL) is demonstrated. This charge generation layer is a combination of HAT-CN (hexaazatriphenylene-hexacarbonitrile) and TAPC (1,1-bis[(di-4-tolylamino)phenyl]cyclohexane) materials which generate electrons and holes, correspondingly. Moreover, in this work, the proposed device (D₂) is compared with other four non-CGL (D₁) and CGL based (D₃, D₄ and D₅) devices. In all the CGL based devices, positional variation of the CGL layer is incorporated. In the proposed device (D₂), the CGL is situated outside the active layer in such a manner like HAT-CN is placed near acceptor and TAPC is near donor layer. In this way, the proposed device is showing the remarkable improvements in terms of photocurrent and dark current as 134.2 nA and 10.2 nA, respectively. The value of photocurrent of D₂ is 34 times increased of the reference device (D₁). Furthermore, on comparing with other CGL based devices D₃, D₄ and D₅, photocurrent of D₂ is approx 1.6, 1.4 and 9 times enhanced, correspondingly. Moreover, the thickness optimization and internal analysis of the proposed device are also performed to show the novelty of the presented work.

© 2024 The Electrochemical Society ("ECS"). Published on behalf of ECS by IOP Publishing Limited. [DOI: 10.1149/2162-8777/ad2401]

Manuscript submitted December 7, 2023; revised manuscript received January 14, 2024. Published February 7, 2024.

Organic semiconductor devices are gaining great interest and have become the first choice of various researchers over inorganic devices nowadays. These organic devices are promising alternates of inorganic devices as they contain unique combination of mechanical advantage of polymers along with electronic benefits of semiconductors.¹⁻⁵ These salient properties provide robustness, large area fabrication, flexibility, inexpensiveness, lightweight etc. to organic devices.⁶⁻¹¹ In particular, all these features are true for photodetector field as well. Photodiodes based on silicon are very sensitive to a wide range of wavelengths (ultraviolet to in-red). On the other hands, organic semiconductor-based photodiodes can particularly identify a designated range of light wavelengths because of specific molecular design.¹²⁻¹⁶ Materials used in OPDs can be altered chemically which leads to faster charge extraction and dynamic range adjustments.¹⁷⁻²⁰

Organic photodiodes (OPD) have been explored widely by various researchers using several techniques to improve the performance parameters such as photocurrent, responsivity, dark current, external quantum efficiency (EQE) etc. Ng et al.²¹ presented a bulk heterojunction photodiode on a flexible substrate using inkjet printing. In this research, efficient charge collection was reported with low dark current ($<1 \text{ nA cm}^{-2}$). Additionally, Lee et al.²² proposed a highly efficient fullerene-free BHJ OPD with the materials N,N-dimethyl quinacridone (DMQA) and dibutyl-substituted dicyanovinyl-terthiophene (DCV3T) for donor and acceptor, respectively. The device exhibited external quantum efficiency of about 67% at 540 nm. Moreover, Deckman et al.²³ fabricated a fully printed OPD with the capability of RGB light separation. This proposed OPD achieved EQE of $\sim 37\%$ at -4 V with the dark current of 0.5 nA cm^{-2} . Afterwards, Jang et al.²⁴ demonstrated a non-fullerene acceptor based OPD and compared it with fullerene acceptor based OPD. The non-fullerene based OPD showed faster time response and higher detectivity as $2.7 \mu\text{s}$ and $1.61 \times 10^{13} \text{ cm Hz}^{1/2} \text{ W}^{-1}$, respectively.

In this paper, a novel structure of charge generation layer (CGL) based OPD is presented. The utilized materials for CGL are 1,1-bis[(di-4-tolylamino)phenyl]cyclohexane (TAPC) and 1,4,5,8,9,11-hexaazatriphenylene-hexacarbonitrile (HAT-CN). Herein, TAPC material provides additional free positive charge carriers (holes) and HAT-CN is used for generation of additional negative charge carriers (electrons). This CGL layer significantly

enhances the performance of device parameters and the proposed device exhibits remarkable performance in comparison with reference device.²⁵ The performance parameters such as photocurrent and dark currents are obtained as 134.2 nA and 10.2 nA, correspondingly.

The completer paper is arranged in total six sections. First section starts with the introduction of OPD. Afterwards, second section explains the working principle of OPD. Thereafter, third section incorporates validation work of the reference device. Moreover, in fourth section the proposed novel device is discussed. This section also includes comparison of the proposed device with other CGL based devices as well as the section performs thickness optimization of the proposed device. Addition to this, the paper incorporates the vertical cutline analysis in fifth section. Eventually in sixth section, necessary conclusions are mentioned.

Working Principle of OPD

Photodiodes is used to convert the light into electricity. Hence, the major application of photodiode is to detect the brightness.²⁶ The structure of OPDs is very similar as organic solar cells (OSCs) but both vary in terms of their mode of operations. An OPD consists of basically five layers: (1) cathode, (2) anode, (3) acceptor, (4) donor and (5) substrate as demonstrated in Fig. 1.

The photodiode operates in reverse bias. First, the cathode is connected to the positive terminal of the battery and anode is connected to the negative terminal of the battery. Now, when the incident light falls on the active layer (combination of acceptor & donor), the bounded electrons and hole pairs inside active layer will gain some energy and free electrons and holes are generated. These free charge carriers will be further collected at the electrodes and eventually, a current is produced which is called photocurrent. In the other case, when there is no incident light on the active layer, a small amount of current still flows inside the photodiode. This current is called dark current.²⁶ The mentioned working steps are also depicted in Fig. 2.

Characteristic Analysis and Parameters Extraction of OPD

In this section, a multilayered organic photodiode²⁵ is validated using Silvaco Atlas 2-D device simulator. For the simulation, a model i.e. Langevin's recombination rate is applied in Silvaco Atlas 2-D device simulator for the validation of the reference device. The expression for the model is as follows:

^zE-mail: sugandhayadav555@gmail.com; poornimamittal@dtu.ac.in; shubhamnegi0192@gmail.com

Covid-19 Detection Using Organic LED and Photodiode-Based Sensor Device

Sugandha Yadav, Poornima Mittal¹, Senior Member, IEEE, and Shubham Negi, Member, IEEE

Abstract—The utilization of fluorescence detection for various biomedical applications such as oximeter sensors, cancer detection, monitoring of protein-DNA interactions, heart stroke detection, etc. has been on the rise which was first introduced by Heyduk and Lee in 1990. The integration of organic light emitting diode and organic photodiode (OPD) is well suited for these kinds of health-care detections. In this article, a methodology is proposed for Covid-19 detection which consists of a highly flexible blue organic LED (OLED), an OPD, and a human saliva sample. An in-depth investigation is being performed on both the OLED and OPD devices to make these devices suitable for the detection of the SARS-COV-2 virus inside human saliva samples. The presented methodology is based on fluorescence detection. Herein, the OLED emits an excitation wavelength of 470 nm and OPD produces two different currents 63.5 and 37.2 mA corresponding to the emission wavelengths of 490 and 525 nm, correspondingly. It is concluded here that if the OPD produces 63.5 mA current, the person is infected by Covid-19 and if it produces 37.2 mA current, the person is healthy. This article also compares the proposed methodology with some other researcher's work. The proposed OLED-OPD integration may be utilized for other sensing applications such as environmental monitoring, multispectral sensing, optical sensing, IoT devices, etc.

Index Terms—Covid-19, organic LED (OLED), organic photodiode (OPD), sensor, V-OTFT.

I. INTRODUCTION

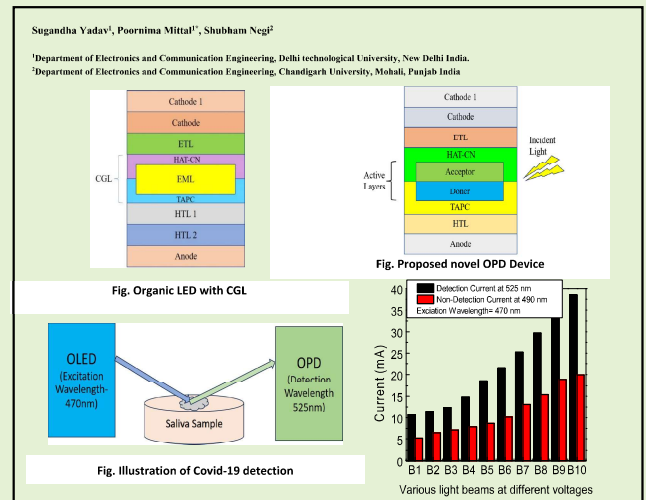
ULTRATHIN and flexible sensors are highly promising for health care applications [1], [2], [3], [4], [5], [6]. To produce flexible wearable sensors, two devices are vital which are; 1) organic LED (OLED) and organic photodiode (OPD). OLED is generally used for light emission which falls on the sample and OPD receives the light which is emitted by the sample. Various researchers have utilized these two devices for so many health care-based sensor applications to make flexible devices. Titov et al. [7] utilized a combination of OLED and OPD which is suitable for low-cost compact optical detection for the sensing applications. Furthermore, Katchman et al. [8] demonstrated the quantitative detection of IgG antibodies using human serum with the help of a light-emitting diode and photodiode.

Received 3 September 2024; revised 16 October 2024; accepted 16 October 2024. Date of publication 30 October 2024; date of current version 13 December 2024. The associate editor coordinating the review of this article and approving it for publication was Dr. Juan A Lenero-Bardallo. (Corresponding author: Poornima Mittal.)

Sugandha Yadav and Poornima Mittal are with the Department of Electronics and Communication Engineering, Delhi Technological University, Delhi, New Delhi 110042, India (e-mail: poornimamittal@dtu.ac.in).

Shubham Negi is with the Mohali Electronics and Communication Department, Chandigarh University, Mohali, Punjab 140413, India.

Digital Object Identifier 10.1109/JSEN.2024.3485702



Lim et al. [9] presented an oxygen sensor device using the same OLED-OPD combination. Herein, simultaneous monitoring of tcpO_2 is incorporated for the detection in any part of the human body. In addition to this, Lochner et al. [10] reported a low-cost flexible pulse oximeter using organic devices; LED and photodiode. The proposed device is able to measure oxygenation and pulse rate with errors of 2% and 1%, correspondingly. Furthermore, Khan et al. [11] demonstrated a reflectance oximeter sensor device using a light emitter, a detector, and an optical barrier between the emitter and detector. Using this method, the researchers designed three sensor geometries which are rectangular geometry, bracket geometry, and circular geometry. Additionally, Lee et al. [12] proposed a compact flexible OLED-OPD sensing device for Covid-19 detection. The device successfully detects SARS-CoV-2 RNA within 20 min using fluorescence detection.

This work presents a detection methodology for Covid-19. This is done by detecting the SARS-CoV-2 virus in saliva samples using OLED and OPD devices. An in-depth discussion of the methodology is provided in the below sections. The complete paper is categorized into five different sections. As discussed already above, Section I is about the introduction which includes various sensing applications using OLED and OPD. Afterward, Section II showcases the light-emitting device which further discusses the OLED driving circuit as well. Moreover, the Covid-19 detection technique is discussed

Parametric Analysis of Organic LED and Photo-Diode Based Sensor for Heart Rate Detection

Sugandha Yadav, Poornima Mittal,* and Shubham Negi

Conventional Light emitting diode and photo-diode integration is the best suitable combination for point-of-care diagnostic in the field of sensor applications. However, these approaches based on inorganic devices are not scalable to incorporate multiple bio-marker. As a solution, this work proposes the methodology for bio-medical application using organic LED (OLED) and photo-diode to make a highly efficient, ultra-flexible, and low-cost sensor. In this paper, a green charge generation based OLED and organic photo diode (OPD) are utilized for heart rate measurements. The methodology is basically based on the fluorescence emission where green light having wavelength of 497 nm falls on the blood cells. Furthermore, a different intensity wavelength is sensed by the photodiode. The proposed OLED exhibits current and luminescence parameters of 0.92 A and 8 363.6 cd m⁻², correspondingly. Moreover, the presented OPD demonstrates dark currents and photocurrent of 10.2 and 174.5 nA, subsequently. This proposed technique can be also investigated in terms of other biomedical applications such as oxygen sensor, cancer detection, corona detection etc.

1. Introduction

Ultra-thin and flexible sensors are highly promising for health-care applications.^[1–7] To produce flexible wearable sensors, two devices are vital: 1) organic LED (OLED) and 2) organic photo diode (OPD). OLED is generally used for light emission which falls on the sample and OPD receives the light which is emitted by the sample. Various researchers have utilized these two devices for so many health-care based sensor applications to make flexible devices. Titov et al.^[8] utilized a combination of OLED and OPD which is suitable for low-cost compact optical detection for the sensing applications. Furthermore, Katchman et al.^[9] demonstrated quantitative detection of IgG antibodies using human serum with the help of light emitting diode and photo diode.

Lim et al.^[10] presented an oxygen sensor device using the same OLED-OPD combination. Herein, simultaneous monitoring of

tcpO₂ is incorporated for the detection in any part of the human body. Addition to this, Lochner et al.^[11] reported a low-cost flexible pulse oximeter using organic devices, LED and photo diode. The proposed device is able to measure oxygenation and pulse rate with the errors of 2% and 1%, correspondingly. Furthermore, Khan et al.^[12] demonstrated a reflectance oximeter sensor device using a light emitter, a detector and an optical barrier between emitter and detector. Using this method, the researchers designed three sensor geometries which are rectangular geometry, bracket geometry, and circular geometry. Additionally, Lee et al.^[13] proposed a compact flexible OLED-OPD sensing device for covid-19 detection. The device successfully detects SARS-CoV-2 RNA within 20 min using fluorescence detection.

Our work investigates few biomedical applications based on the light detection methodology using OLED-OPD integration. The in-depth discussion about the methodology is provided in the below sections. The complete paper is categorized in seven different sections. As discussed already above, Section I is about the introduction which includes various sensing applications using OLED and OPD. Afterward, Section II showcases the light detection methodology using these devices. Moreover, Section III illustrates the novel OLED structure for heart rate detection. Thereafter, in Section IV, OPD is investigated in order to measure the heart rate in human. Additionally, Section V depicts the methodology for the heart rate detection. Next, Section VI incorporates the comparison of few researchers' work for heart rate detection. Eventually, Section VII incorporates the necessary conclusions.

2. Light Detection Methodology Using OLED-OPD Integration

The block diagram in Figure 1 depicts methodology for light-based detection technique using OLED and photo-diode. Here, OLED is used as light emitting device whereas, organic photo-diode is utilized as light detector as per their basic characteristics. The light from LED falls on sample which further excites the sample based on the nano particles present inside the sample and fluorescence emission occurs.

Eventually, photodiode provides current values at the specific wavelengths as per the detection technique. This idea of excitation and absorption in terms of wavelength is very promising for

S. Yadav, P. Mittal
Department of Electronics and Communication
Delhi Technological University
New Delhi 110042, India
E-mail: poornimamittal@dtu.ac.in

S. Negi
Department of Electronics and Communication Engineering
Chandigarh University
Mohali, Punjab 140413, India

The ORCID identification number(s) for the author(s) of this article can be found under <https://doi.org/10.1002/adts.202500037>

DOI: 10.1002/adts.202500037

Parametric Analysis of CGL based OLED-OPD Integration for Ovarian Cancer Detection

Sugandha Yadav¹, Poornima Mittal^{1*}, Shubham Negi²

¹Department of Electronics & Communication Engineering, Delhi Technological University, New Delhi, 110042, India

²Department of Electronics and Communication Engineering, Chandigarh University, Mohali Punjab, 140413 India

E-mail: ¹sugandhayadav555@gmail.com, ^{1*}poornimamittal@dtu.ac.in,

²shubhamnegi0192@gmail.com

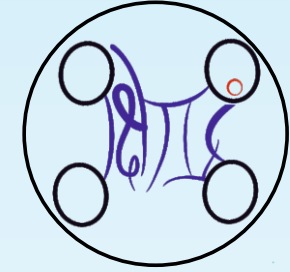
*Corresponding Author: poornimamittal@dtu.ac.in

Abstract: In the field of sensor applications, conventional LEDs and photodiode are vital devices. Their combination provides precise point-of-care diagnostic for various applications such as cancer detection, PPG sensor, corona virus detection etc. However, conventional inorganic LEDs and photodiodes are not capable of producing flexible and more compact arrangements. To overcome this, organic devices such as OLED, OPD and OTFT etc. are gaining attention in order to produce ultra-thin and flexible devices in the field of bio-marker based detection applications. This work proposed such organic LED and photodiode using charge generation layer to design an ovarian cancer detection device. The presented OLED generates the current density and luminescence values as 37.02 mA/cm² and 3636.38 cd/m², correspondingly. Addition to this, the novel OPD provides dark current and photo current of 10.2 and 174.5 nA, subsequently. The novel OLED emits the target light beam of 350nm which falls on the urine sample. Thereafter, the altered light beam is sensed by the proposed photodiode and produces output current. In this work, two current values are produced corresponding to the two light beams of 420nm and 440nm to decide whether the person is diagnosed with ovarian cancer or not.

Keywords- Organic Light Emitting Diode (OLED), Organic Photo-Diode (OPD), Charge Generation Layer (CGL), Luminescence, Ovarian Cancer, Bio-Sensor



IIT Roorkee



Drone Research Centre

IEEE International Conference On Electrical, Electronics, Communication and Computers (ELEXCOM'23)

CERTIFICATE


This is to certify that Prof./Dr./Mr./Ms. Sugandha Yadav of
Delhi Technological University, ~~participated~~ / presented in Elexcom'23 Jointly Organized by: Drone
Research Centre, IIT Roorkee, in Collaboration with IEEE Roorkee Subsection and IEEE Uttar Pradesh GRSS
Chapter at Indian Institute of Technology Roorkee, Roorkee, Uttarakhand, INDIA during 26th-27th August,
2023.

Paper Title..... Analysis and comparison of a high-K dielectric vertical channel based organic thin film transistor

Authors..... Sugandha Yadav; Dr Poornima Mittal; Dr. Shubham Negi


Prof. Ekant Sharma
Organizing Chair


Prof. Deep Kiran
Organizing Chair


Prof. Dharmendra Singh
General Chair

Certificate of Participation

This is to certify that

Sugandha Yadav, Poornima Mittal, Shubham Negi

have successfully Presented the Paper Entitled

Positional Analysis and Comparison of Different Charge Generation Layer based Blue OLEDs

at the **2nd IEEE International Conference on Device Intelligence, Computing, and Communication Technologies (DICCT-2024)** organised by the Department of Electronics and Communication Engineering, Graphic Era (Deemed to be University) Dehradun, India held on **15-16 March, 2024**.



Dr. Abhay Sharma
Convener



Dr. Mridul Gupta
Convener



Dr. Chandni Tiwari
Convener



Prof. (Dr.) Md. Irfanul Hasan
Conference Chair



DELHI TECHNOLOGICAL UNIVERSITY

(Formerly Delhi College of Engineering)

Shahbad Daulatpur, Main Bawana Road, Delhi-42

PLAGIARISM VERIFICATION

Title of the Thesis: **Design and Structural Analysis of Organic Semiconductor based Electronic Devices for Bio-medical Applications**

Total Pages: **196**

Name of the Scholar: **Ms. Sugandha Yadav**

Supervisor (s):

(1) **Prof. Poornima Mittal**, Professor, Department of Electronics and Communication Engineering, Delhi Technological University, Delhi, India

(2) **Dr. Shubham Negi**, Department of Electronics and Communication Engineering, Chandigarh University, Mohali, India

Department: **Electronics and Communication Engineering**, Delhi Technological University

This is to report that the above thesis was scanned for similarity detection. Process and outcome is given below:

Software used: **Turnitin**

Similarity Index: **7%**

Total Word Count: **63,823**

Date: 19-11-2025

A handwritten signature in blue ink, appearing to read 'Sugandha Yadav'.

Candidate's Signature

A handwritten signature in blue ink, appearing to read 'Shubham Negi'.

Signature of Joint Supervisor

A handwritten signature in blue ink, appearing to read 'Poornima Mittal'.

Signature of Supervisor

Ph.D. Thesis_2K20PHDEC09_Sugandha Yadav.pdf

 Delhi Technological University

Document Details

Submission ID

trn:oid:::27535:121512011

Submission Date

Nov 15, 2025, 3:25 PM GMT+5:30

Download Date

Nov 15, 2025, 3:40 PM GMT+5:30

File Name

Ph.D. Thesis_2K20PHDEC09_Sugandha Yadav.pdf

File Size

5.3 MB

196 Pages

63,823 Words

333,189 Characters



7% Overall Similarity

The combined total of all matches, including overlapping sources, for each database.





Filtered from the Report

- Bibliography
- Small Matches (less than 10 words)




Exclusions

- 13 Excluded Sources

Match Groups

-  **264 Not Cited or Quoted 7%**
Matches with neither in-text citation nor quotation marks
-  **2 Missing Quotations 0%**
Matches that are still very similar to source material
-  **8 Missing Citation 0%**
Matches that have quotation marks, but no in-text citation
-  **0 Cited and Quoted 0%**
Matches with in-text citation present, but no quotation marks

Top Sources

- 4%  Internet sources
- 5%  Publications
- 4%  Submitted works (Student Papers)

Integrity Flags

0 Integrity Flags for Review

No suspicious text manipulations found.

Our system's algorithms look deeply at a document for any inconsistencies that would set it apart from a normal submission. If we notice something strange, we flag it for you to review.

A Flag is not necessarily an indicator of a problem. However, we'd recommend you focus your attention there for further review.




Match Groups

- 264** Not Cited or Quoted 7%
Matches with neither in-text citation nor quotation marks
- 2** Missing Quotations 0%
Matches that are still very similar to source material
- 8** Missing Citation 0%
Matches that have quotation marks, but no in-text citation
- 0** Cited and Quoted 0%
Matches with in-text citation present, but no quotation marks

Top Sources

- 4% Internet sources
- 5% Publications
- 4% Submitted works (Student Papers)

Top Sources

The sources with the highest number of matches within the submission. Overlapping sources will not be displayed.

- 1** Internet
ouci.dntb.gov.ua <1%
- 2** Internet
coek.info <1%
- 3** Submitted works
Indian Institute of Technology Roorkee on 2015-04-22 <1%
- 4** Internet
dspace.dtu.ac.in:8080 <1%
- 5** Submitted works
Delhi Technological University on 2024-05-23 <1%
- 6** Publication
Poornima Mittal, Sugandha Yadav, Shubham Negi. "Advancements for organic thi... <1%
- 7** Internet
idoc.tips <1%
- 8** Internet
mrs.org <1%
- 9** Submitted works
Delhi Technological University on 2025-05-06 <1%
- 10** Submitted works
King Abdullah University of Science and Technology (KAUST) on 2023-07-13 <1%

11	Internet	www.renta.com.tw	<1%
12	Submitted works	Sabancı Universitesi on 2016-08-11	<1%
13	Internet	www.researchgate.net	<1%
14	Submitted works	Heriot-Watt University on 2011-12-05	<1%
15	Submitted works	Universiti Teknologi MARA on 2025-11-06	<1%
16	Submitted works	dtusimilarity on 2024-05-29	<1%
17	Publication	David Knepe, Felix Talnack, Bahman K. Boroujeni, Cecilia Teixeira da Rocha et al....	<1%
18	Publication	Sugandha Yadav, Poornima Mittal, Shubham Negi. "Architectural design, fabricat...	<1%
19	Internet	www.mendeley.com	<1%
20	Internet	ir.niist.res.in:8080	<1%
21	Submitted works	Jaypee University of Information Technology on 2018-03-16	<1%
22	Internet	www.science.gov	<1%
23	Internet	ir.kluniversity.in	<1%
24	Internet	s7c093c6ff6cff6e7.jimcontent.com	<1%

25	Internet	www.tandfonline.com	<1%
26	Publication	Woongsik Jang, Shafket Rasool, Byung Gi Kim, Jehan Kim, Jinhwan Yoon, Sergei M...	<1%
27	Publication	Guo-Qiang Zhang, Zhiyuan Gao, Jingtian Zhang, Hanlin Ou, Heqi Gao, Ryan T.K. K...	<1%
28	Publication	Poornima Mittal, Yuvraj Singh Negi, R. K. Singh. "Mapping of performance limitin...	<1%
29	Internet	www.lumtec.com.tw	<1%
30	Submitted works	Amrita Vishwa Vidyapeetham on 2025-10-14	<1%
31	Publication	Shubham Negi, A. K. Baliga, Yamini Pandey, Poornima Mittal, Brijesh Kumar. "Per...	<1%
32	Internet	hyoka.ofc.kyushu-u.ac.jp	<1%
33	Internet	www.rcsb.org	<1%
34	Publication	Zhizhi Li, Denghui Liu, Shi-Jian Su. "Management of charge and exciton for high-p...	<1%
35	Publication	Brajesh Kumar Kaushik, Brijesh Kumar, Sanjay Prajapati, Poornima Mittal. "Orga...	<1%
36	Publication	Rashmi Rathi, Rais Ahmad, Shubham Negi, Varij Panwar. "Performance Analysis o...	<1%
37	Internet	worldwidescience.org	<1%
38	Publication	P.P. Lima, F.A.A. Paz, C.D.S. Brites, W.G. Quirino et al. "White OLED based on a tem...	<1%

39	Publication	Lu, L., J.N. Yu, L. Long, F.F. Yu, J.H. Zhang, H. Zhang, and B. Wei. "Low-voltage and ...	<1%
40	Publication	Paritosh Chamola, Poornima Mittal. "Impact of ZnTe, SbZnTe and SnZnTe absorbe...	<1%
41	Publication	Yalian Weng, Guixiong Chen, Junyang Nie, Sihua Que et al. "Hybrid Device of Blue...	<1%
42	Publication	Shubham Negi, Poornima Mittal, Brijesh Kumar, Pradeep Kumar Juneja. "Organic ...	<1%
43	Publication	Yanwei Liu, Xiaofang Wei, Zhiyi Li, Jianjun Liu et al. "Highly Efficient, Solution-Proc...	<1%
44	Internet	www.frontiersin.org	<1%
45	Internet	ia804504.us.archive.org	<1%
46	Publication	N. Thejo Kalyani, S.J. Dhoble. "Novel materials for fabrication and encapsulation o...	<1%
47	Publication	Shih, Cheng-Hung, Pachaiyappan Rajamalli, Cheng An Wu, Wei-Ting Hsieh, and Ch...	<1%
48	Internet	d-scholarship.pitt.edu	<1%
49	Submitted works	Davao Del Sur State College on 2023-07-25	<1%
50	Publication	Kazunori Watanabe, Yuji Iwaki, Yutaka Uchida, Daiki Nakamura et al. "18.3: An 8....	<1%
51	Submitted works	Ngee Ann Polytechnic on 2024-08-23	<1%
52	Submitted works	University of Edinburgh on 2022-08-14	<1%

53	Internet	d-nb.info	<1%
54	Submitted works	King Abdullah University of Science and Technology (KAUST) on 2025-05-16	<1%
55	Publication	Yu-Hsiang Tsai, Yi-Lin Wu, Wei-Tong Liou, Yu-Ruei Kung, Yi-Hsiang Huang, Kuo-Ch...	<1%
56	Publication	Chang Yeol Lee, Ismail Degani, Jiyong Cheong, Jae-Hyun Lee, Hyun-Jung Choi, Jin...	<1%
57	Publication	Poornima Mittal. "Ditch and elevated organic thin film transistor-based improved...	<1%
58	Submitted works	University of Science and Technology on 2015-11-24	<1%
59	Submitted works	University of Washington on 2015-11-20	<1%
60	Internet	vdoc.pub	<1%
61	Publication	Ashish Pal, Brijesh Kumar, G. S. Tripathi. "Effect of electrode-thickness on electric...	<1%
62	Internet	static.datasheets.com	<1%
63	Submitted works	GLA University on 2015-05-02	<1%
64	Submitted works	Kaunas University of Technology on 2025-04-16	<1%
65	Submitted works	Kaunas University of Technology on 2025-10-21	<1%
66	Publication	Kleemann, Hans, Alrun A. Günther, Karl Leo, and Björn Lüssem. "High-Performan...	<1%

67	Publication	Ritu Srivastava, M.N. Kamalasanan, Gayatri Chauhan, Arunandan Kumar, Priyank...	<1%
68	Submitted works	Universiti Malaysia Perlis on 2018-05-28	<1%
69	Submitted works	Leiden University on 2025-06-13	<1%
70	Internet	arxiv.org	<1%
71	Publication	Huang-Yu Lin, Chin-Wei Sher, Chih-Hao Lin, Hsien-Hao Tu et al. "Fabrication of Fle...	<1%
72	Publication	Jang, J.. "High-performance OTFT and its application", Current Applied Physics, 20...	<1%
73	Publication	Mengdi Wang, Wenqing Zhu, Zhengyuan Yin, Lu Huang, Jun Li. "Synergistic effect...	<1%
74	Submitted works	University of Leeds on 2017-04-26	<1%
75	Internet	doczz.net	<1%
76	Internet	onlinelibrary.wiley.com	<1%
77	Internet	uwspace.uwaterloo.ca	<1%
78	Submitted works	Birla Institute of Technology and Science Pilani on 2018-12-13	<1%
79	Publication	Lionel Derue, Simon Olivier, Denis Tondelier, Tony Maindron, Bernard Geffroy, Elé...	<1%
80	Publication	Mittal, Poornima, Y.S. Negi, and R.K. Singh. "A depth analysis for different structu...	<1%

81	Publication	Mozena, Emily N. R.. "Understanding Perspectives and Resilience of Adolescents ..."	<1%
82	Internet	ip.ios.semcs.net	<1%
83	Internet	ksascholar.dri.sa	<1%
84	Internet	patents.google.com	<1%
85	Internet	researchspace.ukzn.ac.za	<1%
86	Publication	Arvind Sharma, T.D. Das. "Highly efficient OLED device based on the double emiss..."	<1%
87	Publication	Dinesh Chandra, Aryan Kannaujiya, Anupam Sahu, Brijesh Kumar. "Analysis of m..."	<1%
88	Publication	E. Angioni, M. Chapran, K. Ivaniuk, N. Kostiv et al. "A single emitting layer white O..."	<1%
89	Publication	Haji Talik Sisin, Noor Azrina. "Efficiency Enhancement of Solution Processable Org..."	<1%
90	Submitted works	Kaunas University of Technology on 2024-08-20	<1%
91	Submitted works	University of College Cork on 2022-12-02	<1%
92	Publication	Xialei Lv, Rongjuan Huang, Shuaiqiang Sun, Qing Zhang, Songpo Xiang, Shaofeng ...	<1%
93	Internet	www.freepatentsonline.com	<1%
94	Publication	"Physics and Technology of Crystalline Oxide Semiconductor CAAC-IGZO", Wiley, ...	<1%

95	Publication	Abhishek Bhattacharjee, Marampally Saikiran, Sudeb Dasgupta. "A First Insight t...	<1%
96	Publication	Amirah Basir, Hanan Alzahrani, Khaulah Sulaiman, Fahmi F. Muhammadsharif et ...	<1%
97	Submitted works	Bahcesehir University on 2024-09-19	<1%
98	Publication	Chan Hyuk Ji, Seon Ju Lee, Se Young Oh. "P3HT-based visible-light organic photod...	<1%
99	Publication	Jianhui Luo, Yibing Wu, Chengwei Lin, Shu Xiao, Xianfeng Qiao, Dezhi Yang, Yanfe...	<1%
100	Publication	Kumar, Brijesh, Brajesh Kumar Kaushik, and Yuvraj Singh Negi. "Analysis of electr...	<1%
101	Publication	Li, Weixin (Wayne). "A hybrid device approach to high performance in organic lig...	<1%
102	Publication	Marius Klein, Nicholas Rau, Mirco Wende, Jörg Sundermeyer, Gang Cheng, Chi-Mi...	<1%
103	Publication	Marlene Della. "The Impacts of the COVID-19 Pandemic on the Lives of Disabled P...	<1%
104	Publication	Menna Mostafa, Ahmed Barhoum, Ekin Sehit, Hossam Gewaid et al. "Current tren...	<1%
105	Submitted works	Nanyang Technological University on 2024-08-20	<1%
106	Publication	Rui Liu, Shujat Ali, Suleiman A. Haruna, Qin Ouyang, Huanhuan Li, Quansheng Ch...	<1%
107	Publication	Shao-Yu Lu, Sukrit Mukhopadhyay, Robert Froese, Paul M. Zimmerman. "Virtual S...	<1%
108	Publication	Shubham Negi, Poornima Mittal, Brijesh Kumar. "Characteristic Performance of ...	<1%

109	Publication	Shubham Negi, Poornima Mittal, Brijesh Kumar. "Modeling and Analysis of High-...	<1%
110	Publication	Shuqing Yuan, Yuying Hao, Yanqin Miao, Qinjun Sun, Zhanfeng Li, Yanxia Cui, Hu...	<1%
111	Submitted works	University of Birmingham on 2023-05-31	<1%
112	Submitted works	University of Hong Kong on 2013-04-29	<1%
113	Submitted works	University of Hong Kong on 2025-05-07	<1%
114	Submitted works	University of Hong Kong on 2025-06-18	<1%
115	Submitted works	University of Liverpool on 2025-04-27	<1%
116	Submitted works	University of Strathclyde on 2019-05-15	<1%
117	Publication	Xin-Feng Wei, Wan-Yi Tan, Jian-Hua Zou, Qing-Xun Guo, Dong-Yu Gao, Dong-Ge M...	<1%
118	Publication	Zhuangmiao Wang, Yu Tang, Mingsheng Gao, Jiayin Han, Furong Zhu. "Advanced ...	<1%
119	Publication	Zijuan Hao, Zhiyun Wu, Shuren Liu, Xiaowu Tang, Jinzhou Chen, Xuying Liu. "High...	<1%
120	Internet	dokumen.pub	<1%
121	Internet	dro.dur.ac.uk	<1%
122	Internet	faculty.kashanu.ac.ir	<1%

123	Internet	fundacioncreo.org.ar	<1%
124	Internet	pmc.ncbi.nlm.nih.gov	<1%
125	Internet	research-repository.st-andrews.ac.uk	<1%
126	Internet	www.extrica.com	<1%
127	Internet	www.repository.cam.ac.uk	<1%
128	Publication	"Handbook of Advanced Lighting Technology", Springer Science and Business Me...	<1%
129	Publication	Aanchal Verma, Poornima Mittal. "Performance analysis of different novel organi...	<1%
130	Submitted works	Academia Sinica Life Science Library on 2020-07-17	<1%
131	Publication	Akanksha Jetly, Rajesh Mehra. "Design of Tandem Organic Light Emitting Diode u...	<1%
132	Publication	Ameri, Lydia Nezhat. "High Performance White Organic Light-Emitting Diodes", A...	<1%
133	Publication	Brijesh Kumar, Brajesh Kumar Kaushik, Yuvraj Singh Negi, Vidhi Goswami. "Single...	<1%
134	Publication	Brijesh Kumar, Brajesh Kumar Kaushik, Yuvraj Singh Negi. "Analysis of electrical ...	<1%
135	Publication	Changhun Yun, Jonghee Lee, Jaehyun Lee, Björn Lüssem, Fabian Ventsch, Karl Le...	<1%
136	Publication	Changting Wei, Jinyong Zhuang, Dongyu Zhang, Wenrui Guo et al. "Pyridine-Base...	<1%

137	Publication	Chuan-Yi Yang. "<![CDATA[Pentacene-Based Planar- and Vertical-Type Organic Thi...	<1%
138	Publication	Da Yin, Shi-Xin Jia, Hao-Yang Zhang, Su-Heng Li, Yue-Feng Liu, Jing Feng. "Applicat...	<1%
139	Publication	Evin Yigit, Ömer Sevgili, Sinan Bayindir, Feride Akman, İkrım Orak, Osman Dayan...	<1%
140	Submitted works	Hoseo University on 2015-12-16	<1%
141	Submitted works	Imperial College of Science, Technology and Medicine on 2021-08-26	<1%
142	Submitted works	Indian Institute of Technology Jodhpur on 2016-05-28	<1%
143	Submitted works	Indian Institute of Technology Roorkee on 2013-04-08	<1%
144	Submitted works	Institute of Technology, Nirma University on 2013-09-05	<1%
145	Submitted works	Kaunas University of Technology on 2021-05-31	<1%
146	Publication	Ketan Priyadarshi, Vijaya Lakshmi Nag, Sarika P. Kombade, Ravi Sekhar Gadepalli...	<1%
147	Publication	Krishan Kumar, Kiran Kishore Kesavan, Sunil Kumar, Subrata Banik et al. "Decora...	<1%
148	Publication	M. Riede, B. Lüssem, K. Leo. "Organic Semiconductors", Elsevier BV, 2011	<1%
149	Publication	Mangey Ram Nagar, Shahnawaz, Rohit Ashok Kumar Yadav, Jin-Ting Lin, Jwo-Hue...	<1%
150	Publication	Mingliang Xie, Xun Chao, Chenglin Ma, Tengyue Li, Xin Wang, Yannan Zhou, Qiku...	<1%

151	Publication	Nannan Wang, Xiaohui Kang, Wumeng Liu, Wenjie Wu, Kexu Ren, Xiaohui Bao. "I...	<1%
152	Submitted works	Polytechnic of Turin on 2018-03-15	<1%
153	Publication	Pooja Maurya, Poornima Mittal, Brijesh Kumar. "Performance improvement for o...	<1%
154	Publication	Poornima Mittal, Yuvraj Singh Negi, R. K. Singh. "An analytical approach for para...	<1%
155	Submitted works	Rochester Institute of Technology on 2022-04-29	<1%
156	Publication	S. Manasa, Shubham Negi, Garima Chandel. "A Comprehensive Compilation of th...	<1%
157	Submitted works	The Hong Kong Polytechnic University on 2024-04-30	<1%
158	Submitted works	The Hong Kong Polytechnic University on 2025-04-30	<1%
159	Submitted works	University of Hong Kong on 2017-04-11	<1%
160	Submitted works	University of Hong Kong on 2023-09-21	<1%
161	Submitted works	University of North Texas on 2017-04-25	<1%
162	Submitted works	University of South Florida on 2014-06-26	<1%
163	Submitted works	University of Surrey on 2013-05-14	<1%
164	Submitted works	University of Sydney on 2024-05-26	<1%

165	Internet	aaltodoc.aalto.fi	<1%
166	Internet	conservancy.umn.edu	<1%
167	Internet	daten-quadrat.de	<1%
168	Internet	drpress.org	<1%
169	Internet	dspace.lboro.ac.uk	<1%
170	Internet	dtu.ac.in	<1%
171	Internet	faculty.iitmandi.ac.in	<1%
172	Internet	ilps.uobaghdad.edu.iq	<1%
173	Internet	ir.lib.nycu.edu.tw	<1%
174	Internet	publications.polymtl.ca	<1%
175	Internet	pure.mpg.de	<1%
176	Internet	www.lmpv.nl	<1%
177	Internet	www.mdpi.com	<1%
178	Internet	www.qucosa.de	<1%

SUGANDHA YADAV

#75/type IV, Gautam Buddha
University, Greater Noida (UP)

sugandhayadav555@gmail.com

(+91)9899494690

OBJECTIVE

I aim to secure a full-time academic role that allows me to contribute meaningfully to research and development in science and technology.

TEACHING EXPERIENCE

SN	Institute Name	Designation	Mode	Duration
1.	Gautam Buddha University, Greater Noida	Assistant Professor	Contract	August 2022 to June 2025
2.	Gautam Buddha University, Greater Noida	Assistant Professor	Contract	July 2019 to June 2020
3.	Guru Ghasidas Central University, Bilaspur (C.G.)	Assistant Professor	Contract	January 2018 to June 2018
4.	Bundelkhand Institute of Engg. & Technology, Jhansi (U.P.)	Assistant Professor	Contract	August 2015 to May 2017

EDUCATIONAL QUALIFICATIONS

SN	Course	Institute	Specialization	Duration	Division
1.	PhD.	Delhi Technological University, Delhi	Organic and Flexible Electronics	Pursuing (From August 2020)	Status: Thesis submitted
2.	M. Tech.	NIT Kurukshetra	VLSI Design	2012-2014	1st
3.	B. Tech.	HIT Greater Noida	Electronics & Communication Engineering	2008-2012	1st
4.	Intermediate	S. B. V. M. Sadar, Jhansi (U.P.)	Physics, Chemistry, Mathematics, Hindi, English	2007-2008	1st
5.	High school	B. D. G. V. M. Jhansi (U.P.)	Hindi, English, Mathematics, Science, Social Science, Drawing	2005-2006	1st

RESEARCH EXPERIENCE

Ph.D. Research Scholar, DTU Delhi (Pursuing from August 2020)

Supervisor: Prof. Poornima Mittal (DTU Delhi).

- Research topic: Design and structural analysis of organic semiconductor-based electronics devices for bio-medical applications.
- Published 09 SCI/SCIE research papers as first author.

Post Graduate Student, NIT Kurukshetra (2012-2014)

Supervisor: Dr. Sudhanshu Choudhary (Assistant Professor, NIT Kurukshetra).

- Conducted research in SAR ADC.
- Successfully reduced the power of SAR ADC using double tailed dynamic comparator.